CORA Cork Open Research Archive
Cartlann Taighde Oscailte Chorcaí

Title	Functional characterisation of LNX1 and LNX2 proteins
Authors	Lenihan, Joan A.
Publication date	2022
Original Citation	Lenihan, J. A. 2022. Functional characterisation of LNX1 and LNX2 proteins. PhD Thesis, University College Cork.
Type of publication	Doctoral thesis
Rights	© 2022, Joan Anne Lenihan. - https://creativecommons.org/licenses/by-nc-nd/4.0/
Download date	2024-05-18 15:18:20
Item downloaded from	https://hdl.handle.net/10468/15421

UCC
University College Cork, Ireland
Coláiste na hOllscoile Corcaigh

FUNCTIONAL CHARACTERISATION OF LNX1 AND LNX2 PROTEINS

A thesis submitted to the National University of Ireland, Cork, in fulfilment of the requirements for the degree of

Doctor of Philosophy

by

Joan Anne Lenihan, BSc.

School of Biochemistry & Cell Biology

University College Cork, Ireland

Supervisor: Dr. Paul Young

January, 2022

Table of Contents

Declaration 7

Acknowledgements 8

Publications 9

Abstract 10

Lay Abstract 12

List of Abbreviations 13

Chapter 1: General Introduction 17

1.1 Protein ubiquitination: mechanisms and consequences 18

1.1.1 E1 ubiquitin-activating enzymes 18

1.1.2 E2 ubiquitin-conjugating enzymes. 18

1.1.3 E3 ubiquitin ligases 19

1.1.3.1 HECT family E3 ligases 19

1.1.3.2 RING-type E3 ligases 21

1.1.4 Consequences of protein ubiquitination 23

1.1.4.1 Proteasomal degradation of ubiquitinated proteins 23

1.1.4.2 Lysosomal degradation of ubiquitinated proteins 24

1.2 The LNX1/2 family of proteins 26

1.2.1 Evolution of LNX1/2 proteins 26

1.2.2 Structure of LNX1/2 proteins 27

1.2.3 LNX2 and LNX2b functions in Zebrafish 28

1.2.4 LNX1/2 mRNA expression in mammals 30

1.2.5 LNX1/2 protein expression in mammals 32

1.2.6 Interactions of LNX1 and LNX2 with Numb and Numb-like 33

1.2.6.1 LNX1 and LNX2 as ligands of Numb 33

1.2.6.2 LNX1/2 as regulators of Notch signalling via Numb 34

1.2.7 Role of LNX1/2 proteins in neurogenesis and neuronal differentiation 35

1.2.8 Other interactions of LNX1/2 proteins 37

1.2.8.1 BCR 40

1.2.8.2 CD8 40

1.2.8.3 Claudins 41

1.2.8.4 ErbB2 42

1.2.8.5 ERC2 42
1.2.8.6 JAM4 43
1.2.8.7 PBK 43
1.2.8.8 RhoC 44
1.2.8.9 SKIP 44
1.2.8.10 c-Src 44
1.2.9 Disease associations of LNX1 and LNX2 46
1.2.9.1 Immune function and infectious disease 46
Chapter 2: Expression & regulation of LNX proteins 47
2.1 Introduction 48
2.2 Materials & Methods 52
2.2.1 Animals and animal procedures 52
2.2.2 Antibodies and reagents 52
2.2.3 Plasmids, primers, cDNA constructs and bioinformatic analysis 52
2.2.4 Immunoprecipitation of endogenous LNX proteins 54
2.2.5 Cell culture and transfection 54
2.2.6 Dual luciferase assays 55
2.2.7 RNA isolation and real time qPCR analysis 55
2.2.8 Analysis of LNX1 protein stability 56
2.2.9 Ubiquitination assays 57
2.2.10 Statistical analysis 58
2.3 Results 59
2.3.1 Examination of LNX protein expression in the nervous system 59
2.3.2 uORFs attenuate translation of LNX1p70 but not LNX1p80 or LNX2 63
2.3.3 Additional 5' UTR elements regulate LNX1 p70 protein expression 66
2.3.4 Proteasomal degradation and turnover of LNX1p80 protein. 70
2.4 Discussion 74
Chapter 3: Characterisation of LNX1 & LNX2 protein interactomes 79
3.1 Introduction 80
3.2 Materials & Methods 82
3.2.1 Reagents and cell lines 82
3.2.2 cDNA constructs and cloning 83
3.2.3 Antibodies 83
3.2.4 Animals and tissue harvesting 84

3.2.5 Expression and purification of GST-LNX1-PDZ2 and GST-LNX2-PDZ2 85
3.2.6 Cell culture conditions 85
3.2.7 Cryopreservation and recovery of cell lines 86
3.2.8 Maintenance of established cell lines 86
3.2.9 Seeding and transfection of cells 87
3.2.10 Protein extraction from mammalian cells 87
3.2.11 Determination of protein concentration in mammalian cells 87
3.2.12 SDS-PAGE 88
3.2.13 Coomassie blue staining 88
3.2.14 Western immunoblotting 88
3.2.15 Immunocytochemistry 89
3.2.16 Purification of LNX1 complexes from stably transfected cells 90
3.2.17 Purification of LNX1-PDZ2 and LNX2-PDZ2 complexes from brain lysates 91
3.2.18 Identification of Proteins by Peptide Fragment Fingerprinting (PFF) 91
3.2.19 Characterisation of interactions by GFP pull-down assays. 92
3.2.20 Ubiquitination assays 92
3.2.21 Analysis of functional associations of LNX interacting proteins. 93
3.2.22 Statistical analysis 93
3.3 Results 95
3.3.1 Affinity purification and identification of LNX1 interacting proteins 95
3.3.2 Confirmation of LNX1 interacting proteins 97
3.3.3 Mapping LNX1 interactions to regions within LNX1 100
3.3.4 Identification of LNX1 and LNX2 PDZ2 domain interacting proteins 102
3.3.5 Verification of PDZ2 interacting proteins ability to interact with full-length LNX 104
3.3.6 Investigation of colocalization events between LNX and novel interacting proteins 105
3.3.7 Characterisation of LNX-Liprin-α1 interaction 111
3.3.7.1 Liprin-α1 interacts with LNX via it carboxy-terminus 111
3.3.7.2 LNX enhances ubiquitination of Liprin-α1 113
3.3.7.3 LNX1p80 does not target Liprin-α1 for proteosomal degradation 115
3.3.7.4 LNX-mediated ubiquitination of Liprin-α1 is dependent on the interaction between LNX and Liprin-α1 116
3.3.7.5 Examination of the regions of LNX required for substrate recognition of Liprin-α1 118
3.3.8 KLHL11, KIF7 and ERC2 are substrates for LNX-mediated ubiquitination 121
3.3.9 Interaction of LNX1 with members of the TRIM E3 ubiquitin ligase family 121

3.4 Discussion **124**

Chapter 4: Exploration of the neuronal functions of LNX proteins *in vivo* **134**

4.1 Introduction **135**

4.2 Materials & Methods **136**

4.2.1 Animals 136

4.2.2 Breeding, housing and animal care 138

4.2.3 Genotyping 138

4.2.4 Tissue homogenization for western blot analysis and immunoprecipitation 139

4.2.5 Immunoprecipitation (IP) 140

4.2.6 Phenotypic characterisation of Lnx1 $^{exon3-/-}$ /Lnx2$^{-/-}$ mice. 141

4.2.6.1 Body weight and growth analysis. 141

4.2.6.2 Order of behavioural testing 141

4.2.6.3 Conditions common to all tests 141

4.2.6.4 Primary Observations 142

4.2.6.5 Y-maze 142

4.2.6.6 Open field 142

4.2.6.7 Light-dark box test 143

4.2.6.8 Elevated plus maze 144

4.2.6.9 Gait analysis 144

4.2.6.10 Rotarod test 145

4.2.6.11 Grip Strength 145

4.2.6.12 Hotplate test 146

4.2.6.13 Auditory fear conditioning 146

4.2.6.14 Forced swim test 148

4.2.7 Tissue harvesting 148

4.2.8 Statistical analysis 149

4.3 Results **150**

4.3.1 Confirmation of genotype 150

4.3.2 General appearance, body weight, survival 153

4.3.3 Lnx1$^{exon3-/-}$/Lnx2$^{-/-}$ knockout effects on physiology: organ masses 157

4.3.3.1 Brain mass 157

4.3.3.2 Spleen mass 157

4.3.3.3 Heart mass 158

4.3.3.4 Kidney mass 159

4.3.3.5 Lung mass....159
4.3.3.6 Liver mass....160
4.3.4 Lnx1$^{exon3-/-}$/Lnx2$^{-/-}$ knockout effects on Numb levels....162
4.3.5 Behavioural battery....164
4.3.5.1 Anxiety-like behaviour....164
4.3.5.1.1 Open field test....164
4.3.5.1.2 Light-dark box test....167
4.3.5.1.3 Elevated-plus maze test....169
4.3.5.2 Motor coordination and balance....172
4.3.5.2.1 Rotarod....172
4.3.5.2.2 Footprint analysis....174
4.3.5.2.3 Grip strength....177
4.3.5.3 Sensory responses....178
4.3.5.3.1 Hot plate test....178
4.3.5.4 Learning and memory....179
4.3.5.4.1 Y-maze test....179
4.3.5.4.2 Conditioned fear paradigm....182
4.3.5.5 Depression-like behaviour....184
4.3.5.5.1 Forced swim test....184
4.4 Discussion....185
4.4.1 General appearance, body weight, survival and organ weights....187
4.4.2 Anxiety-like behaviour....188
4.4.3 General locomotion, motor coordination and balance....190
4.4.4 Sensory responses....193
4.4.5 Learning and memory....193
General Discussion & Future Perspectives....197
Bibliography....203
Appendix A: Supplementary tables & figures....212
Appendix B: Publications....229

Declaration

This is to certify that the work I am submitting is my own and has not been submitted for another degree, either at University College Cork or elsewhere. All external references and sources are clearly acknowledged and identified within the contents. I have read and understood the regulations of University College Cork concerning plagiarism and intellectual property.

_____

Joan Lenihan

Acknowledgements

I wish to thank my supervisor Dr. Paul Young for his guidance, constant support and encouragement. Thanks to the Irish Research Council for supporting this work. Thanks to all members of the School of Biochemistry & Cell Biology past and present. A special thanks to the technical team – Pat Allen, Noreen Casey, Trish Fowler and Jenny Duane. Thanks to Prof. John Cryan, and to Pat Fitzgerald and James O'Leary for their generous assistance and advice regarding behavioural experiments. My thanks to Orthis Saha and Louise Mansfield for their contributions to the work. A special thanks to Anita Murphy – it was a pleasure to work alongside you.

Publications

Lenihan, J.A.*, Saha, O*., Mansfield, L.M. and Young, P.W. (2014) 'Tight, cell type-specific control of LNX expression in the nervous system, at the level of transcription, translation and protein stability', *Gene*, 552(1), 39-50, available: ***http://dx.doi.org/10.1016/j.gene.2014.09.011***.

*These authors contributed equally to this work.

Lenihan, J.A., Saha, O. and Young, P.W. (2017) 'Proteomic analysis reveals novel ligands and substrates for LNX1 E3 ubiquitin ligase', *PLoS One*, 12(11), e0187352, available: ***http://dx.doi.org/10.1371/journal.pone.0187352***.

Lenihan, J.A., Saha, O., Heimer-McGinn, V., Cryan, J.F., Feng, G. and Young, P.W. (2017) 'Decreased Anxiety-Related Behaviour but Apparently Unperturbed NUMB Function in Ligand of NUMB Protein-X (LNX) 1/2 Double Knockout Mice', *Mol Neurobiol*, 54(10), 8090-8109, available: ***http://dx.doi.org/10.1007/s12035-016-0261-0***.

Note:

Chapter 2 of this thesis incorporates the data/figures from the *Gene* paper that I generated or contributed to. One of the five figures from the paper, to which I did not contribute, has not been included in the thesis.

Chapter 3 of this thesis incorporates data/figures from both the *PLoS One and Mol Neurobiol* papers (all of which I generated or contributed to).

Chapter 4 of this thesis incorporates data/figures from the *Mol Neurobiol* paper (all of which I generated or contributed to), as well as some additional unpublished data.

Abstract

Ligand of Numb protein X1 (LNX1) and LNX2 are E3 ubiquitin ligases that contain a catalytic RING (Really Interesting New Gene) domain and four PDZ (PSD-95, DlgA, ZO-1) domains. LNX1 and LNX2 can interact with Numb – a key regulator of neurogenesis and neuronal differentiation. LNX1 can target Numb for proteasomal degradation, and *Lnx* mRNAs are prominently expressed in the nervous system, suggesting that LNX proteins play a role in neural development. This hypothesis remains unproven, however, and our understanding of LNX protein function is very limited – largely because LNX proteins are present at very low levels *in vivo*.

Chapter 2 of this thesis addresses this – investigating possible reasons for the low levels of LNX proteins observed *in vivo*, at both transcriptional and translational levels, and also in terms of protein stability. Luciferase reporter assays show that the 5' untranslated region of the *Lnx1_variant 2* mRNA, that generates the LNX1p70 isoform, strongly suppresses protein production. This effect is mediated in part by the presence of upstream open reading frames (uORFs), but also by a sequence element that decreases both mRNA levels and translational efficiency. By contrast, uORFs do not negatively regulate LNX1p80 or LNX2 expression. Instead, some evidence is presented that protein turnover via proteasomal degradation may influence LNX1p80 levels in cells.

To gain functional insights into the LNX family, Chapter 3 details the first physiologically relevant affinity purification/mass spectrometry-based analysis of the LNX interactome. In the context of mammalian cells, this approach identified a large number of novel LNX1-interacting proteins, as well as confirming known interactions with NUMB and ERC2. Many of the novel interactions mapped to the LNX PDZ domains, particularly PDZ2, and many showed

specificity for LNX1 over the closely related LNX2. It was shown that LIPRIN-α1, KLHL11, KIF7 and ERC2 are substrates for ubiquitination by LNX1. LNX1 ubiquitination of LIPRIN-α1 is dependent on a PDZ binding motif containing a carboxyl terminal cysteine that binds LNX1 PDZ2. Surprisingly, the neuronally-expressed LNX1p70 isoform, that lacks the RING domain, was found to promote ubiquitination of Liprin-α1 and KLHL11, albeit to a lesser extent than the longer RING-containing LNX1p80 isoform. Of several E3-ligases identified in the LNX1 interactome, interactions of LNX1 with MID2/TRIM1 and TRIM27 were confirmed. On this basis, a model is proposed, whereby LNX1p70 - despite lacking a catalytic RING domain, may function as a scaffold to promote ubiquitination of its ligands through recruitment of other E3-ligases. Proteomic analysis of LNX-interacting proteins in the context of brain tissue identified and/or confirmed interactions of LNX1 and LNX2 with proteins known to have presynaptic and neuronal signalling functions, including the presynaptic active zone constituents ERC1, ERC2, and LIPRIN-αs (PPFIA1, PPFIA3), as well as the F-BAR domain proteins FCHSD2 (nervous wreck homolog) and SRGAP2.

To examine the role of LNX proteins *in vivo*, mice lacking both LNX1 and LNX2 expression in the brain were generated. Surprisingly, these mice are viable, fertile and physically healthy (Chapter 4). Behavioural analysis of LNX1/LNX2 double knockout mice revealed decreased anxiety-related behaviour, as assessed in the open field and elevated plus maze paradigms. By contrast, no major defects in learning, motor or sensory function were observed.

The proteomic analysis (Chapter 3) revealed several novel neuronal LNX-interacting protein candidates that might contribute to the anxiolytic phenotype observed. Overall, these findings provide novel functional insights into the LNX protein family and identify promising candidates to mediate LNX functions in the central nervous system.

Lay Abstract

LNX1 and LNX2 proteins are found in the brain, where they are believed to be important. These proteins are not very well understood however, and little is known about how they work. Understanding how proteins function, and the biological processes they are involved in, is crucial for the development of targeted drug therapies to treat disease. Different approaches to ultimately provide insights into the functions of LNX1 and LNX2 are described herein. Investigation of LNX-interacting proteins identified several promising candidates for future study, by which – through interaction, LNX may function. Loss of LNX1 and LNX2 in mice lead to decreased anxiety-like behaviours. This finding provides a foundation for follow-up studies on LNX1 and LNX2 as potential novel drug targets in the treatment of anxiety and anxiety-related disorders, for which there is a real need.

List of Abbreviations

AP - affinity purification

BCR - breakpoint cluster region

BOZ - Bozozok

CAR - coxsackievirus and adenovirus receptor

CASPR4 - contactin-associated protein-4

CAZ - cytomatrix at the active zone

CMA – chaperone mediated autophagy

CNS - Central Nervous System

Co-IP - co-immunoprecipitation

COS - C-terminal subgroup one signature

CP - core particle

CRC - colorectal cancer

DHET - $Lnx1^{exon3+/-}$;$Lnx2^{+/-}$ double heterozygous knockout

DKO - $Lnx1^{exon3-/-}$;$Lnx2^{-/-}$ double knockout

DMSO - dimethyl sulphoxide

DUB - deubiquitinating enzyme

E6 - early protein 6

E6-AP - E6 - associated protein

EDTA - ethylenediamine tetra-acetic acid

EMT - epithelial to mesenchyme transition

EPM - elevated plus maze

ERC - ELKS/Rab6-interacting/CAST

FBS - foetal bovine serum

FN3 - fibronectin type III

FST - forced swim test

GAP - GTPase activating protein

GFP - green fluorescent protein

GST - glutathione-S-transferase

GWAS - genome-wide association study

HECT - homologous to E6-AP carboxy-terminus

HEK - human embryonic kidney cells

IP - immunoprecipitation

IPTG - isopropyl-β-D-thiogalactopyranoside

JAM - junctional adhesion molecule

JNK - c-Jun N-terminal kinase

KD - Kawasaki disease

LIR – LC3 interacting protein

LD - light-dark box

LNX - Ligand of numb protein X

M-CSF - macrophage colony stimulating factor

MDCK - Madin-Darby Canine Kidney cells

MS - mass spectrometry

MUPP1 - multiple PDZ domain containing protein-1

NEM - N-ethylmaleimide

NF-κB - nuclear factor kappa B

NMJ - neuromuscular junction

NPC - neural precursor cell

OF - open field

PBK - PDZ binding kinase

PBS - phosphate buffer saline

PCR - polymerase chain reaction

PDB - Protein Data Bank

PDZ - PSD-95, DlgA, ZO-1

PDZRN - PDZ and RING

PFA - paraformaldehyde

PFF - peptide fragment fingerprinting

PM - plasma membrane

PNS - peripheral nervous system

PSC - perisynaptic Schwann cells

PTB - phosphotyrosine binding domain

RANKL - receptor activator of nuclear factor kappa B ligand

RGL - radial glial cells

RHOGEF - RHO guanine nucleotide exchange factor

RING - Really Interesting New Gene

RLDs - RCC1-Like Domains

RP - regulatory particle

SDS - sodium dodecyl sulfate

SHC - Src homology 2 domain-containing

SKIP - Ski interacting protein

SNP - single nucleotide polymorphism

SVZ - subventricular zone

TGF-β - transforming growth factor β

TJ - tight junction

TRIM - tripartite motif

Ub - ubiquitin

UBC - ubiquitin-conjugating

uORF - upstream open reading frame

UTR - untranslated region

WB - Western blot

WT - wild-type

ZnF - zinc finger motif

Chapter 1: General Introduction

1.1 Protein ubiquitination: mechanisms and consequences

Protein ubiquitination is a post-translational modification of proteins that is of great importance in cells. It is a multistep process involving the sequential action of three categories of enzymes termed E1s, E2s and E3s [1] (see Figure 1.1). In this section the ubiquitination cascade and the consequences of protein ubiquitination are described.

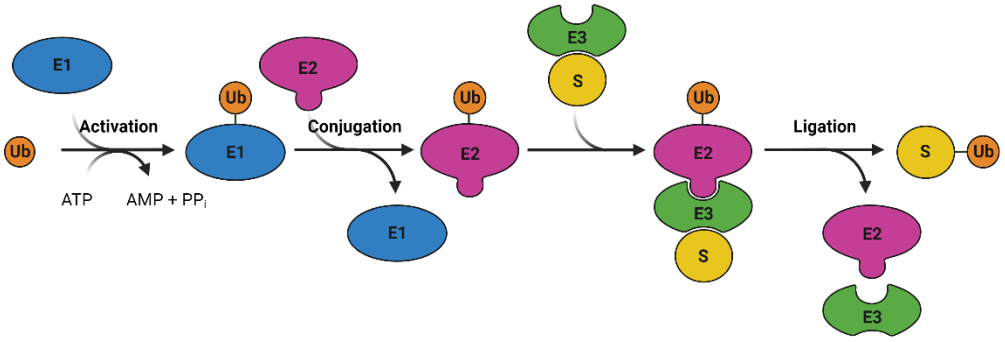

Figure 1.1: Schematic representation of the ubiquitin pathway. The ubiquitin pathway relies on sequential action of three categories of enzymes: ubiquitin-activating enzymes (E1s), ubiquitin-conjugating enzymes (E2s), and ubiquitin-ligating enzymes (E3s), which conjugate ubiquitin to target proteins. First, ubiquitin is activated by an E1 enzyme in an ATP-dependent manner, resulting in its attachment to a cysteine residue in the active site of the E1 enzyme. The ubiquitin is then transferred to the active cysteine in E2 enzyme. Finally, upon association with an E3 enzyme, ubiquitin is conjugated to its target substrate.

1.1.1 E1 ubiquitin-activating enzymes

The ubiquitination process begins with activation of ubiquitin by an E1 ubiquitin-activating enzyme. Two E1 enzymes, UBA1 and UBA6, are known to initiate ubiquitin conjugation in humans [2].

1.1.2 E2 ubiquitin-conjugating enzymes.

Ubiquitin molecules activated by the E1 enzyme are accepted by E2 or ubiquitin-conjugating enzymes, which form another thiol-ester bond with G76 of ubiquitin [1]. About forty E2

enzymes are encoded by the human genome [3]. E2 enzymes are distinguished by the presence of a catalytic ubiquitin-binding cysteine residue and a 140-200 amino acid ubiquitin-conjugating (UBC) domain required for binding of specific E3s [4].

1.1.3 E3 ubiquitin ligases

E3 ubiquitin ligases accept ubiquitin molecules from E2 enzymes and catalyze their addition to specific target substrates. Some E3s accept ubiquitin in a thioester linkage from E2s prior to ligation of ubiquitin to the substrate, while others bring the E2s and the substrates together and facilitate the direct transfer of ubiquitin to substrates. Typically, ubiquitin forms an isopeptide bond with the ε-amino group on substrate lysine residues, but ubiquitin ligation to the N-terminal α-amino group, or to serine, threonine or cysteine substrate residues on substrate proteins has also been described – forming peptide, ester or thioester linkages, respectively [4]. Since the target substrate binds to the E3 ligase, either directly or indirectly, via ancillary proteins, prior to conjugation, the substrate specificity of ubiquitin system is essentially determined by E3s. Two major classes of E3 enzymes exist, distinguished by conserved homologous to E6-AP carboxyl terminus (HECT) or really interesting new gene (RING) domains.

1.1.3.1 HECT family E3 ligases

Discovery of the HECT domain ubiquitin ligases ensued from studies on tumours arising from human papilloma virus (HPV) infection. Early protein 6 (E6) is a viral protein encoded by oncogenic strains of HPV. Following infection, E6 associates with a host cell ubiquitin ligase called E6-associated protein (E6-AP), causing degradation of the p53 tumour repressor [5]. Sequence alignment identified a family of protein ubiquitin ligases with homology to the 350

amino acid, carboxy-terminal, catalytic domain of E6-AP [6]. These ubiquitin ligases came to be called homologous to E6-AP carboxy-terminus (HECT) domain E3s, and were the first family of E3s described.

The HECT E3s are unique among the E3s in that they possess intrinsic catalytic activity. HECT domain E3s form an E3-ubiquitin thioester intermediate between an active site cysteine – located at the carboxy-terminus of the HECT domain, and the ubiquitin carboxy-terminus, following binding of an ubiquitin charged E2 [7]. The formation of a thioester intermediate with ubiquitin is unique to HECT domain E3s and is not observed with other types of E3 ligases. The HECT domain then directly catalyzes the formation of an isopeptide bond between the ε-amino group of the substrate lysine side chains and the ubiquitin carboxy terminus [7]. Thus, unlike the RING-finger E3s – which, although able to promote the formation of ubiquitin chains, lack a catalytic site, the HECT E3s directly catalyze substrate ubiquitylation.

The HECT domain adopts a bilobular structure [8]. The larger amino-terminal lobe of the HECT domain contains the E2 binding site, whereas the smaller carboxy-terminal lobe contains the conserved catalytic cysteine residue – which serves as the site of ubiquitin thioester formation [7]. These two lobes are linked by a flexible hinge region which is crucial for juxtaposing the catalytic cysteine residues of the E2 and E3 during ubiquitin transfer [7, 9]. A conformational change altering the relative orientation of the two lobes is thought to facilitate the transfer of ubiquitin.

Whereas the HECT domain represents the catalytic domain, the substrate specificity of HECT E3s is determined by their individual amino-terminal extensions. Human HECT domain E3s can be further grouped into three subfamilies based on the presence of distinct amino acid sequence motifs or domains within these amino-terminal extensions: the Nedd4 family – which contain WW (tryptophan-tryptophan) domains, the HERC family – harbouring RLDs (RCC1-Like Domains), and "other" HECTs – that contain neither RLDs nor WW domains [7].

1.1.3.2 RING-type E3 ligases

RING (Really Interesting New Gene)-type E3s are the second and largest class of E3 ubiquitin ligases, comprising over 600 genes [10]. True to their name, RING-finger E3s are characterised by a RING-finger domain. RING-finger-domains are a specialised type of zinc-finger containing seven conserved cysteine and one histidine residue arranged non-consecutively, that coordinate a pair of zinc ions in a cross-braced arrangement [11]. Unlike the HECT domain E3s, RING-finger E3s do not form a thioester intermediate with ubiquitin. Rather, RING-finger E3s directly transfer ubiquitin from E2 to substrate [7].

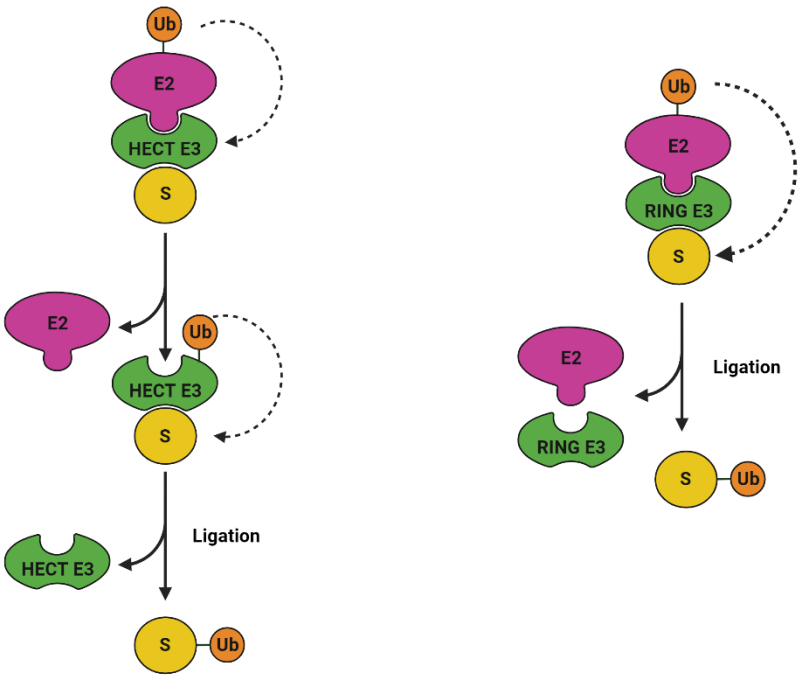

Figure 1.2: Schematic representation of the RING and HECT domain classes of E3 ubiquitin ligases and their mechanisms of action. RING E3 ubiquitin ligases (on right) facilitate the direct transfer of ubiquitin from the E2 to the target protein. HECT E3 ubiquitin ligases (on left) require an additional step for ubiquitin transfer, where ubiquitin is first transferred to a cysteine residue in the active site of the HECT domain and is then transferred to the target protein.

1.1.4 Consequences of protein ubiquitination

Attachment of ubiquitin to a protein can have diverse consequences. These can include regulating the function of the protein in some way or alternatively, targeting the protein for degradation. Degradative pathways are most relevant to the work described in this thesis and the two major degradation pathways associated with ubiquitination are outlined below.

1.1.4.1 Proteasomal degradation of ubiquitinated proteins

The 26S proteasome is composed of a core particle (CP) and a regulatory particle (RP) [12]. The 20S CP's cylindrical and hollow shape results from the compact stacking of four seven-subunit rings – two central β-subunit rings flanked on either side by an α-subunit ring. The proteolytic active sites reside in the interior of the 20S CP – specifically on β subunits 1, 2 and 5, providing caspase-like, trypsin-like and chymotrypsin-like cleavage activity respectively [13] – thereby shielding cellular proteins from non-specific proteolytic cleavage. Access to these proteolytic active sites can only be gained through a narrow aperture at either end of the CP, entry to which is gated by the N-termini of the α subunits and controlled by the 19S RP [14].

The 19S regulatory particle assembles onto one or both ends of the 20S CP and is composed of two sub-complexes, the "base" and the "lid" [15]. The base consists of six AAA-ATPases, Rpt1-Rpt6, arranged in a ring formation, and four non-ATPases –Rpn1, Rpn2, Rpn10 and Rpn13. The ATPase C-termini intercalate into pockets that exist between adjacent α subunits of the CP, tethering the 19S RP to the 20S CP. Rpn10 and Rpn13 subunits act as ubiquitin receptors, recognise and bind to poly-ubiquitin tags on proteins destined for proteasomal

degradation [15]. At just 13 A in diameter [16], substrates require unfolding prior to entering the translocation pore – a ATP-dependent process carried out by Rtp1-6 [17].

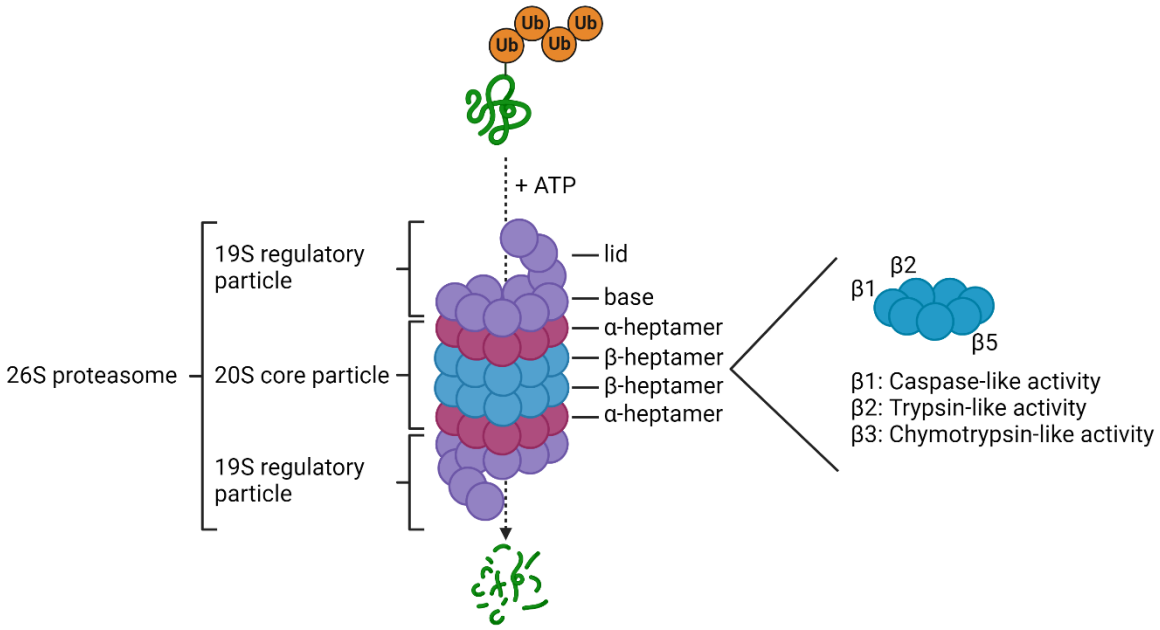

Figure 1.3: Schematic representation of the 26S proteasome. The 26S proteasome is composed of two 19S regulatory particles, composed of "lid" and "base" subunits, and a 20S core particle, composed of two inner β subunit rings flanked either side by an α subunit ring. The proteolytic active sites reside on β subunits, illustrated in the diagram.

1.1.4.2 Lysosomal degradation of ubiquitinated proteins

Lysosomes mediate autophagy-lysosomal degradation. The autophagy-lysosomal pathway can be subdivided into three distinct pathways: macroautophagy microautophagy and chaperone-mediated autophagy (CMA) – depending on the way in which substrates reach the lysosomal lumen [18]. Macroautophagy - generally referred to as autophagy, is a multi-step process, involving the formation of a double-membraned structure known as autophagosomes around cytoplasmic proteins and organelles, for eventual fusion with the lysosome, and degradation of the sequestered cargo by acidic-hydrolases of the lysosome [18]. Autophagy adaptor proteins p62 and NBR1 (neighbor of BRCA1 gene 1) provide a molecular link between ubiquitination

and autophagy-lysosomal degradation – a ubiquitin-associated domain (UBA) binds ubiquitin on mono and polyubiquitinated proteins, and a short LC3 interacting region (LIR) binds to the autophagy-specific ubiquitin-like modifier LC3, linking ubiquitinated cargoes to the autophagosomes for degradation [19, 20]. Microautophagy, by contrast, does not require the formation of an autophagosome. Rather, proteins are directly engulfed by invagination or protrusion of the lysosomal membrane [20]. As for CMA, the chaperone protein HSP70 recognises the KFERQ motif – a motif exposed in proteins damaged by oxidative stress, and transports them to the lysosome [20].

1.2 The LNX1/2 family of proteins

Ligand of Numb Protein-X1 (LNX1) and LNX2 comprise a protein family with a domain structure containing an amino-terminal RING finger domain – classifying it as a RING-type E3 ligase, and four carboxyl-terminal PDZ (PSD-95, DlgA, ZO-1) domains. LNX1 and LNX2 are the focus of this thesis. This section provides a brief review of the literature about these intriguing proteins.

1.2.1 Evolution of LNX1/2 proteins

The poriferan or sponge *Amphimedon queenslandica* has a clear LNX1/2 ortholog – thus, the ancestral LNX1/2-like gene is said to have evolved in the basalmost metazoan lineage, prior to the divergence of porifera from other metazoans [21]. The authors report subsequent loss of this gene from several invertebrate lineages. For example, a LNX1/2 ortholog was identified in cephalochordate and platyhelminth lineages, but not in urochordates, arthropods, nematodes or molluscs. Thus, whatever the ancestral function of LNX1/2, it appears that this function is not essential in invertebrates, since many invertebrate lineages lack a LNX1/2-like protein [22]. Duplication of the ancestral LNX1/2-like gene in vertebrates gave rise to the paralogous LNX1, LNX2 and LNX2b genes [21]. These three genes appear to be conserved in virtually all vertebrate lineages, except for Eutherian mammals. Gene loss of LNX2b occurred in Eutherians when it underwent pseudogenization and contributed several exons to the non-coding Xist RNA – the master regulator of the X chromosome inactivation process in Eutherian mammals [23].

Conservation of at least two LNX1/2 like genes in all vertebrate lineages proposes evolutionary acquirement of essential vertebrate-specific functions [22]. Interestingly, vertebrate LNX1/LNX2 proteins contain a Numb binding motif, NPAY and NPAF respectively – that is absent in non-vertebrate LNX1/2 orthologs [21], and can interact with and regulate Numb [24-28]. This may be an essential vertebrate specific function, explaining the presence of LNX1/2 orthologs in all vertebrates [22]. The *A. queenslandica* LNX1/2 ortholog has an identical domain architecture to vertebrate LNX1, -2 and -2b proteins except for the absence of the Numb NPAY/F binding motif [21]. The ancestral LNX1/2 protein is thus likely to have evolved in very primitive metazoans to perform a cellular function independent of an interaction with Numb [22]. It is possible that vertebrate LNX1/2 proteins retained some of these ancestral functions. Thus, despite their name LNX1/2 proteins are likely to have significant functions unrelated to their interaction with Numb and subsequent regulation of Notch.

1.2.2 Structure of LNX1/2 proteins

Vertebrate LNX1, -2 and -2b share an identical protein domain architecture consisting of an amino-terminal RING domain, flanked on either side by a zinc-finger motif, a Numb PTB domain binding motif (NPAY/F), four PDZ domains and carboxy-terminal consensus PDZ domain binding motif [22, 24, 25, 27, 29] (see Figure 1.4)

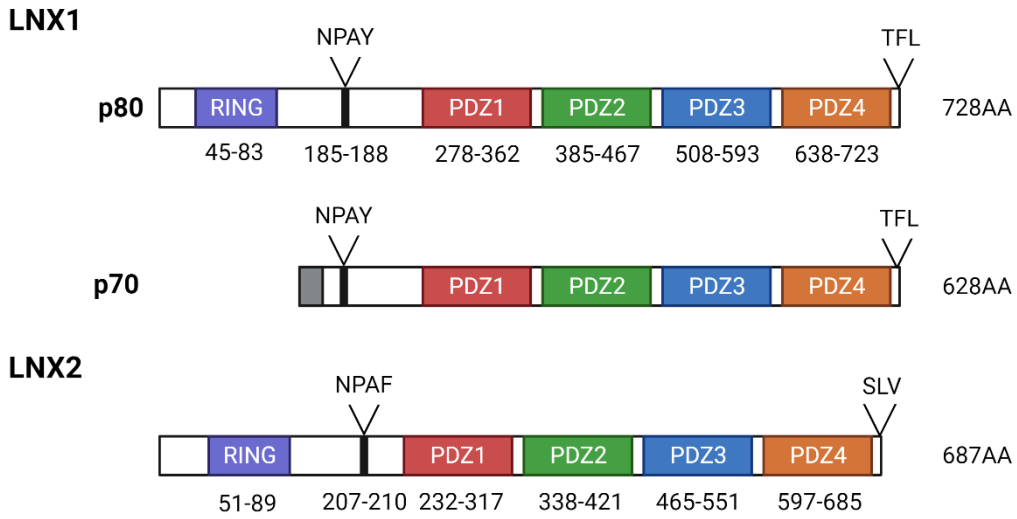

Figure 1.4: Domain structures of LNX1 and LNX2 proteins. Two domain structures are shown for LNX1, representing both p80 and p70 isoforms. LNX1p80 and LNX2 have identical domain structures, containing a RING domain, NPAY and NPAF motifs respectively, and four PDZ domains. LNX1p70 lacks the catalytic RING domain and is expressed exclusively in the brain and spinal cord. LNX1 and LNX2 PDZ binding motifs and are also indicated.

1.2.3 LNX2 and LNX2b functions in Zebrafish

The major model organism in which the *in vivo* functions of LNX1/2 proteins have been studied is the zebrafish. Morpholino antisense oligonucleotide-mediated knockdown of *lnx2b* in zebrafish resulted in embryonic defects characteristic of dorsalization – a phenomenon they confirmed by analysis of several dorso-ventral markers [30]. In this study, Boz was identified as a binding partner of LNX2b. Boz, a homeodomain-containing transcriptional repressor protein, favours dorsal organiser formation, by suppressing the expression of ventralizing genes. Boz was found to be a substrate for LNX2b-mediated, K-48 linked, polyubiquitination, targeting it for degradation by the proteasome [30]. Thus, LNX2b negatively regulates Boz. Overexpression of LNX2b resulted in embryonic defects reminiscent of Boz loss-of-function mutant phenotype, including anterior notochord and forebrain malformations [30]. Furthermore, LNX2b reversed the dorsalized phenotype resulting from Boz overexpression. Simultaneous overexpression of Boz and depletion of LNX2b saw expansion of ectopic

goosecoid (*gsc*) expression into the presumptive ectoderm [31]. Thus, maternally derived Lnx2b represses *gsc* expression in the presumptive ectoderm by negatively regulating Boz stability, presumably through proteasomal mediated degradation. LNX2b modulation of Boz restricts dorsal organiser specification to a defined region of the early zebrafish embryo and thus functions in dorso-ventral patterning.

Ro and Dawid [32] describe a further, distinct role of LNX2b in zebrafish embryogenesis – specifically as a regulator of caudal-type homeobox (*cdx*) transcription factor 4 expression. Cdx transcription factors, including Cdx4, are targets of Wnt signalling, and play roles critical for normal caudal body development in the embryo. In the absence of Wnt, transcription factor 3 (Tcf3), in conjunction with corepressor proteins, represses *cdx4* expression, through direct binding to the regulatory region of c*dx4* [32]. Upon Wnt signalling activation however, the transcriptional regulator E4f1 derepresses *cdx4* expression, by dissociating corepressor molecules from Tcf3. LNX2b was found to interact with E4f1, but was found to stabilise the Tcf3 transcriptional repressor complex and thus counteracts E4f1-dependent expression of *cdx4*. Furthermore, LNX2b was found to antagonize E4f1 independent of its E3 ubiquitin ligase activity. Thus, it appears that LNX2b interaction alone with E4f1 is sufficient for modulation of the Tcf3 transcriptional repressor complex, however interaction with other components of the complex may be important for this.

The most recent study on the *in vivo* function of Lnx2 and Lnx2b in zebrafish development describes a role of Lnx2 – referred to as Lnx2a – and Lnx2b in pancreatic exocrine cell differentiation [28]. In this study, Lnx2 and Lnx2b were found to function in a redundant manner in the zebrafish pancreas – loss of expression of either paralog alone produced no

phenotype. However, a reduction in the expression of the early exocrine cell specific marker, *ptfa1* – required for differentiation of these cells – and another exocrine cell marker, *trypsin*, was noted in embryos where both *lnx2a* and *lnx2b* expression was supressed. Embryos expressing a negative interfering form of Lnx2 displayed the same pancreas deficient phenotype. Conversely, the expression of endocrine specific cell markers was unchanged in these embryos. The phenotype observed correlates with the differential expression of *lnx2* in the ventral, but not the dorsal pancreatic bud; the ventral pancreatic bud is primarily composed of exocrine cell types, whereas cells of the dorsal pancreatic bud are exclusively endocrinal. The authors attributed the increase in Numb and concomitant decrease in Notch signalling in the ventral pancreas to the morphant embryo phenotype. Indeed, reduction of Numb substantially rescued the Lnx2/2b deficient phenotype. LNX2 was shown to ubiquitinate and thus target Numb – an inhibitor of Notch signalling – for degradation. The authors propose Lnx2/2b destabilisation of Numb enables Notch signalling in the ventral bud cell types – required for both the specification and proliferation of exocrine precursor cell population.

1.2.4 LNX1/2 mRNA expression in mammals

Dho et al. [24] noted expression of *Lnx1* in most adult mouse tissues examined, including the heart, brain, lung, skeletal muscle and kidney, but not in the spleen, liver and testis. Human *LNX1* is also expressed in the adult heart, brain and kidney – in addition to the placenta and pancreas [33]. Expression of human *LNX1*was not however, obvious in the adult lung, liver or skeletal muscle, and expression in the testis was not examined. Interestingly, different message sizes, representing alternatively spliced variants of *Lnx1/LNX1* were observed by Northern blot in both these studies. A larger, 2.8 kb message, predicted to encode the 80kDa protein isoform (LNX1p80), was apparent in all tissues expressing *Lnx1/LNX1* except the brain and spinal cord.

In the brain and spinal cord, a smaller, 2.6 kb message was found – predicted to encode the N-terminally truncated 70 kDa protein (LNX1p70), that lacks the ZnF-RING-ZnF domain. Therefore, *Lnx1/LNX1* is expressed in many adult tissue, the splice variants of *Lnx1/LNX1* are differentially expressed, and only the p70 variant is expressed in the brain and spinal cord.

Lnx2 was detected in all adult mouse tissues examined by Northern blot, including the brain, skeletal muscle, liver, spleen, lung, heart, kidney and thymus [25]. Thus, like *Lnx1*, *Lnx2* is expressed in a wide variety of tissues. A single *Lnx2* message, of uniform size, was apparent in all tissues examined except for the lung, where an additional, smaller band was noted.

The expression patterns of *Lnx1* and *Lnx2* in the developing embryo, postnatal, and adult mouse brains were examined by *in situ* hybridisation [25]. The earliest expression of *Lnx*, specifically *Lnx2*, was observed at embryonic day 11.5 (E11.5), in neuroepithelial cells of the developing forebrain. Notably, *Lnx1* was not expressed at detectable levels here at this age. At E14.5, *Lnx2* was expressed in several tissues throughout the developing embryo, with highest levels of expression apparent in the forebrain. Though *Lnx1* expression was obvious at this age, expression was confined to the spinal cord and other brain regions. Expression of *Lnx1* and *Lnx2* persists postnatally and into adulthood [25]. *Lnx1* is expressed throughout the postnatal and adult brain, except for the cerebellum, where *Lnx1* expression is minimal. *Lnx2* is highly expressed in the cerebellum, in addition to the hippocampus, cortex and olfactory bulb. The expression of *Lnx* genes thus overlap in some brain regions and differ in others.

Several studies have documented differential *Lnx1* expression in certain situations, providing clues on the function of LNX1 [22]. *Lnx1* is highly expressed in the pineal gland relative to other tissues [34, 35]. Transcriptome-wide analysis reported in these studies identified differential *Lnx1* expression in the pineal gland in response to the light:dark cycle, where *Lnx1* was up-regulated during the dark phase [34, 35]. While this is suggestive of a possible role of LNX1 in the pineal gland, a comprehensive study examining this has yet to be reported. Furthermore, high relative *Lnx1* expression has been reported in diverse stem and progenitor cell populations including oligodendrocyte precursor cells [36], limbal side-population stem cells of the eye [37] and quiescent skeletal muscle satellite cells [38]. These observations provide clues on the function of LNX1. LNX1 protein levels were not assessed in these studies however – therefore the functional significance of these observations is unclear.

1.2.5 LNX1/2 protein expression in mammals

Western blot detection of endogenous LNX1/2 proteins generally requires prior immunoprecipitation from tissue lysates [28, 39-41] with few exceptions. Wang et al. [42] did detect LNX2 directly in embryonic (day 18.5) E18.5 mouse brain lysate by Western blot – specifically forebrain lysate [42]. Furthermore, LNX2 was detected directly in colorectal cancer cell line lysates by Western blot [43], but has not been widely reported in other cell lines. Thus – despite widespread mRNA expression, LNX1 and LNX2 proteins are expressed at very low levels *in vivo* [22]. Few reports describe the expression patterns of endogenous LNX1 and LNX2 proteins. Immunohistochemistry staining detected endogenous LNX1 in perisynaptic Schwann cells at neuromuscular junctions of mice, from embryonic day 16/E16, through adulthood (P42) – reaching peak levels around postnatal day 14-21 [44], while IHC on E16.5 mouse embryo detected endogenous LNX2 widely in most organs [39].

Immunocytochemistry revealed endogenous expression of both LNX1 and LNX2 in mouse spermatozoa, albeit in distinct subcellular compartments – LNX2 localized to the acrosome, while LNX1 appeared to localize to the acroplaxome [45].

1.2.6 Interactions of LNX1 and LNX2 with Numb and Numb-like

1.2.6.1 LNX1 and LNX2 as ligands of Numb

LNX1 was originally discovered in a yeast two-hybrid screen, designed to identify murine Numb PTB interacting proteins [24]. The Numb PTB domain binding site mapped to the NPAY sequence motif of LNX1 – in agreement with the binding specificity described for other PTB domain interactions. Replacement of the NPAY tyrosine with phenylalanine had no effect on Numb PTB binding [24], thus – like the majority of other PTB domains, phosphorylation of the NPAY tyrosine is not required for Numb PTB binding. LNX1 can also interact with the PTB domain of Numb-like, a closely related paralogue of Numb [24]. LNX2 shares the ability to interact with Numb and Numb-like, via it's NPAF sequence motif [25]. The absence of a tyrosine residue in the LNX2 NPAF PTB binding motif supports the notion that LNX1/2 interactions with Numb and Numb-like are phosphorylation independent [22]. Interestingly, the interaction of the Numb PTB domain binding to the NPAY/F motifs seems to be exclusive to LNX1/2 – NPXY containing peptides from EGFR or TRKA failed to interact with the Numb PTB domain [24]. Furthermore, binding of other PTB domain containing proteins to the NPAY/F motifs of LNX1/2 have not been reported, with one exception: a LNX1 peptide was found to interact with the PTB domain of SHC [24], however phosphorylation of the tyrosine residue within the NPAY PTB domain binding motif was necessary for binding. Phosphorylation of LNX1 has yet to be reported *in vivo* thus the physiological relevance of the SHC-LNX1 interaction is unclear [22]. LNX1 was subsequently discovered to function as a

RING-type E3 ubiquitin ligase, and Numb was identified as a substrate for LNX1-mediated ubiquitination [26]. LNX2 ubiquitination of human and zebrafish Numb has also been documented [27, 28]. Both LNX1- and LNX2-mediated ubiquitination targets Numb to the proteasome for degradation. [26, 28]. Four major mammalian Numb protein isoforms have been described: p65, p66, p71 and p72 [46]. LNX1 can interact with all four Numb isoforms, however, LNX1-mediated ubiquitination of Numb is isoform-specific, and only the p66 and p72 isoforms are ubiquitinated by LNX1 [46]. Numb p66 and p72 differ from the other two isoforms by the presence of an 11 amino acid insert in their PTB domain, and so are termed PTBi domain variants. Numb PTB domain binding to both the canonical PTB domain binding motif NPAY and first PDZ domain of LNX1 if required for effective recognition of Numb as a substrate for LNX1-mediated ubiquitination [46]. Interaction with either site alone is not sufficient for LNX1 ubiquitination of Numb. Only the Numb PTBi domain variant interacts with the first PDZ domain of LNX1, thus only PTBi domain containing Numb isoforms, p66 and p72, are substrates for LNX1 ubiquitination.

1.2.6.2 LNX1/2 as regulators of Notch signalling via Numb

Numb interacts with the Notch receptor and antagonises Notch signalling. The mechanism by which Numb antagonises Notch remains elusive and is the subject of controversy. Numb may negatively regulate Notch by promoting endocytosis of the Notch receptor from the plasma membrane into endosomes or, alternatively, by altering Notch receptor trafficking through the endocytic pathway post-endocytosis [47]. LNX1/2 ubiquitinates Numb, targeting it for proteasomal degradation [24-26, 28]. Considering Numb's ability to negatively regulate Notch signalling, one would expect LNX-mediated proteolytic degradation of Numb to promote Notch signalling [22]. Indeed, LNX1 expression and the consequent ubiquitination and

decrease in Numb protein levels led to a ~30% increase in Notch signalling, as measured by a *Hes1* promoter-driven luciferase reporter assay [26].

Evidence in support of alteration in LNX1/2 expression affecting Notch signalling includes the following: (i) zebrafish embryos expressing a dominant negative form of LNX2 showed an increase in the number of Numb-positive cells and a decrease in the number of Notch-active cells in the pancreas as assessed using a transgenic mouse line in which a Notch-responsive element drives expression of a fluorescent protein reporter [28] and (ii) knockdown of LNX2 in bone marrow-derived macrophages led to an increase in Numb protein levels, a decrease in the level of NOTCH2 and a reduction in the expression of the NOTCH2 target gene *Hes1* [48]. Others report no change in Notch signalling despite alterations in LNX1/2 expression. Gli3 knockout mice for example, exhibit increased LNX2 expression and a decrease in Numb protein levels [42]. Reduced expression of Numb in these mice, however, did not alter levels of Notch activity. Furthermore, knockdown of LNX2 in a pancreatic cancer cell line had no impact on Notch signalling [49].

1.2.7 Role of LNX1/2 proteins in neurogenesis and neuronal differentiation

Wang et al. [42] describe a possible role of LNX2 in neurogenesis in mice – namely in the subventricular zone (SVZ). NSCs and ependymal cells of the SVZ originate from a common developmental origin, radial glial cells (RGCs). The authors noted defects in the glial cell specification and abnormal cryoarchitecture in the SVZ of Gli3-/- mice and partially attribute these defects to a reduction in the levels of Numb in these mice [42]. Increased levels of LNX2 were also noted in these mice, particularly in the SVZ. The authors thus propose that this overexpression ultimately targets NUMB for degradation in these mice.

Yin et al. [50] propose the interaction of contactin-associated protein 4 (Caspr4) and LNX2 to play a role in neuronal differentiation. Caspr4 – a transmembrane protein and member of the neurexin superfamily – is expressed in neural progenitor cells (NPCs) in the subventricular zone (SVZ) region of the developing cortex. The intracellular cytoplasmic domain of Caspr4 interacts with LNX2 in a PDZ-dependent manner [50]. Moreover, Caspr4 and LNX2 are co-expressed by NPCs in the SVZ. LNX2 and Caspr4 inhibit proliferation and promote neuronal differentiation of NPCs *in vitro*. LNX2 rescued the decreased neuronal differentiation in Caspr4 knockdown NPCs and hence is proposed to act downstream of Caspr4 in promoting neuronal differentiation.

1.2.8 Other interactions of LNX1/2 proteins

Many other interactions of LNX proteins have been described. Some of the better characterised interactions are summarised in Figure 1.5 and Table 1.1, and discussed below (in alphabetical order).

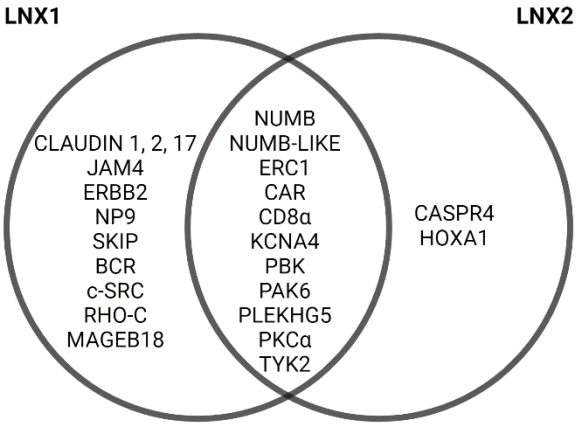

Figure 1.5: Schematic representation of known LNX1 and LNX2 interacting proteins. Venn diagram illustrating LNX1 and LNX2 specific interacting proteins, and interactions common to both. Only protein interactions that have been confirmed in mammalian cells, and using full-length proteins are shown.

Table 1.1: Known interactions of LNX1/2 proteins (prior to undertaking this study). Data in this table was extracted from [22].
Only interactions that have been verified using full-length proteins expressed in mammalian cells are listed. For interacting proteins that are LNX1/2 substrates the consequence of ubiquitination is stated (if known). Abbreviations: Y2H = yeast two-hybrid; GFP-PD or GST-PD = "pull down" experiment using a green fluorescent protein or glutathione-S-transferase tag respectively; Co-IP(h) or Co-IP(e) = co-immunoprecipitation of heterologously-expressed or endogenous proteins respectively. Co-L = co-localization in cells or tissues. n/d = not determined

Interacting protein	Description / Function	Binds to:	Domain(s) involved	Methods used	Substrate for ubiquitination	References
NUMB	Cell fate determinant	LNX1, LNX2	NPAY/F, PDZ1	Y2H, GST-PD, Co-IP(h)	Yes; proteasomal degradation	[24-27, 46]
NUMB-like	Cell fate determinant	LNX1, LNX2	NPAY/F motif	Y2H, GST-PD, Co-IP(h)	n/d	[24, 25]
CASPR4	Neurexin family protein	LNX2	PDZ2	Y2H, GST-PD, Co-IP(h), Co-L	n/d	[50]
CLAUDIN-1, 2, 4	Tight junction	LNX1	PDZ1, PDZ2	Y2H, GST-PD, Co-IP(h)	Yes; endocytosis	[51, 52]
JAM4	Tight junction	LNX1	PDZ2	Y2H, Co-IP(h), Co-local	n/d	[53]
CAR	Tight junction	LNX1, LNX2	PDZ2	Y2H, GST-PD, Co-IP(h)	n/d	[39, 45, 54]
ERC1	Presynaptic	LNX1, LNX2	PDZ2	Y2H, Co-IP(h), GFP-PD, Co-L	Yes	[55-57]
ERBB2	Receptor Tyr kinase	LNX1	PDZ1-4	Y2H, Co-IP (h,e)	n/d	[44]
CD8-α	T-cell co-receptor	LNX1, LNX2	PDZ1/2	Y2H, Co-IP(e), GST-PD, Co-L	Yes; lysosomal degradation	[41]
KCNA4	K^+ channel	LNX1, LNX2	PDZ1	Y2H, Co-IP(h)	n/d	[58, 59]
E4F1	Transcription factor	LNX1, LNX2	n/d	Co-IP(h), GST-PD	Yes; not degraded	[32]
NP9	Nuclear protein	LNX1	PDZ2-4	Y2H, GST-PD, Co-L	n/d	[60]
SKIP	Nuclear protein	LNX1	n/d	Y2H, Co-IP(h), Co-L	n/d	[61]
HOXA1	Transcription factor	LNX2	n/d	Y2H, Co-IP(h), BiFC	n/d	[62]
PBK	MAP kinase kinase	LNX1, LNX2	PDZ1 or PDZ1-4	Y2H, Co-IP(h)	Yes; proteasomal degradation	[51, 58, 59]

Table 1.1 (continued): Known interactions of LNX1/2 proteins

Abbreviations: Y2H = yeast two-hybrid; GFP-PD or GST-PD = "pull down" experiment using a green fluorescent protein or glutathione-S-transferase tag respectively; Co-IP(h) or Co-IP(e) = co-immunoprecipitation of heterologously-expressed or endogenous proteins respectively. Co-L = co-localization in cells or tissues. n/d = not determined

Interacting protein	Description / Function	Binds to:	Domain(s) involved	Methods used	Substrate for ubiquitination	References
BCR	GTPase activating protein	LNX1	PDZ3	Y2H	Yes, proteasomal degradation	[51]
c-SRC	Tyr kinase	LNX1	PDZ3, PDZ1	PDZ array, Co-IP(h,e), Co-L	Yes, proteasomal degradation	[40]
RHO-C	GTPase	LNX1	PDZ1	Y2H, Co-IP(h), Co-L	n/d	[63]
PAK6	Ser/Thr kinase	LNX, LNX2	PDZ2,4	Y2H, Co-IP(h)	n/d	[58, 59]
PLEKHG5	RhoGEF protein	LNX1, LNX2	PDZ1,3	ProtoArray, Co-IP(h)	n/d	[59]
PKCα	Ser/Thr kinase	LNX1, LNX2	PDZ2,4	Peptide Array, Co-IP(h)	n/d	[59, 64]
TYK2	Non-receptor Tyr kinase	LNX1, LNX2	PDZ2	Y2H, Co-IP(h)	n/d	[58, 59]
MAGEB18	Tumor antigen	LNX1	-	TAP, Co-IP(h)	n/d	[65]

1.2.8.1 BCR

The carboxy-terminus of breakpoint cluster region (BCR) protein was found to interact with the third PDZ domain of LNX1 [51]. BCR is a GTPase activating protein (GAP) for Rho family GTPases CDC42 and RAC1. Expression of LNX1 promoted ubiquitination of endogenous BCR, resulting in decreased levels of BCR, and treatment with an inhibitor of proteasomal degradation reversed this decrease [51]. Thus, LNX1-mediated ubiquitination enhanced proteasome-dependent degradation of BCR. Several other intracellular signalling proteins have been identified as LNX1 interacting proteins including the non-receptor tyrosine kinase TYK2, serine/threonine kinases PAK6 and PKCα, and the RHOGEF (RHO guanine nucleotide exchange factor) PLEKHG5 [59]. Furthermore, MAGE-B18 – a tumour associated antigen – was found to interact with LNX1, between its RING and first PDZ domain in this study. No further information on these interactions or their functional relevance is available, however.

1.2.8.2 CD8

The interaction of LNX1/2 with CD8α has been described [41]. Specifically, the carboxy-terminal residues of CD8α were found to interact with the PDZ domain region of both LNX1 and LNX2 [41]. Furthermore, *LNX1* and *LNX2* were both found to be expressed in human blood purified T-cells – a cell type known to express CD8α – and endogenous CD8α and LNX1/2 co-immunoprecipitated from human HPB-ALL T-cells. LNX1 showed cytosolic and nuclear localization when expressed alone, and LNX2 was exclusive to the cytosol, but relocated to the plasma membrane (PM) upon co-expression with CD8α. Both LNX1 and LNX2 induced CD8α ubiquitination, and overexpression of either LNX1 or LNX2 induced downregulation of exogenously expressed CD8α from the PM. LNX1/2 and CD8α staining, concomitant with CD8α reduction from the PM, overlapped with markers of the early

endosome and lysosome. Reduction in the levels of CD8α observed upon co-expression with either LNX1 or LNX2 was partially reversed by treatment with the lysosome inhibitor chloroquine. Thus, LNX1/2-mediated ubiquitination of CD8α triggers its internalisation from the PM and targets it for lysosomal degradation.

1.2.8.3 Claudins

LNX1 was identified as a Claudin-1 binding protein in a yeast two-hybrid screen [52]. The cytoplasmic domain of claudin-1, specifically the carboxy-terminal PDZ binding motif, interacts with LNX1 PDZ domain(s) [52]. Overexpression of LNX1 in the MDCK epithelial cell line resulted in a dramatic and specific reduction in the concentration of claudins -1, -2 and -4 at tight junctions (TJs). Overexpression of LNX1 also led to defects in TJ morphology and remarkably impaired barrier function. LNX1 was found to promote polyubiquitination of claudin-1, -2 and -4. These polyubiquitination chains were found to link through a ubiquitin lysine (K) residue(s) other than K48 – K48 linked polyubiquitin chains are associated with proteasomal degradation of the substrate. Thus, LNX1-mediated claudin-1 ubiquitination does not target claudin-1 for degradation by the proteasome. The level of LNX1-mediated polyubiquitinated claudin-1 increased following treatment with the lysosome inhibitor chloroquine. Furthermore, LNX1 and claudin-2 partially colocalized in vesicular structures and their signals often overlapped with the late endosomal marker Rab7 and the lysosomal protein cathepsin D. Thus, it appears LNX1 ubiquitination triggers selective endocytosis of claudins from TJs, and targets claudins to lysosomes for degradation. While it seems LNX1 has the potential to regulate claudins at TJs, one must bear in mind that these data were largely obtained as a result of LNX1 overexpression. It is not yet known if LNX1/2 are capable of regulating claudins at TJs when expressed at physiological levels [22].

1.2.8.4 ErbB2

ErbB2 was found to interact with the PDZ domain region of LNX1 [44]. This interaction was said to be mediated by internal PDZ binding motifs, in addition to the C-terminal motif on the cytoplasmic domain of ErbB2. Co-immunoprecipitation from mouse brain lysate confirmed LNX1/ErbB2 interaction *in vivo*. LNX1 expression in the peripheral nervous system (PNS) was exclusive to perisynaptic Schwann cells (PSCs) at the neuromuscular synapses and no LNX1 expression was observed in myelinating Schwann cells along motor axons. Axon-derived, neuregulin-1-mediated ErbB2 signalling elicits differentiation of myelinating Schwann cells The exclusive expression of LNX1 and interaction with ErbB2 hints at a potential role of LNX1 in regulating neuregulin-1/ErbB2 signalling, possibly in establishing or maintaining the non-myelinating status of PSCs [22].

1.2.8.5 ERC2

ERC2 (CAST1) is a protein of the presynaptic cytomatrix at the active zone (CAZ). CAZ regulates exocytosis of synaptic vesicles in presynaptic nerve terminals. ERC2 was found to bind LNX1, and this interaction was shown to be mediated through the C-terminal PDZ binding motif of ERC2 and the second PDZ domain of LNX1 [55]. Furthermore, exogenously expressed LNX1 colocalized with endogenous ERC2 at presynaptic terminals in cultured rat hippocampal neurons. LNX1 was diffusely distributed throughout the cell and recovered in the Triton X-100 soluble fraction when expressed alone. ERC2 was observed to recruit LNX1 to large immunoreactive structures and to the Triton X-100-insoluble fraction following co-expression.

1.2.8.6 JAM4

The C-terminal PDZ-binding motif of JAM4 was shown to interact with the second PDZ domain of LNX1 and endogenous LNX1 colocalized with JAM4 at TJs in the epithelial cell line MDCK [53]. LNX1 was found to facilitate endocytosis of JAM4. Numb – another LNX1 interacting protein, and JAM4 bind to different sequences of LNX1, and were discovered to bind to LNX1 simultaneously, forming a tripartite complex [53]. In fact, LNX1-mediated endocytosis of JAM4 depends on Numb. It is important to note that this study focused on LNX1p70 – the isoform of LNX1 that lacks the catalytic RING-finger domain. Thus, a role of LNX1, independent of E3 ubiquitin ligase activity, was proposed, whereby LNX1 acts as a molecular scaffold linking JAM4 to Numb, thereby facilitating endocytosis of JAM4.

1.2.8.7 PBK

The nuclear protein PDZ-binding kinase (PBK) – also known as TOPK – was identified as a LNX1 interacting protein in several independent studies [51, 58, 59]. PBK is a member of the mitogen activated protein kinase kinase (MAPKK) family. PKB is overexpressed in various types of human cancer and is known to suppress p53 – a tumour suppressor protein – function [66, 67]. PBK co-immunoprecipitated with LNX1 from cell lysates exogenously expressing both proteins [59] and was subsequently found to be a substrate of LNX1-mediated ubiquitination, targeting it for proteasomal degradation [51]. Knockdown of endogenous LNX1 using LNX1-specific siRNA resulted in elevated levels of PKB, enhanced cell growth rate and reduced cell sensitivity to doxorubicin-induced apoptosis [51]. Overexpression of LNX1 elicited the opposite effects. Thus, LNX1-mediated ubiquitination and subsequent proteasomal degradation may serve as a mechanism of regulating the cell growth promoting and anti-apoptotic effects of PBK [22].

1.2.8.8 RhoC

RhoC was identified as a LNX1 interacting protein by yeast two-hybrid screen [63]. RhoC is a small GTPase of the Ras superfamily and functions in actin cytoskeletal rearrangement. Co-immunoprecipitation from cells exogenously expressing both proteins confirmed this interaction and the first PDZ domain of LNX1 was found to be indispensable for RhoC binding [63]. RhoC was recruited from the cytoplasm to the nucleus upon co-expression with LNX1. Co-expression of RhoC reversed the increased transcriptional activity of AP-1 mediated by overexpression of LNX1 alone.

1.2.8.9 SKIP

Ski interacting protein (SKIP) – also known as SNW1 – was identified as a LNX1 interacting protein by yeast two-hybrid screen, specifically binding to the first PDZ domain of LNX1 [61]. LNX1 and SKIP co-immunoprecipitated from cell lysate exogenously expressing both proteins, and both proteins showed similar nuclear localization patterns. SKIP is a transcriptional regulator of genes associated with various signalling pathway [68]. SKIP interacts with the Notch intracellular domain and functions in Notch transcriptional complex assembly [69]. Through its interaction with SKIP1, it is possible that LNX1 may regulate Notch signalling, independent of Numb – but this remains to be studied [22].

1.2.8.10 c-Src

c-Src – a non-receptor tyrosine kinase – was found to interact with LNX1, specifically the first and third PDZ domains, through its carboxy terminus [40]. Furthermore, LNX1 and c-Src were shown to co-localize at points of cell-cell contact, peripheral membrane ruffles and in cytoplasmic puncta when overexpressed. LNX1 promoted ubiquitination of activated c-Src,

the level of which increased upon simultaneous inhibition of protein synthesis and proteasomal degradation [40]. Moreover, LNX1 expression resulted in decreased levels of constitutively activated c-Src. c-Src was shown to phosphorylate LNX1 on sites residing in the amino terminal region, upstream of its PDZ domains – the functional relevance of which is unclear. Thus, it appears that LNX1 and c-Src exhibit interdependent regulation, where LNX1 possibly targets activated c-Src for proteasomal degradation [22].

1.2.9 Disease associations of LNX1 and LNX2

1.2.9.1 Immune function and infectious disease

A genome-wide association study identified novel SNPs in *LNX1* associated with increased susceptibility to Kawasaki disease [70]. KD is believed to be triggered by unidentified infection(s). KD is a vasculitis with a propensity for coronary artery damage primarily affecting young children. Differences in whole blood LNX1 transcript levels were also noted at the acute phase compared to convalescence in this study.

Q fever is a disease caused by *Coxiella burnetii* infection [71]. In general, acute Q fever resolves spontaneously. Chronic Q fever, on the other hand, manifests as an endocarditis and is characterized by impaired immune response. Mehraj et al. [71] noted elevated levels of *LNX1* and *LNX2* mRNAs in the blood of patients with chronic Q fever, relative to acute Q fever.

Chapter 2: Expression & regulation of LNX proteins

2.1 Introduction

Ligand of Numb protein X1 (LNX1) and LNX2 are closely related proteins that share an identical domain structure consisting of one amino-terminal RING (Really Interesting New Gene) and four PDZ (PSD-95, DlgA, ZO-1) domains [25]. LNX proteins were originally described as ligands of Numb and its paralog Numb-like [24, 25], and LNX1 has been shown to ubiquitinate and target specific Numb isoforms for proteasomal degradation [26, 46]. Numb is a key protein involved in the specification of cell fates during development. In the nervous system, Numb functions in maintaining neural progenitors at early developmental stages while later, it promotes neuronal differentiation and maturation [72]. The combination of RING and PDZ domains in LNX proteins suggests that their ubiquitin ligase activity may be targeted to specific substrate proteins, by PDZ domain-mediated interactions [21]. Indeed, a large number of other LNX-interacting proteins have also been identified, and several of these are substrates for ubiquitination [51, 59]. LNX substrates include the proto-oncogenes, cSrc and BCR, the cell junction-associated molecule Claudin-1, the T-cell co-receptor CD8α and the protein kinase PBK [40, 41, 51, 52]. However, the *in vivo* relevance of these interactions, including the interactions with Numb proteins, remain unclear. Zebrafish have an additional *Lnx* paralog, *Lnx2b*, that has been well-characterized *in vivo* as a modulator of transcription factors involved in dorso-ventral and antero-posterior axis specification during embryogenesis [30-32]. However, these functions may be unique to Lnx2b, which is not present in mammals. LNX1 and LNX2 function has not been thoroughly explored *in vivo* in any model organism and all studies of LNX1 and LNX2, to date, have relied heavily on exogenously expressed LNX proteins.

Studies of *Lnx* expression showed a widespread distribution of *Lnx1* and *Lnx2* mRNAs in several adult tissues, with the earliest embryonic expression of both genes being observed in the CNS [24, 25]. By contrast, the expression patterns of LNX1 and LNX2 proteins remain poorly characterized. Expression of endogenous LNX1 protein was first reported in perisynaptic Schwann cells, at neuromuscular junctions (NMJs) [44]. Both LNX1 and LNX2 proteins, on the other hand, were detected in the acrosome of spermatozoa, while LNX2 expression was reported in a subset of blood vessels [39, 45]. Detection of LNX proteins by western blotting generally requires prior immunoprecipitation from tissue lysates [39, 40, 44], indicating that despite widespread mRNA expression, LNX1 and LNX2 proteins are present at extremely low levels *in vivo*.

The early expression of *Lnx1* and *Lnx2* in embryonic brain and spinal cord [25] hints at potential functions in neural development, possibly through regulation of Numb proteins. An isoform of LNX1 (LNX1p70), lacking the amino terminal RING domain, is expressed in the CNS using an alternate promoter to the one that drives expression of the longer, RING domain-containing, LNX1p80 isoform, which is expressed in other tissues ([24], Fig. 2.1A, B). This suggests that the functions of LNX1 in the brain, in contrast to LNX2, may be independent of the ubiquitin ligase activity of its RING domain. Amplification of the *Lnx1* and *Lnx2* genes have been reported in brain tumors and colorectal cancer respectively [43, 73, 74], while alterations of *Lnx1* mRNA levels were associated with gliomas, Kawasaki disease and chronic Q fever [61, 70, 71]. In the case of colorectal cancer in particular, a plausible role for *Lnx2* overexpression in activating signaling pathways that drive tumor progression was established [43]. A better understanding of *Lnx* mRNA expression, and how these relate to protein levels, will facilitate the elucidation of the physiological functions of LNX proteins, as well as their proposed roles in disease states.

To address these issues, *Lnx* mRNA and LNX protein expression was examined, focusing especially on the CNS, and a novel LNX1 protein isoform in the brain is described. The presence of uORFs and other sequence elements in the 5' untranslated region (5' UTR) of neuronal *Lnx1* mRNA transcripts is found to attenuate LNX1p70 protein production. The stability and proteasomal degradation of LNX1p80 is also examined. These findings provide a plausible explanation for the lack of correlation between *Lnx1* mRNA and protein levels *in vivo*, and have significant implications for understanding LNX protein function, their roles in disease, and the physiological relevance of the many interactions of LNX proteins that have been identified to date.

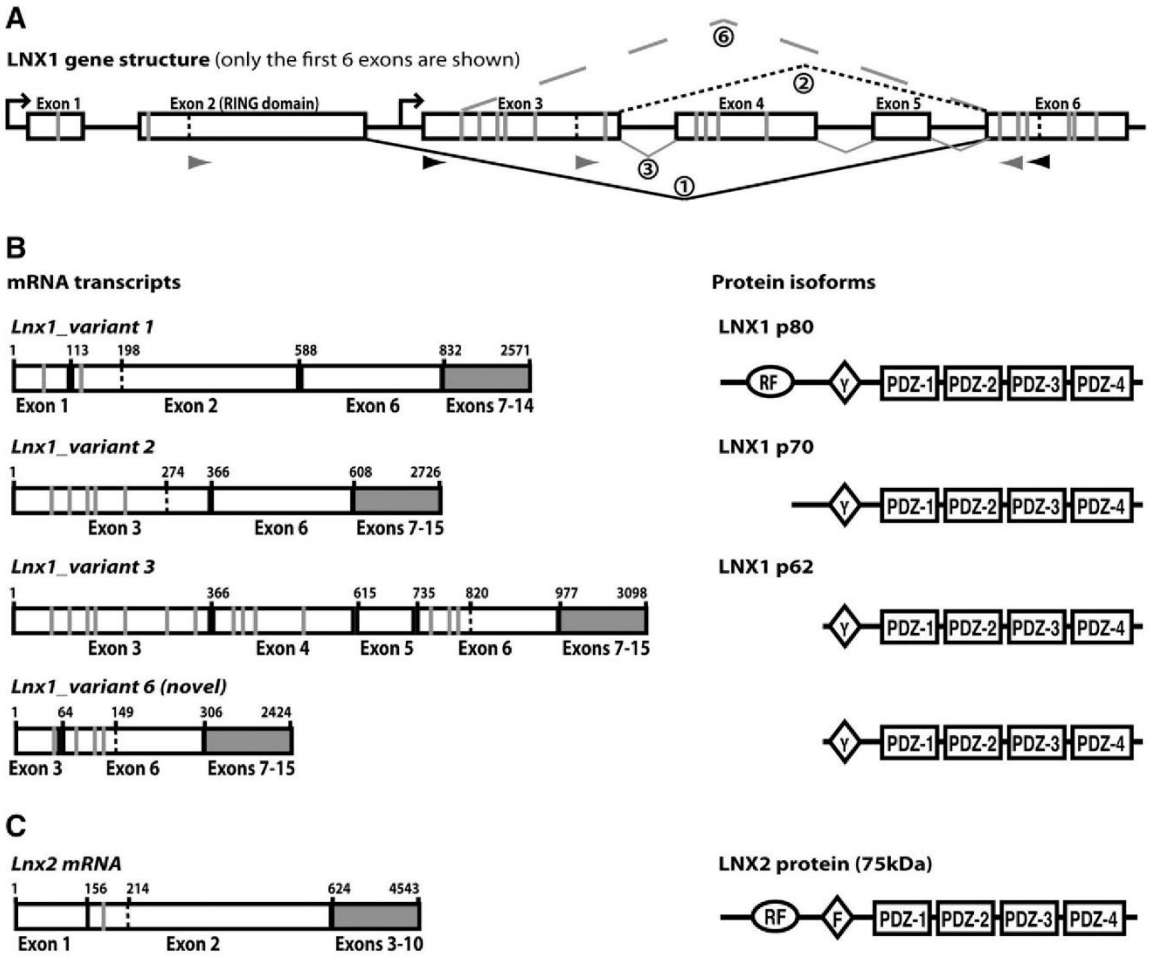

Fig. 2.1. Schematic diagrams of *Lnx1* and *Lnx2* genes, mRNA transcripts and proteins. (A) *Lnx1* gene structure showing the first 6 exons only (rectangles). Two alternate promoters (arrows) generate transcripts that start with either exon 1 or exon 3. The splicing events that generate *Lnx1* transcript variants 1, 2, 3 and 6 are numbered (in circles) and indicated by the black, black-dotted, grey and grey-dashed lines respectively. Vertical grey lines within the exons indicate non-initiation AUG codons, while the initiation codons for the main *Lnx1* coding sequences are shown as vertical dashed black lines. Arrowheads indicate the positions of primers used for reverse transcriptase PCR (see Fig. 2.3). **(B)** *Lnx1* mRNA transcript variants 1, 2, 3 and a novel variant - termed transcript variant 6, are depicted on the left, with the corresponding predicted protein products on the right. *Lnx1_variant 1* contains exon 2 that codes for the RING finger domain (RF) while the other variants, expressed from the alternate promoter, start with exon 3 and lack the RING domain. The NPAY motif (Y) that binds Numb and the four PDZ domains are common to all isoforms and are encoded by exon 6 and downstream exons (indicated by the grey box). Upstream AUG (uAUG) and initiation AUG codons for each transcript are indicated by vertical grey and dashed lines respectively. Nucleotide positions of splice junctions and the initiation AUG are indicated above each mRNA. *Lnx1_variant 6* is generated by splicing from an internal site within exon 3 to exon 6 and is predicted to give rise to the same 62kDa protein product as *Lnx1_variant 3*. **(C)** The first two exons of the *Lnx2* mRNA transcript are depicted on the left with AUG codons and downstream exons indicated as in B (above). LNX2 protein (right) has an identical domain structure to LNX1p80 except that it has an NPAF (F) rather than an NPAY motif.

2.2 Materials & Methods

2.2.1 Animals and animal procedures

Lnx1$^{exon3-/-}$ mice, originally generated by Lexicon pharmaceuticals, were obtained from the Mutant Mouse Regional Resource Center, University of California, Davis (Stock No: 032436-UCD; Strain Name: B6;129S5-Lnx1<tm1Lex>/Mmcd) and were maintained on a C57BL/6J genetic background. *Lnx2*$^{-/-}$ mice were generated recently in our laboratory and are described in detail Chapter 4. All animal experiments were performed as per institutional guidelines set by the University College Cork, Ethics Committee and conducted under license (No: B100/3814) issued by the Department of Health and Children.

2.2.2 Antibodies and reagents

The guinea pig polyclonal anti-LNX antibodies, that are either LNX1-specific (anti-LNX1-PDZ3/4), or that recognize both LNX1 and LNX2 (anti-LNX1/2-PDZ3/4) (Young et al., 2005), and the rabbit polyclonal anti-LNX antibody (anti-LNX1/2-RING/NPAY), that recognizes both LNX1 and LNX2 (Dho et al., 1998), have been described previously. The guinea pig and rabbit antibodies that recognize both LNX1 and LNX2 were used for immunoprecipitation and immunoblotting respectively. Secondary antibodies were from Jackson ImmunoResearch Laboratories and LI-COR, Biosciences. All chemicals and other reagents were purchased from Sigma-Aldrich unless otherwise stated.

2.2.3 Plasmids, primers, cDNA constructs and bioinformatic analysis

Lnx cDNA constructs were based on the following GenBank sequences: NM_001159577.1 for *Lnx1_variant 1*, NM_010727 for *Lnx1_variant 2*, NM_001159578 for *Lnx1_variant 3* and

AF401681.1 for *Lnx2*. The *Lnx1_variant 6* sequence described here has been deposited in GenBank, with the accession number KJ418422. For luciferase reporter assays, 5′ UTR constructs were either amplified by PCR, or synthesized as gBlock™ Gene fragments (Integrated DNA Technologies), and cloned into the HindIII and BamHI sites of the p2luc vector (Grentzmann et al.,1998), replacing the *Renilla* luciferase sequence in this vector and placing the *Lnx* sequence upstream of the Firefly luciferase coding sequence that lacks its own initiation AUG codon. A vector that expresses *Renilla* luciferase (pDluc-*Renilla*) was cotransfected with the p2luc-Lnx constructs, to control for transfection efficiency. For LNX1 protein stability studies, the coding sequences for LNX1p80 or LNX1p80 C48A were cloned into an expression vector (pCMV-N-FLAG) that drives expression of these proteins with an N-terminal FLAG epitope tag. An expression plasmid encoding HA-ubiquitin was a generous gift from Dr. J.McCarthy (University College Cork, Cork, Ireland). The sequences of primers used for reverse transcriptase PCR were as follows. For detection of *Lnx1 variant_1* and variant_2 (Fig. 2.3, left panel) the forward primers Lnx1v1-F (ATGAACCAACCGGACCTTG) and Lnx1v2-F (ATGAAGGCGCTGCTGCTTCTGG) respectively, were used in combination with the reverse primer Lnx1-R1 (CGCTCTCAAGATGGCTGTCCTG) for PCR amplification from cDNA prepared from adult mouse tissues. For detection and cloning of *Lnx1 variants_2 and 6*, the primers Lnx1v2-5UTR-F-HindIII (5′-TTTAAGCTTCCATCCCTCTCCCAGGCATTCATCAGCC-3′) and Lnx1v3-5UTR-R-BamHI (5′-TTTGGATCCTGCCATGAGGCTGGCGCAACCATC-3′) were used for PCR amplification from P3 mouse spinal cord and P8 brain cDNA, prepared as previously described (Foley and Young, 2013). For quantification of mRNAs for firefly and *Renilla* luciferase, the primers Fluc-F (5′-GACCAACGCCTTGATTGACA-3′), Fluc-R (5′-GGGCCACCTGATATCCTTTG-3′), Rluc-F (5′-CCCTGATCAAGAGCGAAGAG-3′) and Rluc-R (5′-GTCTAACCTCGCCCTTCTCC-3′) were used. For bioinformatic analysis of *Lnx*

5′ UTRs, *Lnx* sequences with well-annotated 5′ UTRs were retrieved from the GenBank database and uAUGs were counted using Lasergene software (DNAstar). Expected AUG frequencies were calculated as described by Rogozin et al. (2001).

2.2.4 Immunoprecipitation of endogenous LNX proteins

Three P14 whole mouse brains were homogenized using a Dounce homogenizer in a volume of lysis buffer (20 mM, pH 7.5, 10 mM NaCl, 1% NP40, 0.1% sodium deoxycholate, 1mM EDTA and 1× Complete protease inhibitors (Roche Applied Sciences)) which was 10 times the weight of the tissue. Following centrifugation at 16,000 g for 30 min at 4 °C immunoprecipitation was performed by addition of 10 µl guinea pig anti-LNX1/2-PDZ3/4 serum (Young et al., 2005) for 4 h and 50 µl Protein A sepharose beads (Thermo Scientific Pierce) for 2 h at 4 °C. Following 5 × 5 minute washes in lysis buffer, immunoprecipitated proteins were eluted by boiling in 2× SDS-PAGE gel loading buffer. Western blotting was performed using rabbit anti-LNX1/2-RING/NPAY antibody and enhanced chemiluminescent detection (Thermo Scientific Pierce, Rockford, IL, USA).

2.2.5 Cell culture and transfection

HEK293T cells (ATCC) were maintained in Dulbecco's Modified Eagle's Medium supplemented with 10% fetal bovine serum, 2 mM L-glutamine and antibiotics, at 37 °C, 100% humidity and 5% CO_2. For dual-luciferase assays performed without RNA quantification, 8 × 10^4 HEK293T cells in 100 µl of growth media without antibiotics were transfected per well in a 96-well plate, using 40 ng of p2-luc luciferase reporter plasmid construct, 10 ng of pDluc-Renilla vector and 0.4 µl lipofectamine 2000 in 50 µl Optimem I media (Invitrogen). Transfections for dual-luciferase assays and parallel RNA isolation were performed in a 6-well

dish with 1 μg of DNA (0.8 μg of p2-luc luciferase reporter plasmid constructs, 0.2 μg of pRL-SV40 Renilla vector) using a calcium phosphate based method (Schenborn and Goiffon, 2000). Cells were harvested 40 h after transfection and divided for dual-luciferase assays and RNA isolation. To study LNX1 levels following proteosomal inhibition 3×10^6 HEK293T cells were seeded on a 10 cm diameter plate and transfected the following day with 4 μg of DNA constructs using calcium phosphate precipitation. Media was changed 18 hour post-transfection and cells were sub-cultured onto a 6-well plate for MG132 treatment. For ubiquitination assays, and to study LNX1 stability following inhibition of translation, 7.5×10^5 HEK293T cells were seeded per well of a 6-well plate and transfected the following day with 2 μg of DNA constructs using calcium phosphate precipitation. Media was changed 20 hour post-transfection for MG132 or cycloheximide treatment.

2.2.6 Dual luciferase assays

Transfected cells were washed once with PBS followed by lysis in 25 μl 1× passive lysis buffer (Promega). 12.5 μl of cell extract was assayed for Firefly and Renilla luciferase activities using the Dual-Luciferase assay kit (Promega) and a Veritas Microplate Luminometer (Turner Biosystems) as described [75]. The relative level of reporter gene expression was calculated as the ratio of firefly luciferase activity to co-transfected control plasmid expressing Renilla luciferase.

2.2.7 RNA isolation and real time qPCR analysis

Total RNAs were isolated using TriPure Isolation Reagent (Roche Applied Sciences). Following quantification by spectroscopy, 5.5 μg of total RNA was treated using 1 unit of DNAseI (New England Biolabs). One step quantitative reverse transcriptase PCR (qRT-PCR)

reactions were carried out in a Opticon DNA Engine thermocycler (MJ Research) using 10 ng of DNAseI treated total RNA, 2× SensiFAST™SYBR No-ROX one-Step reagent (Bioline, UK), and 400 nM of each primer. The thermocycling conditions were as follows: 10 min at 45 °C (reverse transcription), 2 min at 95 °C (polymerase activation), 30 cycles of 5 s at 95 °C, 10 s at 60 °C and 5 s at 72 °C. Fluorescent signal was recorded during the 60 °C step. The baseline fluorescence was set as the mean fluorescence for cycles 3–10 and a threshold of 10 standard deviations above the mean baseline fluorescence was set to determine the cycle threshold (C_t) values. A standard curve was constructed using 4-fold serial dilutions of total RNA, (spanning 100 ng to 0.1 ng), assayed in duplicate with mean C_t values plotted versus the log [RNA]. Curve fitting was performed using KaleidaGraph software (Synergy Software). Relative values for [firefly mRNA] were divided by [Renilla mRNA] to control for differences in transfection efficiency. The mean of these normalized values were plotted for each construct. A minimum of three biological and three technical replicates were tested for each sample. To correct relative luciferase activity values for mRNA levels, the mean relative luciferase activity for a given sample was divided by the mean relative mRNA levels for that same sample.

2.2.8 Analysis of LNX1 protein stability

To assess proteasomal dependent degradation of LNX1, cells that had been transfected with FLAG epitope-tagged LNX1 constructs were treated with 10 μM MG132 for 6 h (n = 6). For this an MG132 stock solution at a concentration of 10 mM in DMSO was diluted 1 to 1000 in culture media and added to cells by changing the media. The control groups were treated with media containing an equal volume of DMSO only. To examine LNX1 turnover rates, cells were treated with cycloheximide in ethanol (100 μg/ml) at time-points up to 10 h (n=3). A solution of 20 mg/ml cycloheximide in ethanol was diluted 1 in 200 with media prior to addition

to cells. The control groups were treated with media containing an equal volume of ethanol only. Following drug treatment, cells were washed in PBS, pelleted by centrifugation, lysed in 150 µl of lysis buffer (20 mM Tris/Cl− pH 7.5, 150 mM NaCl, 1 mM EDTA, 1% NP-40, plus protease inhibitors) on ice for 20 min and centrifuged at 4 °C for 20min at 13,000 rpm. Protein concentrations of cleared lysates were determined using a Bicinchoninic acid (BCA) protein assay kit (Thermo Scientific Pierce). Equivalent amounts of protein lysate were analyzed by SDS gel electrophoresis and western blotting, and detected with the Odyssey Infrared Imaging System (LI-COR Biosciences). Immunoblots were quantified using Image Studio Lite software, version 2.1.

2.2.9 Ubiquitination assays

Twenty-four hours after transfection, cells were incubated in fresh medium containing either 10 µM MG132 (Merck Millipore) or vehicle only for 6 h. Cells were then washed twice with ice-cold PBS, and pelleted by centrifugation at 4000 rpm for 3 min at 4 °C. Pellets were resuspended in 100 µl 1% (w/v) Sodium Dodecyl Sulfate (SDS) supplemented with 15mMN-ethylmaleimide (NEM) and 1× Complete protease inhibitors (Roche Applied Sciences), and boiled for 5min. Following cooling on ice, samples were diluted with 900 µl of ice cold buffer that contained 50 mM Tris (pH 8.0), 150 mM NaCl, 1% Triton, 0.5% sodium deoxycholate, 50 mM sodium fluoride, 0.1 mM sodium orthovanadate and 1× Complete protease inhibitors (Roche Applied Science). Lysates were cleared by centrifugation at 13,000 rpm for 30min at 4 °C. The supernatant was collected and protein concentrations were determined. Equivalent amounts (800 µg) of lysates were immunoprecipitated overnight at 4 °C, with rotation, using 0.5 µg of the indicated antibody, followed by incubation with 20 µl Protein A/G agarose beads (Thermo Scientific Pierce) for 4 h. Protein A/G agarose beads were washed three times in the

dilution buffer. Proteins were eluted by boiling the Protein A/G agarose in 2× SDS PAGE sample buffer for 5 min and then analyzed by western blotting.

2.2.10 Statistical analysis

Microsoft Excel software was used to perform two tailed Student's T tests to evaluate changes in luciferase activities for constructs lacking uORFs (Fig. 2.4) and changes in LNX protein levels following proteasomal inhibition. To test the significance of changes in luciferase and mRNA levels in Fig. 2.7-2.9 a one-way ANOVA was performed using SPSS software (IBM). ANOVA revealed significant differences between groups in all cases. A Dunnett T3 post hoc test was chosen since the assumption of homogeneity of variances was violated. Similar results were obtained using a Games–Howell post hoc test.

2.3 Results

2.3.1 Examination of LNX protein expression in the nervous system

Despite clear mRNA expression, endogenous LNX2 protein has not been detected in the nervous system and LNX1 protein has only been detected following immunoprecipitation from brain lysates [40]. Using antibodies that recognize both LNX1 and LNX2, three LNX bands were detected by western blotting following immunoprecipitation from brain lysates (Figure 2.2). None of these bands are directly detected in brain lysates, in agreement with the notion of endogenous LNX proteins being present at very low levels. To examine the identity of these bands, an available mouse line in which *Lnx1* exon 3 has been deleted was utilized [76]. These mice are referred to as mice as $Lnx1^{exon3-/-}$. Exon 3 is the first exon of *Lnx1_variant 2* mRNA (Figure 2.1 B), that gives rise to the p70 LNX1 protein, and so these mice should lack this isoform. However, the absence of LNX protein in these mice was never confirmed, and no obvious phenotype was reported for this line (***https://www.mmrrc.org/***). The middle and lower bands, observed by western blotting, are absent in immunoprecipitates from $Lnx1^{exon3-/-}$ brains (Figure 2.2, left panel), confirming that they both correspond to LNX1 isoforms, probably arising from transcripts that contain exon 3. The middle band corresponds to the size of the brain-specific LNX1p70 isoform, while the identity of the lower band, at approx 60kDa, is unclear. The top band, migrates at approximately the molecular weight of LNX2 (75kDa), and is absent in immunoprecipitates from $Lnx2^{-/-}$ mice, identifying it as corresponding to LNX2 protein (Figure 2.2, right panel).

The lower molecular weight LNX1 protein identified above may represent a novel LNX1 isoform arising from alternative splicing of a transcript that contains exon 3. The Genbank sequence database lists three *Lnx1* transcript variants, in addition to *Lnx1 variant 1* and *2* that generate the well-characterized p80 and p70 protein isoforms respectively. *Lnx1_variant 3*

contains exon 3 and two additional exons (exons 4 and 5) that are not present in *variants 1* and *2* (Figure 2.1B). This transcript is predicted to produce a protein of 62kDa, though there has been no experimental evidence for the existence of this protein isoform to date. The predicted LNX1p62 isoform was expressed in HEK293 cells. This protein migrates at the same molecular weight as the lower band observed in anti-LNX immunoprecipitates from brain tissue (Figure 2.2, middle panel), strongly suggesting that this band corresponds to LNX1p62.

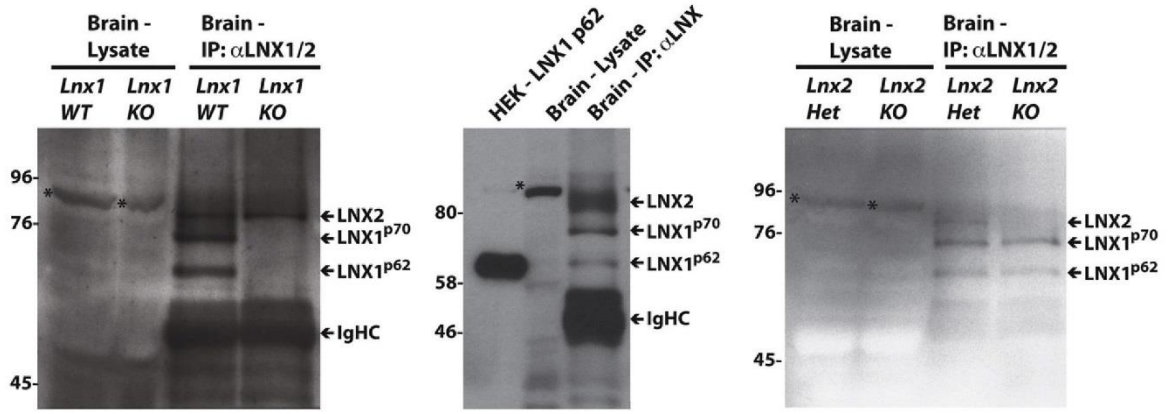

Figure 2.2: LNX protein expression in the nervous system examined using LNX1$^{exon3-/-}$ mice. LNX protein expression in the brain was examined by western blotting of lysates and immunoprecipitates (IP) from P17 mouse brain. Immunoprecipitation and immunoblotting were performed with guinea pig anti-LNX1/2-PDZ3/4 and rabbit anti-LNX1/2-RING/NPAY antibodies respectively that recognize both LNX1 and LNX2. Left panel shows immunoprecipitations from LNX1$^{+/+}$ (WT) and LNX1$^{exon3-/-}$ (KO) tissues. Middle panel shows immunoprecipitates from wild-type mice run side-by-side with lysate from HEK cells overexpressing LNX1p62 (left lane). Right panel shows immunoprecipitations from LNX2$^{+/-}$ (Het) and LNX2$^{-/-}$ (KO) mice * = non-specific band detected in brain lysates, IgHC = immunoglobulin heavy chains from the antibody used for immunoprecipitation. n=2.

To examine which *Lnx1 mRNA* transcripts are expressed in the CNS and identify transcripts that could give rise to the novel LNX1p62 protein, rtPCR was first performed using primers designed to detect the well-characterized transcript *variants_1* and *2* (Figure 2.3, left panel). In line with previous reports [24] , *Lnx1 variant_1* was readily detected in non-neuronal tissues (liver and muscle) but was not detected in spinal cord and only just detectable in the brain,

whereas *Lnx1 variant_2* expression was specific to the CNS tissues. To examine if *Lnx1 variant_3,* or other exon 3-containing variants distinct from *variant_2,* are expressed in the brain, rtPCR was performed using a primer at the 5' end of exon 3 in combination with a primer within exon 6. The major product obtained corresponds to *Lnx1_variant 2*. No product of the size expected for *Lnx1_variant 3* was obtained, but instead, a minor product of much smaller size was present (Figure 2.3, right panel). Sequencing identified this as a novel transcript variant, in which splicing occurs between an internal site within exon 3 and exon 6 (Figure 2.1B). This transcript, now called *Lnx1_variant 6,* is predicted to give rise to the same 62kDa protein product as *Lnx1_variant 3*, but has a much shorter 5' UTR. Thus, this novel *Lnx1_variant 6* mRNA could give rise to the lower band detected by western blotting in the region of 60kDa. While *Lnx1_variant 6* seems to be much less abundant than *Lnx1_variant 2* in the brain, PCR results suggest that its expression, relative to *Lnx1_variant 2*, is somewhat higher in the spinal cord (Figure 2.3, right panel). These observations provide evidence at both the mRNA and protein levels for a novel LNX1 p62 isoform in the CNS.

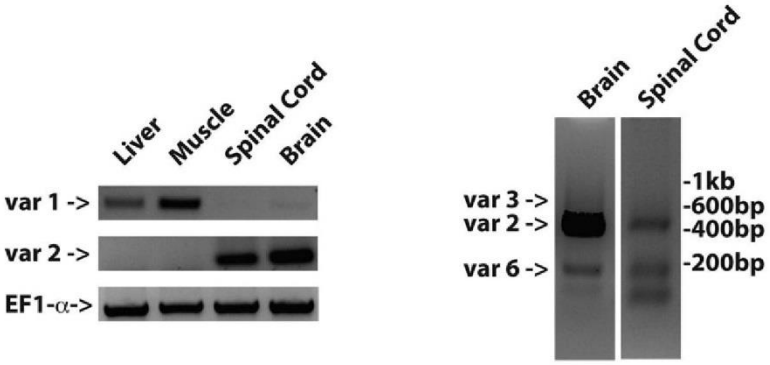

Figure 2.3: Reverse transcriptase PCR of *Lnx1* mRNA transcripts expressed in neuronal and non-neuronal tissues analyzed by gel electrophoresis. In the left panel, primers designed to detect *Lnx1_variants 1* and *2* were employed (indicated by grey arrowheads in Fig. 2.1A). In the right panel, primers designed to detect any exon 3-containing transcripts were used (indicated by black arrowheads in Fig. 2.1A). Expected positions of products corresponding to *Lnx1_variants 2, 3* and *6* are indicated on the left. n=1.

Previous reports show LNX1 protein expression in the perisynaptic glial cells at the NMJ by immunofluorescent staining using several anti-LNX1 antibodies [44]. However, the identity of the LNX1 isoform expressed in these cells had not been established [44]. Immunofluorescence staining of NMJs, from *Lnx1*$^{exon3-/-}$ mice, shows that the LNX1 staining is still present (Figure 2.4). This indicates that it is, in fact, the p80 isoform, rather than the p70 isoform, of LNX1 that is expressed in perisynaptic glial cells at the NMJ. Immunohistochemistry with anti-LNX antibodies was also performed on brain sections, but this did not reveal any specific staining pattern, indicating perhaps that the low levels of LNX proteins in the brain cannot be detected by immunostaining.

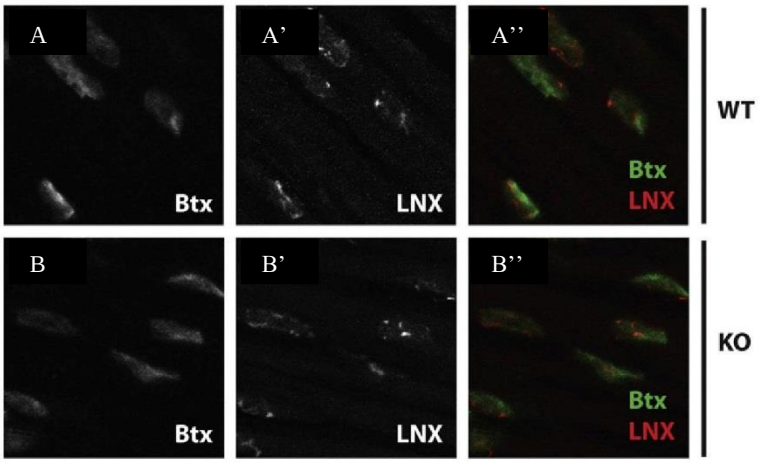

Figure 2.4: Immunofluorescent staining of neuromuscular junctions in P14 diaphragm muscle from wild type (A-A") and LNX1$^{exon3-/-}$ (B-B") mice. LNX1 protein is detected in perisynaptic Schwann cells using an anti-LNX1 specific antibody that does not recognize LNX2 (A',B'). α-bungarotoxin (Btx) was used to stain acetylcholine receptors at the neuromuscular junctions (A,B). Merged images are shown in panels A" and B" with a-bungarotoxin in green and anti-LNX staining in red.

Overall, these observations suggest that LNX1 and LNX2 proteins are both expressed in the brain, albeit at low levels. In addition, the absence of LNX1 and LNX2 protein expression in the brains of *Lnx1*$^{exon3-/-}$ and *Lnx2*$^{-/-}$ mice validates them as models to study the function of LNX proteins in the central nervous system.

2.3.2 uORFs attenuate translation of LNX1p70 but not LNX1p80 or LNX2

The miniscule levels of endogenous LNX proteins detected, despite relatively widespread expression of *Lnx* mRNA [25], suggest that LNX protein synthesis is tightly regulated. The presence of uORFs in the 5'-UTR of genes has been shown to be a common mechanism to inhibit translation of the main coding sequence [77]. To see whether this mechanism might regulate LNX protein expression, the 5'-UTRs of *Lnx1p80*, *Lnx1p70* and *Lnx2* transcripts were examined from ten diverse vertebrate species (Table 2.1). At least one upstream initiation codon (uAUG) was found in virtually every transcript examined for both *Lnx1* and *Lnx2*, suggesting that uORFs could play an evolutionarily conserved role in regulating translation of LNX proteins.

Table 2.1. Analysis of uAUG codons in *Lnx1* and *Lnx2* 5' UTRs

5' UTR length and number of uAUG codons are presented for a diverse selection of vertebrate LNX transcripts. n/a = sequence not available or 5' UTR not annotated. Bt = *Bos taurus* (cattle); Dr = *Danio rerio* (zebrafish); Gg = *Gallus gallus* (chicken); Hs = *Homo sapiens* (human); Mm = *Mus musculus* (house mouse); Ol = *Oryzias latipes* (Japanese medaka) Oo = *Orcinus orca* (killer whale); Or = *Odobenus rosmarus divergens* (Pacific walrus); Rn = *Rattus norvegicus* (Norway rat); Xt = *Xenopus tropicalis* (western clawed frog); Fa = *Ficedula albicollis* (collared flycatcher); Cc = *Condylura cristata* (star-nosed mole)

	Lnx1_variant 1		***Lnx1_variant 2***		***Lnx2***	
Species	**Length (ntd)**	**# uAUG**	**Length (ntd)**	**# uAUG**	**Length (ntd)**	**# uAUG**
Bt	228	1	225	3	281	1
Dr	359	3	n/a	n/a	243	5
Gg	111	1	376	5	255	4
Hs	285	4	304	1	309	1
Mm	197	2	273	5	213	1
Ol	n/a		483	4	n/a	n/a
Oo	268	2	246	4	n/a	n/a
Or	263	3	306	2	317	1
Rn	190	2	201	3	197	1
Xt	195	2	315	7	116	1
Fa	74	0	138	1	162	5
Cc	n/a	n/a	n/a	n/a	105	1
Average	217	2	287	3.5	220	2.1
uAUG frequency /1000ntd						
Observed:		9.2		12.2		9.6
Expected:		13.9		14.7		13.7

To test this hypothesis, dual luciferase reporter assays were employed. *Lnx* 5'-UTRs, and the first two codons of the murine *Lnx* coding sequences, were cloned upstream and in frame with a firefly luciferase coding sequence that lacked its own initiation AUG codon. Reporter constructs containing wild type 5'-UTRs, as well as 5'-UTRs in which the uAUGs had been mutated to AAA, were prepared and co-transfected into HEK293T cells, along with a vector encoding *Renilla* luciferase that acted as a control for transfection efficiency. Normalized firefly/*Renilla* luciferase activity was measured to assess protein production. For *Lnx2*, the wild type 5' UTR construct exhibited relatively high luciferase activity, and mutation of the single uAUG had no effect (Fig. 2.5, right panel). Surprisingly, for *Lnx1_ variant 1*, mutation of two uAUGs to AAA decreased protein production. By contrast, the wild type *Lnx1_variant 2 5' UTR* construct, which contains 5 uAUGs, exhibited relatively low luciferase activity, that was increased approximately 2-fold when these uAUGs were mutated to AAA (Figure 2.5, left panel). This indicates that the presence of uORFs may negatively regulate the efficiency of correct translation initiation for *Lnx1_variant 2*, but not for *Lnx1_variant 1* or *Lnx2.*

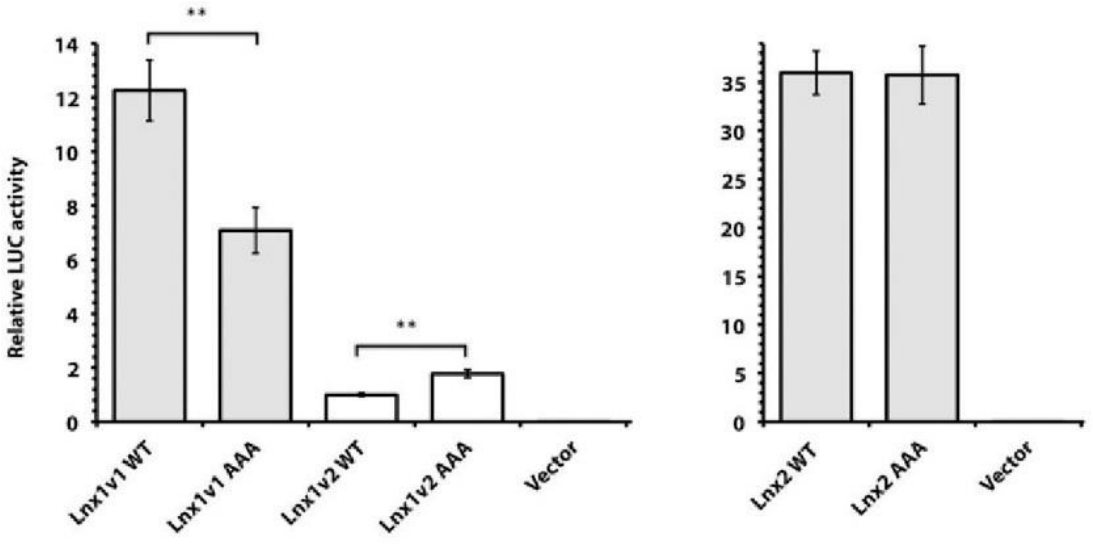

Figure 2.5: The effects of uORFs on translation of *Lnx* mRNAs assessed using a dual luciferase reporter assay. Relative luciferase activity for either wild type (WT) 5' UTRs or 5' UTR constructs in which all uAUGs have been mutated to AAA (AAA) is plotted for *Lnx1_variant 1* (*Lnx1v1*; light grey bars), *Lnx1_variant 2* (*Lnx1v2*; white bars) and *Lnx2*. Data for *Lnx1 and Lnx2* are from the same experiment and can be directly compared, but are shown with different y-axis scales for clarity. ** P<0.01 Students T-test, Error bars represent S.E.M. n=5. Experiment performed by Ms. Louise Mansfield.

2.3.3 Additional 5' UTR elements regulate LNX1 p70 protein expression

The relative luciferase activity observed for the wild-type *Lnx1_variant 2* 5' UTR was very low compared to *Lnx1_variant 1* and *Lnx2* (12 and 36-fold less respectively). Even after mutation of all five uAUGs, the 5' UTR of *Lnx1_variant 2* does not support protein expression levels comparable to the other 5' UTRs (Fig. 2.5). This suggested that there might be other inhibitory elements in the 5' UTR of the *Lnx1_variant 2* mRNA. A number of 5' and 3' deletion constructs were generated to explore this possibility (Figure 2.6).

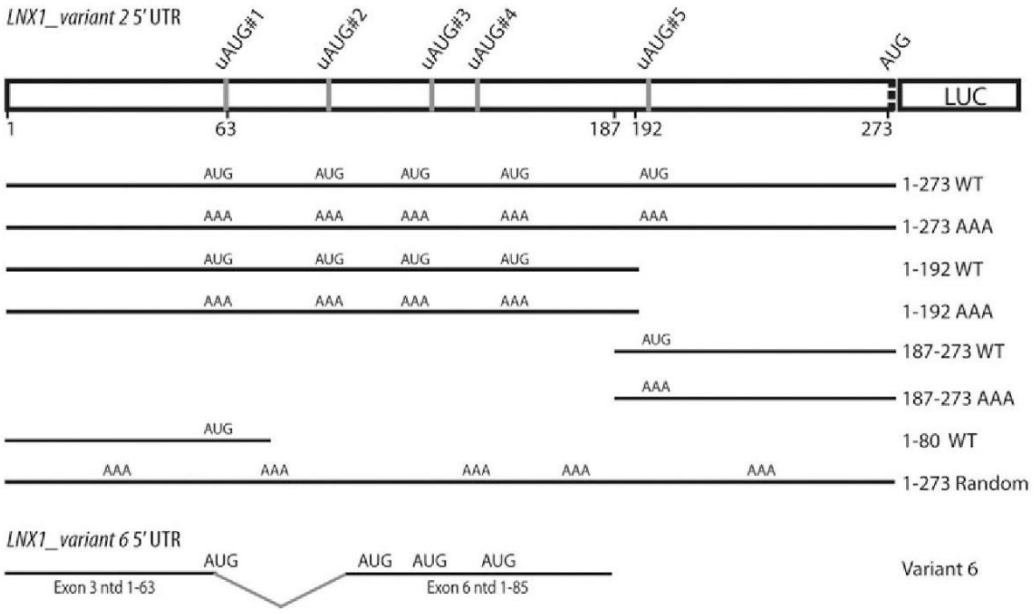

Figure 2.6: Schematic representation of luciferase reporter constructs used in Figures 2.7-2.9 below. The *Lnx1_variant 2* 5' UTR consists of 273 nucleotides and contains five uAUGs as shown on top. Truncated constructs and those with uAUGs mutated to AAA are depicted below. In the construct designated 1-273 Random, the wild type 5' UTR sequence has been randomized and any AUG codons changed to AAA. The 5' UTR of *Lnx1_variant 6* containing part of exon 3 spliced into exon 6 is depicted at the bottom and contains four uAUGs.

Luciferase activity for a construct containing nucleotides 1-192 was similar to the wild type 273 nucleotide 5' UTR (Figure 2.7). Mutation of the four uAUGs in this truncation construct increased luciferase activity approximately 5-fold. However, a construct containing

nucleotides 187-273, or this construct with its one uAUG mutated to AAA, exhibited 23-fold and 30-fold increased activity respectively, compared to the wild type 5' UTR. Luciferase activity for a construct containing nucleotides 1-80, with a single uAUG, was 8-fold higher than the wild type. To rule out the possibility that these observations were just a consequence of shorter 5' UTR length of the truncated constructs, the *Lnx1_variant 2* 5' UTR sequence was randomized to generate a construct of the same length, and similar nucleotide composition as the wild-type 5' UTR (but lacking uAUGs). Luciferase activity for this construct was 22-fold higher than the wild-type 5' UTR and 8-fold higher than the full length UTR lacking uAUGs (Figure 2.7). Taken together, these observations indicate the presence of a sequence-specific element in the region between nucleotides 80 and 192 of the *Lnx1_variant 2* 5' UTR, that has a significant negative impact on protein expression, additional to the effect of uAUGs.

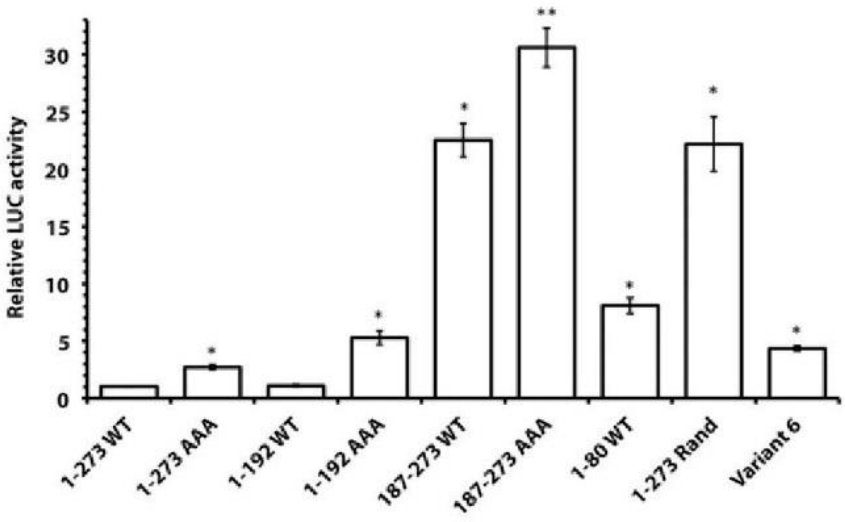

Figure 2.7: Relative luciferase activity is shown for the constructs described in Figure 2.6 above. The values for the 1-273 WT is arbitrarily set to one for ease of comparison of fold changes in luciferase levels. Statistical significance of differences in luciferase activity relative to the 1-273 WT construct as determined using the Dunnett T3 posthoc test are indicated; * $P<0.05$, ** $P<0.01$. Error bars represent S.E.M. n=4.

To examine the mechanism by which this element suppresses protein production, the relative luciferase mRNA levels for the various constructs was measured (Figure 2.8). A very consistent 3-4 fold increase in mRNA levels was observed for constructs that lack the nucleotide 80-192 region of the 5' UTR. This strongly suggests that this region either inhibits mRNA transcription, or increases mRNA degradation.

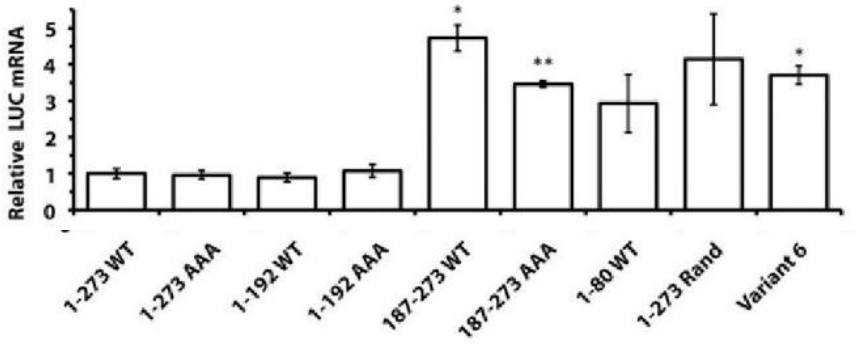

Figure 2.8: mRNA levels are shown for the constructs described in Figure 2.6 above. The values for the 1-273 WT is arbitrarily set to one for ease of comparison of fold changes in mRNA levels. Statistical significance of differences in mRNA levels relative to the 1-273 WT construct as determined using the Dunnett T3 posthoc test are indicated; * $P<0.05$, ** $P<0.01$. Error bars represent S.E.M. n=3.

To ascertain whether these effect on mRNA expression account for the large differences in luciferase activity observed, the luciferase activities were normalized for mRNA levels (Figure 2.9). Even correcting for mRNA levels, luciferase activity for the nucleotide 187-273 construct, lacking uAUGs, is significantly higher than the wild type 5' UTR, or the 5' UTR lacking uAUGs. The corrected activity for the nucleotide 1-80 and randomized constructs is also higher, though it does not reach statistical significance. This indicates that, in addition to decreasing mRNA levels, the nucleotide 80-192 region of the *Lnx1_variant 2* 5' UTR inhibits protein translation, by some mechanism other than through the presence of uORFs.

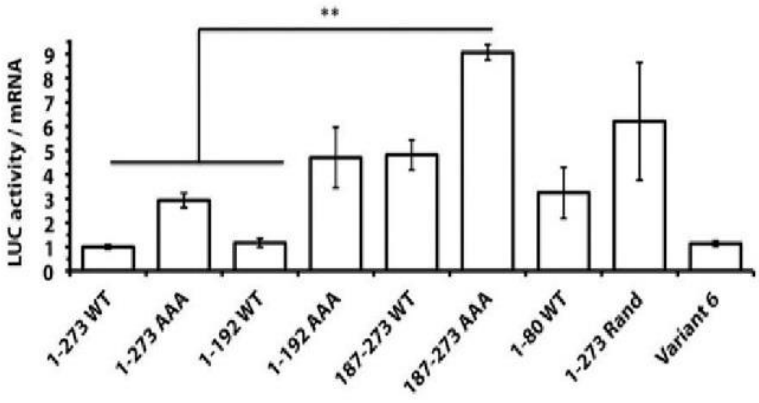

Figure 2.9 Luciferase activity corrected for mRNA levels are shown for the constructs described in Figure 2.6 above. The values for the 1-273 WT is arbitrarily set to one for ease of comparison of fold changes in luciferase or mRNA levels. Statistically significant differences relative to the 1-273 WT construct as determined using the Dunnett T3 posthoc test are indicated; * $P<0.05$, ** $P<0.01$. Error bars represent S.E.M. n=3.

Interestingly, the novel splicing of *Lnx1_variant 6* described in Sect. 2.3.1 above, skips this inhibitory region and joins nucleotides 1-63 of exon 3 directly to exon 6. Thus, a reporter construct containing the 5' UTR of *Lnx1_variant 6* exhibits higher luciferase activity than *Lnx1_variant 2* (Figure 2.6, 2.7). This difference can be accounted for by higher mRNA levels, similar to other constructs lacking the inhibitory region of exon 3 (Figure 2.8). *Lnx1_variant 6* contains 4 uAUGs that may modulate translational efficiency, though their effect has not been examined. Overall, these findings demonstrate that the expression of the CNS-specific LNX1 protein isoforms is tightly regulated, both at the level of mRNA transcription/stability, and translation by elements within the 5' UTR. This regulation is likely to contribute significantly to the low levels of LNX1 protein that are observed in the CNS *in vivo*.

2.3.4 Proteasomal degradation and turnover of LNX1p80 protein.

The *Lnx1_variant 1* mRNA, that codes for the RING finger domain-containing p80 protein isoform, is expressed widely in non-neuronal tissues [24, 25], but endogenous LNX1 p80 protein is not readily detected, except in perisynaptic Schwann cells. One possible explanation for the low levels of LNX proteins *in vivo* is that the protein is intrinsically unstable, or is turned over at a high rate. The stability of several ubiquitin ligases is known to be regulated by ubiquitination and proteasomal degradation [78]. To examine whether LNX1 is regulated in this manner, levels of exogenously-expressed LNX1p80 in cultured cells were examined following a 6 hour treatment with the proteasomal inhibitor MG-132 (Figure 2.10). Wild-type LNX1p80 levels were increased by close to 100% under these conditions. Proteasomal targeting of LNX1p80 could occur through either auto-ubiquitination, or ubiquitination mediated by a distinct E3 ubiquitin ligase [78]. It was found that a mutant LNX1 protein, lacking ubiquitin ligase activity (LNX1p80-C48A [26]), was stabilized to a similar extent following proteasomal inhibition as wild type LNX1, indicating that proteasomal degradation of LNX1 is probably not a consequence of auto-ubiquitination.

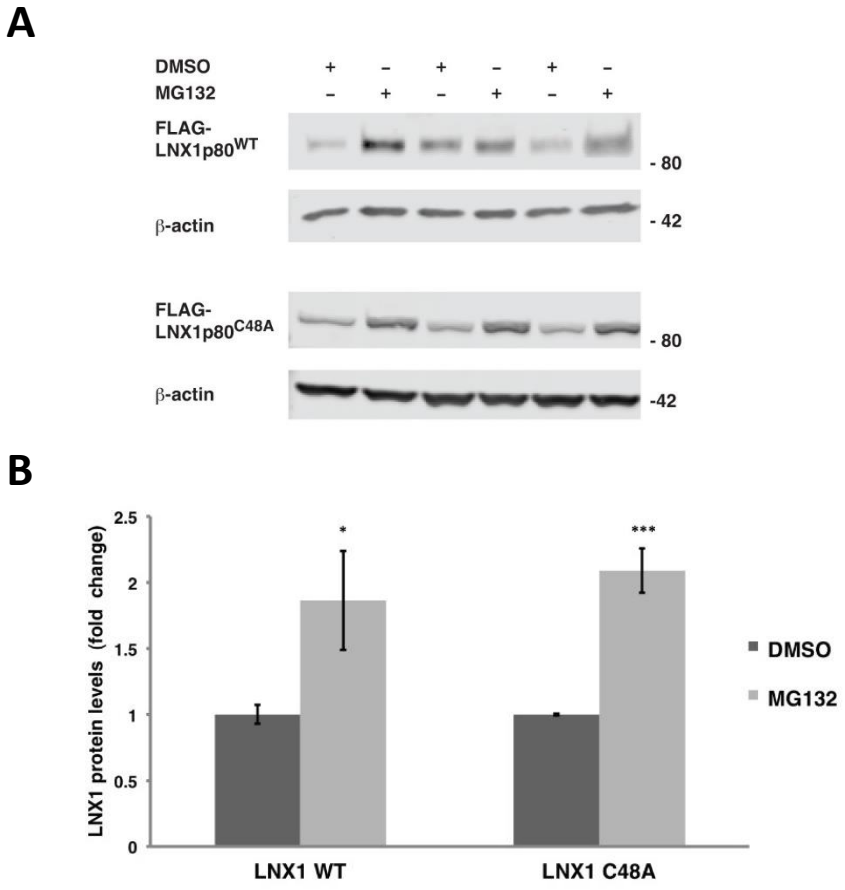

Figure 2.10: Proteasomal inhibition increases LNX1 protein levels. HEK293T cells were transfected with FLAG-tagged LNX1p80 or a mutant (LNX1 $p80^{C48A}$) lacking ubiquitin ligase activity and treated for 6 hours with either 10μM of the proteasomal inhibitor MG132 or vehicle only (DMSO). LNX1 protein was detected by immunoblotting using an anti-FLAG antibody (A). LNX1 protein levels were quantified and normalized against β-actin levels (B). (n=6, *P<0.05, ***P<0.001 Students T-test).

To directly demonstrate ubiquitination of LNX1p80, LNX1p80 constructs and HA epitope-tagged ubiquitin were co-expressed and ubiquitinated proteins were immunoprecipitated from cell lysates that had been boiled in the presence of SDS to disrupt protein-protein interactions. Ubiquitinated LNX1p80 and LNX1p80-C48A are both detected and accumulate in the presence of proteasomal inhibitor (Figure 2.11).

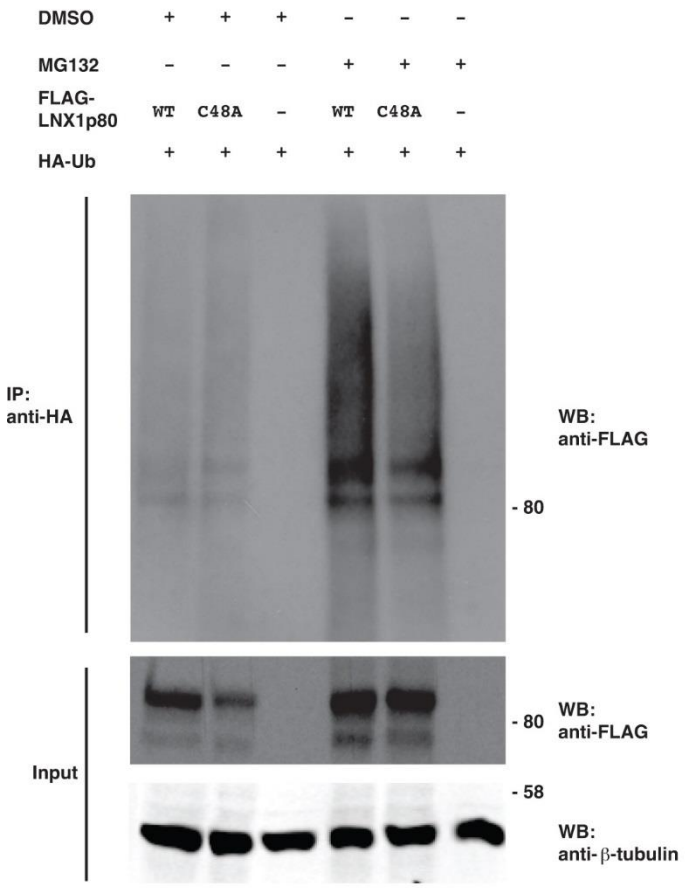

Figure 2.11: Ubiquitination of LNX1p80 and LNX1p80^{C48A} assessed by immunoprecipitation (IP) following co-expression with HA-tagged ubiquitin (HA-Ub). The indicated constructs were expressed in HEK293T cells that were then treated with either the proteasomal inhibitor MG132 or vehicle only (DMSO) for 6 hours. Ubiquitinated proteins were immunoprecipitated from cell lysates (Input) using an anti-HA antibody. A high molecular weight smear corresponding to ubiquitinated LNX1 is detected by Western blot (WB) for both the wild type and mutant protein and accumulates in the presence of MG132. n=2.

To examine the turnover rate of LNX1, a "cycloheximide chase" experiment was performed in which levels of transfected FLAG epitope-tagged LNX1p80 were monitored in HEK293 cells following inhibition of protein synthesis (Figure 2.12). A clear decline in LNX1p80 levels was seen at 8 and 10 hours post-cycloheximide treatment (100ug/ml). This observation indicates that LNX1p80 is turned over at an appreciable rate in cells, although deterioration of the health of the cycloheximide-treated cells prevented extension of this time-course beyond 10 hours.

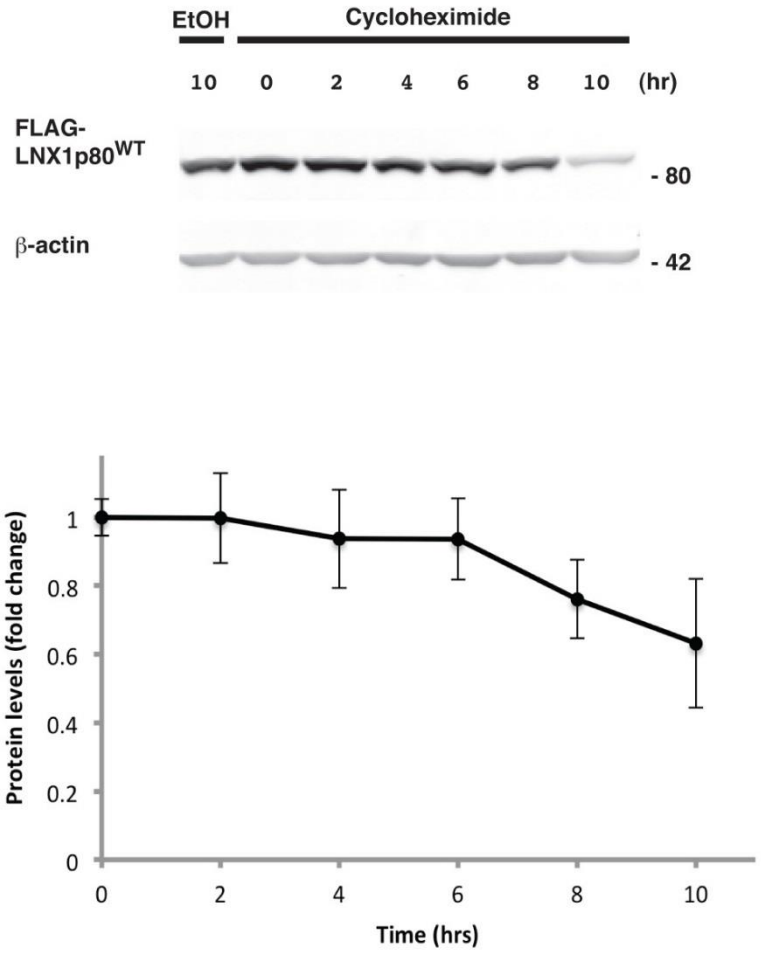

Figure 2.12: LNX1 protein levels decrease following inhibition of protein synthesis. HEK293T cells transfected with LNX1p80 were treated with 100μg/ml cycloheximide or vehicle only (EtOH) and harvested at the indicated time points post-treatment. LNX1 protein levels were detected as described above, quantified and plotted versus time after treatment (n=3). Error bars represent S.E.M.

2.4 Discussion

A detailed understanding of the cell-type specific expression of *Lnx* mRNA, and more importantly LNX proteins, is a prerequisite to elucidating their physiological functions and the *in vivo* significance of their interactions with Numb and other proteins. The first *in vivo* localization of LNX1 protein has previously been reported, in perisynaptic glial cells, at neuromuscular synapses [44]. In the present study, immunostaining for LNX1 at the NMJ persists in *Lnx1*$^{exon3-/-}$ knockout mice, and thus, it is likely to be *Lnx1 variant_1* (coding for LNX1p80 protein) that is expressed in perisynaptic glial cells of the PNS. A surprising observation, when LNX proteins were immunoprecepitated from brain lysates, was the detection of two LNX1 bands by western blotting, both of which were absent from immunoprecipitates from brains of LNX1$^{exon3-/-}$ mice (Figure 2.2). The upper band corresponds to LNX1p70 while the lower band migrates with a molecular weight of approximately 60kDa. The *Lnx1_variant 3* mRNA transcript, annotated in sequence databases, is predicted to produce a protein of 62kDa. This transcript has two additional exons, exons 4 and 5, compared to *Lnx_variant 2*, generating an 820 nucleotide 5' UTR, with 13 uORFs prior to the predicted start codon. A novel transcript, *Lnx1_variant 6* – predicted to produce the same 62kDa product as *Lnx1_variant 3*, but has a 150bp 5' UTR with 4 uORFs, was also detected in both brain and spinal cord. Reverse transcriptase PCR, with flanking primers that should amplify all three transcripts, only yields a product for transcript *variant 2* and *6*, but not *3*. *Lnx1_variant 3*-specific primers, located in exons 4 and 5, do amplify a product from brain cDNA, suggesting that this variant is expressed in the brain. However, it would not appear to be very abundant, and given the presence of so many (13) uORFs in this transcript, it seems more likely that the novel *Lnx1_variant 6* transcript may give rise to the 62kDa protein detected by Western blotting.

As reported previously [40], it was found that LNX1 can only be detected in brain tissue following immunoprecipitation. Here, using the same approach, LNX2 protein expression was shown in the brain for the first time. Detection of either protein required immunoprecipitation from a large volume of brain lysate. The presence of LNX protein at very low levels *in vivo*, despite the mRNA for these genes being readily detectable, suggests that protein expression is tightly regulated post-transcriptionally. One mechanism that has emerged for translational regulation is the presence of uORFs in the 5'-UTR of gene transcripts, which divert the translation machinery away from translation of the main coding sequence [79]. The degree to which uORFs affect translation of the main coding sequence is variable, and factors that seem to contribute to this include the context (Kozak sequence) of the uAUG codon, the presence of multiple uORFs, and distance of the uORF from the 5' cap of the transcript. Overlap between the uORF and main coding sequence, proximity of the uORF to the main coding sequence and uORF length may also be important factors in some cases [77, 79].

Examining sequences from diverse species, *Lnx* 5' UTRs are longer than average (Table 2.1). In addition, uAUGs are found in virtually every *Lnx* sequence examined and uAUG frequency is higher than values previously reported for large gene sets [77, 80]. This is noteworthy given that over half of all genes lack uAUGs in most vertebrate species. The above points are especially true of *Lnx1_variant 2* mRNAs, which have longer 5' UTRs and more uAUGs than *LNX1_variant 1* or *LNX2* transcripts. Generally, uAUGs in 5' UTRs occur at significantly lower frequency than would be expected by chance [80], but for *Lnx1_variant 2* the uAUG frequency is closer to that expected by chance, based on 5' UTR nucleotide composition (Table 2.1). Thus the bioinformatic evidence points towards an evolutionarily conserved regulatory role for uORFs in *Lnx* transcripts, particularly *Lnx1_variant 2*. In agreement with this, luciferase reporter assays indicate that the presence of uORFs in *Lnx1_variant 2* serve to

negatively regulate translation. Thus luciferase activity is 2-3 fold higher, when the five uAUGs in the LNX1p70 encoding *Lnx1_variant 2* 5' UTR are mutated to AAA. These uAUGs are not very close to the AUG of the LNX1p70 coding sequence and the predicted uORFs do not overlap the main ORF. The 1st uORF, at 25 codons, is significantly longer than the others, a factor that is thought to prevent ribosome reinitiation [81]. In addition, the 1st uAUG has a strong Kozak consensus sequence, suggesting that the 1st uORF may contribute significantly to the observed inhibition of translation, but this needs to be tested experimentally. The presence of a uORF in the *Lnx2* 5'UTR doesn't appear to affect translation. Strangely, mutation of two uAUGs in the *Lnx1_variant 1* 5'UTR seemed to decrease protein production somewhat, a result that cannot be explained, at present.

In addition to identifying a role for uORFs in suppressing translation of *Lnx1_variant 2*, evidence for an element within the 5' UTR of *Lnx1_variant 2* was found, that decreases mRNA levels and also seems to suppress translation by a mechanism independent of uORFs. At present, the underlying mechanisms of these effects are unknown, but it is clear that expression of LNX1p70 protein is tightly regulated by sequences present in the 5' UTR of the *Lnx1_variant 2 mRNA*. The assays did not reveal such inhibitory effects for the 5' UTR of *Lnx1_variant 1* or *Lnx2*, suggesting that other mechanisms operating at the level of protein translation may contribute to the low endogenous levels of these proteins. Possible regulatory mechanisms could include microRNAs, or natural antisense transcripts that may cause repression of translation.

Another explanation for low levels of LNX1 p80 and LNX2 protein could be that LNX proteins have a short half-life. Proteasomal degradation is a likely pathway for LNX1p80 and LNX2 turnover, since they contain a RING domain that, at least for LNX1, has been shown to have

ubiquitin ligase activity. It was found that LNX1p80 levels double in 6 hours following proteasomal inhibition, suggesting that there is significant, ongoing, proteasomal degradation of LNX1. However, similar results for a mutant LNX1, that lacks ubiquitin ligase activity, implicate ubiquitination by another E3 enzyme, rather than LNX auto-ubiquitination in this process. One caveat to this observation is that proteasomal degradation of transiently transfected LNX in these experiments may be elevated, compared to that of endogenous protein. A decline in LNX1p80 levels within 8 hours following cycloheximide treatment also indicates that LNX1p80 is turned over at an appreciable rate. To definitively determine that this observation is, in fact, due to protein turnover - and not as a result of cycloheximide-induced cell death, it would be important to conduct a cell viability assay in the future. It appears, however, that protein turnover, mediated at least in part by proteasomal degradation, may thus contribute to the very low levels of endogenous LNX1 proteins that are observed *in vivo*.

The low expression levels of LNX1 and LNX2 proteins, and the identification of mechanisms that negatively regulate LNX1p70 protein expression, has implications for understanding LNX protein function. It may be that LNX proteins have a very general function in the many tissues for which *Lnx* mRNA expression has been reported, but that they are only required at extremely low levels, and that excess LNX protein expression may be deleterious. Alternatively, synthesis of LNX proteins may simply be suppressed and be non-essential under most circumstances, in order to allow them to play a very specific role in certain cell types or scenarios, when inhibition of LNX protein production is relieved. One may speculate that some such mechanism may exist to overcome the effects of uORFs, or other inhibitory elements in cells that exhibit significant levels of LNX proteins, such as perisynaptic Schwann cells (LNX1p80) and spermatazoa (LNX1 and LNX2). Notably, amplification of the *Lnx1* and *Lnx2*

genes have been reported in gliomas and colorectal cancer respectively. Any transcriptional or post-transcriptional inhibition of protein synthesis would also have to be overcome if amplification of *Lnx* genes is to result in LNX protein overexpression in these cancers. Overall, the identification of mechanisms that regulate LNX protein expression is a significant step toward understanding the physiological functions of these enigmatic proteins and their postulated roles in diseases such as glioma, colorectal cancer, Kawasaki disease and Q fever [43, 61, 70, 71, 73, 74].

Chapter 3: Characterisation of LNX1 & LNX2 protein interactomes

3.1 Introduction

Ligand of Numb protein X1 (LNX1) was first characterised based on its ability to bind to the cell fate determinant protein, Numb [24]. This ability is shared by the closely related LNX2 protein [25]. LNX1 and LNX2 have the same domain structure, comprising an amino-terminal RING (Really Interesting New Gene) domain, a Numb-binding motif (NPAY or NPAF) and four carboxyl-terminal PDZ (PSD-95, DlgA, ZO-1) domains (Figure 2.1A). Two major isoforms of LNX1 have been described; LNX1p80 and a shorter, brain-specific, LNX1p70 isoform, that lacks the RING domain. LNX1p80, through its RING domain, can ubiquitinate specific isoforms of Numb, thereby targeting Numb for proteasomal degradation [26, 46]. Studies of *Lnx* expression showed a widespread distribution of *Lnx*1 and *Lnx2* mRNAs in several adult tissues, with the earliest embryonic expression of both genes being observed in the central nervous system (CNS) [24, 25]. These observations suggest a role for LNX1 and LNX2 in neural development, possibly through their interaction with Numb – an important regulator of neurogenesis and neuronal differentiation. However, LNX proteins are present at very low levels in the brain and other tissues ([40], P.Y. unpublished observations) – hence the *in vivo* significance of the LNX-Numb interaction remains unclear.

The combination of a RING and one or more PDZ domains is a unique feature of the LNX family [21]. PDZ domains function as protein-protein interaction modules, most commonly binding to the carboxyl-termini of other proteins. Wolting et al. [59] compiled a list of 220 LNX-interacting proteins both from their own work and the published literature, while a subsequent study by Guo et al. [51] added approximately 30 additional proteins to this list. Most of these interactions are PDZ domain-mediated and were identified using either yeast-two hybrid assays or arrays of PDZ domains and PDZ-binding motifs. To date, only a small number of the described LNX-interacting proteins have been shown to be substrates for

ubiquitination by LNX. For example, ubiquitination of c-Src and PBK (PDZ binding kinase) by LNX1 targets them for proteasomal degradation [40, 51], while LNX-mediated ubiquitination of claudins and CD-8α appears to cause their internalisation from the cell surface, via endocytic pathways [41, 52]. Nevertheless, these examples indicate that the ubiquitin ligase activity of LNX proteins can be targeted to specific substrates via PDZ-mediated interactions. Given the low and potentially cell-type restricted expression patterns of LNX proteins [40, 44], the identification of physiologically relevant interacting proteins and substrates will be key to elucidating the *in vivo* functions of LNX proteins.

To gain further insights into the poorly understood LNX proteins, the molecular interactions of LNX proteins in mammalian cells and tissues were examined under conditions that are more physiologically relevant than previous studies. To that end, LNX1 and LNX2 interactomes have been characterised using affinity purification and mass spectrometry. The results validate some known LNX interactions and identify a significant number of new ones. Analysis and comparison of the LNX1 and LNX2 interactomes described here provides valuable clues about both the common and unique functions of these closely-related proteins *in vivo*.

3.2 Materials & Methods

3.2.1 Reagents and cell lines

All salts and reagents were purchased form Sigma-Aldrich (Arklow, Ireland) unless otherwise stated. Restriction enzymes, T4 DNA ligase and pre-stained molecular weight markers were purchased from New England Biolobs (Hitchin, UK). Immobilon® PVDF (polyvinylidene difluoride) membrane was obtained from Millipore (Carrigtwohill, Cork, Ireland). dNTPs, Phusion™ Hot Start II DNA Polymerase, Pierce™ BCA Protein Assay Kit, GelCode™ Blue Safe Protein Stain, Pierce™ ECL Western Blotting Substrate, Pierce™ CL-XPosure™ Film and Pierce™ Protein A/G Plus Agarose beads were procured from Thermo-Fisher Scientific (Dublin, Ireland). Proteinase K, cOmplete™ protease inhibitor cocktail tablets and DNase I were purchased from Roche Applied Sciences (Dublin, Ireland). GFP-Trap®_M were purchased from ChromoTek GmbH (Planegg-Martinsried, Germany). Glutathione-sepharose® 4B beads were obtained from GE Healthcare (Carrigtwohill, Cork, Ireland). HyperLadder™ I and IV, agarose and IPTG were procured from Bioline (London, UK) through Medical Supply Company Ltd. (Dublin, Ireland). MG132 was purchased from Caltag Medsystems (Buckingham, UK). SafeView™ nucleic acid stain was obtained from NBS Biologicals (Huntingdon, UK). QIAprep® Spin Miniprep Kit was purchased from Qiagen (Manchester, UK). Pureyield™ Plasmid Midiprep System was procured from Promega (Wisconsin, USA) through Medical Supply Company Ltd. (Dublin, Ireland). *Taq* DNA polymerase used routinely for PCR amplifications was prepared in-house following a protocol obtained from Charles Spillane, NUI Galway, Ireland. Primers and oligonucleotides designed by us for this study were purchased from Integrated DNA Technologies, Inc. (Leuven, Belgium). Human Embryonic Kidney 293T (HEK 293T) and MCF-7 cells were originally purchased from ATCC, and were received as kind gifts from Prof. Rosemary O' Connor (University College Cork, Ireland).

3.2.2 cDNA constructs and cloning

The coding sequences of *Lnx1* (p80 isoform) and *Lnx2* were cloned into the pEGFP-C2 vector (Clontech). Empty pEGFP-C2 vector was used to express EGFP alone. LNX1 sequences in pEGFP-C2, for mapping interactions, encoded the following amino acids (aa): RING-NPAY motif, aa1-277; PDZ1-4, aa268-728; PDZ1, aa271-384; PDZ2, aa377-470; PDZ3, aa500-598; PDZ4, aa630-725. Constructs encoding the second PDZ domains of LNX1 and LNX2, corresponding to aa377-470 and aa330-423 respectively, were cloned into the vector pET24d-GST to produce GST-tagged proteins. Coding sequences for LNX interacting proteins were cloned into the vectors pCMV-N-HA or pCMV-N-FLAG to produce proteins with amino-terminal HA and FLAG tags respectively. For ubiquitination assays, the coding sequences for *Lnx1* (p80 and p70 isoforms) and *Lnx2* were cloned into the pCMV mammalian expression vector to eliminate possible interference from an epitope tag. An expression plasmid encoding HA-ubiquitin was a generous gift from Dr. J. McCarthy (University College Cork, Cork, Ireland). Cloning procedures employed have been described elsewhere [44]. Sequences were verified by GATC Biotech (Konstanz, Germany).

3.2.3 Antibodies

The following commercially available antibodies were used at the indicated dilutions: anti-green fluorescent protein (GFP, catalogue number ab290, Abcam, 1:3000 dilution), anti-FLAG (catalogue number F3165, Sigma-Aldrich, 1:2000 dilution), anti-GST (Glutathione-S-Transferase, catalogue number G1160, Sigma-Aldrich, 1:1000 dilution), anti-HA (catalogue number MMS-101R, Covance, 1:1000 dilution), anti-HA (catalogue number sc-805, Santa-Cruz Biotechnology, 1:1000 dilution), anti-LIPRIN-α1 (catalogue number ab26192, Abcam, 1:500 dilution), anti-LIPRIN-α3 (catalogue number 169102, Synaptic Systems, 1:1000

dilution), anti-KIF7 (catalogue number ab95854, Abcam, 1:1500 dilution), anti-AKAP13 (catalogue number NB100-68214, Novus Biologicals, 1:500 dilution), anti-NUMB (catalogue number NB500-178, Novus Biologicals, 1:7500 dilution), anti-β-actin (catalogue number A5441, Sigma-Aldrich, 1:3000 dilution). The guinea pig polyclonal anti-LNX antibodies that are either LNX1-specific (anti-LNX1-PDZ3/4) (1:100 dilution), or that recognize both LNX1 and LNX2 (anti-LNX1/2-PDZ3/4) (1:400 dilution) have been described previously (Young et al., 2005) and were used for immunostaining and immunoblotting respectively. Secondary antibodies were from Jackson ImmunoResearch Laboratories (West Grove, PA, USA) and LI-COR Biosciences (Cambridge, UK).

3.2.4 Animals and tissue harvesting

Brain lysates were prepared from P16 C57/BL6J mice that were bred and housed at University College Cork as per institutional guidelines set by the University College Cork Animal Experimentation Ethics Committee and conducted under license issued by the Department of Health and Children in accordance with the European Union Directive 2010/63/EU for animals used for scientific purposes.

Mice were anesthetized by isofluorane inhalation and perfused through the left ventricle of the heart using a peristaltic pump. Ice-cold phosphate buffered saline (PBS) (pH 7.4) was used to flush out blood from all vessels and tissues. Whole brains were harvested and snap-frozen in liquid nitrogen prior to storage at -80 ^{o}C.

3.2.5 Expression and purification of GST-LNX1-PDZ2 and GST-LNX2-PDZ2

Expression constructs encoding GST, GST-LNX1-PDZ2 and GST-LNX2-PDZ2 described in section 3.2.2 were transformed into *Escherichia coli* BL21 cells. Protein expression was induced at 37 ^{o}C by addition of 0.1 mM isopropyl-β-D-thiogalactopyranoside (IPTG) and cells were harvested 4 h post induction. Cells pellets were resuspended in PBS, 0.2% Triton X-100, 20 mM β-mercaptoehanol and 1 mM PMSF. Cells were lysed by addition of 0.1 mg/ml lysozyme for 30 min on ice, followed by 0.1 mg/ml DNase I for a further 10 min on ice, before finally sonicating. Lysates were cleared by centrifugation at 10,200 rpm for 30 min at 4 ^{o}C. For GST purifications, the supernatent were loaded on a glutathione-sepharose® 4B column, pre-equilibrated with wash buffer (PBS, 0.1% Triton X-100, 5 mM β-mercaptoethanol). Columns were washed twice with 10 ml wash buffer and bound proteins were eluted in 10 mM glutathione, 50 mM Tris-HCl, pH 8.0.

3.2.6 Cell culture conditions

Cell culture was performed under sterile conditions using biological safety class II vertical laminar flow cabinets. Cells were maintained in Dulbecco's Modified Eagle Media (Sigma-Aldrich, catalogue number D6429) supplemented with 10% foetal bovine serum (FBS), 2mM L-glutamine and antibiotics (100 units/ml penicillin and 50 μg/ml streptomycin). Cells were grown as a monolayer in 10 cm tissue culture dishes, in a humidified 37 °C incubator with 5% CO_2.

3.2.7 Cryopreservation and recovery of cell lines

For cryopreservation cells were collected as described in section 3.2.8. Cells from a 80% confluent 10 cm tissue culture dish were resuspended in 3 ml complete media supplemented with 10% dimethyl sulphoxide (DMSO) and aliquoted into cryopreservation vials. Vials were stored at -80 ^{o}C overnight and were then transferred for long term storage in liquid nitrogen. When recovering cells from liquid nitrogen, vials were thawed at 37 ^{o}C and then the cell suspension was carefully added dropwise to 10 ml complete media in a 10 cm tissue culture dish, and incubated overnight in a 37 ^{o}C, 5% CO_2, 95% air incubator. The following day, cells were trypsinised as outlined in section 3.2.8 and the entire cell suspension re-plated.

3.2.8 Maintenance of established cell lines

Cells were routinely passaged at approximately 80% confluence to prevent outgrowth and loss of surface contact in culture flasks. The cells and media used are described in sections 3.2.1 and 3.2.6 respectively. To passage, cells were washed once in PBS and incubated with 1 ml trypsin-ethylenediamine tetra-acetic acid (trypsin-EDTA). Once detached cells were collected in 3 ml complete media (media supplemented with 10% (v/v) fetal bovine serum (FBS), 2 mM L-glutamine and antibiotics (100 units/ml penicillin and 50 μg/ml streptomycin) which inactivates the trypsin. Cells were centrifuged at 1000 rpm for 5 min. Media and trypsin-EDTA were aspirated off and the cell pellet resuspended in complete media for passaging or plating. To accurately seed cell culture dishes or plates with a known number of cells, cells were counted using a haemocytometer.

3.2.9 Seeding and transfection of cells

7.5×10^5 HEK293T cells were seeded per well of a 6-well plate and transfected the following day with 2 µg of DNA constructs using the calcium phosphate precipitation method [82]. Media was changed 18 h post-transfection or, for ubiquitination assays, 20 h post-transfection for 6 h treatment with 10 µM MG132, a potent proteosome inhibitor. 24-48 h post transfection, cell cultures were washed twice in ice-cold PBS and then detached from plates by gentle scraping in 1 ml PBS. Cells were pelleted by centrifugation at 4000 rpm for 3 min at 4 °C.

3.2.10 Protein extraction from mammalian cells

For all assays, except for ubiquitination assays (section 3.2.20), cells were lysed in lysis buffer (10 mM Tris/Cl pH 7.5; 150 mM NaCl; 0.5 mM EDTA; 0.5% NP-40 and 1x cOmplete protease inhibitors (Roche Applied Sciences) for 30 min on ice. Post incubation, lysates were centrifuged at 16 000×*g* for 30 min at 4 ºC.

3.2.11 Determination of protein concentration in mammalian cells

The concentration of protein in cell lysates was determined using the Pierce™ bicinchoninic acid assay (BCA) Protein Assay Kit (Thermo-Fisher Scientific), a colorimetric detection and quantification protocol, as per manufacturer's instructions. A protein standard curved was generated using BSA at concentrations of 2000, 1500, 1000, 750, 500, 250, 125 and 25 µg/ml. 100 µl of BCA working reagent was added to 5 µl of cell lysate or standard, in triplicate in a 96-well plate. The plate was incubated at 37 ºC for 30 min in the dark. The absorbance was measured at 562 nm on a microplate reader (Tecan Group Ltd., Männedorf, Switzerland).

3.2.12 SDS-PAGE

Protein concentration in the samples were quantified as described in section 3.2.11 and samples were prepared by combination with 2X, 3X or 5X SDS gel loading buffer (1X: 50 mM Tris-HCl pH 6.8, 2% (v/v) SDS, 10% (v/v) glycerol, 0.1% (w/v) bromophenol blue, 5% (v/v) β-mercaptoethanol). In order to denature the protein, samples were heated at 95 ^{o}C for 5 min prior to loading equal concentrations of extracts on SDS-PAGE gels of varying percentages. 3 µl of prestained protein ladder (catalogue number P7708S, New England Biolabs) was also added to the gel as a marker of protein size. Samples were electrophoresed at 100 V in running buffer (25 mM Tris, 192 mM glycine, 0.1% (v/v) SDS). The gel was then either subjected to Coomassie blue staining (section 3.2.13) or to further processing and Western immunoblotting (section 3.2.14).

3.2.13 Coomassie blue staining

SDS-PAGE gels were rinsed thoroughly with water and stained in Gel-Code™ Blue Safe Protein Stain (Thermo-Fisher Scientific) at room temperature with gentle shaking for 1 h. The stain was discarded and the gel washed in deionised water twice, for 1 h each, with gentle shaking. The stained gel was visualised using an Odyssey infra-red imaging system (LI-COR Biosciences, Cambridge, UK).

3.2.14 Western immunoblotting

The proteins from the SDS- PAGE (section 3.2.12) were transferred to Immobilon® membrane (Millipore) by electroblotting at 100 V in cold transfer buffer (25 mM Tris, 192 mM glycine, 20% (v/v) methanol). After transferring, Ponseau S stain was applied to verify successful

protein transfer and then washed off using distilled water. Protein-containing membranes were washed briefly (2-3 min) in TBST (10 mM Tris, 150 mM NaCl, 0.05% (v/v) Tween 20, pH 7.4) and then blocked in 4% (w/v) fat free milk powder dissolved in TBST (blocking buffer) for 1 h at room temperature. Primary antibody incubation was performed overnight at 4 ^{o}C in a humidified chamber. The membrane was washed three times in TBST, for 5 min each, at room temperature, whilst shaking. Secondary antibody incubation was performed at room temperature, in a dark container, for 1 h, whilst shaking. The membrane was then washed three times, twice in TBST and once in TBS (10 mM Tris, 150 mM NaCl, pH 7.4), for 5 mins each, whilst shaking. Primary and secondary antibodies were diluted in blocking solution. The blot was visualised using either an Odyssey infra-red imaging system (LI-COR Biosciences, Cambridge, UK), where a fluorescent secondary antibody was used, or by enhanced chemiluminescence (ECL), where peroxidase secondary antibodies were used, following the manufacturer's instructions. Briefly, equal quantities of the two solutions from the Pierce™ ECL Western blotting substrate kit (Thermo-Fisher Scientific) were mixed and poured onto the membrane. After 1 min, the excess ECL substrate was drained off and films were exposed for various lengths of time ranging from 5 sec to overnight prior to development using a table top film processor (Agfa CP 1000).

3.2.15 Immunocytochemistry

Sterile glass coverslips were coated, by incubation, with 0.1 mg/ml poly-D-lysine solution for 30 min. Coverslips were then washed ten times with sterile water and allowed to dry. Cells were seeded onto coated coverslips at a cell density of 2.5×10^5 and allowed to adhere overnight. 24 h post-transfection cells were washed twice in PBS and were fixed with 4% PFA for 10 mins at room temperature. After fixation, cells were washed three times in PBS for 5

min each and permeabilised and blocked in blocking solution (PBS containing 0.2% Triton X-100, 5 % normal goat serum and 2% bovine serum albumin) for 1 hr at room temperature. Coverslips were then incubated with the indicated primary antibody for 3 hr at room temperature, washed in PBS three times and incubated with the appropriate secondary antibody for 1 hr, in the dark, at room temperature. All antibodies were diluted in PBS containing 5% (v/v) normal goat serum and 2% (v/v) bovine serum albumin. For antibody dilutions see section 3.2.3. Following three washes with PBS for 5 min each, the coverslips were mounted onto glass slides using Fluoromount™ and dried overnight before imaging. Cells were imaged using a Leica DMI 3000 microscope (Leica, Milton Keynes, UK).

3.2.16 Purification of LNX1 complexes from stably transfected cells

HEK 293T cells, cultured under standard conditions, were transfected with GFP and GFP-LNX1 expression constructs using calcium phosphate precipitation, and stable cell pools were selected using G418 antibiotic. To purify GFP-LNX1 and GFP protein complexes, ten confluent 15 cm diameter dishes of cells were harvested and GFP affinity purifications performed using magnetic GFP-Trap®_M beads, as per manufacturer's instructions (ChromoTek GmbH). Purified complexes were separated by gel electrophoresis and stained using GelCode^{TM} Blue Safe Protein Stain (Thermo Scientific Pierce). Each lane was cut into slices for mass spectrometry analysis.

3.2.17 Purification of LNX1-PDZ2 and LNX2-PDZ2 complexes from brain lysates

To prepare brain lysates, 0.8 g of brain tissue from P16 mice was resuspended in 2.5 volumes (w/v) of lysis buffer (10 mM Tris/Cl pH 7.5; 150 mM NaCl; 0.5 mM EDTA; 0.5% NP-40 and 1x cOmplete™ protease inhibitors (Roche Applied Sciences)). After homogenisation using a Dounce homogeniser, the samples were incubated on ice for 30 mins with frequent agitation. Samples were then clarified by centrifugation at 16 000×*g* for 30 min at 4°C. The supernatant was collected and diluted to a final volume that was 10 times the weight of the tissue in lysis buffer lacking NP-40. GST, GST-LNX1-PDZ2 and GST-LNX2-PDZ2 recombinant proteins were produced in *Escherichia coli* BL21 cells, purified with glutathione-sepharose® 4B beads (GE Healthcare) (section 3.2.5) and dialysed into binding buffer (20 mM Tris pH7.5, 50 mM NaCl, 5 mM β-mercaptoethanol). 300 µl of 58 µM GST or GST fusion protein was incubated with 1 ml of brain lysate for 90 min at 4 °C. 40 µl of glutathione-sepharose beads were added, incubated for 10 min at 4 °C with rotation and washed three times in binding buffer for 5 min each at 4 °C. Bound proteins were eluted in 10 mM glutathione, 50 mM Tris/Cl pH 8. Purified samples were prepared for mass spectrometry analysis as described above for LNX1 complexes.

3.2.18 Identification of Proteins by Peptide Fragment Fingerprinting (PFF)

PFF was performed at the FingerPrints Proteomics Facility, University of Dundee, Scotland, UK. Protein identification and data analysis was performed as previously described. In brief, peptides were obtained using an in-gel digestion protocol and extracted prior to analysis by 1D nLC-MS/MS using an LTQ Orbitrap Velos Pro mass spectrometer (Thermo Scientific, Hemel Hempstead, United Kingdom). MS/MS data was searched against the IPI-human or mouse

database (European Bioinformatics Institute ***www.ebi.ac.uk***) using in-house Mascot software (Matric Science, London, UK). Proteins identified in LNX complexes, but not in the control samples, were ranked according to Mascot protein scores and listed using protein symbols as identifiers. A Mascot protein score of 100 was then applied as a cut off value to limit results to proteins that have been reliably identified, and probable environmental contaminants or false positives (Trinkle-Mulcahy *et al*, 2008; www.peptracker.com) were eliminated as previously described [83].

3.2.19 Characterisation of interactions by GFP pull-down assays.

Expression vectors encoding GFP-tagged LNX1 or LNX2 constructs, or GFP alone, were transfected into HEK 293T cells, together with constructs encoding a LNX interacting protein. Cultures were harvested 24 - 48 h post-transfection, and GFP affinity purification performed using 10µl GFP-Trap_M® beads (ChromoTek GmbH) essentially according to the manufacturer's protocol. In some cases, the stringency of the wash conditions were increased by increasing the sodium chloride concentration in the standard wash buffer up to 500 mM. Protein were eluted by boiling in 2X SDS sample buffer and analysed by Western blotting.

3.2.20 Ubiquitination assays

Pellets were resuspended in 100 µl 1% (w/v) Sodium Dodecyl Sulfate (SDS) supplemented with 15 mM N-ethylmaleimide (NEM) and 1× cOmplete™ protease inhibitors (Roche Applied Sciences), and boiled for 5min. Following cooling on ice, samples were diluted with 900 µl of ice cold buffer that contained 50 mM Tris (pH 8.0), 150 mM NaCl, 1% Triton, 0.5% sodium deoxycholate, 50 mM sodium fluoride, 0.1 mM sodium orthovanadate and 1× cOmplete™ protease inhibitors (Roche Applied Sciences). Lysates were cleared by centrifugation at 13,000 rpm for 30 min at 4 °C. The supernatant was collected and protein concentrations were

determined. Equivalent amounts of lysates were immunoprecipitated overnight at 4 °C, with rotation, using 0.5 μg of the indicated antibody, followed by incubation with 20 μl Protein A/G agarose beads (Thermo Scientific Pierce) for 4 h. Protein A/G agarose beads were washed three times in the dilution buffer. Proteins were eluted by boiling the Protein A/G agarose in 2× SDS PAGE sample buffer for 5 min and then analysed by Western blotting.

3.2.21 Analysis of functional associations of LNX interacting proteins.

To compare interactions identified here with those from previous studies, lists of interacting proteins were taken from Wolting *et al.* [59] and Guo *et al.* [51] and gene identifiers converted to gene symbols. These lists were combined and compared to the proteins identified here using Excel software. For analysis of functional associations, lists of gene symbols (from Tables 3.1, 3.2 and 3.3) were submitted to the functional annotation tool in DAVID (Database for Annotation, Visualisation and Integrated Discovery; http://david.abcc.ncifcrf.gov/) using default settings.

3.2.22 Statistical analysis

Western blot signal intensities were quantified with Odyssey V2.1 software (LI-COR Biosciences, Cambridge, UK) or ImageJ software (National Institutes of Health, Bethesda, MD, USA) in the case of fluorescent or ECL Western blot detection respectively, using β-actin as a loading control. Microsoft Excel software was used to perform two tailed Student's *t*-test to evaluate changes in ubiquitination of wild-type versus carboxyl-terminal mutant liprin-α1 when co-expressed with LNX. Data from all other assays were analysed by one-way Analysis of Variance (ANOVA) using GraphPad Prism v.6.0 (La Jolla, CA, USA), followed by

Bonferroni post-hoc test where appropriate. P values of less than 0.05 were considered significant. Unless stated otherwise, all data are presented as mean ± SEM.

3.3 Results

3.3.1 Affinity purification and identification of LNX1 interacting proteins

While many LNX-interacting proteins are known [51, 59], most were identified by yeast two-hybrid assays and protein/peptide arrays, and only a minority of these have been confirmed in mammalian cells using full-length proteins, that are targeted to their normal subcellular location. To directly identify interactions of LNX1 in a physiologically relevant context, stably-transfected HEK cell pools expressing GFP-tagged LNX1p80 were established. LNX1-containing protein complexes were then affinity purified from these cells using GFP-Trap® magnetic beads. Cells expressing GFP alone were used as a negative control for non-specific binding to either the beads or GFP tag. Purified proteins from both samples were separated by electrophoresis and analysed by nano-liquid chromatography and MS/MS mass spectrometry. Proteins were identified by searching against the IPI protein database. Non-specific interactions present in control GFP complexes, and likely false positives or environmental contaminants, were eliminated (see Materials & Methods, 3.2.18) to generate a list of over 70 proteins specifically identified in affinity purified GFP-LNX1 complexes. The well-characterised LNX1-interacting proteins Numb, Numblike and ERC2/CAST1 were specifically identified in GFP-LNX1 complexes – validating the overall approach (underlined in Table 3.1). Examination of the carboxyl-terminal sequence of proteins identified indicates that many of them potentially contain PDZ binding motifs. Particularly noteworthy were proteins containing a carboxyl-terminal cysteine residue, a motif reportedly recognised by LNX1 PDZ2.

Table 3.1. Proteomic analysis of GFP-LNX1 interacting proteins purified from HEK293 cells. The top 30 proteins identified, as ranked by Mascot score, are shown. The full table is available as an appendix (Table A3). Previously known interactions are underlined, as are carboxyl-terminal cysteine residues. [a] Indicates proteins selected for further analysis.

Gene Symbol	Mascot Score	Name	Carboxyl terminus
PPFIA1[a]	5644	Isoform 1 of Liprin-alpha-1	DSATVRTYSC
LNX1	3662	Isoform 1 of E3 ubiquitin-protein ligase LNX	TIVSWPGTFL
MID2[a]	2641	Isoform 1 of probable E3 ubiquitin-protein ligase MID2	PYVSGMKTCH
USP9X	2229	Isoform 2 of probable ubiquitin carboxyl-terminal hydrolase FAF-X	EVSPPQTKDQ
MYCBP2	1995	Probable E3 ubiquitin-protein ligase MYCBP2	CGVCRNAHTF
KIF7[a]	1131	Kinesin-like protein KIF7	GMIDVRKNPL
KLHL11[a]	1056	Kelch-like protein 11	RRVPSSQIEC
MID1	1030	Isoform 1 of Midline-1	DHLDCTEQLP
IARS	1020	Isoleucyl-tRNAsynthetase, cytoplasmic	VSVLPTTADF
PPFIA3[a]	791	Isoform 1 of Liprin-alpha-3	DGVSVRTYSC
KIF14	629	Kinesin-like protein KIF14	ECTPSRIQWV
AKAP13[a]	510	Isoform 6 of A-kinase anchor protein 13	VSAEGEEIFC
PEX1	494	Peroxisome biogenesis factor 1	FRPGQKVTLA
NUMB	438	Isoform 1 of Protein numb homolog	DLQKTFEIEL
RPL4	391	60S ribosomal protein L4	PTTEEKKPAA
NUMBL	356	Numb-like protein	DLQKTFEIEL
AP2M1	352	Isoform 1 of AP-2 complex subunit mu	GRSGIYETRC
PLEK	341	Pleckstrin	AIQMASRTGK
PPP1CA	294	Serine/threonine-protein phosphatase PP1-alpha catalytic subunit isoform 3	PPRNSAKAKK
TRIM27	279	Isoform Alpha of Zinc finger protein RFP	NHGHSMETSP
DUSP14	265	Dual specificity protein phosphatase 14	SRHLMPYWGI
TMED10	253	Transmembrane emp24 domain-containing protein 10	RFFKAKKLIE
ZNF24	248	Isoform 1 of Zinc finger protein 24	AEKLLNVVKV
ZCRB1	247	Zinc finger CCHC-type and RNA-binding motif-containing protein 1	YFSDEEELSD
AP2A1	246	Isoform B of AP-2 complex subunit alpha-1	HLCELLAQQF
LARS	244	Leucyl-tRNAsynthetase, cytoplasmic	IGDTIIYLVH
IQGAP1	242	RasGTPase-activating-like protein IQGAP1	FLLNKKFYGK
RPS27L	237	40S ribosomal protein S27-like	
CHD2	234	Isoform 2 of Chromodomain-helicase-DNA-binding protein 2	PDYNWNVRKT
ERC2	226	ERC protein 2	DQDDEEGIWA

3.3.2 Confirmation of LNX1 interacting proteins

DAVID Bioinformatics Resource was employed to identify enriched biological associations and functional annotation terms in the LNX interactomes, in an attempt to guide us towards proteins that warranted further investigation. However, as discussed later in section 3.4, numerous functional annotation terms were enriched – and while these novel associations provide useful information on the function of LNX proteins, it did not help us to identify those that most merited further investigation. We therefore chose six of those proteins that ranked among the highest in terms of peptide abundance following affinity purification and mass spectrometry for further characterisation (PPFIA1/liprin-α1, PPFIA3/liprin-α3, MID2, KIF7, KLHL11 and AKAP13). Two proteins (EPHA7 and SYNGAP) previously demonstrated to interact with both LNX1 and LNX2 in yeast two hybrid assays were also examined [84].

The specificity of the interaction of these proteins with LNX1 and LNX2 was first assessed. The indicated constructs were co-transfected into HEK 293T cells, GFP expression was confirmed by fluorescence microscopy, cell lysate was prepared and GFP-Trap® pull-down assays were performed either with GFP fused to the N-terminus of LNX1 or LNX2, or the GFP moiety alone. Bound proteins were separated on SDS-PAGE gels, transferred to membrane and visualised by Western blot analysis using the indicated antibodies (Figure 3.1). Unbound cell lysates (input lanes) were included as a control for transfection efficiency and to show that proteins of the expected sizes were expressed.

As expected from previous yeast two hybrid data, SynGAP1 and EphA7 were able to bind both LNX1 and LNX2 in a GFP pull-down assay, as was KLHL11. By contrast, the remaining five novel LNX1-interacting proteins identified in this proteomics screen interacted specifically with LNX1 but not LNX2. Importantly, no interacting protein specific signal was detected

when binding was performed with the GFP moiety alone, with the exception of SynGAP1. SynGAP1 showed some non-specific binding to the GFP tag-alone. However, despite equal amounts of SnyGAP1 in the input samples, the amount bound to the GFP-tag alone was far less than with either LNX1 and LNX2, indicating an enhanced and somewhat specific interaction with LNX 1 and LNX2.

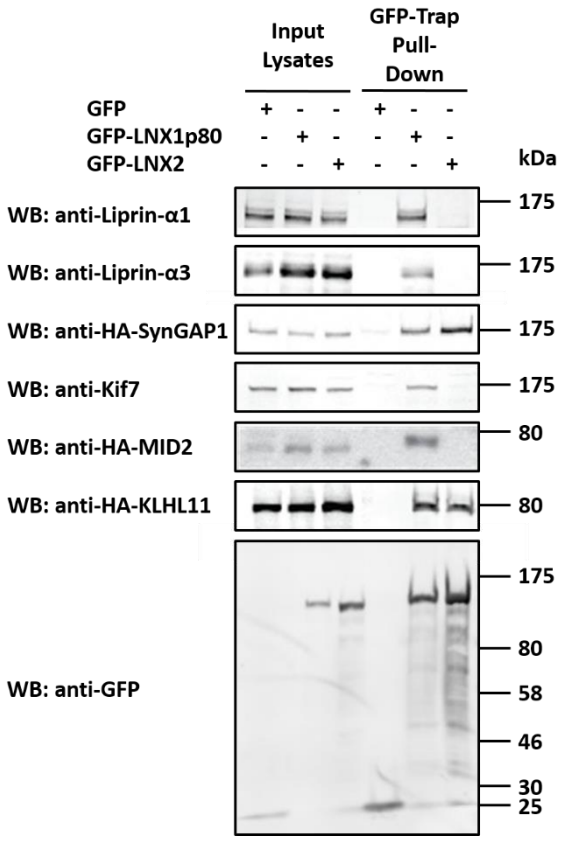

Figure 3.1: Specificity of interactions for LNX1 versus LNX2. The ability of the indicated proteins to interact with transfected GFP-tagged LNX constructs was assessed in HEK 293T cells. For each interacting protein, Western blots of cell lysates confirmed expression of the indicated construct, and the output of a GFP "pull-down" assay is shown. Binding of endogenous proteins to LNX was assessed for liprin-α1, liprina-α3, KIF7 and Numb. For the other proteins, interactions of transfected HA or GST epitope-tagged proteins were assessed. Successful expression and pull-down of GFP-tagged LNX proteins was verified in all assays by Western blot using an anti-GFP antibody, and a representative blot probed for GFP is shown (bottom panel). n = 2.

3.3.3 Mapping LNX1 interactions to regions within LNX1

To identify the region in LNX1 responsible for these interactions, GFP-epitope tagged full-length LNX1 and a series of truncation constructs indicated were constructed and their interaction with the indicated interacting protein tested by GFP-Trap pull-down assays, following cotransfection into HEK 293T cells. Amino-terminal (RING-NPAY motif) and carboxyl-terminal (PDZ1-PDZ4) fragments of LNX1, as well as constructs encoding the individual LNX1 PDZ domains, were employed to map these interactions within LNX1. Bound proteins were separated on SDS-PAGE gels, transferred to membrane and visualised by Western blot analysis using the indicated antibodies (Figure 3.2). Unbound cell lysates (input lanes) were included as a control for transfection efficiency and to show that proteins of the expected sizes were expressed. While failing to associate with GFP alone, as before, all interacting proteins bound strongly to full-length GFP-epitope tagged LNX. All the novel interactions mapped to the C-terminal PDZ domain region of LNX. By comparison, Numb was observed to bind the N-terminal fragment, as reported previously, which serves as a positive control to show that this construct was fully functional in the assay. Interactions with individual PDZ domains were generally less prominent than with full-length LNX or PDZ1-PDZ4 fragments, despite equivalent amounts of GFP-tagged LNX constructs being expressed and pulled-down in the assays. Nevertheless, the interactions of PPFIA1/liprin-α1, PPFIA3/liprin-α3, KLHL11 and AKAP13 could be clearly mapped to LNX1 PDZ2, whereas KIF7 seemed to bind PDZ2 and PDZ4. SynGAP1 showed interactions with PDZ1, and to a somewhat lesser extent PDZ2, while MID2 and EphA7 interactions could not be mapped clearly to an individual PDZ domain, indicating that these interactions are not limited to one domain of LNX.

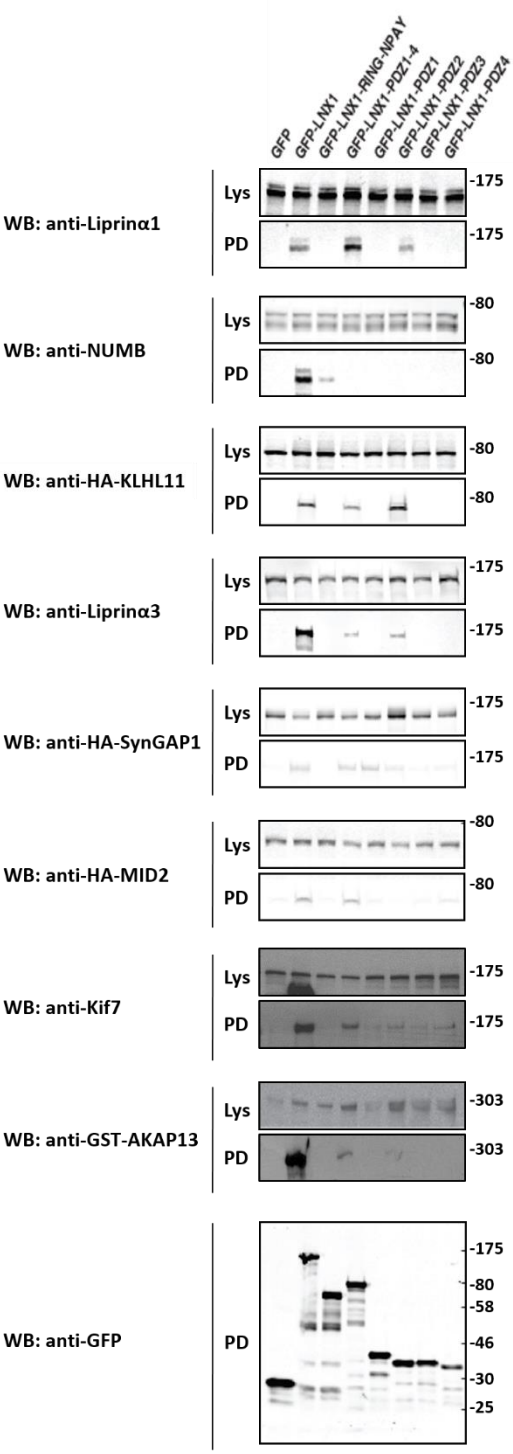

Figure 3.2: Mapping interactions to individual protein domains of LNX. The ability of the indicated proteins to interact with the various transfected GFP-tagged LNX constructs shown was assessed in HEK 293T cells. For each interacting protein, top panels show Western blots of cell lysates (Lys) confirming expression of the indicated construct, while the bottom panels show the output of a GFP "pull-down" assay (PD). Binding of endogenous proteins to LNX was assessed for liprin-α1, liprina-α3, KIF7 and Numb. For the other proteins, interactions of transfected HA or GST epitope-tagged proteins were assessed. Successful expression and pull-down of GFP-tagged LNX proteins was verified in all assays by Western blot using an anti-GFP antibody, and a representative blot probed for GFP is shown (bottom panel). n = 2.

3.3.4 Identification of LNX1 and LNX2 PDZ2 domain interacting proteins

Noting that most of the aforementioned LNX1-specific interactions identified involved PDZ2, and a large proportion of previously reported LNX1 and LNX2 interactions involve their second PDZ domain [51, 59], analysis of PDZ2 may thus be sufficient to capture a significant fraction of all LNX1- and LNX2-interacting proteins.

To compare the range of ligands that bind LNX1 and LNX2 PDZ2 in a neural context, recombinant GST-tagged PDZ2 domains were expressed, purified and used to "pulldown" interacting proteins from mouse brain lysates. The top 15 proteins identified by mass spectrometry as interacting with the PDZ domain, but not the GST tag alone, are listed in Table 3.2, with full lists available in supplementary Tables A2 and A3. In agreement with the above data, liprin-α proteins (PPFIA1, PPFIA3 and PPFIA4) were identified as LNX1-PDZ2 specific interacting proteins. KLHL11's interaction with LNX1 was also confirmed, although it was not detected in LNX2-PDZ2 complexes. The known LNX interacting proteins ERC1 and ERC2 were abundant components of both LNX1 and LNX2 complexes, as were several novel proteins such as LRRC16A, FCHSD2, FERMT2, SHPKAP, and AKAP11. Putative LNX2-PDZ2 specific interactors included SRGAP2, ATP2A2 and EML3.

Table 3.2. Proteomic analysis of GST-LNX1 and LNX2 PDZ2 domain interacting proteins purified from mouse brain lysates. The top 15 proteins, as ranked by Mascot score, are shown for each experiment. Full tables are available as appendices (Table A2 and A3). Previously known interactions are underlined, as are carboxyl-terminal cysteines. An asterisk indicates proteins identified as interacting with both LNX1 and LNX2 PDZ2 domains. . [a] Indicates proteins selected for further analysis.

Gene Symbol	Mascot Score	Name	Carboxyl terminus
A. GST-LNX1-PDZ2-interacting proteins purified from mouse brain lysates			
Erc1*[a]	7959	Erc1 ELKS/Rab6-interacting/CAST family member 1	DQDEEEGIWA
Ppfia3	4094	Ppfia3 Liprin-alpha-3	DGVSVRTYSC
Erc2*[a]	2235	Erc2 ELKS/Rab6-interacting/CAST family member 2	DQDDEEGIWA
Lrrc16a*	2180	Lrrc16a Leucine-rich repeat-containing protein 16A	EEAEKEFIFV
Fchsd2*[a]	2109	Fchsd2 FCH and double SH3 domains protein 2	KMEDVEITLV
Ppfia4	1549	Ppfia4 liprin-alpha-4	EPSTVRTYSC
Fermt2*[a]	1467	Fermt2 Fermitin family homolog 2	MFYKLTSGWV
Ppfia2	1441	Ppfia2 Liprin-alpha-2	DNSTVRTYSC
Ppfia1	1358	Ppfia1 Liprin-alpha-1	DSATVRTYSC
Ppp2r5d	968	Ppp2r5d Protein phosphatase 2A B56 delta subunit	TGSRNGREGK
Prkcc	843	Prkcc Protein kinase C gamma type	PTSPVPVPVM
Akap11*	792	Akap11 A-kinase anchor protein 11	ANRLQTSMLV
Ndrg3	749	Ndrg3 Protein NDRG3	DRHQTMEVSC
Ppp2r5c	724	Ppp2r5c Isoform 2 of Serine/threonine-protein phosphatase 2A 56 kDa regulatory subunit gamma isoform	ASELLSQDGR
Pafah1b1*	710	Pafah1b1 Isoform 1 of Platelet-activating factor acetylhydrolase IB subunit alpha	DQTVKVWECR
B. GST-LNX2-PDZ2-interacting proteins purified from mouse brain lysates			
Erc1*[a]	3181	Erc1 ELKS/Rab6-interacting/CAST family member 1	DQDEEEGIWA
Sphkap*	2692	Sphkap A-kinase anchor protein SPHKAP	EQKERTPSLF
Lrrc16a*	2270	Lrrc16a Isoform 1 of Leucine-rich repeat-containing protein 16A	EEAEKEFIFV
Fchsd2*[a]	1938	Fchsd2 Isoform 2 of FCH and double SH3 domains protein 2	KMEDVEITLV
Srgap2[a]	1935	Srgap2 SLIT-ROBO Rho GTPase-activating protein 2	PQATDKSCTV
Akap11*	1576	Akap11 A-kinase anchor protein 11	ANRLQTSMLV
Fermt2*[a]	1287	Fermt2 Fermitin family homolog 2	MFYKLTSGWV
Erc2*[a]	1139	Erc2 ELKS/Rab6-interacting/CAST family member 2	DQDDEEGIWA
Atp2a2	1125	Atp2a2 Isoform SERCA2B of Sarcoplasmic/endoplasmic reticulum calcium ATPase 2	DTNFSDMFWS
Rrbp1	1059	Rrbp1 ribosome-binding protein 1 isoform a	GSSSKEGTSV
9030409G11 Rik*	560	9030409G11Rik Isoform 1 of Kazrin	GYGSLEVTNV
Eml3	549	Eml3 Echinoderm microtubule-associated protein-like 3	SLSPASSLDV
Prkar1b*	507	Prkar1b cAMP-dependent protein kinase type I-beta regulatory subunit	RYNSFISLTV
Prkar1a*	504	Prkar1a cAMP-dependent protein kinase type I-alpha regulatory subunit	QYNSFVSLSV
Ktn1	500	Ktn1 Uncharacterized protein	EVNQQLTKET
Kcnj10	327	Kcnj10 ATP-sensitive inward rectifier potassium channel 10	SALSVRISNV

3.3.5 Verification of PDZ2 interacting proteins ability to interact with full-length LNX

The ability of a selection of these proteins to interact with full-length LNX1 and LNX2 proteins was assessed following co-transfection in cultured cells (Figure 3.3), as described above. Fchsd2, SRGAP2, ERC1 and ERC2 all interacted with both full-length LNX1 and LNX2. Notably, SRGAP2 was able to interact with full-length LNX1, even though it was only detected in LNX2-PDZ2 and not LNX1-PDZ2 complexes from brain lysates. By contrast, Fermt2 failed to directly associate with full-length LNX1 or LNX2 proteins in GFP pull-downs. This analysis thus provides a putative catalogue of both common and LNX1 and LNX2-specific interacting proteins.

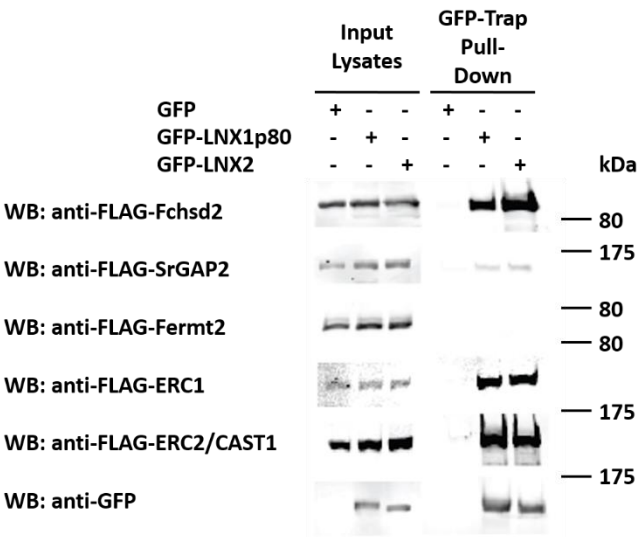

Figure 3.3: Verification of the ability of candidate interacting proteins to bind full length LNX1 and/or LNX2. Selected proteins that co-purified with either LNX1-PDZ2 or LNX2-PDZ2 from brain lysates were tested for their ability to interact with full-length, GFP-tagged LNX1 and LNX2 by GFP pull-down assays following co-transfection into HEK 293T cells. LNX interacting proteins were detected by Western blotting FLAG epitope tags. Successful expression and pull-down of GFP-tagged LNX proteins was verified in all assays by Western blot using an anti-GFP antibody, and a representative blot probed for GFP is shown (lowest box). GFP alone was used as a negative control (not visible on blots due to its small size). n = 2.

3.3.6 Investigation of colocalization events between LNX and novel interacting proteins

Physical association between these novel interacting proteins and LNX *in vivo* would demand colocalization. Immunofluorescence microscopy was used to discern the distribution pattern and potentially highlight any colocalization events.

To examine the intracellular localization of LNX1p80 in mammalian cells, a construct encoding the protein was generated and expressed in MCF-7 cells. The cellular distribution of LNX was observed in paraformaldehyde-fixed cells by indirect immunofluorescence microscopy. LNX1p80 exhibited both a cytosolic and nuclear localization (Figure 3.4A).

Where an antibody was not immediately available to directly detect a protein in immunofluorescence experiments, the cellular distribution was assessed by transfecting MCF-7 cells with a plasmid which could express an epitope (FLAG- or HA-) tagged version of the protein, and antibodies directed against the tag were used in indirect immunofluorescence experiments.

Figure 3.4A shows diffuse Liprin-α1 expression in both the cytoplasmic and nuclear compartments of transfected cells – predominantly in the former. To investigate potential colocalization with LNX, MCF-7 cells were co-transfected with LNX1 and FLAG-tagged Liprin-α1. Transfected cells, dual labelled with anti-LNX and anti-FLAG antibodies suggested colocalization events between LNX and Liprin-α1, as indicated by the yellow colour in the merged image (Figure 3.4B). This demonstrated that LNX and Liprin-α1 were targeting the same subcellular location and supports *in vivo* interaction.

Potential colocalization between KLHL11 and LNX1 in MCF-7 cells was also investigated. MCF-7 cells were transfected with a plasmid expressing an N-terminally HA-tagged version of KLHL11 either alone, or together with LNX1. Images taken of these cells by indirect immunofluorescence microscopy indicated that KLHL11 displayed a punctate, cytoplasmic distribution (Figure 3.4A). Images of co-transfected cells, dual labelled with anti-LNX and anti-HA antibodies, displayed strong colocalization between the two proteins, as indicated by almost complete overlap between the two sets of labelled punctae (Figure 3.4B).

ERC2 appeared to be diffusely distributed throughout the cell, including the nucleus, and was present to some extent in as-yet-unidentified dot-like structures (Figure 3.4A). LNX1 appeared to redistribute and colocalise with FLAG-ERC2 in these dot-like structures upon co-transfection (Figure 3.4B).

EphA7 displayed a mostly punctate, cytoplasmic distribution (Figure 3.4A). The merge image (Figure 3.4B) shows some overlapping expression with LNX, however this is most likely due to the diffuse expression of LNX rather than a site specific association between these two proteins, since colocalization was not obvious in any punctate structures where EphA7 predominantly localized.

SRGAP2 localized diffusely to both the cytoplasmic and nuclear compartments – predominantly in the latter, of MCF-7 cells. Upon coexpression, clear colocalization of LNX and SRGAP2 was observed throughout the cytoplasm and in punctate cytoplasmic structures, particularly along the plasma membrane and at some cell protrusions (Figure 3.4B)

ERC1 showed a diffuse, somewhat punctate, cytoplasmic and nuclear distribution (Figure 3.4A). Partial colocalization with LNX was evident in the cytoplasm and in punctate structures observed in a small number of cells.

FCHSD2 was distributed diffusely and predominantly in the cytoplasm – distinct to LNX, whose expression was primarily nuclear (Figure 3.4B). Furthermore, FCHSD2 failed to localise with LNX in any dot-like structures observed, suggesting that these two proteins do not colocalise – in MCF-7 cells at least.

SynGAP2 was diffusely distributed throughout the cell, including the nucleus, and appeared particularly concentrated at the plasma membrane and at sites of cell-cell contact (Figure 3.4A). Colocalization of LNX1 and SynGAP2 was apparent upon co-transfection - indicated by an overlap in staining patterns in the cytoplasm and punctate structures throughout (Figure 3.4B).

MID2 localized diffusely to both the cytoplasmic and nuclear compartments, predominantly in the former, and displayed a slightly punctate distribution pattern within transfected cells (Figure 3.4A). LNX did not colocalise with MID2 in these punctae however (Figure 3.4B), implying that cytoplasmic colocalization of LNX and MID2 is likely a consequence of the diffuse staining patterns of both proteins, rather than evidence to support their interaction.

Incidences of colocalization in specific subcellular compartments provide additional evidence for the interaction between LNX1p80 and the candidate protein, and strongly suggest a functional role of these interactions *in vivo*.

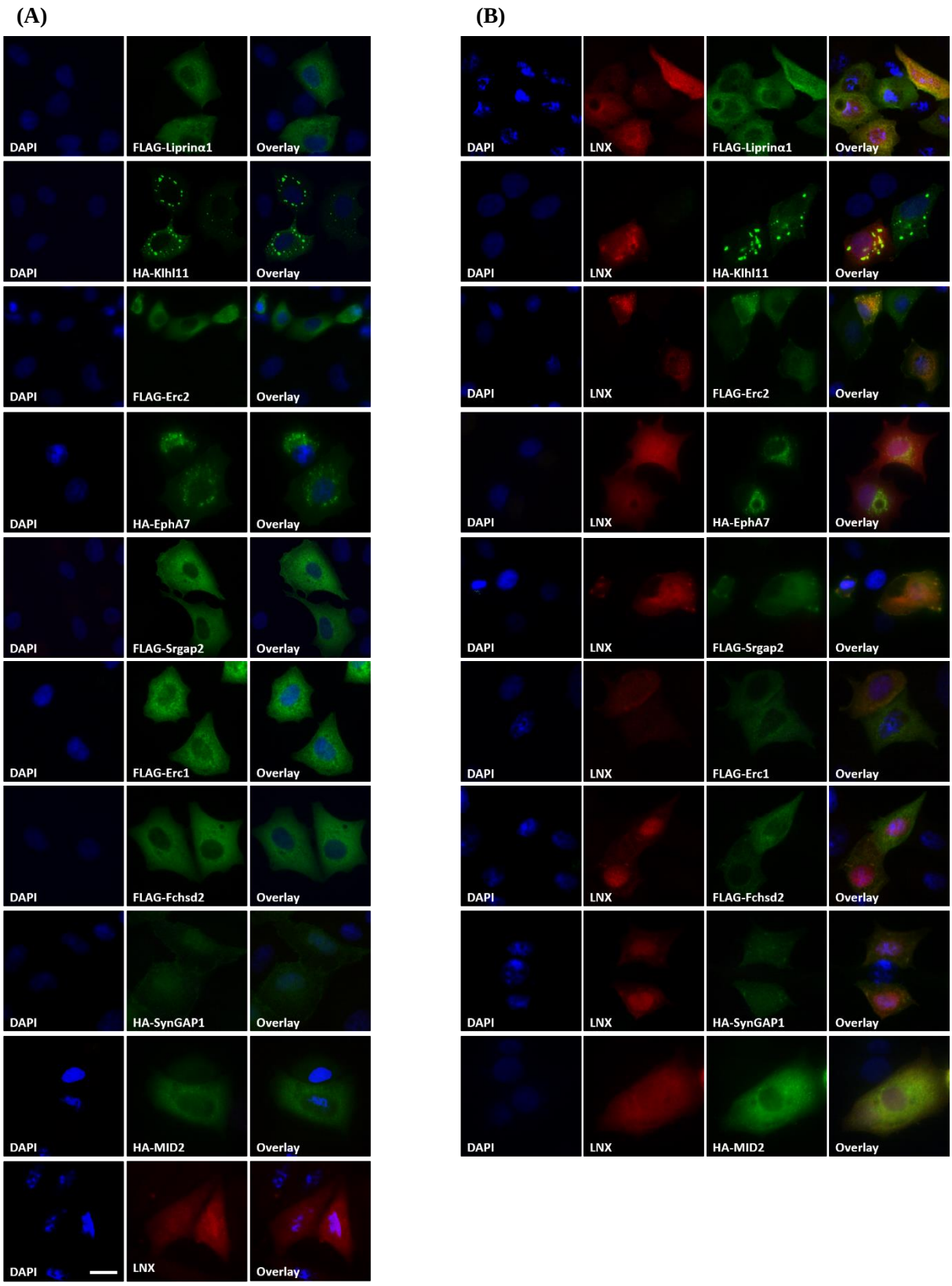

Figure 3.4: Representative of n=2 fluorescence immunocytochemistry images examining localisation of the indicated fusion proteins following transient expression in MCF-7 cells, either **(A)** individually or **(B)** in combination with LNX, for 24 h. Anti-FLAG (green), anti-HA (green) and anti-LNX (red) were used to visualize the proteins of interest. Nuclei were stained with DAPI (blue). The different wavelengths were scanned individually and digitally merged. Regions of overlap indicating colocalization are represented by yellow staining in the merged image ((B) *overlay*). Scale bar indicated 10 µm.

To identify or eliminate potential sites of localisation, a limited number of available marker antibodies for subcellular structures were employed: namely, F-actin, focal adhesions, cis-Golgi and early endosomes (supplementary Figure A1). No colocalisation events or similarities in expression pattern to those proteins in Figure 3.4 were observed, suggesting that the above proteins do not accumulate at these particular sites in MCF-7 cells.

3.3.7 Characterisation of LNX-Liprin-α1 interaction

3.3.7.1 Liprin-α1 interacts with LNX via it carboxy-terminus

Next, the LNX-binding domain of liprinα1 was examined. LNX1 PDZ2 has been reported to select peptides with a carboxy-terminal cysteine residue [58]. Furthermore, ligand positions 0 and -2 are particularly crucial for recognition and binding of PDZ domains to target proteins [85]. Since Liprin-α1 contains a PDZ binding motif with a cysteine at its C-terminus, it seemed reasonable that the C-terminal YSC residues should prove important for binding to LNX1. With this in mind, a mutant of Liprin-α1, where the C-terminal tyrosine (Y) at -2 and the hydrophobic amino acid cysteine (C) at position 0 are replaced with alanine (D) and glutamic acid (E) respectively, was generated and its binding to both full length LNX1 and also to LNX1 PDZ2, the region in LNX1 responsible for the interaction with Liprin-α1, examined by GFP-Trap pull-down assays from transfected cell lysates (Figure 3.2). As before, wild-type FLAG-Liprin-α1 interacted with full length GFP-LNX1, and to a similar extent with GFP-LNX1-PDZ2 (Figure 3.5). On the contrary, mutant FLAG-Liprin-α1 failed to interact with either full-length GFP-LNX1 or GFP-LNX1-PDZ2. These results indicate that the binding of Liprin-α1 and LNX1 is mediated through the C-terminal consensus motif of Liprin-α1 and the second PDZ domain of LNX.

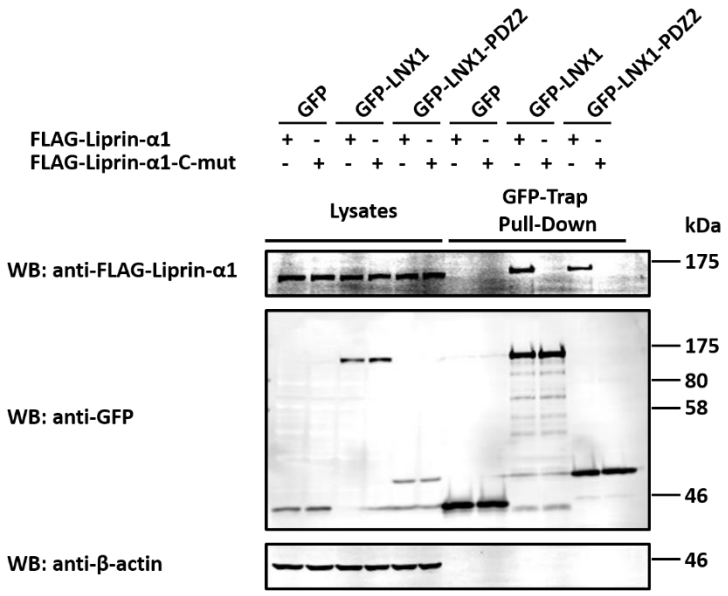

Figure 3.5: Liprin-α1 interacts with LNX1 via its C-terminus. HEK 293T cells were transiently transfected with either wild-type FLAG-Liprin-α1 or a similar Liprin-α1 construct with a carboxy-terminal YSC to DSE mutation (FLAG-Liprin-α1-C-mut) and either GFP-LNX1, GFP-LNX1-PDZ2 or GFP only for 24 h. Cell lysates were prepared and subjected to GFP pull-down assays for GFP-tagged proteins, followed by FLAG-tag immunoblotting for wild-type or mutant Liprin-α1. Western blot of whole cell lysates with the indicated antibodies confirms expression of all constructs. Successful pull-down of GFP-tagged LNX proteins was verified in the pull-down blot probed for GFP. n = 2.

3.3.7.2 LNX enhances ubiquitination of Liprin-α1

Next, an examination on whether LNX1p80 was able to ubiquitylate Liprin-α1, and also whether LNX2 was capable of ubiquitylation activity, was carried out (Figure 3.6). For this purpose, Liprin-α1, HA-tagged ubiquitin and LNX1p80 were coexpressed in HEK 293T cells. 20 hours post transfection, cells were treated for a further 6 h with the potent proteasome inhibitor MG132 prior to harvesting. To detect ubiquitination on Liprin-α1 specifically, rather than on non-covalent interacting proteins, the cell lysates were boiled in the presence of SDS to disrupt protein–protein interactions and then immunoprecipitated with anti-HA.

One-way ANOVA revealed significant differences to the ubiquitination status of Liprin-α1 in the presence of LNX ($p < 0.0001$, $F_{4,15} = 17.15$). The smear pattern of Liprin-α1 signal in the precipitates with LNX1p80 on the blotted membrane was significantly stronger than that with the control vector ($p < 0.0001$), as revealed by Bonferroni post-hoc test, indicating that LNX1p80 promotes ubiquitylation of Liprin-α1. Remarkably, when the catalytically inactive RING-finger domain mutant of LNX1p80, in which a conserved cysteine residue (C48) of the RING-finger domain was substituted with alanine (LNX1p80C48A) [26], was transfected instead of LNX1p80, Liprin-α1 was modified in anti-HA immunoprecipitates from boiled lysates compared to the control vector, although this did not quite reach significance and occurred at a much lesser extent than immunoprecipitates transfected with wild-type LNX1p80. Bonferroni post-hoc test further revealed significant ubiquitination of Liprin-α1 in immunoprecipitates transfected with the truncated LNX1p70 isoform ($p < 0.05$), which lacks the RING finger domain required for ubiquitination, or LNX2 ($p < 0.05$), compared to the control vector, and occurred at a similar level to samples transfected with the catalytically inactive RING-finger domain mutant of LNX1p80 (LNX1p80C48A).

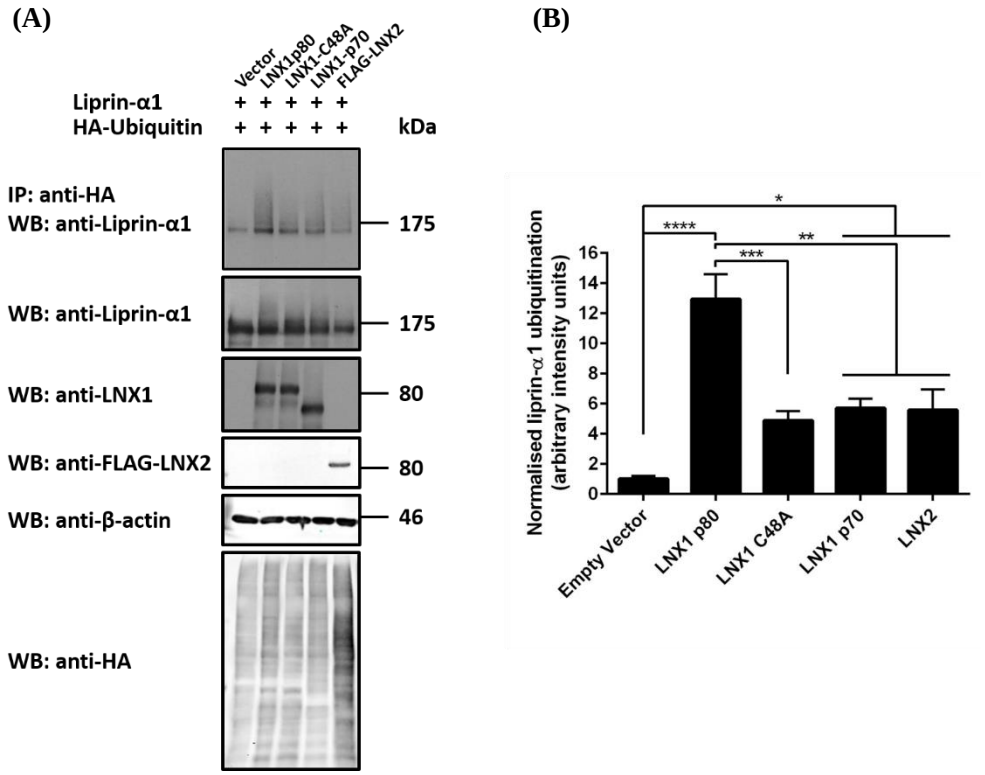

Figure 3.6: Liprin-α1 is a substrate for LNX-mediated ubiquitination. HEK 293T cells were transiently transfected with the indicated constructs. 20 h post-transfection cells were treated with 10 μm of the proteosomal inhibitor MG132 for 6 h. Under stringent SDS-denaturing conditions, cell lysates were then prepared and ubiquitinated proteins were immunoprecipitated from cell lysates using an anti-HA antibody. The ubiquitination status of liprin-α1 was then revealed by Western blot analysis using an anti-liprin-α1 antibody. **(A)** A high molecular weight smear corresponding to ubiquitinated liprin-α1 was detected, at varying levels, by Western blot (WB) for the wild-type and mutant LNX proteins. Western blot of whole cell lysates confirmed expression of all constructs. **(B)** Levels of ubiquitinated liprin-α1 were quantified by densitometry and normalised for liprin-α1 expression in whole cell lysates. Data are expressed as mean ± SEM. n = 4. *$p < 0.05$, **$p < 0.01$, ***$p < 0.001$, ****$p < 0.0001$; one-way ANOVA followed by Bonferroni post-hoc test.

3.3.7.3 LNX1p80 does not target Liprin-α1 for proteosomal degradation

The ubiquitination of cellular proteins often leads to their degradation by the proteasome. To assess possible degradation of Liprin-α1 induced by wild-type LNX1p80, FLAG-Liprin-α1, HA-ubiquitin and LNX1p80, LNX1p80C48A or vector only were cotransfected into HEK 293T cells. Western analysis of total cell lysates with anti-FLAG antibodies followed by one-way ANOVA indicated a significant effect of LNX on the levels of Liprin-α1 in transfected cell lysates (p = 0.0134, $F_{2,9}$ = 7.236) (Figure 3.7). Bonferroni post-hoc analysis, however, revealed no significant reduction of Liprin-α1 in wild-type LNX1p80 or mutant LNX1p80C48A transfected cell lysates, compared to the control vector. These results suggest that ubiquitination of Liprin-α1 by wild-type LNX1p80 does not target Liprin-α1 for proteosomal degradation.

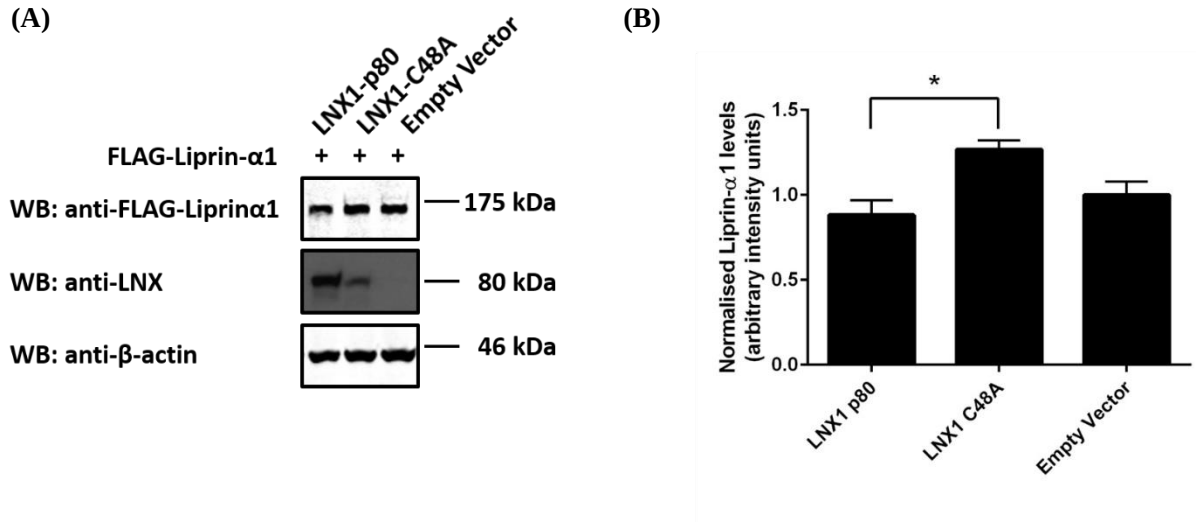

Figure 3.7: Liprin-α1 protein levels are not altered by LNX. HEK 293T cells were transiently transfected with wild-type LNX1p80, a mutant (LNX1 $p80^{C48A}$) lacking ubiquitin ligase activity or vector only and FLAG-Liprin-α1 for 24 h. **(A)** Whole cell lysates were analysed by Western blot using anti-FLAG, anti-LNX1/2-PDZ3/4 and anti-β-actin antibodies. **(B)** Liprin-α1 protein levels were quantified and normalised to β-actin levels. No significant effect of LNX on Liprin-α1 protein levels was detected by one-way ANOVA followed by Bonferroni post-hoc test. Data are expressed as mean ± SEM. n = 4.

3.3.7.4 LNX-mediated ubiquitination of Liprin-α1 is dependent on the interaction between LNX and Liprin-α1

As shown in Figure 3.5, mutation of the C-terminal YSC sequence motif of Liprin-α1 appeared to abolish its interaction with LNX. Additionally, this mutation dramatically reduced, and appeared to abrogate, LNX mediated ubiquitylation of Liprin-α1 (Figure 3.8). Densiometric analysis followed by two-way ANOVA revealed no significant LNX x Liprin-α1 interaction ($p = 0.0706$, $F_{2,8} = 3.759$). A significant effect of LNX on the ubiquitination status of Liprin-α1 was detected however ($p = 0.0410$, $F_{2,8} = 4.890$), as was a significant effect of the Liprin-α1 protein present ($p = 0.0311$, $F_{1,8} = 6.812$). A significant reduction in LNX1p80 mediated ubiquitination of Liprin-α1 was detected in samples transfected with carboxy-terminal mutant Liprin-α1 compared to wild-type liprin-α1 ($p < 0.05$). Interestingly, levels of ubiquitinated Liprin-α1 detected in LNX1p80 and LNX1p80C48A samples, cotransfected with the carboxy-terminal mutant Liprin-α1, were comparable to the vector only control suggesting that mutation of the carboxy-terminus, required for interaction with LNX, abolished the ability of LNX to enhance Liprin-α1 ubiquitination.

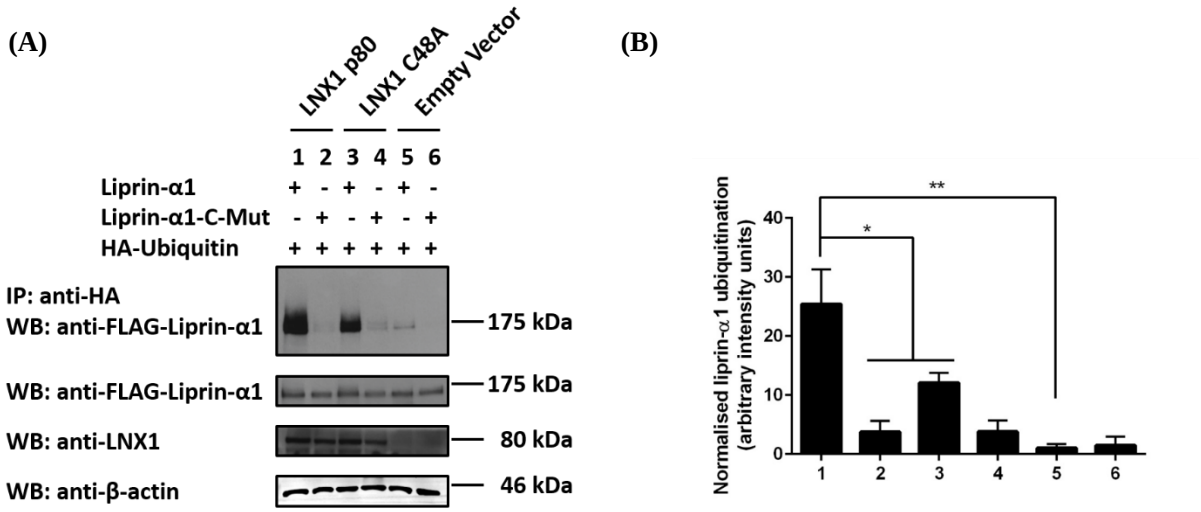

Figure 3.8: LNX-mediated ubiquitination of Liprin-α1 is dependent on the interaction of LNX and Liprin-α1, via Liprin-α1's carboxyl terminus. HEK 293T cells were transiently transfected with the indicated constructs. 20 h post-transfection cells were treated with 10 µm of the proteosomal inhibitor MG132 for 6 h. Under stringent SDS-denaturing conditions, cell lysates were then prepared and ubiquitinated proteins were immunoprecipitated from cell lysates using an anti-HA antibody. The ubiquitination status of Liprin-α1 was then revealed by Western blot analysis using an anti-FLAG antibody. **(A)** An obvious high molecular weight smear corresponding to ubiquitinated wild-type Liprin-α1, but not Liprin-α1 with a carboxy-terminal mutation, was detected by Western blot (WB) for both wild-type and mutant LNX. Western blot of whole cell lysates confirmed expression of all constructs. **(B)** Levels of ubiquitinated Liprinα1 were quantified by densitometry and normalised for Liprin-α1 expression in whole cell lysates. Data are expressed as mean ± SEM. n = 3. *$p < 0.05$, **$p < 0.01$; two-way ANOVA.

3.3.7.5 Examination of the regions of LNX required for substrate recognition of Liprin-α1

The regions of LNX required for substrate recognition were determined in HEK293T cells co-transfected with mammalian expression vectors encoding either FLAG epitope-tagged LNX1p80, the LNX truncation mutants indicated or LNX1p70, HA epitope-tagged ubiquitin and Liprin-α1. 20 h post-transfection, cells were treated for a further 6 h with 10 μm of the proteosomal inhibitor MG132. Cells were harvested under stringent denaturing conditions and the cell lysates were immunoprecipitated with and anti-HA antibody. Ubiquitination of Liprin-α1 was determined by Western blotting using an anti-Liprin-α1 antibody. In the presence of wild-type LNX and the LNX truncation mutants Liprin-α1 was modified to various degrees in anti-HA immunoprecipitates as indicated by the shift in migration of the input Liprin-α1 protein into discrete bands and a high molecular weight smear (Figure 3.9A). Densiometric analysis of immunoreactive bands and smears followed by one-way ANOVA revealed a significant effect of LNX on the ubiquitination status of Liprin-α1 ($p < 0.0001$, $F_{4,9} = 65.11$). Bonferroni post-hoc analysis revealed a very consistent and statistically significant 6-fold increase in the levels of ubiquitinated in anti-HA immunoprecipitates from cell lysates transfected with wild-type LNX1p80 compared to the vector control ($p < 0.0001$). Remarkably, expression of LNX truncation mutants enhanced polyubiquitination of Liprin-α1, albeit significantly less efficiently than wild-type LNX1p80 ($p < 0.0001$). In the presence of RING-NPAY and PDZ1-4 truncation mutants, Bonferroni post-hoc analysis revealed a significant 3-fold increase in the levels of ubiquitinated Liprin-α1 was observed in anti-HA immunoprecipitates compared to control vector ($p < 0.01$, $p < 0.05$ respectively), although the increase in ubiquitinated Liprin-α1 was not quite statistically significant in the case of LNX1p70 transfected cell lysates. The increase in ubiquitinated Liprin-α1 seen in immunoprecipitates from RING-NPAY and PDZ1-4 transfected cell lysates is similar to that observed in immunoprecipitates from cell lysates transfected with LNX1p70, which is not surprising for PDZ1-4 at least given their identical domain structure. Although PDZ1-4 can

interact with Liprin-α1 via PDZ2, like LNX1p70, it lacks the RING finger domain required for E3 ubiquitin ligase activity, and thus the increased levels of ubiquitinated Liprin-α1 seen in the immunoprecipitates from cell extracts transfected with either of these constructs can most likely be attributed to another E3 ubiquitin ligase in the cells, for which PDZ 1-4 and LNXp70 may act as a scaffold proteins to bring the two proteins within close proximity. Since the RING-NPAY construct does not encode the LNX PDZ2 domain binding site and thus cannot interact with Liprin-α1, ubiquitination observed in immunoprecipitates from cell extracts transfected with this construct is most likely as a result of indirect interaction with another cellular protein. In agreement with this notion, the isolated RING finger domain has previously been reported to function as an E2-dependent E3 ubiquitin ligase *in vitro*. Interestingly, the summation of levels of ubiquitinated Liprin-α1 in immunoprecipitates from cell extracts transfected with RING-NPAY or PDZ1-4 domains results in ubiquitination levels similar to that observed in the presence of full-length wild-type LNX1p80, which consists of both of these domains.

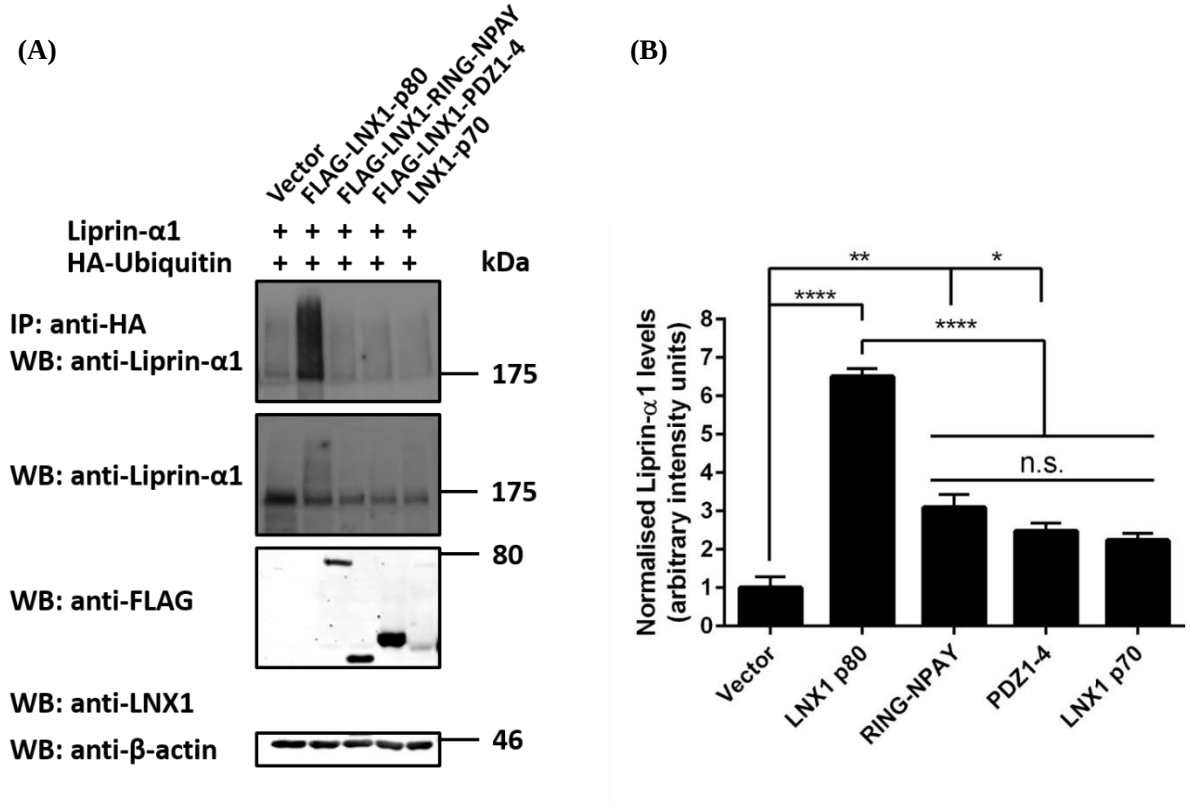

Figure 3.9: LNX truncation mutants mediate ubiquitination of Liprin-α1 to a similar extent as LNX1p70, but to a much lesser degree than LNX1p80. HEK293T cells were transiently transfected with the indicated constructs. 20 h post-transfection cells were treated with 10 μm of the proteosomal inhibitor MG132 for 6 h. Under stringent SDS-denaturing conditions, cell lysates were then prepared and ubiquitinated proteins were immunoprecipitated from cell lysates using an anti-HA antibody. The ubiquitination status of Liprin-α1 was then revealed by Western blot analysis using an anti-Liprin-α1 antibody. **(A)** A high molecular weight smear, corresponding to ubiquitinated Liprin-α1, of varying intensities, was detected by Western blot (WB) for both the wild-type and truncated mutant LNX proteins. Western blot of whole cell lysates confirmed expression of all constructs. **(B)** Levels of ubiquitinated Liprin-α1 were quantified by densitometry and normalised for Liprin-α1 expression in whole cell lysates. Data are expressed as mean ± SEM. n = 3. *$p < 0.05$, **$p < 0.01$, ****$p < 0.0001$; one-way ANOVA followed by Bonferroni post-hoc test.

3.3.8 KLHL11, KIF7 and ERC2 are substrates for LNX-mediated ubiquitination

Having shown that Liprin-α1 is ubiquitinated by LNX, a number of other novel LNX interacting proteins were also investigated as potential LNX substrates in similar cell-based ubiquitination assays. HEK 293T cells were transiently transfected with GFP-KLHL11, GST-KIF7, GFP-ERC2, or FLAG-SRGAP2, HA-Ub and LNX1p80, LNX1p70 or vector only. LNX1p80 increased ubiquitination of KLHL11, KIF-7, ERC2 and possibly SRGAP2 to a much lesser extent (appendix Figure A2, A-D respectively). As was the case for Liprin-α1, expression of LNX1p70 increased ubiquitination of KLHL11 (appendix Figure A2, A), but appeared to have no effect on KIF7, ERC2 or SRGAP2 (appendix Figure A2, B-D respectively). These results suggest a function of LNX in enhancing protein ubiquitination that is both dependent on and independent of its RING domain.

3.3.9 Interaction of LNX1 with members of the TRIM E3 ubiquitin ligase family

LNXp70 may act as a scaffold to recruit other E3 ubiquitin ligases to substrates that bind to its PDZ domains. Six E3 ubiquitin ligases (MID1, MID2, MycBP2, TRIM27, TRAF4 and DZIP3) were identified in the LNX1 interactome (Table). it was decided to further characterize some of these interactions , focusing on the three members of the tripartite motif (TRIM) family identified in the mass spectrometry data - MID1/TRIM18, MID2/TRIM1 and TRIM27. Transfected, epitope-tagged MID2 interacted with the PDZ domain region of LNX1, but this interaction could not be mapped to an individual PDZ domain (Figure 3.2). Furthermore, the histidine residue present at the carboxyl terminus of MID2 (Table 3.1) does not fit with consensus sequences for PDZ binding motifs [51, 86]. These observations suggest that MID2

does not bind LNX via a typical carboxyl terminal: PDZ domain interaction. An investigation into which part of MID2 mediates this interaction found that a region containing the FN3 and SPRY domains of MID2 is necessary and sufficient to bind LNX1, with no interaction being observed for constructs containing the RING, B-BOX, coiled-coil or microtubule binding COS domains (appendix Figure A3, A and B).

With regard to interaction of LNX1 with MID1 and TRIM27, surprisingly, no interaction with LNX1p80 was seen for transfected epitope-tagged MID1 under the same experimental conditions for which MID2 binding was observed (appendix Figure A3, C). However, when MID1 and MID2 were co-transfected with LNX1, MID1 co-purified with LNX1, suggesting that MID1 interacts indirectly with LNX1, due to its ability to heterdimerize with MID2 via the coiled coil regions of both proteins [87]. By contrast, interaction of transfected epitope-tagged TRIM27 with LNX1 was observed without having to co-transfect MID2, confirming this interaction and suggesting that it is direct rather than mediated by heterodimerization with MID2 (appendix Figure A3, D).

Given the robust interaction of MID2 with the LNX1 PDZ domains, the LNX1p70 isoform, while lacking its own RING domain, may target the ubiquitin ligase activity of the MID2 RING domain to proteins that bind the LNX1 PDZ domains. To test this hypothesize, the ability of MID2, LNX1p70 and the LNX1 ligand Liprin-α1 to form a ternary complex was examined (appendix Figure A3, D). While LNX1p70 was seen to interact strongly with GFP-tagged MID2, co-purification of Liprin-α1 with LNX1p70 and MID2 was not observed. It is thus unlikely that the recruitment of MID2 E3 ligase activity by LNX1p70 could explain the ability of LNX1p70 to promote Liprin-α1 ubiquitination. However, confirmation of the ability of

LNX1p70 to bind strongly to MID2 indicates that LNX1p70 might recruit MID2 to mediate ubiquitination of other LNX1 interacting proteins.

3.4 Discussion

In an analysis of the human PDZ domain-ligand interactions network (PDZNet), LNX1 ranked third in terms of total number of interactions [88]. The large number of interactions that have been reported for LNX1 is remarkable, given that they are not a well-studied family of proteins. Considering that LNX protein levels are tightly regulated, establishing which LNX interactions are physiologically relevant is a key challenge. To complement previous approaches, the first affinity purification/mass spectrometry-based analysis of the LNX interactome was performed in the context of mammalian cells and tissues, where expression of LNX mRNAs, and more importantly LNX proteins, is known [40, 65].

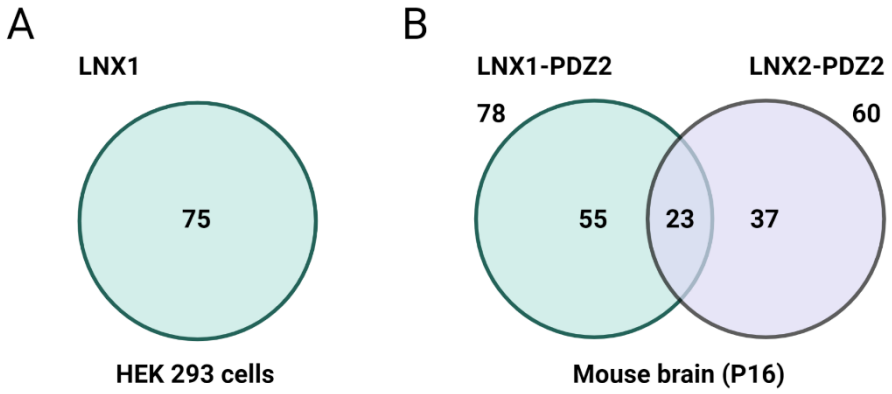

Figure 3.10: Venn diagram analysis of LNX1 and LNX2 interacting proteins purified from (A) mammalian HEK cells and (B) mouse brain lysate.

The results provide confirmation of just seven of the approximately 250 previously reported LNX interactions [51, 59]. These were AP2M1, BCR, CTNND2, ERC2, KRT15, NUMB and NUMBL (Table 3.1 and 3.2.). The identification of well-characterised interaction partners, such as Numb and ERC2, validates the methodology, and supports the veracity of these interactions. The failure to confirm more reported interactions may simply be because these

proteins are not expressed in HEK cells or P16 mouse brain tissue. However, this seems unlikely to be true in all cases, and it may be that some previously reported LNX binding protein were not detected in this study because, (1) they do not interact with full-length LNX proteins, (2) they are localised in a different subcellular compartment from LNX, or (3) they are out-competed by ligands present in the cell or tissue lysates that have a higher affinity. Thus, some interaction pairs that have been identified by yeast-two-hybrid or protein/peptide arrays may not be significant in a mammalian cellular context, with many potential ligands binding competitively to LNX proteins. In addition, indirect interactions detected by the affinity purification approach may partly explain the lack of overlap with previously identified LNX ligands. Overall though, these data confirm the propensity of LNX proteins to interact with a large number of ligands and may highlight those interactions that are physiologically relevant.

Comparative analysis of LNX1 and LNX2 interactomes

Many of the proteins identified have carboxyl terminal sequences that fit consensus sequences previously identified for LNX1 and LNX2 PDZ2 [51], suggesting that they interact with LNX proteins directly. The identification of putative LNX1 PDZ2 interacting proteins with carboxyl terminal cysteines is particularly noteworthy, with ten such proteins found in LNX1 complexes as compared to just one for LNX2 PDZ2. Notable LNX1-specific interactors with carboxyl terminal cysteines are members of the Liprin- (PPFIA1,-2,-3,-4) and N-myc downstream regulated gene (NDRG1,-2,-3) families. The LNX1-specific interaction of Liprin-α3 was confirmed in assays using full-length LNX proteins. In addition, some indirect interactions are likely to have been detected by the affinity purification approach, which may partly explain the lack of overlap with LNX ligands previously identified using methods that favoured detection of direct interactions. For example, the protein phosphatase 2A regulatory subunits (PPP2R5C

and PPP2R5D) lack a carboxyl terminal PDZ-binding consensus sequence, but are known to interact with Liprin-αs [89, 90]. This suggests that their specific co-purification with LNX1 PDZ2 may be due to an indirect interaction mediated by Liprin-α. In any case, such isoform-specific interactions, whether direct or indirect, provide clues regarding differential functions of LNX1 and LNX2 – an area that has not previously been explored.

Comparing the lists of 78 LNX1- and 60 LNX2-interacting proteins, there is considerable overlap (23 proteins) (Figure 3.10). Notable interactions common to PDZ2 of both LNX1 and LNX2 are the ELKS/Rab6-interacting/CAST family members ERC1 and ERC2. LNX1 is known to interact with ERC2 [55]. The data here confirms this and indicates that this ability is shared by LNX2. Interestingly, ERC and Liprin−α proteins interact with each other and are evolutionarily conserved core components of the presynaptic active zone complex that underpins synapse formation and maturation, as well as neurotransmitter release [91, 92]. ERC1/2 and Liprin−αs are likely to bind competitively to LNX1-PDZ2; however, LNX1 is known to dimerise [25], and so a LNX1 dimer could potentially form a tripartite complex binding both ERC and Liprin−α proteins simultaneously. Higa et al. [55] reported that LNX1 and ERC2 colocalize at nerve terminals in cultured neurons. Findings that LNX2 also binds ERC1/2, and that LNX1 binds Liprin−α, now provide further support for a potential function for LNX proteins at the active zone. While probably not abundant enough to play a structural role, they might regulate some aspect of active zone formation or plasticity. Kazrin (KAZN) was another interaction shared by LNX1 and LNX2 and interestingly has been described as belonging to the Liprin protein family [93]. The SLIT-ROBO Rho GTPase-activating proteins, SRGAP1 and SRGAP2 were co-purified with LNX1 and LNX2 PDZ2 domains respectively. However, in confirmatory assays using full-length LNX proteins, SRGAP2 bound both LNX1 and LNX2 and so was not isoform-specific in its interaction. SRGAP2 acts as a regulator of

neuronal migration, neurite outgrowth and dendritic spine formation, and plays important roles in cortical development, with human-specific duplications of SRGAP2 hypothesised to have played a role in the evolution of the human neocortex [94-97]. FCHSD2 – identified as binding to both LNX1 and LNX2 via PDZ2, is evolutionarily related to the SRGAP proteins, having in common the presence of an F-BAR and SH3 domains in its domain structure, but lacking the GTPase-activating domain. FCHSD2 is a mammalian homolog of *nwk* (*nervous wreck*) – a regulator of synaptic growth in *Drosophila* [98]. Other putative LNX1- and LNX2-interacting proteins identified include regulatory subunits of protein kinase A (PRKAR1A and PRKAR1B) and a GABA neurotransmitter transporter (SLC6A1). Overall, this analysis confirms the propensity of LNX proteins to interact with a large number of ligands via their PDZ domains and provides a catalogue of putative interacting partners that will be a valuable resource in exploring the molecular mechanism of LNX function in the CNS.

Functional annotation & gene enrichment analysis

The goal in characterising the LNX interactome was to gain insights into potential functions of these proteins and to identify differential functions of LNX1 and LNX2. DAVID Bioinformatics Resource [99] was employed to identify significant biological associations of proteins present in LNX1 and LNX1/2-PDZ2 complexes. Functional annotation terms that are enriched in the LNX1 and LNX2 interactomes include: ATP/nucleotide binding, microtubule cytoskeleton/microtubule-based process, translation/protein biosynthesis, ER-Golgi intermediate compartment, protein transport/localisation, peroxisome membrane, protein kinases, protein phosphatases, cell projection morphogenesis/organisation, synaptosome, regulation of synaptic transmission, ubiquitin conjugation pathway, cell division, zinc/RING finger domain-containing and emp24 domain-containing. Examination of the proteins identified, also reveals several incidences of multiple members of a protein family being identified. These families (with family members identified in parentheses) include: Numb

(NUMB, NUMBL), Midline probable E3 ligases (MID1, MID2), peroxisome biogenesis/assembly factors (PEX1, PEX6), tRNA synthetases (IARS, LARS, MARS, WARS), ELKS/Rab6-interacting/CAST family (ERC1, ERC2), Flotillin (FLOT1, FLOT2), Kinesin-like proteins (KIF7, KIF14, Kif5A), Liprin-α proteins (PPFIA1, PPFIA2, PPFIA3, PPFIA4), N-myc downstream-regulated gene proteins (Ndrg1, Ndrg2, Ndrg3) and Transmembrane emp24 domain-containing proteins (TMED2, TMED4, TMED5, TMED9, TMED10). These novel associations represent valuable clues regarding putative functions of LNX proteins and merit further investigation.

Potential LNX1 ubiquitin ligase independent functions

The *Lnx1* and *Lnx2* genes arose by gene duplication early in the vertebrate lineage [21]. The invertebrate *Lnx1/2-like* gene is more similar to *Lnx2*, indicating that *Lnx1* may have may have undergone neofunctionalisation following the gene duplication[21]. The expression of a LNX1 isoform in the brain, that lacks the catalytic RING domain, suggests that LNX1 may have ubiquitin ligase-independent functions [24]. Several LNX1-specific interactions (Liprin-α1 and α3, MID2, AKAP13, KIF7), that could mediate functions that are unique to LNX1, were identified.

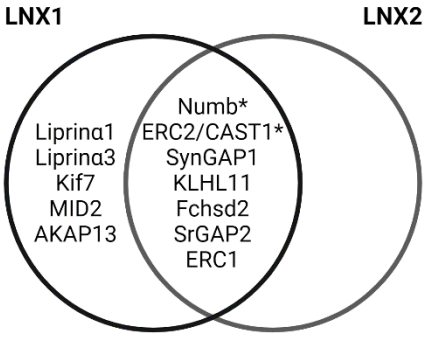

Figure 3.11: Schematic representation of novel and previously known (indicated by an asterisk) LNX interacting proteins confirmed in this study.

Liprin-α1, Liprin-α3 and AKAP13 have putative PDZ binding motifs, with a carboxyl-terminal cysteine residue, and interact specifically with LNX1-PDZ2. By contrast, KLHL11, which also has a carboxyl-terminal cysteine, could interact with both LNX1 and LNX2 when co-transfected in HEK cells, but was co-purified only with LNX1-PDZ2 (and not LNX2-PDZ2) from brain lysates. Thus, in agreement with previous reports [51], LNX1-PDZ2 seems to have a preference for ligands with carboxyl-terminal cysteines compared to LNX2-PDZ2.

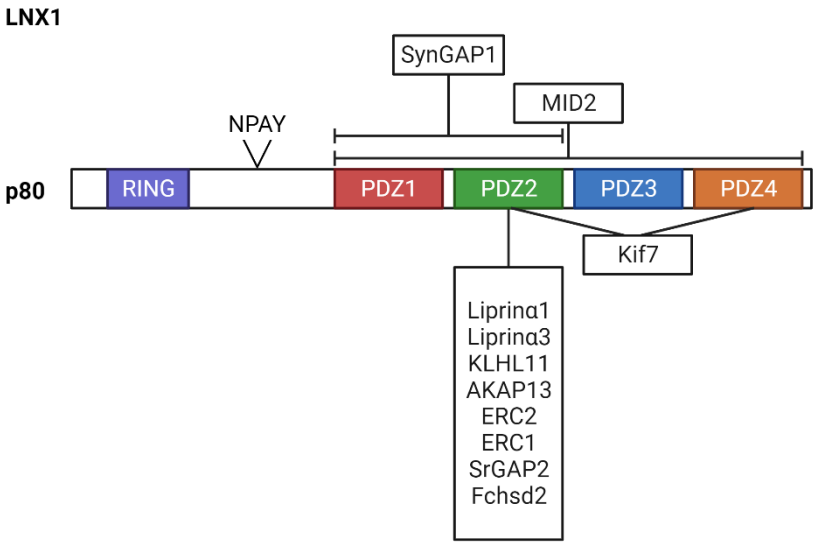

Figure 3.12: Diagram illustrating the regions of LNX1 involved in interaction with the proteins shown.

The molecular basis for the specificity of these interactions with LNX1 versus LNX2 is not obvious however, as key residues involved in ligand recognition are conserved between the PDZ2 domains of LNX1 and LNX2 [21]. and some interacting proteins with a carboxyl-terminal cysteine such as KLHL11, seem to interact equally well with both LNX1 and LNX2.

LNX1 interaction with Liprin-α1 was characterised in more detail by verifying that the interaction is dependent on the carboxyl-terminal –YSC* motif, and showing that Liprin-α1 is

a substrate for ubiquitination by LNX1p80. However, ubiquitination of Liprin-α1 by LNX1 did not significantly alter Liprin-α1 protein levels. This suggests that LNX1-mediated ubiquitination does not target Liprin-α1 for proteasomal (or lysosomal) degradation, but perhaps affects some other aspect of Liprin-α1 function. While Liprin-α1 is widely expressed in many tissues, Liprin-αs are best characterised as a component of the presynaptic cytomatrix of the active zone (CAZ) complex, that is involved in synapse maturation in neurons [100]. While LNX1p80 could ubiquitinate Liprin-α1 in non-neuronal tissues, neurons are thought to exclusively express the LNX1p70 and LNX1p62 isoforms that lack the catalytic RING domain. Surprisingly, LNX1p70 was found to promote ubiquitination of Liprin-α1, albeit to a lesser extent than LNX1p80. A similar effect was observed for ubiquitination of KLHL11.

These findings suggest that the neuronal LNX1p70 isoform may be able to recruit other E3 ligases to mediate ubiquitination of substrates that bind to its PDZ domains. Notably, six E3-ubiquitin ligases were identified in the LNX1 interactome (MID1, MID2, MYCBP2, TRIM27, TRAF4 and DZIP3) and some were identified in previous studies [101]. MID1/TRIM18, MID2/TRIM1 and TRIM27 are members of the large TRIM family of E3-ubiquitin ligases [102]. The interaction of MID2 and TRIM27 with LNX1 was confirmed, however MID1 seemed to require the co-expression of MID2 to interact with LNX1, suggesting its interaction is indirect and mediated by its known ability to heterodimerize with MID2 [87]. The MID2 interaction mapped to the PDZ region of LNX1, though not clearly to any one PDZ domain, while the FN3 and SPRY domains of MID2 are required for the interaction. The carboxyl terminal sequences of MID2 and TRIM27 are not closely related and don't match consensus PDZ binding motifs, arguing against a canonical carboxyl terminal: PDZ domain mode of binding. Since TRIM27 lacks an FN3 domain it may be the SPRY that mediates the interaction of LNX with MID2 and TRIM27. However there is evidence in the IntAct database

(http://www.ebi.ac.uk/intact/) that MID2 can dimerize with TRIM27, and so one cannot completely rule out the possibility that the interaction of TRIM27 with LNX1 might be mediated by endogenous MID2 in these experiments.

To explore whether MID2 might be responsible for the ability of LNX1p70 to promote ubiquitination of liprin-α1, the ability of these three proteins to form a ternary complex was tested. Robust binding of LNX1p70 to GFP-tagged MID2 was observed, but co-purification of Liprin-α1 was not observed in this experimental setup. It may be that binding of MID2 and Liprin-α1 to LNX1 is competitive, or that the formation of a ternary complex is very transient. While no direct evidence was observed for LNX1p70 acting to scaffold an interaction of MID2 with Liprin-α1 in this case, it will be interesting to test this hypothesis for other combinations of LNX1-interacting E3 ligases and substrates including TRIM27 and KLHL11. Such a mechanism, if proven, could explain the existence and conservation of the LNX1p70 isoform in diverse vertebrate species despite its lack of catalytic activity [21].

LNX interactomes: candidate genes with functions in neuronal development and synapse formation

Another component of the presynaptic CAZ complex identified is the known LNX1 interacting protein ERC2/CAST1. ERC2 was previously shown to bind to LNX1-PDZ2 via a carboxyl terminal IWA* motif and to co-localise with LNX1 in neurons [55]. For the first time, it was shown that LNX1p80 but not LNX1p70 causes ubiquitination of ERC2. However, this may not be so relevant *in vivo* since ERC2 (and the isoform of ERC1 that has the IWA* motif) are exclusively expressed in the brain [103], whereas LNX1p80 is expressed in non-neuronal tissues [104]. Instead LNX2, which can also interact with ERC1 and ERC2 [105], is perhaps more likely to promote their ubiquitination in neurons *in vivo*. Many other proteins with well-established functions in neuronal development and synapse formation in the LNX1 interactome

were identified. For example, KIF7, a kinesin motor protein involved in Hedgehog signalling, and MID2, an E3 ubiquitin ligase, both function in neural development [106, 107], as does SRGAP2[94], while MYCBP2 (Pam/highwire/rpm-1) is a well-known regulator of synapse formation. Overall, the LNX1 interacting proteins and substrates identified and characterised here are plausible candidates that may, in addition to NUMB, mediate physiological functions of LNX proteins in the CNS as well as other tissues.

A striking observation about the LNX1-interacting proteins identified from kidney-derived HEK cells was the identification of many proteins with well-established functions in neuronal development, and particularly in synapse formation. This was confirmed, less surprisingly perhaps, in the PDZ2 complexes purified from brain lysates. For example, ERC1, ERC2 and liprin-α proteins are components of the presynaptic active zone complex that are involved in synapse maturation [100]. LNX1 is known to interact with ERC2 [55] and this data indicates that this ability is shared by LNX2, whereas Liprin-α1 and α3 only bind LNX1. All these interactions seem to be mediated by LNX1-PDZ2, but since LNX1 can dimerise [25], it could potentially form a tripartite complex with both ERC and Liprin. KIF7, a kinesin motor protein involved in Hedgehog signalling, and MID2, an E3 ubiquitin ligase, both function in neural development [106, 107], as does SRGAP2[94]. MYCBP2 (Pam/highwire/rpm-1) – an E3 ubiquitin ligase and well-known regulator of synapse formation, was also identified as a putative LNX1 interacting protein, though this interaction was not characterised further. In addition, two proteins with neuronal functions, SynGAP1 and EphA7 – previously described as interacting with LNX1 and LNX2 in yeast two-hybrid assays, using carboxyl-terminal peptides [21], were confirmed here as LNX-binding proteins in mammalian cells using full length proteins. The earliest expression of *Lnx1* and *Lnx2* mRNAs is in the embryonic brain and spinal cord, and expression of both mRNAs occurs predominantly in neurons rather than

glia in the CNS ([25], Paul Young and Orthis Saha unpublished observations). The interacting proteins identified and characterised here are thus plausible candidates that may, in addition to Numb, mediate neuronal functions of LNX proteins in the CNS.

Chapter 4: Exploration of the neuronal functions of LNX proteins *in vivo*

4.1 Introduction

Ligand of NUMB protein X (LNX) proteins were first characterized based on their ability to bind to NUMB and NUMBLIKE [24, 25]. LNX1 and LNX2 are closely related E3 ubiquitin ligases that can ubiquitinate specific isoforms of NUMB and LNX-mediated ubiquitination, at least in the case of LNX1, has been shown to target NUMB for proteasomal degradation [26, 27, 46]. NUMB is a negative regulator of Notch signalling and degradation of NUMB upon LNX1 overexpression was shown to moderately enhance Notch signalling in cultured cells ([26]). However, LNX2 knockdown in colorectal cancer cell lines caused a decrease in NUMB levels, a result that does not fit with the notion of LNX2 targeting NUMB for degradation [43]. Developmentally, expression of both *Lnx*1 and *Lnx2* mRNA is prominent in the embryonic and adult central nervous system (CNS) [24, 25]. This observation suggests a role for LNX1 and LNX2 in modulating neural development, possibly through their interactions with NUMB and/or its paralog NUMBLIKE – key regulators of mammalian neurogenesis and neuronal differentiation [72]. However, LNX proteins are present at very low levels in the brain, despite the presence of *Lnx* mRNAs [40], and there have not been any *in vivo Lnx* loss-of-function studies in a mammalian context. Hence, the physiological significance of the LNX-NUMB interaction remains unclear. To explore the neuronal functions of LNX proteins *in vivo,* double knockout mice were generated, that lack LNX protein expression in the CNS. These mice are viable, fertile and physically healthy, but exhibit decreased anxiety-related behaviours, in the apparent absence of any sensory, motor or learning deficits.

4.2 Materials & Methods

4.2.1 Animals

Lnx1$^{exon3-/-}$ knockout mice (originally made by Lexicon Pharmaceuticals, Inc.) were obtained through the MMRRC (Mutant Mouse Regional Resource Centre) at University of California - Davis, California, USA (Stock No: 032436-UCD; Strain Name: B6;129S5-Lnx1<tm1Lex>/Mmcd) and were maintained on a C57BL/6J genetic background. In these mice, exon 3, which is the first exon of the transcripts that codes for the p70 and p62 neuronal isoforms of LNX1, is replaced by a neomycin resistance gene (Fig. 4.1). This is expected to abolish transcription of these neuronal isoforms but should not affect the expression of the non-neuronal LNX1 p80 isoform that is transcribed from a different upstream promoter.

Lnx2 conditional knockout mice were generated through homologous recombination in mouse R1 ES cells by using standard procedures as previously described [108] These *Lnx2* conditional knockout mice were designed so that a neomycin resistance gene, used as a selectable marker, and the adjacent exon 2 of the *Lnx2* gene, are flanked by LoxP sites (Fig. 4.1). Exon 2 and the neomycin resistance gene were deleted by crossing these mice to a cre recombinase-expressing transgenic mouse line from Jackson Laboratories, Bar Harbor, ME, USA (*Strain Name: B6.C-Tg(CMV-cre)1Cgn/J; Stock Number: 006054*). The heterozygote (*Lnx2*$^{+/-}$) mice, so obtained, were then crossed with each other to obtain knockout (*Lnx2*$^{-/-}$) mice.

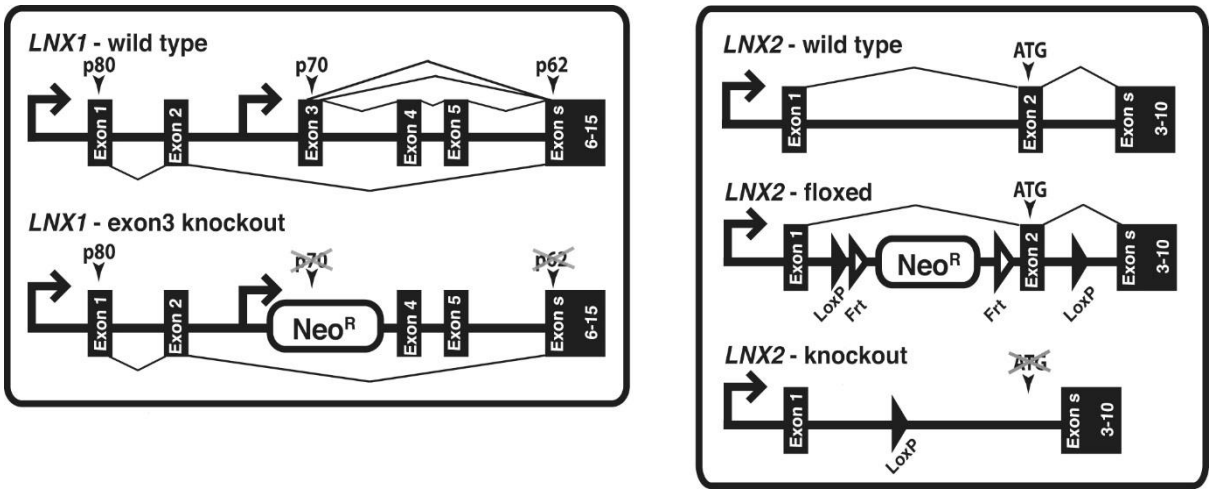

Figure 4.1: Schematic representation of the targeting strategy used to generate Lnx1^{exon3} and Lnx2 knockout mice. Wild-type Lnx1 and Lnx2 alleles, outlining protein-coding alternatively spliced transcripts, the target allele with exon 3 or exon 2, in the case of Lnx1 and Lnx2 respectively, and a neomycin resistance cassette (Neo) flanked by loxP recombination sites, and the null alleles obtained by Cre recombinase-mediated deletion of the floxed region are shown.

In *Lnx2*$^{-/-}$ mice removal of exon 2 deletes the ATG start codon and the coding region for the RING finger domain. If, following deletion of exon 2, exon 1 were to splice into exon 3 or a downstream exon, and the first available in-frame ATG (in exon 7) was used to initiate translation, a protein of 211 amino acids in length could theoretically be produced. However, several out of frame ATGs in exons 3-6 would likely attenuate translation of any such product. Thus, deletion of *Lnx2* exon 2 is likely to result in the production of at most very small quantities of a severely truncated LNX2 polypeptide lacking E3 ligase activity and can be regarded as a null or severely hypomorphic allele.

Lnx2$^{-/-}$ mice were crossed to Lnx1$^{exon3-/-}$ mice [84]. Compound heterozygous mice Lnx1$^{exon3+/-}$ *Lnx2*$^{+/-}$ were obtained and back crossed for at least eight generations to the C57/BL6J strain to

ensure a uniform genetic background. After back crossing, double knockout mice (Lnx1$^{exon3-/-}$ *Lnx2*$^{-/-}$) and the other genotypes required were bred for the experiments described hereafter.

4.2.2 Breeding, housing and animal care

Male and female mice, at least 7 weeks of age, were mated, fathers were removed before parturition after which mothers were singly housed with their pups. Pups were weaned at 3 weeks of age and group-housed in groups of 2-4 mice of mixed genotype. Male and female pups were housed separately. Cages contained minimally enriched living conditions with regular sawdust bedding, paper shred, and a cardboard play tunnel. Dry food pellets in a food hoper and water were available *ad libitum* and cages regularly changed on a weekly basis. Mice were maintained on a 12 h hour light/dark cycle (lights on at 07:30 and off at 19.30), with temperature (22 ± 1 ºC) and humidity (~55 %) controlled conditions. All animal experiments were approved by the Animal Experimentation Ethics Committee of University College Cork (No: 2013/028) and were conducted under license (No: AE19130/P013) issued by the Department of Health and Children, in accordance with the European Union Directive 2010/63/EU for animals used for scientific purposes. All efforts were made to minimize animal suffering and to reduce the number of animals used.

4.2.3 Genotyping

Genomic DNA was extracted from tail biopsies (approx. 2-3 mm) of P7-P10 pups by digestion in 100µl tail digestion buffer (50 mM Tris-HCl pH8.0, 1 mM CaCl2, 1% Tween-20) plus 10µl proteinase K (10 mg/ml) (Roche Applied Sciences) overnight at 55 ºC. Samples were further incubated for 10 minutes at 95 °C to inactivate proteinase K, centrifuged briefly to pellet debris and stored at -20 °C. Genotypes were determined by PCR using the following primer pairs:

- *Lnx1* WT PCR – DNA274-3 [5'-TGCCTTAATCTACAGGCTCC-3'] and DNA274-4 [5'-GAGTTGTGGGCACTGAGAG-3']
- *Lnx1* KO PCR – Neo3a 5' – [5'-GCAGCGCATCGCCTTCTATC-3'] and DNA274-7 5' – [5'-GTCACAAAGCACTAAGCGTG-3']
- *Lnx2* WT PCR – *Lnx2*GENO-F1 [5'-CGCAGCCTTAGGCATGGTTGG-3'] and *Lnx2*GENO-R1 [5'-CTGACTGTGGGTTACAGTTCTGG], 210 bp
- *Lnx2* KO PCR – *Lnx2*GENO-F2 [CCCCATCATGCAGAGCAAAGTC] and *Lnx2*GENO-R1, 368 bp

PCR reaction mixtures included 10X Taq buffer, 0.25 µM of each primer, 0.25 mM of each dNTP, 0.25 µl of Taq polymerase and 2 µl of genomic DNA in a 25 µl reaction volume. Cycling conditions used were: 96°C - 3 min, 40 cycles [96 °C - 40 sec, 60 °C - 40 sec, 68 °C - 1 min 30 sec], 68 °C - 10 minutes and 4 °C indefinitely. The presence of specific amplicons was confirmed by running amplified DNA samples on a 2% agarose gel. A representative gel is depicted in Fig. 4.4.

4.2.4 Tissue homogenization for western blot analysis and immunoprecipitation

Whole P18 mouse brains were homogenized on ice using a Dounce homogenizer in a volume of lysis buffer (20 mM, Tris pH 7.5, 10 mM NaCl, 1% NP40, 0.1% sodium deoxycholate, 1mM EDTA and 1× Complete protease inhibitors (Roche Applied Sciences)) which was 9 times the weight of the tissue. Following incubation on ice for 30 min, tissue lysates were centrifuged at 16,000 g for 30 min at 4 °C. The supernatent was collected and measured for total protein concentration using a BCA assay kit (Thermo Scientific Pierce). A sample was stored at -20

°C for future analysis. Prior to immunoprecipitation, lysates from 3 brains per genotype were pooled together.

4.2.5 Immunoprecipitation (IP)

Brain lysates prepared as described in Section 4.2.3 were pre-cleared for 30 min at 4°C using 40 µl of Protein A/G Sepharose beads (Thermo Fisher Scientific, Dublin, Ireland). Pre-cleared lysates were then immunoprecipitated for 1.5 h at 4°C by incubation with 5 µl guinea pig anti-LNX1/2-PDZ3/4 serum (Young et al., 2005). Pre-clearing and immunoprecipitation were performed under constant mixing using a nutator mixer. Protein A/G beads (40 µl/sample) were then washed with 1X PBS, blocked with 1% BSA for 30 minutes at 4°C (with mixing), washed again, and then centrifuged. The 1X PBS was removed and lysis buffer was added to the blocked beads in a 1:1 ratio. 80 µl of this mixture was added to each of the pre-cleared protein lysates and incubated with constant mixing for 1 h at 4°C. Following immunoprecipitation, the beads were washed 5 x 5 minutes in lysis buffer, with centrifugation steps performed 1,000 g for 2 minutes at 4°C. After the final wash and centrifugation, wash buffer was removed except for the last 40 µl (containing the beads), and 40 µl 2X gel loading buffer was added. 2X gel loading buffer was also added to protein lysates kept aside as input protein samples. All samples were boiled for 5 minutes, centrifuged briefly and resolved by SDS-polyacrylamide electrophoresis. Western blotting was performed using rabbit anti-LNX1/2-RING/NPAY antibody and enhanced chemiluminescent detection (Thermo Scientific Pierce, Rockford, IL, USA).

4.2.6 Phenotypic characterisation of Lnx1 $^{exon3-/-}$ /Lnx2$^{-/-}$ mice.

4.2.6.1 Body weight and growth analysis.

Body weight was measured on a weekly basis to the nearest 0.1 g, beginning at 1 week of age, for 13 weeks.

4.2.6.2 Order of behavioural testing

At adulthood (8 weeks old), mice underwent a battery of behavioural tests, conducted in sequence from the least to the most stressful test, over a period of 5 weeks. A schematic depicting the timeline of behavioural experiments is shown in Fig 4.2. There was a minimum of at least 24 h between each test. At 13 weeks old, animals were either sacrificed, and their tissues collected, or used for breeding purposes.

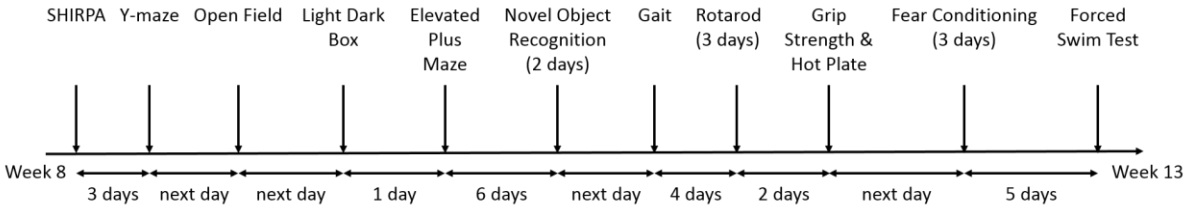

Figure 4.2: Timeline illustrating the sequence of behavioural testing and intervals between tests.

4.2.6.3 Conditions common to all tests

For all procedures, animals were brought to the room at least 30 min prior to testing. All experiments were conducted during the light phase of the day, between 9 a.m. and 7 p.m. All apparatus were cleaned between animals with 70% ethanol to remove odours. Genotypes were

blinded for the duration of the behavioural battery, and for subsequent scoring. The order of testing was random regarding litters and groups.

4.2.6.4 Primary Observations

A primary observational assessment following a modified SHIRPA protocol was performed for male and female mice of each genotype [109-111]. In total 36 observations were quantified including, spontaneous activity, respiration rate, fur, skin and whisker condition, tremor, body position, palpebral closure, piloerection, gait, pelvic elevation, tail elevation, touch escape, positional passivity, transfer arousal, trunk curl, limb grasping, body tone, pinna reflex, corneal reflex, tail pinch reflex, skin colour, heart rate, limb tone, abdominal tone, lacrimation, provoked biting, righting reflex and negative geotaxis.

4.2.6.5 Y-maze

Spontaneous alternation behaviour in the Y-maze is used to assess spatial memory [112]. The maze consisted of a black plastic 3-arm Y-maze (15 cm × 5 cm × 10 cm, $L \times W \times H$). Mice were individually placed in one of the 3 arms and allowed 5-min free exploration. The sequence of visited arms was recorded. At the end of the test, mice were returned to their home cage. Parameters measured included the number of entries, as an index of locomotor activity, and the percentage alternation as a measure of spatial memory.

4.2.6.6 Open field

Spontaneous locomotor activity and anxiety-like behaviour was assessed in the open field task. This paradigm is based on the idea that mice will naturally prefer to be near a protective wall rather than exposed to danger out in the open [109]. The apparatus was a grey, plastic, open

box without any bedding (40 cm × 32 cm × 25 cm, *L* × *W* × *H*). After 30 min habituation to the testing room, animals were placed individually in the middle of the arena and allowed 10 min free exploration. Each mouse was video-recorded for the duration of the test, and the researcher left the room after the start of the trial. Total distance travelled, time spent and number of entries into the centre and corner areas were measured post-test using a video-tracking system (Ethovision software, Noldus, The Netherlands). The total distance travelled served as an index of locomotor activity. Time spent and number of entries into the centre and corners zones were considered an inverse-score for anxiety-like behaviour.

4.2.6.7 Light-dark box test

The light-dark box test assesses levels of unconditioned anxiety in rodents based on levels of passive avoidance behaviour [113]. The apparatus was a plexiglas enclosure (44 cm ×21 cm ×21 cm, *L x W x H*) divided unequally into two chambers by a black partition containing a small opening (10 cm x 5 cm). The larger chamber was approximately twice the size of the smaller chamber, had clear walls and an open top and was brightly illuminated (1000 lux) to generate aversive conditions. The small chamber (14 cm length) was enclosed on all sides by black walls except for the small opening between the chambers. Mice were individually placed into the illuminated side facing away from the dark compartment and were allowed to freely explore the apparatus for 10 minutes. During this period the behaviour of the animals was recorded. Mice were manually scored post-test for their initial latency to enter the dark compartment, the time spent in the light compartment and the number of transitions between the two compartments, using the recorded videos. An entry was defined as the mouse placing all four feet into that compartment. An animal was adjudged to have entered a compartment when all four paws had crossed the threshold.

4.2.6.8 Elevated plus maze

The elevated plus maze protocol is designed to test levels of passive anxiety-like behaviour, based on the conflict between the exploratory instinct of mice and their aversion for the elevated, exposed open arms of the maze [113]. The elevated plus maze consisted of four arms, forming the shape of a plus, elevated 91 cm above the floor. Two opposing arms were enclosed by walls, the other two arms were open. All four arms were connected by a centre area. The experiment was performed under dim red light [114]. Each mouse was placed gently on the centre of the maze facing an open arm and allowed to freely explore the maze for 6 min. Each mouse was video-recorded for the duration of the test, and the researcher left the room after the start of the trial. Variables measured manually post-test were the time spent and percent entries into the open and closed arms of the maze as indices of anxiety-like behaviour. Total arm entries were analysed as an index of general locomotor activity. An animal was adjudged to have entered an arm of the maze only when all four paws were inside the arm in question.

4.2.6.9 Gait analysis

Gait analysis was performed from the footprint pattern [109]. The footpads of mice were coated with non-toxic paint. The animals were required to run along a straight narrow tunnel (50 cm x 9 cm x 16 cm, *L x W x H*) with a 40 cm long sheet of white paper on the floor to record the prints. A dark goal box was positioned at the end of the tunnel to encourage the mouse to run towards a dark and safe environment. Footprints at the start and the end of the tunnel were excluded from the analysis as they correspond to the initiation and termination of the movement. Measurements for at least three-step cycles were averaged, considering a cycle as the distance from one pair of hind prints to the next, where there were no pauses in the gait. The footprint patterns of the hind paws were evaluated in terms of the following parameters: (1) stride length, which was taken as the average distance between the central pads of two

consecutive prints for each hind paw; (2) stride width, which was taken as the average perpendicular distance between lines connecting consecutive hind paw prints on each side; and (3) step length, which was measured as the average perpendicular distance between the central pads of alternating steps. A fresh sheet of paper was placed on the floor of the tunnel for each run.

4.2.6.10 Rotarod test

Motor coordination and skill learning were assessed using a rotarod apparatus (UGO Basile, Varese, Italy) [109]. The rotarod task was first introduced to animals by a 5 minute trial at a constant speed of 4 rpm. During this initial training phase, mice were placed back on the rod immediately after falling, allowing them to become familiar with the test. Thereafter, mice were placed on the rotating drum, which accelerated from 4 to 40 r.p.m. over a 5 min period. Time spent walking on top of the rod before falling was recorded. Mice were given 3 trials on 3 consecutive days for a maximum time of 300 s (5 min) per trial. An interval of 30 minutes was given between trials.

4.2.6.11 Grip Strength

Muscle strength was assessed using a grip strength meter (Ugo Basile, Varese, Italy). Mice were held by the tail and brought close to the grip strength apparatus. Mice were allowed to grasp the grid with their front paws and were gently pulled back until they released their grip. The apparatus registered the peak strength for that trial. Each animal had 5 trials, with an inter-trial interval of 15-30 sec. The 5 trial test did not exceed 5 minutes.

4.2.6.12 Hotplate test

Mice were tested for analgesia-related responses using a hotplate apparatus (Columbus Instruments, Columbus, OH, USA). The hotplate was preheated to 55 ^{o}C and then mice were placed one at a time onto the hotplate. The time to first show a hind limb response was recorded. Typical responses are licking or shaking the hindpaw, or jumping. Mice were immediately removed after showing a response. The test was terminated at 30 sec in the absence of a response.

4.2.6.13 Auditory fear conditioning

Auditory fear conditioning was conducted as described previously described [114]. On day 1, mice were placed in conditioning chambers (21.6 cm x 17.8 cm x 12.7 cm), with transparent walls in the front and back, stainless-steel bars, and a metal-grid floor connected to a shock scrambled and generator in sound-attenuating box. After 180 s acclimatisation, mice received 6 pairings (60 s interpairing interval) of a conditioned stimulus (CS; 20 s, light, 10 dB, 10 kHz tone) and an unconditioned stimulus (US; 2 s, scrambled foot shock; 60 mA). The US was presented during the last 2 s of the CS. Following a 60 s no-stimulus consolidation period after the final CS–US pairing, mice were returned to the home cage. Chambers were cleaned with 70% ethanol between each mouse. On days 2 and 3 mice were returned to the same chamber as day one and the procedure repeated, with the absence of electrical footshocks. Activity of mice was monitored by Video Freeze (Med Associates, USA). This paradigm allows for the measurement of the acquisition and extinction of conditioned fear. The design of the procedure additionally allows us to measure both context and cue induced freezing which are measures of hippocampus and amygdala dependent fear behaviours, respectively. An outline of the experimental procedure is given in Fig 4.3. Animals were filmed at rate of 15 frames per

second, with a freezing behaviour represented by movement of less than 255 pixels (to accommodate breathing) over 7 frames.

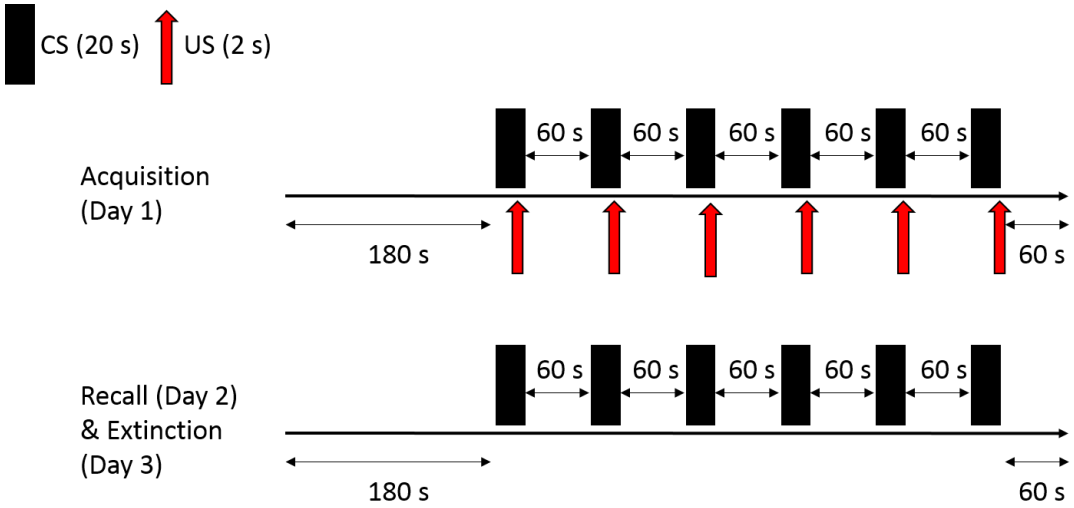

Figure 4.3: Schematic of the auditory fear conditioning protocol. On day one (acquisition training) mice are given 180 seconds acclimatisation to the novel test chamber before presentation of the CS (light, 10 dB, 10kHz tone) for 20 seconds (Black rectangles) with the US (60 mAmp scrambled footshock) presented for the final 2 seconds (red arrow). The US-CS pairing was repeated six times with a 60 second inter-pairing interval and a final 60 second consolidation period. On day two (recall testing) and three (extinction testing) an identical protocol in the same contextual environment, was used with the absence of the footshock.

4.2.6.14 Forced swim test

The forced swim test is a behavioural test commonly used to assess levels of antidepressant-like behavioural activity in mice [115]. Mice are placed in glass cylindrical tank containing 17cm of water at 23-25°C for 6 minutes and their behaviour is recorded. The length of time the mouse spends immobile, i.e. not actively swimming, during the last 4 minutes of the test is scored manually by a trained observer blinded to the treatment group.

4.2.7 Tissue harvesting

Mice were anesthetized by isofluorane inhalation and perfused through the left ventricle of the heart using a peristaltic pump. Ice-cold phosphate buffered saline (PBS) (pH 7.4) was used to flush out blood from all vessels and tissues. Animals whose tissue was intended for

immunohistochemistry were further perfused with 4% paraformaldehyde dissolved in PBS. The brain, heart, kidneys, spleen, liver and lungs were extracted and their wet weights recorded.

4.2.8 Statistical analysis

The normal distribution of data was assessed using the D'Agostino–Pearson test. Since all values passed this test, parametric tests were used for analysis. Chi squared tests were used to compare the Mendelian inheritance of LNX and LNX2 knockout alleles. Two-way repeated measures Analysis of Variance (ANOVA) was carried out to investigate the overall effect of genotype and age on body weight profile, rotarod and conditioned fear data, followed by Bonferroni's post-hoc test where appropriate. Data from all other paradigms were analysed by one-way ANOVA, followed by Bonferroni's post-hoc test where appropriate. Statistical analyses were performed using GraphPad Prism v.6.0 (La Jolla, CA, USA). P values of less than 0.05 were considered significant. Unless stated otherwise, all data are presented as mean ± SEM.

Western blot signal intensities were quantified with Odyssey V2.1 software (LI-COR Biosciences, Cambridge, UK), using β-actin as a loading control. Microsoft Excel software was used to perform two tailed Student's t-tests to evaluate changes in Numb protein levels in DKO brain lysate.

4.3 Results

4.3.1 Confirmation of genotype

To confirm the identity of the mice to be included in each study group,genomic DNA from tail snips of P7 to P10 pups was screened for mutant *Lnx1* and *Lnx2* alleles by PCR, as described in the Materials and Methods section. A representative profile of the three genotypes used in this study, wild-type (WT), double-heterozygous (DHET) and double-knockout (DKO), is presented in Fig 4.4. The wild-type *Lnx1* $^{exon3+/+}$ allele – which gives rise to neuronal *Lnx1* isoforms, produces a PCR product 253 bp in length, while the mutant *Lnx1* $^{exon3-/-}$ allele is detected at 298 bp. The wild-type allele *Lnx2* allele produced a PCR product 260 bp in length, whereas the mutant *Lnx2* allele was observed at 368 bp. The presence of specific bands for the wild-type alleles only for both *Lnx1* and *Lnx2* indicate that the animal belongs to the WT genotype group. Specific bands for both the wild-type and mutant alleles for both *Lnx1* and *Lnx2* indicates a DHET genotype. The presence of specific bands for the mutant alleles only for both *Lnx1* and *Lnx2* indicate a DKO genotype.

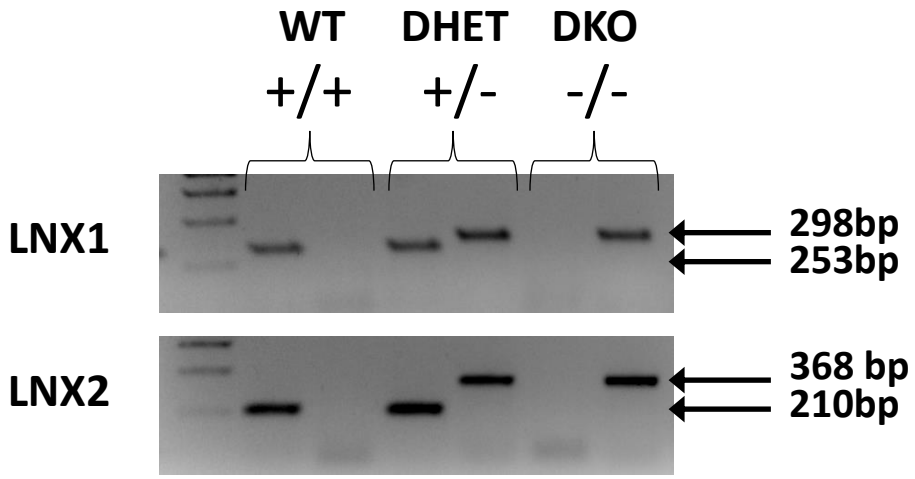

Figure 4.4: PCR-based method for genotyping of DHET and DKO mice. Agarose gel electrophoresis of the PCR products amplified from DNA samples collected from tail biopsies. Arrows (top gel image) indicate a 298 bp amplicon product from the mutant *Lnx1* allele and a 253 bp amplicon product from the *Lnx1* wild-type allele. Arrows (bottom gel image) indicate a 368 bp amplicon product from the mutant *Lnx2* allele and a 210 bp amplicon product from the wild type *Lnx2* allele. Representative WT, DHET and DKO genotypes are shown (left to right). The presence of specific bands for the wild-type alleles only for both *Lnx1* and *Lnx2* indicate that the animal belongs to the WT genotype group. Specific bands for both the wild-type and mutant alleles for both *Lnx1* and *Lnx2* indicates a DHET genotype. The presence of specific bands for the mutant alleles only for both *Lnx1* and *Lnx2* indicate a DKO genotype.

Loss of both $Lnx1^{p70}$ and *Lnx2* was confirmed by immunoblotting (Fig. 4.5). Using antibodies that recognize both LNX1 and LNX2, three LNX bands were detected by Western blot following immunoprecipitation from wild-type brain lysates. As LNX proteins are expressed at very low levels *in vivo*, none of these bands were directly detected in wild-type brain lysates. The middle band corresponds to the size of the brain-specific LNX1p70 isoform (70kDa), while the lower band represents the novel LNX1p62 isoform (62kDa) identified previously. The top band migrates at approximately the molecular weight of LNX2 (75 kDa). All three protein bands are absent in immunoprecipitates from $Lnx1^{exon3-/-}$ /$Lnx2^{-/-}$ brains validating them as suitable models to study the function of LNX proteins in the central nervous system.

Furthermore, Western blot analysis showed no compensatory upregulation of LNX1p80 in the brain of DKO mice – which would run just above LNX2.

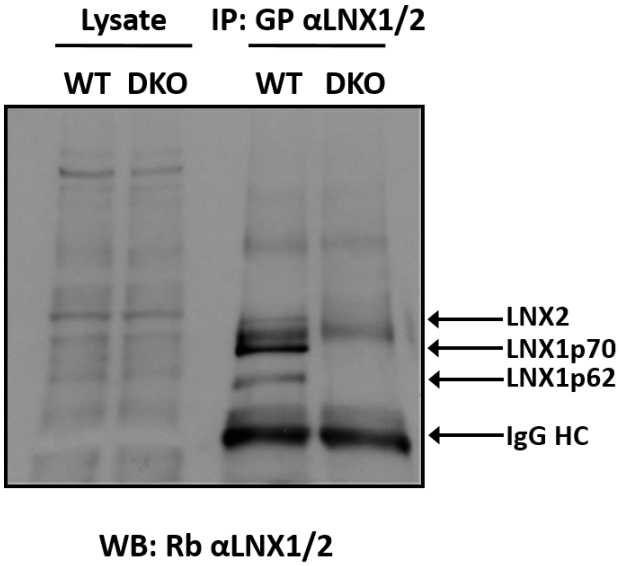

Figure 4.5: Confirmation of LNX1 and LNX2 knockout in the brain of LNX1$^{exon3-/-}$/LNX2$^{-/-}$ (DKO) mice. LNX protein expression in WT and DKO brains was examined by Western blotting of lysates and immunoprecipitates (IP) from P18 mouse brains. Immunoprecipitation and immunoblotting were performed using guinea pig anti-LNX1/2-PDZ3/4 and rabbit anti-LNX1/2-RING/NPAY antibodies, respectively, that recognize both LNX1 and LNX2. The brain specific LNX1p70 isoform, the smaller LNX1 p62 species and LNX2 proteins, indicated by arrows, are all detected in LNX1$^{+/+}$/LNX2$^{+/+}$ (WT) but not LNX1$^{exon3-/-}$/LNX2$^{-/-}$ (DKO) mouse immunoprecipitates, validating them as a suitable model to study LNX proteins in the CNS. No compensatory expression of LNX1p80, which would run just above LNX2, was observed. IgG HC = immunoglobulin heavy chains from the antibody used for immunoprecipitation.

4.3.2 General appearance, body weight, survival.

To determine whether loss of *Lnx1*$^{exon3-/-}$, which gives rise to neuronal *Lnx1* isoforms, or *Lnx2*, or both *Lnx1*$^{exon3-/-}$ and *Lnx2*, results in partial embryonic lethality, the Mendelian inheritance patterns of genotypes in the offspring of numerous matings were analyzed.

Table 4.1 lists the expected and observed frequencies of the possible genotypes arising from double heterozygote matings. Pedigree analysis revealed the presence of all expected nine genotypes among offspring. For eight degrees of freedom, χ^2 would need to be greater than 15.507 in order for the *p*-value to be less than 0.05. Tables 4.2 and 4.3 list the expected and observed frequencies of the possible genotypes arising from *Lnx1exon3*+/– *Lnx2*$^{+/-}$ mated to *Lnx1*$^{exon3-/-}$ *Lnx2*$^{-/-}$ and *Lnx1*$^{exon3+/-}$ *Lnx2*$^{-/-}$ mated to *Lnx1*$^{exon3-/-}$/*Lnx2*$^{+/-}$ respectively. Pedigree analysis revealed the presence of all expected four genotypes among offspring. For three degrees of freedom, χ^2 would need to be greater than 7.815 in order for the *p*-value to be less than 0.05. The χ^2 distribution in each case suggests no significant deviations from expected Mendelian values, both among individual genotypes or the group as a whole indicating no evidence of embryonic lethality across genotypes.

Table 4.1: Frequency of viable pups from *Lnx1*$^{exon3+/-}$ *Lnx2*$^{+/-}$ × *Lnx1*$^{exon3+/-}$ *Lnx2*$^{+/-}$ matings. The nine possible genotypes are listed with the number of recovered viable pups. Expected values are derived from Mendelian inheritance patterns; $\chi^2 = \sum d^2/E$, where d is the expected number – observed number, and E is the expected number, with eight degrees of freedom.

	Genotype									Total
LNX1 allele	+/+	+/+	+/+	+/-	+/-	+/-	-/-	-/-	-/-	
LNX2 allele	+/+	+/-	-/-	+/+	+/-	-/-	+/+	+/-	-/-	
Expected Freq (%)	6.25	12.50	6.25	12.50	25.00	12.50	6.25	12.50	6.25	100.00
Observed Freq (%)	7.89	26.32	2.63	10.53	23.68	7.89	0.00	10.53	10.53	100.00
Observed no. (O)	3	10	1	4	9	3	0	4	4	38
Expected no. (E)	2.375	4.750	2.375	4.750	9.500	4.750	2.375	4.750	2.375	38
O-E	0.625	5.250	-1.375	-0.750	-0.500	-1.750	-2.375	-0.750	1.625	0
$(O-E)^2$	0.39	27.56	1.89	0.56	0.25	3.06	5.64	0.56	2.64	
$\chi^2 = (O-E)^2/E$	0.16	5.80	0.80	0.12	0.03	0.64	2.37	0.12	1.11	11.15

Table 4.2: Frequency of viable pups from *Lnx1*$^{exon3+/-}$ *Lnx2*$^{+/-}$ × *Lnx1*$^{exon3-/-}$ *Lnx2*$^{-/-}$ matings. The four possible genotypes are listed with the number of recovered viable pups. Expected values are derived from Mendelian inheritance patterns; $\chi^2 = \sum d^2/E$, where d is the expected number – observed number, and E is the expected number, with three degrees of freedom.

	Genotype				Total
LNX1 allele	+/-	+/-	-/-	-/-	
LNX2 allele	+/-	-/-	+/-	-/-	
Expected Freq (%)	25.00	25.00	25.00	25.00	100.00
Observed Freq (%)	25.00	26.79	22.32	25.89	100.00
Observed no. (O)	28	30	25	29	112
Expected no. (E)	28	28	28	28	112
O-E	0.00	2.00	-3.00	1.00	0
$(O-E)^2$	0.00	4.00	9.00	1.00	
$\chi^2 = (O-E)^2/E$	0.00	0.14	0.32	0.04	0.50

Table 4.3: Frequency of viable pups from *Lnx1*$^{exon3+/-}$ *Lnx2*$^{-/-}$ × *Lnx1*$^{exon3-/-}$/*Lnx2*$^{+/-}$ matings. The four possible genotypes are listed with the number of recovered viable pups. Expected values are derived from

	Genotype				Total
LNX1 allele	+/-	+/-	-/-	-/-	
LNX2 allele	+/-	-/-	+/-	-/-	
Expected Freq (%)	25.00	25.00	25.00	25.00	100.00
Observed Freq (%)	20.00	32.73	32.73	14.55	100.00
Observed no. (O)	11	18	18	8	55
Expected no. (E)	13.75	13.75	13.75	13.75	55
O-E	-2.75	4.25	4.25	-5.75	0
$(O-E)^2$	7.56	18.06	18.06	33.06	
$\chi^2 = (O-E)^2/E$	0.55	1.31	1.31	2.40	5.58

Mendelian inheritance patterns; $\chi^2 = \sum d^2/E$, where d is the expected number – observed number, and E is the expected number, with three degrees of freedom.

Body weight was monitored weekly from one week of age through to the end of the testing period.

As shown in Fig. 4.6, no differences in the body weights of mice were observed between genotypes of either sex during the first few weeks of life. Postnatal growth curves started to diverge significantly 5 weeks after birth for male mice, as DKO mice began to gain significantly less weight than WT and DHET counterparts. Differences in weight gain persisted throughout adolescence and into adulthood for the indicated period of analysis. This result was supported by a significant effect of week ($F_{12,336}$ = 1564, P < 0.0001), genotype ($F_{2,28}$ = 5.098, P = 0.0129), and interaction between week and genotype ($F_{24,336}$ = 2.653, P < 0.0001) in the overall repeated measures two-way ANOVA. By 12 weeks of age, DKO animals weighed on average 2.7 grams, or 11.2 % less than WT animals and 1.9 grams, or 8.3 % less than DHET mice. No significant differences in body weight were observed between WT and DHET mice.

Female mice displayed a similar age-related difference in weight gain. Differences in body weight in this instance were first observed at 3 weeks after birth, as DHET and DKO mice began to gain significantly less weight in comparison to their WT counterparts. Again, differences in weight gain persisted throughout adolescence and into adulthood for the indicated period of analysis. This result was supported by a significant effect of week ($F_{12,324}$ = 1351, P < 0.0001), genotype ($F_{2,27}$ = 7.213, P = 0.0031), and interaction between week and genotype ($F_{24,324}$ = 2.130, P = 0.0019) in the overall repeated measures two-way ANOVA. By week 12, DKO and DHET mice weighed on average 2.7 grams and 2.1 grams, or 13.2% and 10.2%, less than WT mice respectively.

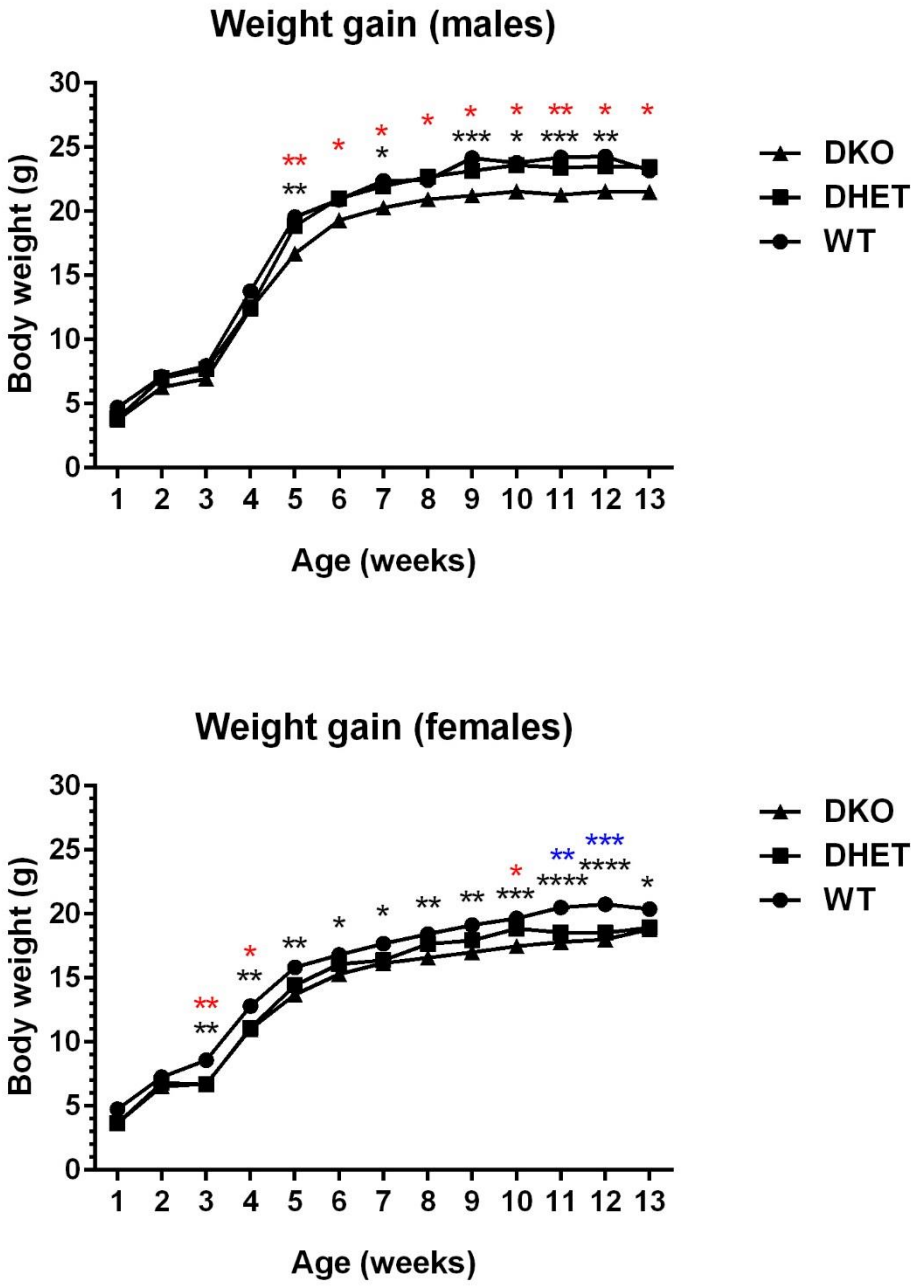

Figure 4.6: Effect of LNX1/LNX2 genotype on body weight gain during postnatal development. Body weights of mice were recorded weekly for the duration of the study. Initially body weights were not different between genotypes of either sex. However, from 5 weeks and 3 weeks of age respectively, DKO male (top) and female (bottom) mice began to gain significantly less weight than their WT and DHET counterparts, and this difference in body weight persisted for the indicated period of analysis. Body weights are expressed as mean ± SEM, n = 7-12/group. *p < 0.05, **p < 0.01, ***p < 0.001, ****p < 0.0001; two-way repeated measures ANOVA followed by Bonferroni post-hoc test. (Black = WT v DKO, Red = DHET v DKO, Blue = WT v DHET).

4.3.3 Lnx1$^{exon3-/-}$/Lnx2$^{-/-}$ knockout effects on physiology: organ masses

4.3.3.1 Brain mass

A significant overall influence of genotype was observed on average absolute brain mass of male mice, as revealed by one-way ANOVA ($F_{2,10}$ = 6.926, P = 0.0130). Bonferroni post-hoc test indicated a significant increase in mean absolute brain mass of DHET animals compared to WT controls (P <0.05). The average absolute brain mass of DKO mice was also increased in comparison to their WT counterparts, although this difference was not statistically significant. When expressed as a percentage of body weight, a significant overall effect of genotype remained, as indicated by one-way ANOVA ($F_{2,10}$ = 87.15, P = <0.0001). Bonferroni post-hoc test revealed a significant increase in the average relative brain mass of DHET and DKO mice when compared to their WT counterpart (P <0.0001).

Again, with regard to female mice, significant differences were observed in absolute brain mass ($F_{2,18}$ = 32.29, P = <0.0001). DKO mice displayed a significant increase in average absolute brain mass compared to WT and DHET counterparts (P <0.01 and P <0.0001 respectively). A significant overall effect of genotype persisted when expressed as a percentage of body weight ($F_{2,18}$ = 43.00, P = <0.0001). Relative brain mass was increased in DKO mice when compared to either WT or DHET mice (P <0.001 and P <0.0001 respectively).

4.3.3.2 Spleen mass

There was a significant overall difference between genotypes on mean absolute spleen mass of male mice, as revealed by one-way ANOVA ($F_{2,10}$ = 13.60, P = 0.0014). Bonferroni post-hoc test revealed the average absolute spleen mass was significantly less in DKO and DHET animals when compared to WT controls (P <0.01). When expressed as a percentage of body weight, a significant overall effect of genotype on spleen mass remained ($F_{2,10}$ = 4.463, P =

0.0412). However, Bonferroni post-hoc test revealed no significant difference between individual groups.

A significant overall effect of genotype on absolute spleen mass was also noted among females ($F_{2,18}$ = 6.809, P = 0.0063). Bonferroni post-hoc analysis revealed a significant decrease on absolute spleen mass in DHET and DKO mice compared to WT control (P <0.05). The significant overall effect of genotype persisted when expressed as a percentage of body weight ($F_{2,18}$ = 6.622, P = 0.0070). Bonferroni post-hoc analysis indicated a significant decrease in relative spleen mass of DHET mice in comparison to their WT counterparts (P <0.01). DKO relative spleen mass was also decreased in comparison to WT controls, although this difference was not statistically significant.

4.3.3.3 Heart mass

One-way ANOVA revealed a significant overall effect of genotype on mean absolute heart mass in male mice ($F_{2,10}$ = 4.317, P = 0.0445). Bonferroni post-hoc test revealed no significant difference between individual groups however. When expressed as a percentage of body weight, a significant overall influence of genotype on average heart mass was further observed ($F_{2,10}$ = 23.21, P = 0.0002). Bonferroni post-hoc test showed the relative heart mass of DKO and DHET mice was significantly increased in comparison to WT controls (P <0.001 and P <0.01 respectively).

A significant overall effect of genotype was also observed on mean absolute heart mass in female mice ($F_{2,18}$ = 5.456, P = 0.0141). Average absolute heart mass was significantly increased in DKO animals compared to DHET mice (P <0.05). Average absolute heart mass also appeared to be increased in DKO mice in comparison to their WT counterparts, although

this difference was not statistically significant. A significant effect of genotype on heart mass persisted even when expressed as a percentage of body weight ($F_{2,18}$ = 10.43, P = 0.0010). The relative spleen mass was increased in DKO mice when compared to either WT or DHET counterparts (P <0.05 and P <0.01 respectively).

4.3.3.4 Kidney mass

No significant influence of genotype was observed on mean kidney mass of male mice regardless of whether expressed as absolute mass ($F_{2,10}$ = 0.1320, P = 0.8779) or percentage of body weight ($F_{2,10}$ = 1.156, P = 0.3534). With regard to females, no significant difference on mean absolute kidney mass was observed ($F_{2,18}$ = 2.026, P = 0.1609) however when expressed as a percentage of body weight, a significant overall effect of genotype was detected ($F_{2,18}$ = 3.740, P = 0.0438). Bonferroni post-hoc test revealed relative kidney mass was decreased in DHET mice when compared to WT animals.

4.3.3.5 Lung mass

There was a significant overall effect of genotype on average absolute lung mass of male mice as illustrated by one-way ANOVA ($F_{2,10}$ = 28.31, P = <0.0001). Bonferroni post-hoc revealed a significant increase in the average lung mass of DHET and DKO mice compared to WT controls (P <0.001). When expressed as a percentage of body weight, an overall significant effect of genotype remained as revealed by one-way ANOVA ($F_{2,10}$ = 36.60, P = <0.0001). Bonferroni post-hoc test indicated that relative lung mass remained significantly increased in DHET and DKO mice in comparison to their wildtype counterpart (P <0.001 and P <0.0001 respectively).

In contrast, no significant difference in lung mass was observed among females regardless of whether expressed as absolute mass ($F_{2,18}$ = 1.039, P = 0.3740) or percent body weight ($F_{2,18}$ = 2.828, P = 0.0855).

4.3.3.6 Liver mass

For both males and females, one-way ANOVA revealed a significant effect of genotype on mean absolute liver mass ($F_{2,10}$ = 6.843, P = 0.0156 and $F_{2,18}$ = 4.739, P = 0.0222 respectively). Bonferroni post-hoc test indicated a significant decrease in the absolute liver mass of male and female DKO mice when compared to WT controls (P <0.05). No overall significant difference was observed however when expressed as a percentage of body weight ($F_{2,10}$ = 1.117, P = 0.3688 and $F_{2,18}$ = 2.886, P = 0.0848 for males and females respectively), as indicated by one-way ANOVA.

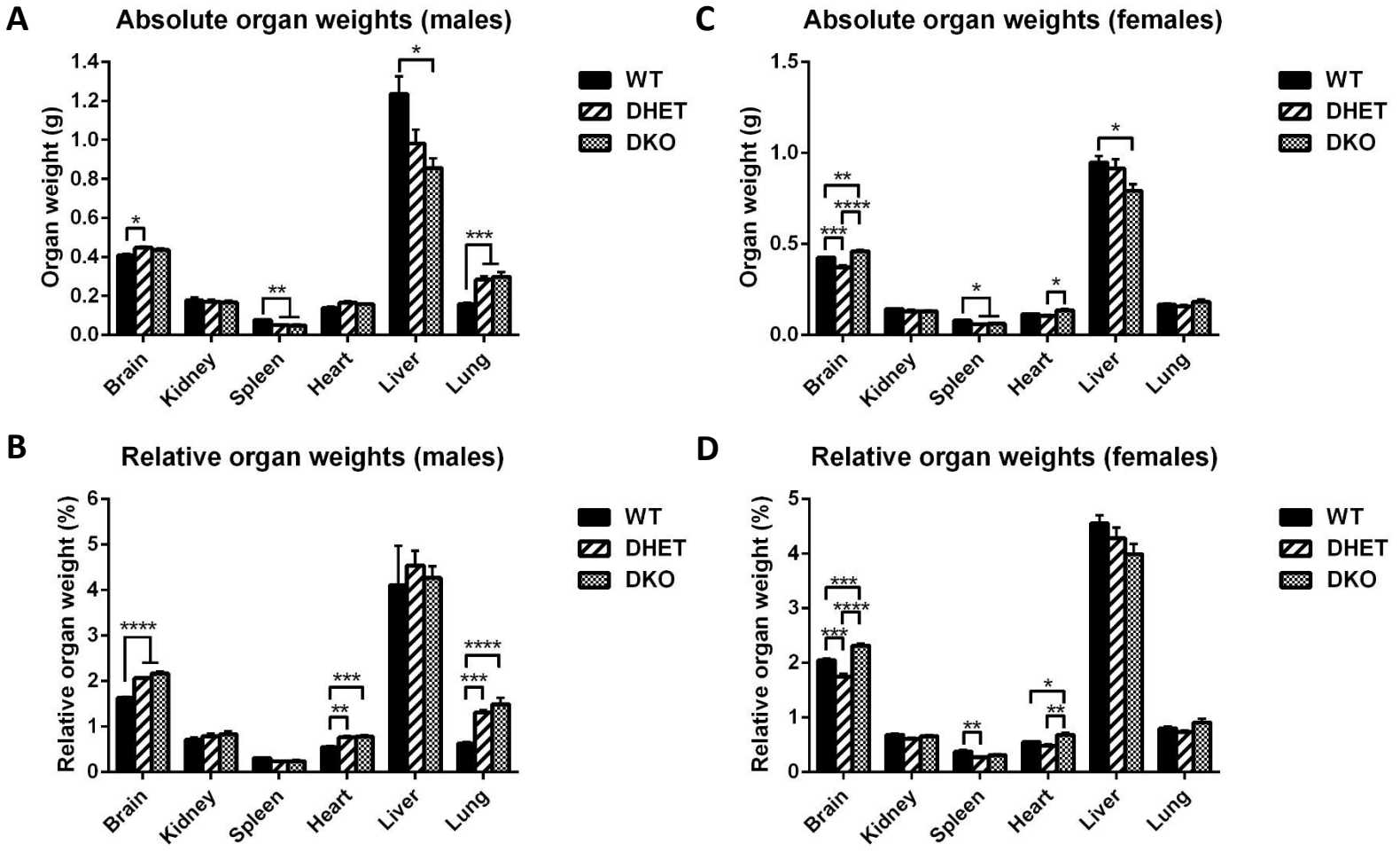

Figure 4.7: Effect of LNX1/LNX2 genotype on organ weights. After sacrifice, the wet weights of each organ shown were measured for (A) male and (B) female genotypes. (C-D) Organ weights were also expressed as a percentage of body weight. Data are expressed as mean ± SEM. n = 4-8/group. *p < 0.05, **p < 0.01, ***p < 0.001, ****p < 0.0001; one-way ANOVA followed by Bonferroni post-hoc test.

4.3.4 Lnx1$^{exon3-/-}$/Lnx2$^{-/-}$ knockout effects on Numb levels

As discussed earlier, LNX proteins were originally identified as ligands of Numb and its paralog Numb-like .Numb is a key protein involved in the specification of cell fates during development [24, 25]. In the nervous system, Numb functions in maintaining neural progenitors at early developmental stages, while later it promotes neuronal differentiation and maturation [72]. LNX1 and more recently LNX2 have been shown to ubiquitinate and target specific Numb isoforms, p72 and p66, for proteasomal degradation [26]. Numb is therefore an obvious candidate protein whose expression could be affected in DKO mice.

Possible alterations to endogenous Numb levels in P18 murine brain lysates of WT and DKO mice were examined by immunoblot assays (Fig. 4.8). The top band most likely corresponds to either the p72 or p71 isoform, whereas the lower bands appear to represent the p66 and p65 isoforms. B-actin served as a loading control. Quantification was performed as outlined in Materials & Methods. No significant change in the levels of Numb was observed in the brains of DKO mice compered to WT controls as revealed by Student's t-test ($P = 0.4237$). Thus, *Lnx1p70* and *Lnx2* ablation appears to have no effect on endogenous NUMB levels in the murine brain.

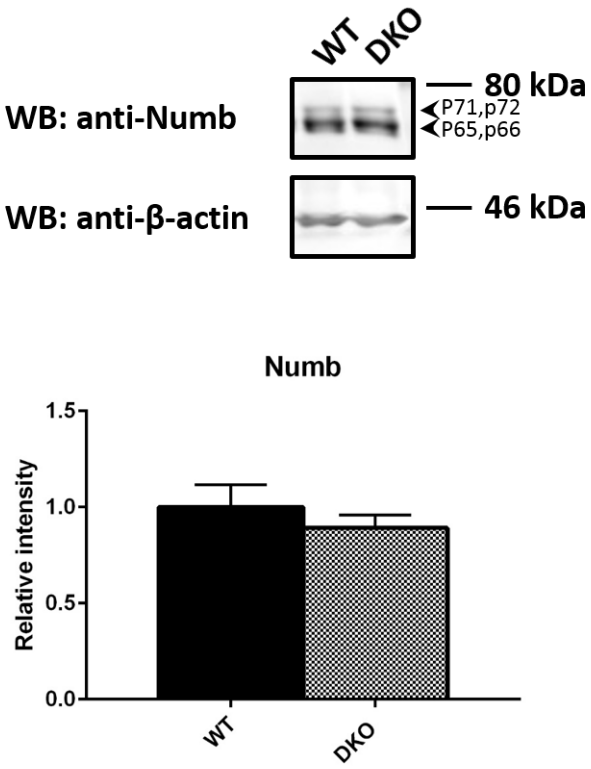

Figure 4.8: Numb proteins are not altered in P18 brains of DKO mice. (A) Protein levels of Numb in brain lysate homogenates of P18 WT and DKO mice were analysed by Western blot. (B) Quantification of Numb protein levels. Relative expression of Numb, normalized to β-actin, is shown. No effect of genotype on Numb proteins levels in DKO mice was detected, as assessed by Student's t-test. Data are presented as mean ± SEM. n =5 (WT), n =6 (DKO).

4.3.5 Behavioural battery

At adulthood (8 weeks old), mice underwent a battery of behavioural tests, conducted in sequence from the least to the most stressful test, over a period of 5 weeks. A schematic depicting the timeline of behavioural experiments is shown in Fig. 4.2.

4.3.5.1 Anxiety-like behaviour

4.3.5.1.1 Open field test

Behaviour of WT, DHET and DKO mice in the open field was examined – a test which is widely used in laboratories to quantify anxiety-like and locomotor behaviours in mice. Mice prefer to move around the periphery of an apparatus when they are placed in an open field of a novel environment. It is thought that the time spent in the central area of the open field is inversely correlated to their level of anxiety-related proneness [109].

In male mice, no overall effect of genotype was found in total distance travelled ($F_{2,31}$ = 1.322, P = 0.2813; Fig. 4.9A), a measure of general locomotor activity, or average speed of movement ($F_{2,31}$ = 1.255, P = 0.2993; Fig. 4.9B) in the open field test. While the distance travelled was comparable across genotypes, one-way ANOVA indicated a significant overall effect of genotype on the number of entries into ($F_{2,31}$ = 5.681, P = 0.0079; Fig. 4.9C) and time spent in the centre area of the open field arena ($F_{2,31}$ = 8.910, P = 0.0009; Fig. 4.9D). Bonferroni post-hoc analysis revealed DKO mice entered the centre area of the arena more frequently and spent significantly more time there than their WT and DHET counterparts (P <0.01). Furthermore, one-way ANOVA indicated a significant overall effect of genotype for the time spent in the corners of the arena ($F_{2,31}$ = 4.694, P = 0.0166; Fig. 4.9E). Bonferroni post-hoc test revealed

DKO spent significantly less time in the corners than either WT or DHET mice ($P < 0.05$). No difference in the number of corner entries were observed ($F_{2,31} = 0.1019$, $P = 0.9034$; Fig. 4.9F).

With regard to females, significant overall differences between genotypes were observed in the total distance travelled ($F_{2,31} = 9.402$, $P = 0.0006$; Fig. 4.9A) in the open field arena, as revealed by one-way ANOVA. Bonferroni post-hoc test indicated that DHET and DKO mice travelled significantly less ($P < 0.001$ and $P < 0.05$ respectively), and in the case of DHET at a significantly slower average speed (Fig. 4.9B) ($P < 0.05$), than WT controls, reflecting hypoactivity. No significant difference in the number of centre entries was detected among genotypes ($F_{2,31} = 0.2967$, $P = 0.7453$; Fig. 4.9C). Although DHET and DKO mice tended to spend an increased amount of time in the centre area compared to WT controls, the effect of genotype was not significant ($F_{2,31} = 1.745$, $P = 0.1913$; Fig. 4.9D). A significant overall effect of genotype was detected in the number of corner entries ($F_{2,31} = 4.262$, $P = 0.0232$; Fig. 4.9E) and time spent in the corners of the area ($F_{2,31} = 4.283$, $P = 0.0228$; Fig. 4.9F), by one-way ANOVA. Bonferroni post-hoc analysis revealed DHET mice entered the corners of the arena significantly less frequently ($P < 0.05$) and spent significantly less time there ($P < 0.05$) than WT controls. Similarly, although not statistically significant, DKO mice also appeared to enter the corner regions of the arena less and spent less time there than their WT counterparts.

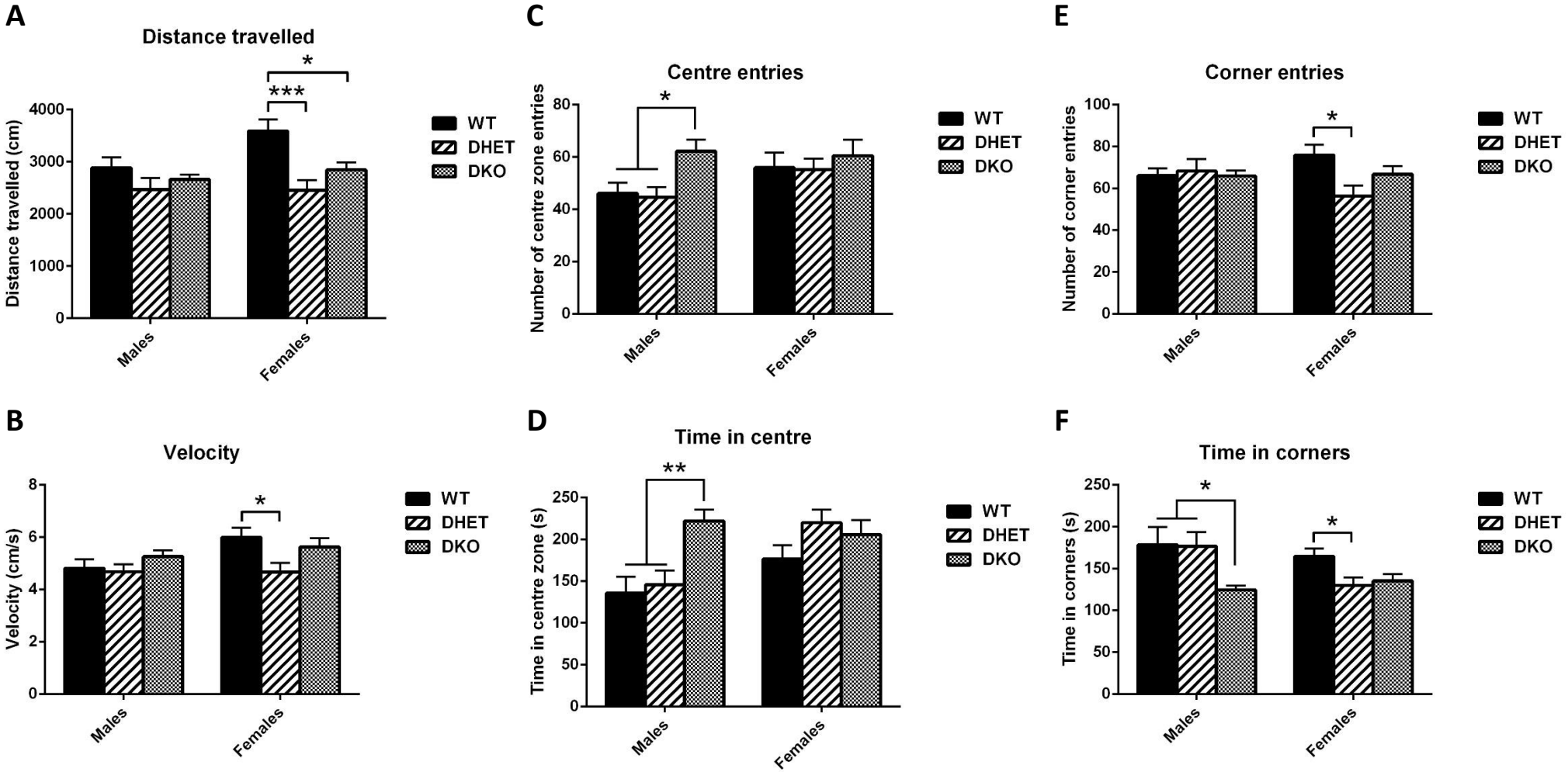

Figure 4.9: Effect of LNX1/LNX2 genotype on anxiety-related behaviour and spontaneous locomotor activity in the open field task. Mice of the indicated genotypes were placed in the centre of the arena and allowed to move freely for 10 minutes. Movement of mice in the open field was tracked using Ethovision software. Distance travelled (A) and velocity (B) were analysed as indices of general locomotor activity. The number of entries into, and amount of time spent in the centre (C and D) versus the corners (E and F) of the open field arena were monitored as indicators of differences in anxiety-like behaviour. Data are expressed as means ± SEM. n = 10-13/group. *p < 0.05, **p < 0.01, ***p < 0.001; one-way ANOVA followed by Bonferroni post-hoc test.

As the results of the open-field experiments suggested that *Lnx1* and *Lnx2* knockout leads to a reduction in anxiety-related behaviours, in males at least, it is interesting to look at other tests from the behavioural battery that relate to anxiety.

4.3.5.1.2 Light-dark box test

In addition to an aversion open spaces, mice also have a natural aversion to brightly illuminated spaces, which is reflected in their behaviour when subjected to the light/dark box test. The light-dark box exploration paradigm, which is based on the innate aversion of rodents to brightly illuminated areas and on the spontaneous exploratory behaviour of the animals, is used primarily to detect anxiogenic behaviour [113].

There were no significant overall differences between male genotypes in latency to first enter the dark compartment ($F_{2,32}$ = 0.07835, P = 0.9248; Fig. 4.10A), number of light–dark transitions ($F_{2,32}$ = 2.501, P = 0.0979; Fig. 4.10C) or total time spent in the light compartment ($F_{2,32}$ = 0.2197, P = 0.8040; Fig. 4.10B), as revealed by one-way ANOVA.

One-way ANOVA also revealed no significant effects of genotype among females on latency to first enter the dark chamber ($F_{2,31}$ = 0.9406, P = 0.4012; Fig. 4.10A) or total number of light-dark transitions ($F_{2,31}$ = 0.7211, P = 0.4947; Fig. 4.10C). Female DKO mice did however tend to spend more time in the light compartment when compared to WT and DHET counterparts, but this difference was not quite statistically significant ($F_{2,31}$ = 3.250, P = 0.0533; Fig. 4.10B), as revealed by one-way ANOVA.

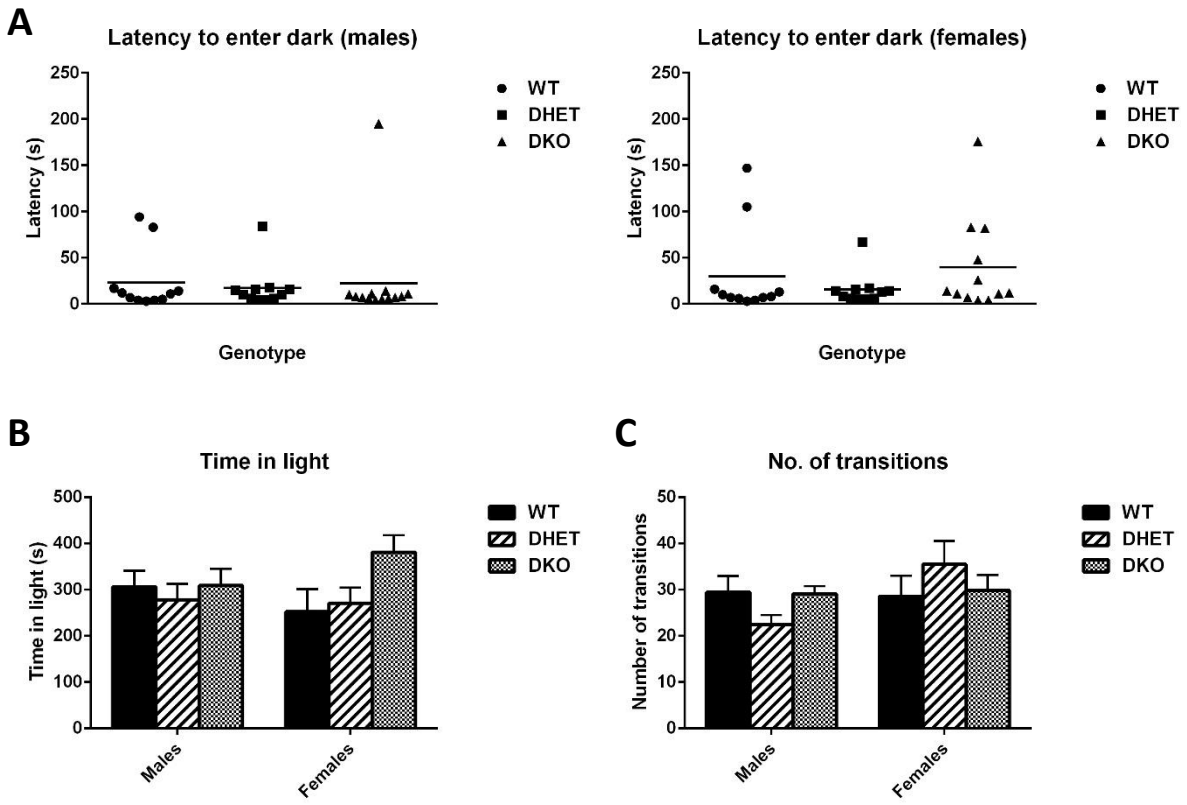

Figure 4.10: Effect of LNX1/LNX2 genotype on anxiety-related behaviour in the light/dark box. Mice were placed in the lighted compartment of the apparatus and latency to enter the dark compartment (A), time in light compartment (B) and the number of transitions between the light and dark compartments in the light-dark box (C) were recorded for mice of the indicated genotypes and sex. Data displayed in panel (A) as mean with individual data points. Data displayed in panels (B) and (C) as mean +/- SEM. Analysis by one-way ANOVA did not reveal any significant effects of genotype on the parameters measured. n = 10-13/group.

4.3.5.1.3 Elevated-plus maze test

The elevated-plus maze is used to analyse anxiety-related behaviour on the basis of that there is greater stress from being in the open arms versus the closed arms of the elevated plus maze [113]. The number of entrances into the open arms and the time spent in the open arms provide indications of anxiety-like behaviour, and the total number of entries into all of the arms is a measure of total activity.

A significant effect of genotype was detected for the percentage of entries into ($F_{2,31}$ = 8.891, P = 0.0009; Fig. 4.11A) and the time spent in the open arms ($F_{2,31}$=21.03, p=<0.0001; Fig. 4.11D) in male mice as revealed by one-way ANOVA. Bonferroni post-hoc analysis revealed that DKO mice entered the open arms more frequently (P < 0.001 and P <0.05) and spent significantly more time in the open arms (P <0.0001 and P <0.001) when compared to WT and DHET counterparts respectively, consistent with a phenotype characterised by a reduced anxiety-like behaviour. Furthermore, examination of closed arm entries revealed a significant effect of genotype on the percentage of entries into ($F_{2,31}$ = 8.891, P = 0.0009; Fig. 4.11B) and the time spent in the closed arms ($F_{2,31}$ = 13.77, P = <0.0001; Fig. 4.11E). DKO mice displayed a significantly lower percentage of closed arms entries (P < 0.001 and P <0.05) and spent significantly less time in the closed arms (P < 0.001) compared to WT and DHET mice respectively. One-way ANOVA indicated a significant overall effect of genotype on total number of arm entries ($F_{2,31}$ = 6.407, P = 0.0047; Fig. 4.11C). Bonferroni post-hoc test revealed that DHET mice exhibited a significantly lower number of total entries in comparison to WT and DKO counterparts (P <0.05 and P <0.01 respectively). No difference in the total number of arm entries was observed between WT and DKO mice however, confirming that the behavioural variability between these genotypes was not as a result of differences in their locomotor activity.

With regard to female mice, significant overall differences in the percentage of entries ($F_{2,31}$ = 7.362, P = 0.0024; Fig. 4.11A) and time spent in the open arms ($F_{2,31}$ = 10.70, P = 0.0003; Fig. 4.11B) of the elevated plus maze were also observed, as indicated by one-way ANOVA. Bonferroni post-hoc analysis revealed that DKO mice showed a significant increase the percent in of entries into the open arms compared to WT controls (P < 0.01) and an increase in the time spent in the open arms compared to WT and DHET counterparts respectively (P <0.001 and P <0.01). Furthermore, no differences in the total number of entries was observed ($F_{2,31}$ = 3.284, P <0.0509; Fig. 4.11E). One-way ANOVA revealed a significant effect of genotype on the percentage of entries into ($F_{2,31}$ = 7.362, P = 0.0024; Fig. 4.11C) and the time spent ($F_{2,31}$ = 8.137, P = 0.0014; Fig. 4.11D) in the closed arms of the elevated plus maze. Bonferroni post-hoc indicated DKO mice entered the closed arms less often than WT mice (P <0.01) and spent less time there (P <0.01) than either WT or DHET mice.

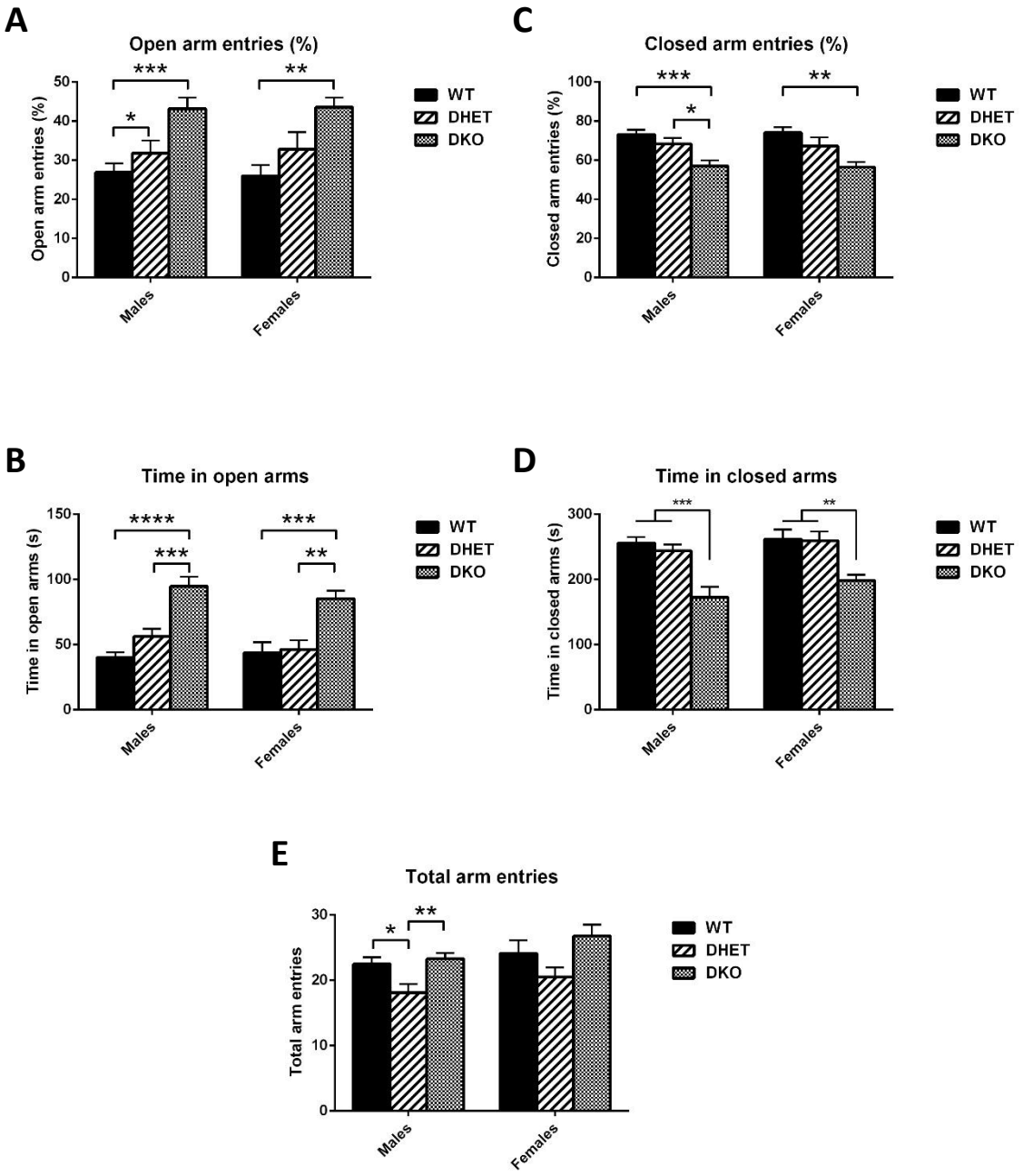

Figure 4.11: Effect of LNX1/LNX2 genotype on anxiety behaviour in the elevated plus-maze. Mice of all genotypes were tested for 6 min on the elevated plus maze. (A) Percent of entries into the open arms, (B) percent of entries into the closed arms, (C) time spent in the open arms, (D) time spent in the closed arms and (E) total arm entries are shown. Increased entries into, and time spent in the open versus the closed arms are indicative of reduced anxiety-like behaviour. The total number of entries is an index of general locomotor activity during the task. (E). Data expressed as means ± SEM. n = 10-13/group. *p < 0.05, **p < 0.01, ***p < 0.001, ****p < 0.0001; one-way ANOVA followed by Bonferroni post-hoc test.

Collectively, the results of the elevated plus maze are consistent with a phenotype characterised by a reduced anxiety-like behaviour.

To conclude, anxiety-like behaviours of DKO mice were reduced in the open field test and the elevated plus maze test, but not in the light/dark transition test.

4.3.5.2 Motor coordination and balance

4.3.5.2.1 Rotarod

Motor coordination and skill learning were evaluated in an accelerating rotarod test. As seen in Fig. 4.12, male mice of all genotypes improved significantly across the days of testing ($F_{2,72}$ = 24.74, P = <0.0001), with mice remaining on the rotarod for a shorter period of time on day one compared with days two and three. There was no overall difference between the genotypes ($F_{2,36}$ = 0.9243, P = 0.4060) and no significant genotype x day interaction ($F_{4,72}$ = 0.7746, P = 0.5453), on latency to fall indicating intact motor performance across genotypes of male mice. Furthermore, female mice of all genotypes also improved significantly across the days of testing ($F_{2,58}$ = 9.850, P = 0.0002). Again, there was no significant overall effect of genotype ($F_{2,29}$ = 0.01303, P = 0.9871) and no significant genotype x day interaction ($F_{4,58}$ = 0.1860, P = 0.9448) was observed on latency to fall indicating unaffected motor performance across genotypes of female mice.

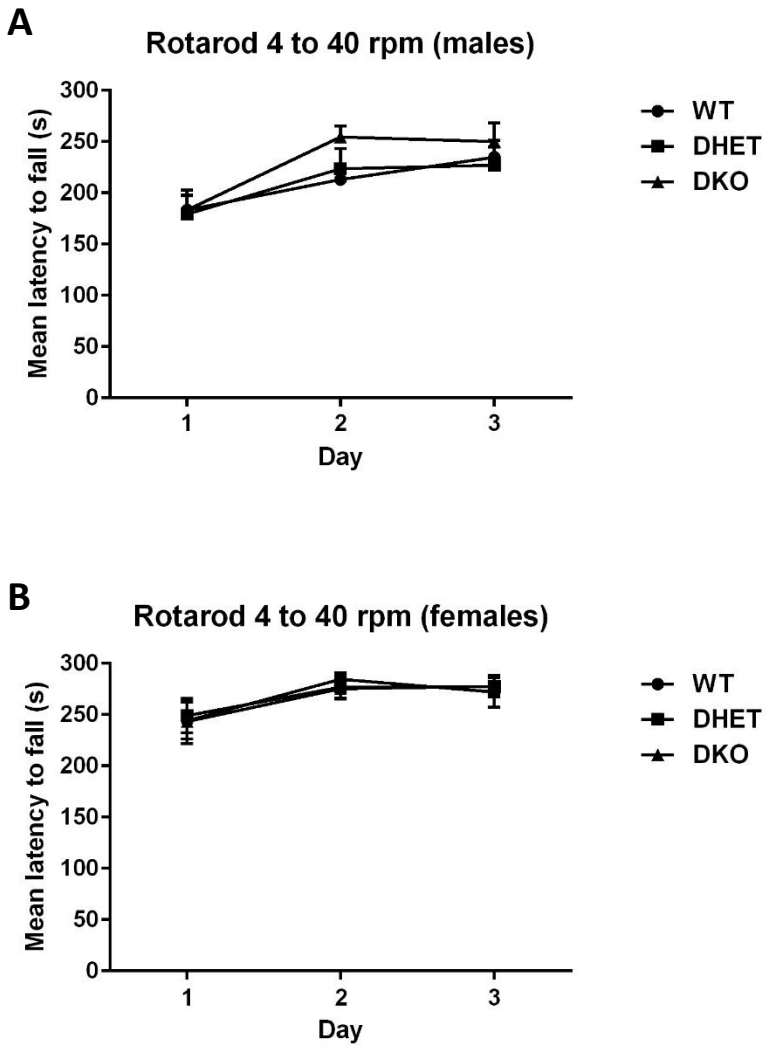

Figure 4.12: Effect of LNX1/LNX2 genotype on motor skill learning and coordination in the accelerating rotarod test. Male (A) and female (B) mice of the indicated genotypes were placed onto an accelerating rotarod and their latency to fall was measured in three trials per day, for three consecutive days. There were no significant differences between genotypes for either sex on any of the days as assessed by repeated measures two-way ANOVA. Improved performance on day 2 and 3 is indicative of normal motor skill learning in the task. Data are presented as mean ± SEM, n= 9-13/group.

4.3.5.2.2 Footprint analysis

Gait abnormalities were assessed by analyzing the footprint pattern of mice while they walked along a narrow corridor. Representative footprint patterns are illustrated in Fig. 4.13A.

Both male and female mice of all genotypes appeared to walk in a relatively straight line. One-way ANOVA revealed no significant effect of genotype on left ($F_{2,32}$ = 3.191, P = 0.0545; Fig. 4.13B) or right ($F_{2,32}$ = 2.789, P = 0.0765; Fig. 4.13C) stride lengths of male mice. Furthermore, no significant difference on stride width was observed ($F_{2,32}$ = 0.6438, P = 0.5320; Fig. 4.13F). With regard to step length, no significant influence of genotype on right to left step length was detected ($F_{2,32}$ = 0.3077; Fig. 4.13E). A significant overall difference on left to right step length was observed however, as indicated by one-way ANOVA ($F_{2,32}$ = 3.912, P = 0.0302; Fig. 4.13D), but Bonferroni post-hoc test revealed no significant differences between individual groups.

With regard to female mice, one-way ANOVA revealed a significant overall effect of genotype on left stride length ($F_{2,31}$ = 5.004, P = 0.0131; Fig. 4.13B), but not right stride length ($F_{2,31}$ = 2.791, P = 0.0768; Fig. 4.13C). Bonferroni post-hoc test showed a decrease in left stride length of DKO mice compared to WT or DHET counterparts (P <0.05). Furthermore, a significant difference in stride width was observed ($F_{2,31}$ = 3.402, P = 0.0464; Fig. 4.13F). Stride width was significantly increased for DHET mice when compared to WT control (P <0.05). However, no difference in stride width between WT and DKO mice was revealed. As was the case among male mice, no significant effect of genotype was observed on right to left stride length ($F_{2,31}$ = 0.3311, P = 0.7206; Fig. 4.13E), but a statistically significant difference on left to right stride

length was detected ($F_{2,31}$ = 3.498, P = 0.0427; Fig. 4.13D). Again, Bonferroni post-hoc test revealed no significant differences between individual groups.

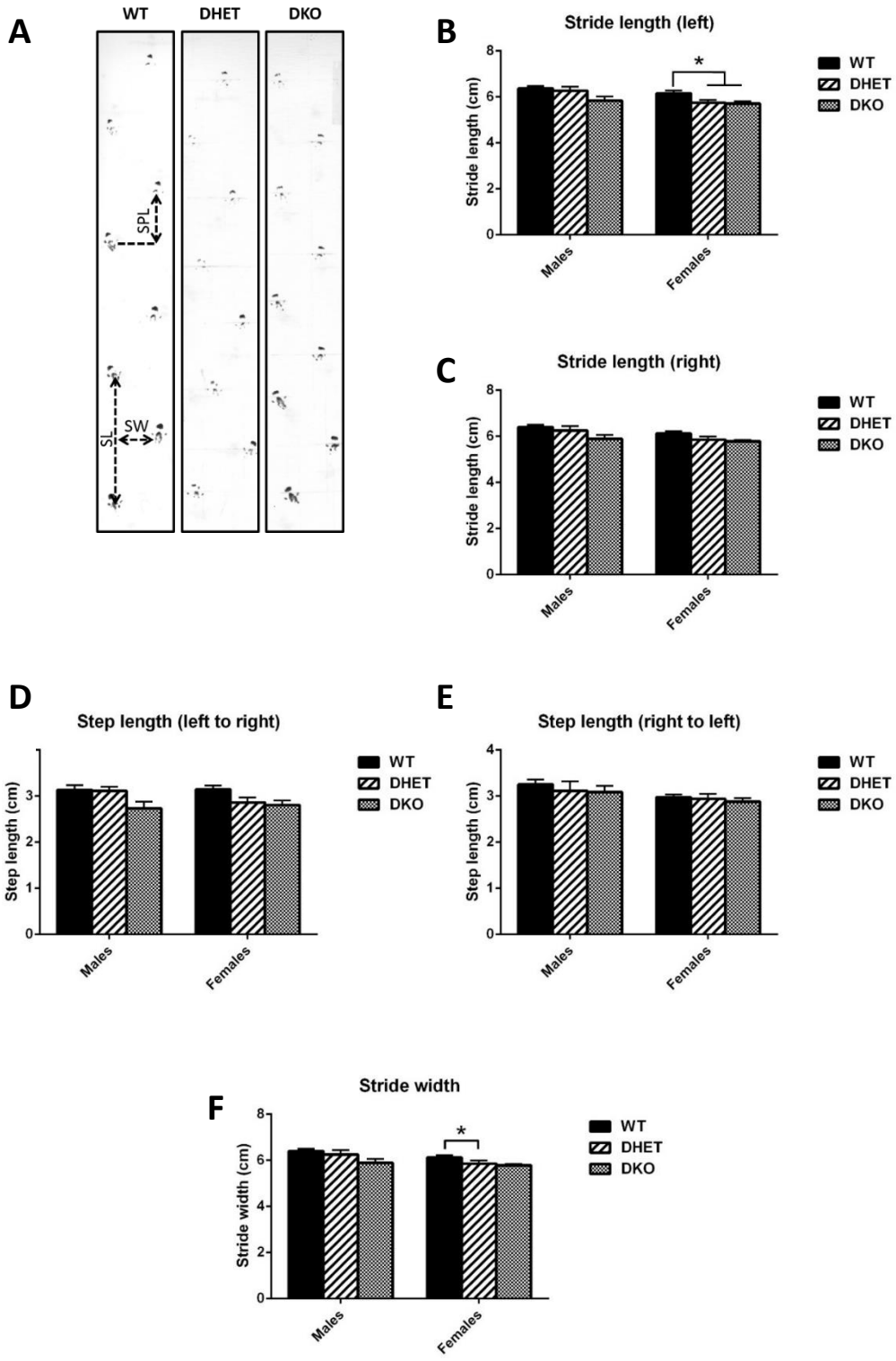

Figure 4.13: Effect of LNX1/LNX2 genotype on gait. (A) Representative footprint patterns of WT, DHET and DKO mice. Parameters measured are indicated by dotted lines. Footprint patterns were assessed quantitatively by measurements of (B) left and (C) right hind limb stride length (SL), (D) left-to-right hind step length, (E) right-to-left hind step length (SPL) and (F) hind limb width (SW). Data for each measure are expressed as mean ± SEM. n = 10-13/group. *$p < 0.05$; one-way ANOVA followed by Bonferroni post-hoc test.

4.3.5.2.3 Grip strength

One-way ANOVA indicated no significant overall differences in grip strength between genotypes of male mice ($F_{2,32}$ = 1.102, P = 0.3446; Fig. 4.14). With regard to females, again no significant effect of genotype was observed on grip strength, with comparable values obtained across groups ($F_{2,31}$ = 1.049, P = 0.3764; Fig. 4.14).

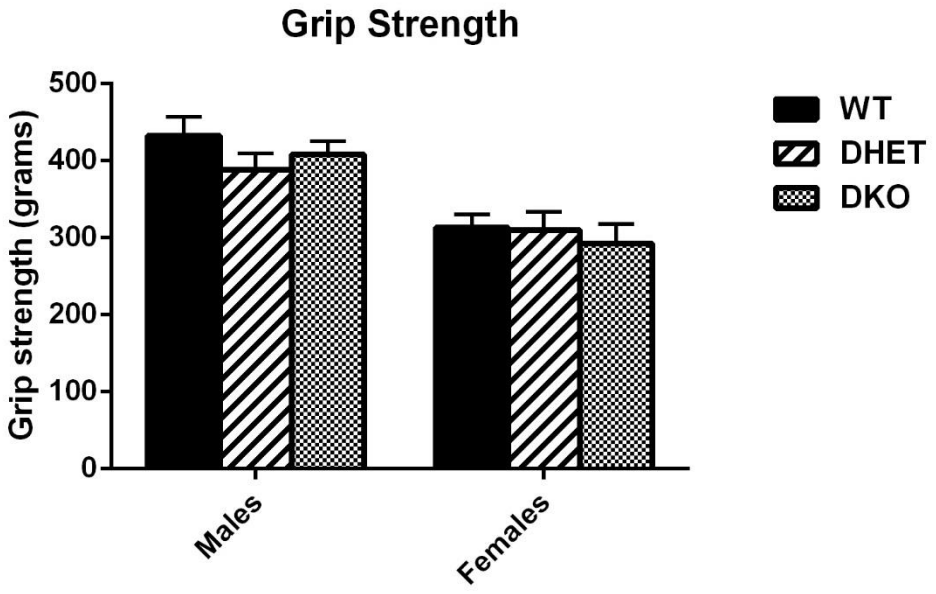

Figure 4.14: Effect of LNX1/LNX2 genotype on muscle strength in the grip strength task. Mice were allowed to grasp a grid with their fore limbs and gently pulled back until release of their grip. Average of 5 trials was recorded for each animal. No significant effect of genotype on muscle strength was observed for either sex as assessed by one-way ANOVA. All results are expressed as mean ± SEM. n = 10-13/group.

4.3.5.3 Sensory responses

4.3.5.3.1 Hot plate test

The hotplate test provides an assessment of sensitivity to painful stimuli, which provides useful information to properly interpret the results of fear conditioning tests. No significant effect of genotype was detected among males in the hotplate test (Fig. 4.15), with comparable latency to first hindlimb response observed across groups ($F_{2,30}$ = 0.7630, P = 0.4751). With regard to females, again no significant differences were observed in latency to first hindlimb response, indicating comparable nociceptive thresholds across genotypes ($F_{2,29}$ = 1.049, P = 0.3631; Fig. 4.15). Furthermore, all groups responded to footshock in the fear conditioning paradigm, suggesting normal pain sensitivity in DKO mice.

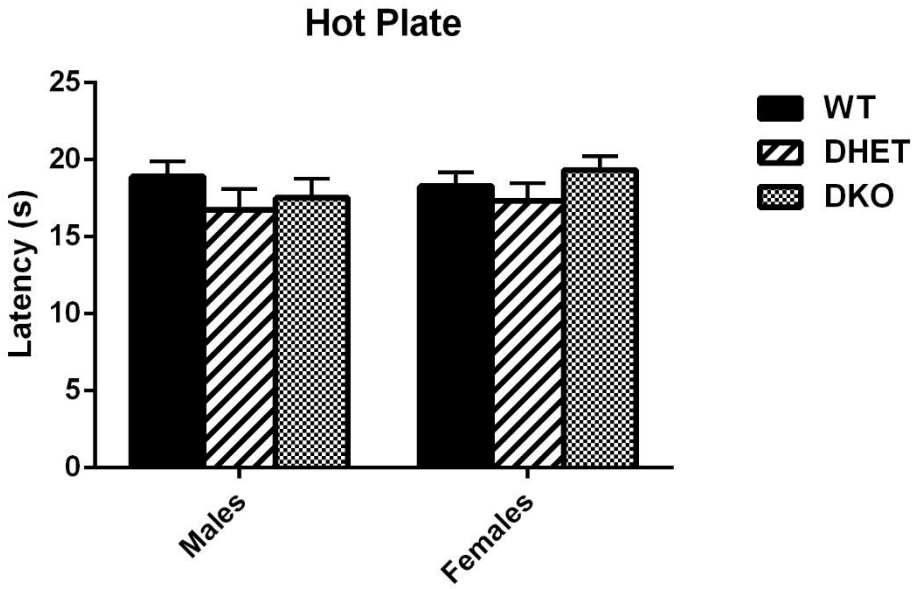

Figure 4.15: Effect of LNX1/LNX2 genotype on analgesia-related responses in the hotplate test. No effect of genotype was observed on pain threshold, with male and female mice of all genotypes showing similar latencies to exhibit a hind-limb response as assessed by one-way ANOVA. Values represent mean+SEM. n = 10-13/group.

4.3.5.4 Learning and memory

4.3.5.4.1 Y-maze test

Short-term spatial working memory and exploratory performance was examined by monitoring spontaneous alternation behaviour in the Y-maze, a hippocampus dependent learning task. The spontaneous alternation performance relies on inherent tendency of mice to enter a less recently visited arm, different from that of the preceding choice. If working memory is impaired, mice fail to remember the preceding arm position selected and the number of alternations should be reduced [112]. Total arm entries serve as a measure of exploratory activity.

A significant overall difference between genotypes was observed in total arm entries in male mice ($F_{2,30}$ = 3.689, P = 0.0370; Fig. 4.16A). DHET mice displayed significantly less arm entries when compared to WT controls (P <0.05). No differences in total arm entries were observed between WT and DKO mice however, indicating comparable exploratory activities between these two groups. No effect of genotype was detected in total alternations ($F_{2,30}$ = 0.7880, P = 0.4642; Fig. 4.16B). There were no overall differences between genotypes in alternation percentage ($F_{2,30}$ = 0.4270, P = 0.6564; Fig. 4.16C), and alternation performances across genotypes were well above the random performance level of 50%, indicating no effect of genotype on spatial-working memory of male mice.

With regard to females, there was no significant overall effect of genotype on the total number of arm entries ($F_{2,29}$ = 0.3615, P = 0.6997; Fig. 4.16A), indicating comparable exploratory activity across groups. Again, no significant overall differences in total alternations ($F_{2,29}$ = 1.294, P = 0.2896; Fig. 4.16B) or in alternation percentage ($F_{2,29}$ = 1.559, P = 0.2275; Fig.

4.16C) were detected. Alternation performances across genotypes were well above the random performance level of 50%.

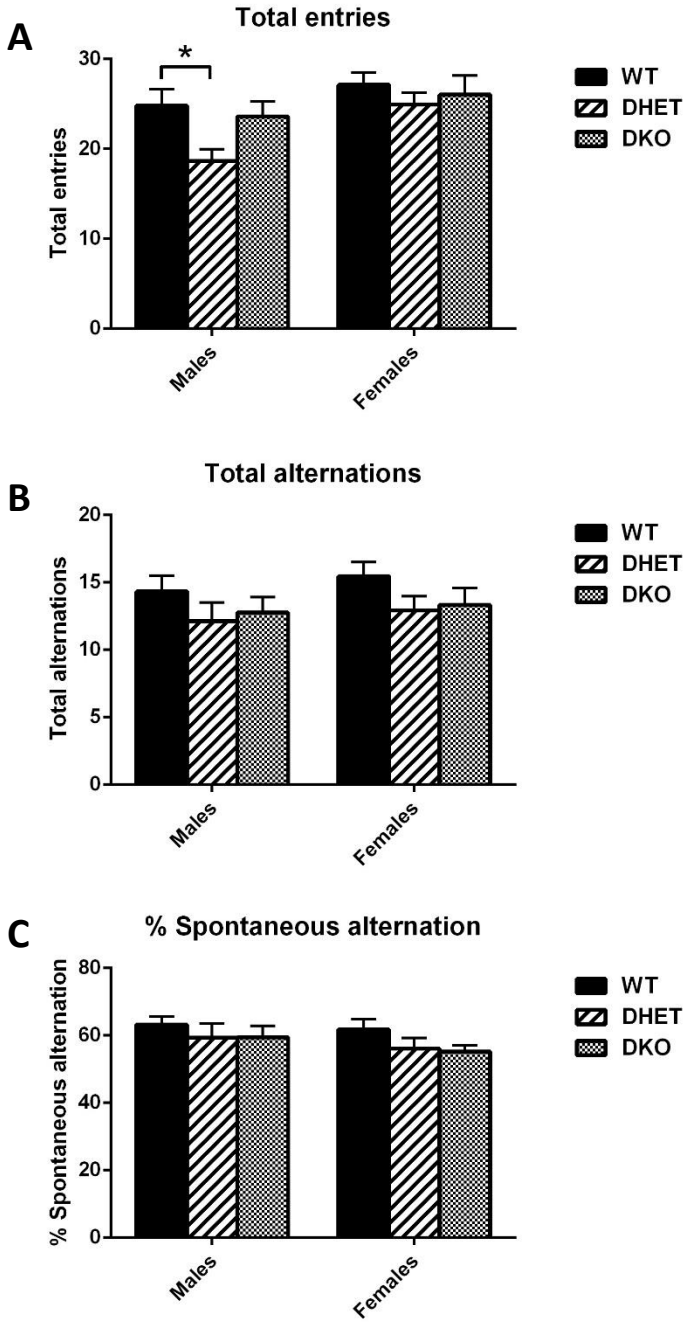

Figure 4.16: Effect of LNX1/LNX2 genotype on spontaneous alternation behaviour in the Y-maze. Total entries into the arms of the maze (A) were measured as an index of locomotor activity in the task. The number (B) and % (C) of alternations – instances where the mouse visits all three arms in sequence, were monitored as a measure of spatial memory. Data expressed as means ± SEM. n = 10-13/group. *p < 0.05; one-way ANOVA followed by Bonferroni post-hoc test.

4.3.5.4.2 Conditioned fear paradigm

Fear conditioning is a commonly used paradigm that assesses the ability of an animal to learn and remember basic associations between environmental cues and an aversive experience. Fig. 4.17 shows the behaviour of WT, DHET and DKO mice in the fear conditioning paradigm. No effect of genotype was observed on the acquisition ($F_{2,32}$ = 2.669, P = 0.0847), recall ($F_{2,32}$ = 0.2580, P = 0.7742) or extinction ($F_{2,32}$ = 2.270, P = 0.1197) of conditioned fear in male mice as measured by freezing responses to both the conditioning chamber context and the light/sound cue. Furthermore, no significant genotype x phase interaction was detected. With regard to females, no significant differences between genotypes was detected on the acquisition ($F_{2,27}$ = 0.5573, P = 0.5792), recall ($F_{2,31}$ = 0.4307, P = 0.6539) or extinction ($F_{2,31}$ = 0.1713, P = 0.8433) of conditioned fear, with all groups exhibiting comparable levels of freezing. No significant genotype x phase interaction was detected.

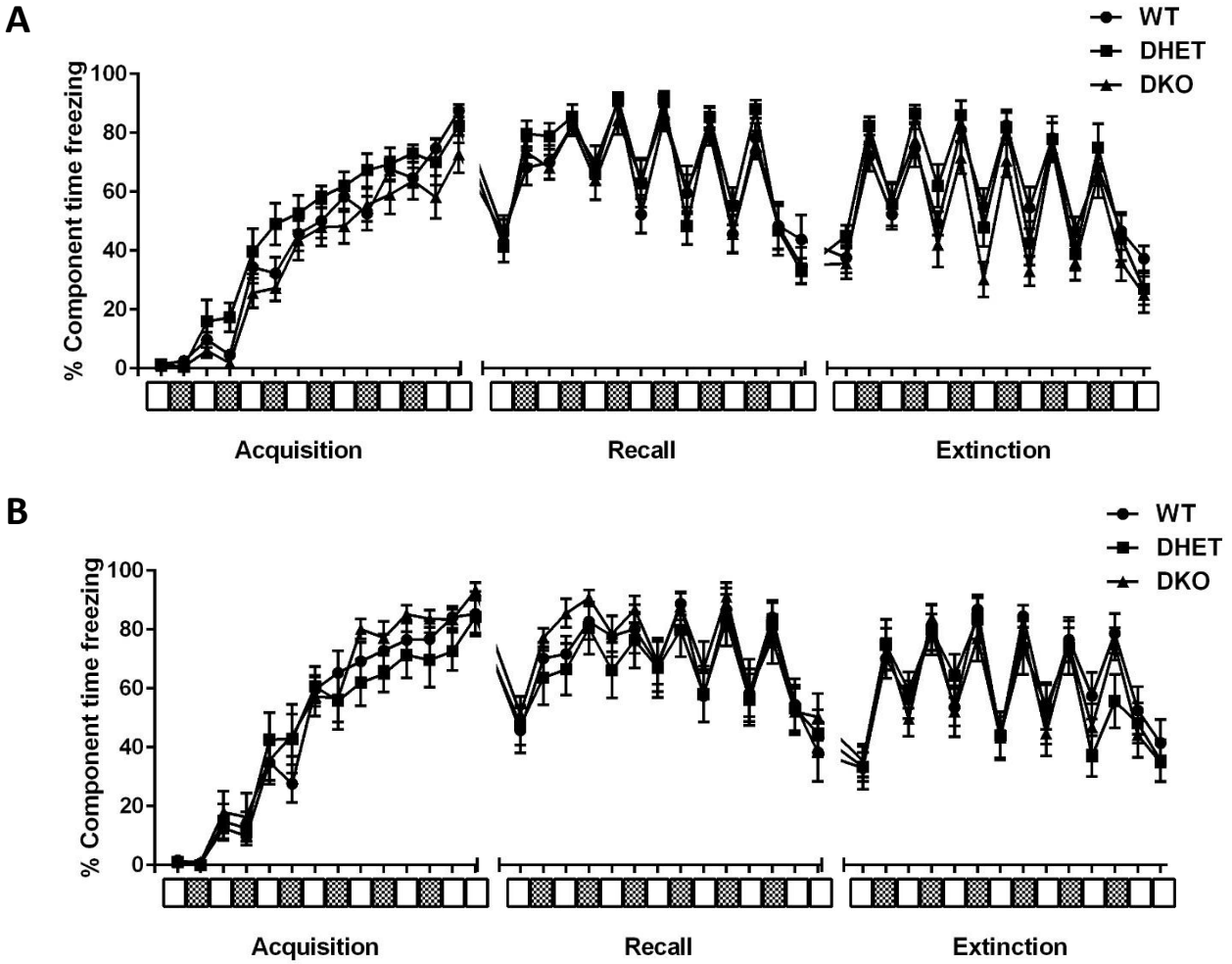

Figure 4.17: Effect of LNX1/LNX2 genotype on freezing behaviour in a paradigm of conditioned fear. Comparable levels of freezing were observed across genotypes for male (top) and female (bottom) mice in both the context and cued components of the conditioned fear paradigm as assessed by repeated measures two-way ANOVA. White boxes on the x-axis represent context components and black boxes signify cue components. Data are expressed as % time spent immobile (freezing) during each stage of the procedure. Data are expressed as mean±SEM. n=10-13/group.

4.3.5.5 Depression-like behaviour

4.3.5.5.1 Forced swim test

Fig. 4.17 shows the behaviour of WT, DHET and DKO mice in the fear conditioning paradigm – a test of depressive behaviour. No effect of genotype on time spent immobile was observed in this test.

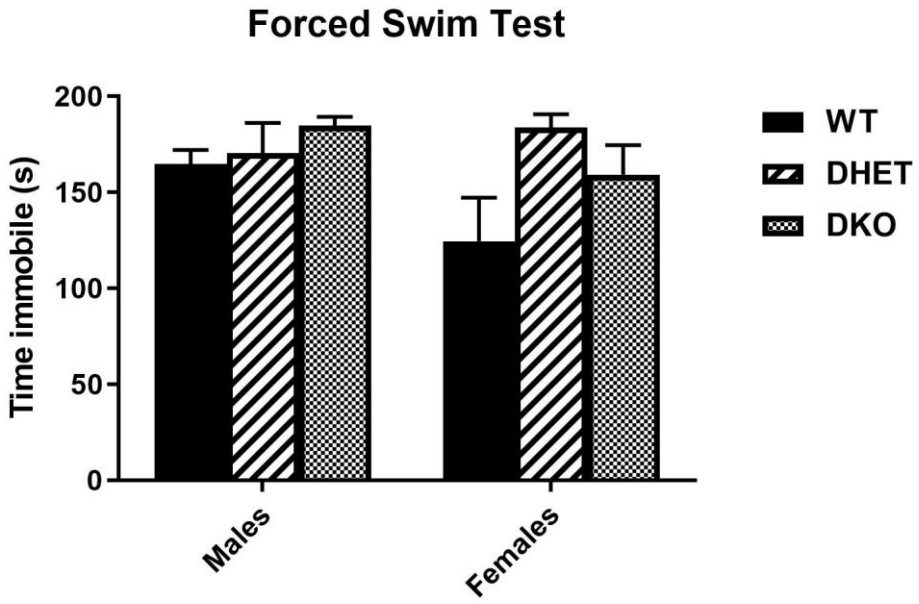

Figure 4.18: Effect of LNX1/LNX2 genotype on time spent immobile in the forced swim test. No significant effect of genotype on time immobile in the final 4 minutes of the forced-swim test was observed for either sex as assessed by one-way ANOVA. Values represent mean+SEM. n = 10-13/group.

4.4 Discussion

Studies of *Lnx* expression showed a widespread distribution of *Lnx1* and *Lnx2* mRNAs in several adult tissues, with the earliest embryonic expression of both genes observed in the CNS [25]. The function of LNX proteins *in vivo* remains unknown however, largely because LNX proteins are expressed at exceedingly low levels in most tissues. LNX1 and LNX2 functions have not been thoroughly explored *in vivo* in any mammalian model organism, and all studies of LNX1 and LNX2, to date, have relied heavily on exogenously expressed LNX proteins. High throughput phenotyping efforts claimed that genetic ablation of either LNX1p70 or LNX2 does not result in overt phenotypical alternations, with the exception of a very minor immunological abnormality for LNX1 p70 KO mice, the significance of which is unclear since only the brain isoform was deleted (www.mmrrc.org). Furthermore, it should be noted that the LNX2 KO mouse analysed targeted a different exon to that described here, and the absence of the LNX2 protein was not validated in this study (www.mousephenotype.org). Based on the sequence homology and partly overlapping tissue distribution of *Lnx1* and *Lnx2* [25], compensation or functional redundancy between these two genes is possible. Therefore, for the very first time LNX1p70/p62 and LNX2 DKO mice were generated. These mice completely lack LNX expression in the brain and are therefore a suitable model to study LNX function in the CNS by behavioural phenotyping. The behavioural phenotyping consisted of a battery of tests, which included tests for simple sensory and motor function, locomotor activity, anxiety-related and depressive responses, motor coordination and skill learning, conditioned fear and spatial learning – the results of which are summarised below, in Table 4.1. The study also examined the role of sex in each of the phenotypes measured.

Table 4.1: Summary of results from the behaviour test battery

Test	Behaviour measured	Parameter	Males		Females	
				P value		P value
Y-maze	Memory	Total entries	↓	WT vs DHET p<0.05	–	ns
		Total alternations	–	ns	–	ns
		% spontaneous alternation	–	ns	–	ns
Open field	Activity, anxiety-like behaviour	Distance travelled	–	ns	↓	WT vs DHET p<0.001
					↓	WT vs DKO p<0.05
		Velocity	–	ns	↓	WT vs DHET p<0.05
		Number of centre entries	↑	WT, DHET vs DKO p<0.05	–	ns
		Time spent in centre	↑	WT, DHET vs DKO p<0.01	–	ns
		Number of corner entries	–	ns	↓	WT vs DHET p<0.05
		Time spent in corners	↓	WT, DHET vs DKO p<0.05	↓	WT vs DHET p<0.05
Light/dark box	Anxiety-like behaviour	Latency to enter dark	–	ns	–	ns
		Time spent in light	–	ns	–	ns
		Number of light/dark transitions	–	ns	–	ns
Elevated plus maze	Anxiety-like behaviour	Total arm entries	↓	WT vs DHET p<0.05	–	ns
			↑	DHET vs DKO p<0.01		
		% open arm entries	↓	WT vs DHET p<0.05	↑	WT vs DKO p<0.01
			↑	WT vs DKO p<0.001		
		Time spent in open arms	↑	WT vs DKO p<0.0001	↑	WT vs DKO p<0.001
			↑	DHET vs DKO p<0.001	↑	DHET vs DKO p<0.01
		% closed arm entries	↓	WT vs DKO p<0.001	↓	WT vs DKO p<0.01
			↓	DHET vs DKO p<0.05		
		Time spent in closed arms	↓	WT, DHET vs DKO p<0.001	↓	WT, DHET vs DKO p<0.01
Gait analysis	Gait, locomotion, motor function	Stride width	–	ns	↓	WT vs DHET p<0.05
		Stride length	–	ns	↓	WT vs DHET, DKO p<0.05
		Step length	–	ns	–	ns
Rotarod	Motor coordination and learning	Latency to fall	–	ns	–	ns
Grip strength test	Muscle strength	Grip strength	–	ns	–	ns
Hot plate test	Nociception	Hindleg response	–	ns	–	ns
Fear conditioning	Memory, learning	% time freezing	–	ns	–	ns
Forced swim	Depression-like behaviour	Time immobile	–	ns	–	ns

4.4.1 General appearance, body weight, survival and organ weights

Characterisation of the DKO mice revealed that these mice are viable and fertile. Genotype distributions at birth matched expected Mendelian ratios indicating no evidence of embryonic lethality. Newborn DKO mice were indistinguishable from WT or DHET mice. However, within 5 weeks for males, and 3 weeks for females, a reduction in their body weight was noticed, and this slower growth continued throughout the period of study. Despite normal tooth development and the continued ability to eat, the growth of these mice was somewhat reduced. At week 12, their mean body weight was approximately 11% and 8% less than that of their WT and DHET counterparts respectively for males, and 13.2% less than WT controls for females. WT, DHET and DKO males consistently weighed more than females of their respective genotype.

Given the expression of *Lnx2* mRNA in the colon [43], it is possible that the reduced weight gain observed in DKO mice may be indicative of an important role of *Lnx2* in the development of the gut. It will be of great interest to determine whether the reduced ability to thrive is due to direct defects or delays in intestine development or function, or whether underlying neuroanatomical defects influence food sensing or eating behaviour in DKO mice. To distinguish between these possibilities it will be necessary to perform detailed analysis of intestine development and function, further behavioural studies on mutant mice and to use a conditional allele to delete *Lnx2* solely from brain or intestine cells and determine which region is responsible for the phenotype. Dual energy x-ray absorbance (DEXA) and nuclear magnetic resonance imaging (MRI) analysis are useful methods for assessing body composition *in vivo* and should also be considered in future studies.

Adult WT, DHET and DKO mice were dissected and all major organs were investigated macroscopically. Compared with WT controls, the overall size and weight of brains from adult DKO mice was significantly increased. Histological examination of DKO brains was since performed to investigate changes at the microscopic level. With the exception of the reduced size of all regions, no abnormalities in the overall structure of the different brain regions examined were observed. *In vivo* magnetic resonance imaging (MRI) is also an excellent non-invasive technique for studying brain anatomy in transgenic and mutant mice (Kooy et al., 2001; Natt et al., 2002). For further characterization of DKO mutant brain anatomy, it may be useful to perform high- resolution 3D MRI as previously described. The increase in DKO brain weights suggests an increase in either neurons or glia and the use of specific cell markers will allow us to assess which cell types are increased in the DKO brains. An increased brain mass was observed in mice overexpressing IGF2 and is also associated with autism spectrum disorders [116]. An increased ratio of organ to body weight was also observed in other DKO tissues examined including the heart and lungs. The increased ratios in mutant mice may be due to compensatory growth, for example as a result or hyperplasia, hypertrophy or increased functional demand, or may be as a result of pathological enlargement. Serological analysis will aid in the evaluation of tissue function, and furthermore will identify changes to metabolism that could contribute to the reduced body weight observed in DKO mice when compared to WT and DHET control animals.

4.4.2 Anxiety-like behaviour

Lnx1 and *Lnx2* mRNAs are expressed in the hippocampus which, along with the amygdala, pre-frontal cortex and bed nucleus of the stria terminalis, is involved in the regulation of

emotional behaviour [117]. Thus, it is plausible that LNX1 and LNX2 may contribute to some aspect of emotional behaviour or mechanism of anxiety.

In order to evaluate anxiety-like behaviour, DKO mice and their WT and DHET counterparts were tested in various approach-avoidance paradigms: the open field test, the light-dark box test and the elevated plus maze. These tests are based on the conflict between the innate exploratory behaviour of rodents and their aversion towards open, bright, or elevated spaces, at risk of predation [109].

In the open field test, with regard to males, DKO mice showed decreased avoidance of the central area, entering this area significantly more frequently and spending significantly more time there than either WT or DHET mice. Furthermore, DKO mice spent significantly less time in the periphery of the arena, including corners, than control animals. Collectively, these results are consistent with a reduced anxiety-like behaviour and increased exploratory behaviour. Similar differences, though not quite statistically significant, were observed among female counterparts. With regard to females, DKO mice tended to enter the centre area of the open field arena more frequently than either WT or DHET animals, and DHET and DKO mice spent more time in this area than WT controls. Furthermore, DHET and DKO mice also spent less time in the periphery, including corners, and entered the corners of the arena less frequently than WT animals, further suggesting a reduced anxiety-like, increased exploratory phenotype.

The elevated plus maze further revealed an anxiolytic phenotype, with DKO mice of both sexes entering and spending more time in the unprotected open arms significantly more than WT and DHET animals.

By contrast, no differences were observed in latency to enter the dark compartment, the number of transitions between light and dark sides, or time spent in the light compartment in the light-dark box test.

While obtaining consistent findings across multiple tests is generally strong evidence for particular phenotype, it is recognized that various tests of anxiety in rodents do not measure exactly the same psychological phenomenon. Rather, each test can be regarded as measuring overlapping, but partially distinct, aspects of anxiety-related behaviour [113]. Thus, knockout models with both anxiogenic and anxiolytic phenotypes that are specific to particular tests have previously been reported [109, 118]. Overall, reports on transgenic and knockout mice with reduced anxiety-like behaviour are not uncommon in the literature, though anxiolytic indications are sometimes found in combination with other behavioural deficits [119].

4.4.3 General locomotion, motor coordination and balance

Integration of the motor cortex, cerebellum and sensory motor neurons provide a network that allows innervation of muscle cells and allow motor function [120]. Due to the complexity of the system, many genes are involved in the regulation of motor function. A mutation in any of these may thus produce an abnormal motor phenotype. *Lnx1* and *Lnx2* mRNAs are widely expressed in motor cortex, the spinal cord and cerebellum [25] – regions of the central nervous

system involved in motor function, therefore, it is possible that LNX1 and LNX2 are involved in some aspect of motor function. DKO mice, along with WT and DHET animals were tested with an expanded repertoire of motor-behavioural testing designed to expose cerebellar-related motor defects.

General locomotor activity was evaluated across three paradigms: the open field test, the EPM and the Y-maze test. As many of the tests employed here have a motor component to their readout of anxiolytic activity, it was important to examine basal locomotor activity of knockout and wild-type mice. It could be argued that alterations in activity may contribute to the observed anxiolytic phenotype of the DKO mice. Although the overall distance travelled by DKO and DHET female mice was significantly shorter than that travelled by wild-type controls in the open-field test, suggesting hypo-activity, no difference was observed between genotypes of male counterparts. Further tests of locomotor function, such as the EPM and Y-maze, also revealed no differences in locomotor activity between WT and DKO genotypes of either sex, as indicated by a comparable number of total entries, suggesting that LNX1 and LNX2 are unlikely to play a critical role in the integration of locomotor information.

The rotarod test is also used to screen locomotor performance measuring motor coordination and balance control [109]. Typically, mice with structural abnormalities in the cerebellum or with disruptions in genes richly expressed in the cerebellum exhibit performance deficits on the rotarod. No abnormalities were detected on the accelerating rotarod for either sex, with comparable latencies to fall observed across genotypes. Overall female mice performed better than male mice on the accelerating rotarod, exhibiting a longer latency to fall, although this could be attributed to their smaller size.

Gait abnormalities were assessed using footprint pattern analysis. Footprint analysis is a useful task to study slight locomotor impairments, which are generally undetectable in terms of motor properties [109]. Slight differences between the hind-paw footprint pathways of the mutant and wild-type mice were detected. Modest decreases in both stride lengths were observed between genotypes, for both sexes, although these differences only reached significance in the case of DHET and DKO females whose left stride length was decreased by 7% compared to WT controls. Left stride length was also decreased for DKO males compared to WT and DHET counterparts, by 8% and 7% respectively, but didn't quit reach statistical significance (P = 0.0545). A similar decrease in right stride length was observed across sexes, although this difference was not statistically significant, most likely because of increased variability in measurements. Stride width was unchanged for DKO mice when compared to WT controls, for both males and females, as was step length. Abnormal gait could be due to reduced muscular tone, impaired cerebellar motor or peripheral neurological function, and/or due to an underlying musculoskeletal anomaly. The slight differences detected by footprint analysis could however be attributed to the modest decrease in size of DKO mice compared to WT controls.

The grip test, as the gait test, is a highly specific test to measure a single aspect of motor function, muscular strength [109]. No impairment of muscular strength was observed in DKO mice of either sex when compared to their WT and DHET counterparts.

When taken together these results suggest that the network that allows innervation of muscle cells and allow motor function, which includes the motor cortex, hindbrain, cerebellum and sensory motor neurons, is not impaired in DKO mice. Given the high expression of *Lnx1* and

Lnx2 mRNAs in the deep cerebellar nuclei, it is surprising that DKO mice did not suffer from functional alterations in the cerebellar circuitry.

4.4.4 Sensory responses

The effect of *Lnx1* and *Lnx2* knockout on pain perception was analysed, using acute noxious stimuli. The results indicate no change in the nociceptive threshold after the application of thermal stimuli (hot plate test), suggesting that the LNX1 and LNX2 encoded proteins do not participate in the perception of thermal pain. The response of *Lnx1* and *Lnx2* deficient mice was also found to be unchanged after the application of a mechanical (tail pinch test) stimulus suggesting the absence of a tonic implication of the LNX1 and LNX2 encoded protein in these responses.

4.4.5 Learning and memory

Hippocampal and neocortical structures contribute to memory function [121]. In addition to testing locomotor and exploratory activity as discussed previously, the Y-maze paradigm is a useful test of hippocampus-dependent spatial working memory as measured by spontaneous alternation in the maze [112]. By nature, rodents seek a new arm of the Y-maze, different from that of the preceding choice, but if working memory is impaired, the number of correct choices should be reduced. No differences in alternation percentage were detected between genotypes for either sex. Furthermore, alternation performances across genotypes were well above the random performance level of 50%, suggesting no impairment of hippocampus-dependent spatial working memory. Furthermore, skill learning was not impaired as revealed by the rotarod test, where mice of all genotypes improved significantly across the days of testing. Fear conditioning is a commonly used paradigm that assesses the ability of an animal to learn and

remember basic associations between environmental cues and an aversive experience. After just a single pairing of the context/auditory cue and electrical footshock, mice exhibit long-lasting freezing when faced with either the context or the cue. Freezing behaviour is used as an index of fear memory. Freezing during the context portion of the task is used to assess hippocampus-dependent memory whereas freezing during the cued-portion of the task is used to assess amygdala-dependent memory. No difference between genotypes, of either sex, was observed on their ability to acquire, retain and extinguish conditioned fear, as measured by freezing responses to both the conditioning chamber context and the light/sound cue, suggesting that hippocampus and amygdala-dependent learning and memory were not impaired in DKO mice. Taken together, these results suggest that the functional networks of hippocampus and amygdala involved in learning and memory are not affected by the deletion of *Lnx1* and *Lnx2* genes.

Studies of *Lnx* expression showed a widespread distribution of *Lnx1* and *Lnx2* mRNAs in several adult tissues, with the earliest expression of *Lnx1* and *Lnx2* observed in the embryonic brain and spinal cord of the CNS [25]. *Lnx1* and *Lnx2* are overwhelmingly expressed in neurons of the CNS. LNX1 and LNX2 interacting proteins identified and characterised to date have well-established functions in neuronal development, and particularly in synapse formation. The phenotypic effects presented in this study are either the direct or indirect result of the absence of LNX1 and/or LNX2. In theory, due to their widespread mRNA expression in the CNS, LNX1 and LNX2 can either directly or indirectly regulate neuronal function, thus affecting their activity, which ultimately can modulate the behavioural traits. Indeed, association studies and expression analysis are in agreement with our findings of a reduced anxiety-like behaviour. *Lnx1* and *Lnx2* are highly expressed in the hippocampus, a brain region known to be involved in the regulation of emotional behaviour. In this regard LNX1 and LNX2 can be implicated in

the regulation of anxiety in DKO mice that exhibit decreased anxiety-related behaviour. Given the normal structural and morphological appearance of the brains of DKO mice it is unlikely that the phenotypic effects outlined in this study are due to degenerative changes, but represent functional abnormalities mediated by loss of LNX1 and/or LNX2. LNX was originally identified as an interaction partner of Numb, a key regulator of neurogenesis and neuronal differentiation [24]. While it is possible that the phenotypic effects observed in this study may be attributed to this interaction, no alterations in protein expression of Numb were observed in the brain of LNX-deficient mice. The interacting proteins identified and characterised to date suggest many other plausible candidates, in addition to Numb, that may mediate the neuronal functions of LNX proteins in the regulation of anxiety. However, a molecular basis for such a role has not been shown so far. Furthermore, the neurobiological circuits and pathways that are altered by ablation of *Lnx1* and *Lnx2* in DKO mice, generating an anxiolytic phenotype, remain to be elucidated. As several genes involved in neuronal circuit activity were found in the mass spectrometry experiments (Chapter3), future behavioural and electrophysiological studies of DKO brains will elucidate the specific role of LNX1 and/or LNX2 in synaptic transmission. Furthermore, microarray analysis should be considered in future studies to examine the gene expression patterns in brains of WT and DKO mice at different time points during postnatal brain development.

To conclude, to my knowledge, this is the first *in vivo* study on the role of LNX1 and LNX2 in the CNS. The findings reveal a novel role of LNX1 and/or LNX2 in the regulation of anxiety-related behaviour, and may therefore implicate LNX as an innovative target for developing therapeutic agents to treat anxiety-related disorders. I further identify a role of LNX in normal body weight and organ weight gain, the significance of which remains to be elucidated. For a

better understanding of LNX function *in vivo*, the molecular mechanisms and the brain regions underlying the behavioural defects should be further investigated.

.

General Discussion & Future Perspectives

This thesis aimed to better characterize LNX1 and LNX2 proteins and to study their functions in a physiologically relevant context.

Role in general health and embryonic development

No gross neuroanatomical defects were noted in DKO mice [56]. DKO mice are viable, fertile and – despite weighing on average 10% less than WT mice by adulthood, physically healthy. The mechanism underlying this slight but significant reduction in body weight is not yet known. Tooth development was normal and DKO mice showed continued ability to eat. Perhaps DKO mice have altered eating behaviours or – given LNX2 mRNA expression in the colon [43], perhaps some defect in gut development or function underpins this phenotype. Importantly, Lee at al. [122] propose an important role of *Lnx2* in early embryonic development. *Lnx2* knockdown in mouse embryos resulted in impaired blastocyst formation, with more than half of the embryos failing to develop into normal blastocysts. The authors attribute this to alteration in the expression of genes critical for early embryonic development, including Notch and Hippo signalling pathway genes. Here however, no evidence of this was seen *in vivo*, in DKO mice that lack LNX2. In fact, genotype distributions at birth matched expected Mendelian ratios indicating no evidence of embryonic lethality.

Role in anxiety-related behaviours

Behavioural phenotyping was conducted on DKO mice as described. LNX1 and LNX2 mRNAs are widely expressed in the motor cortex, spinal cord and cerebellum [25, 123] – areas of the brain that are involved in motor function. Despite this, and perhaps surprisingly, DKO mice exhibited normal motor coordination and motor skill learning, as determined by the rotarod test. DKO mice also showed normal learning and sensory function. The major finding

of the behavioural battery was a decrease in anxiety-like behaviour in DKO mice in EPM and OF test paradigms of anxiety-related behaviour. Importantly, these are both approach-avoidance based test paradigms of anxiety-related behaviour. These tests exploit the tendency of rodents to explore novel environments and their innate aversion to brightly lit, open and elevated spaces, due to fears of predation [113]. It is crucial to note that – while extensively used –approach-avoidance test paradigms cannot distinguish reduced anxiety-related behaviour from increased novelty-seeking or risk-taking behaviours. Future studies should thus assess DKO behaviour in a range of alternative test-paradigms to include non-approach-avoidance tests of anxiety-like behaviour and tests to assess novelty-seeking behaviour, risk-taking and impulsivity.

Given their sequence homology and partial overlap in mRNA expression – spatially and temporally [25], functional compensation between LNX1 and LNX2 seemed likely. Thus, behavioural phenotyping was conducted on DKO and has yet to be conducted on either single knockout line. Importantly, Liu et al. [124] have subsequently reported the normal behaviour of their LNX1 single knockout in the EPM and OF test paradigms. This suggests that the reduced anxiety phenotype observed in DKO mice in these paradigms is due to loss of either LNX2 alone or in combination with LNX1, but this has yet to be determined experimentally.

The use of conditional knockouts, where LNX can be modulated in a spatially and temporally selective manner, may be an interesting direction for further research. These would allow identification of the key brain regions in which LNX functions to modulate anxiety-related behaviour and determination of the developmental stages critical for the reduced anxiety-like phenotype observed in DKO mice. The earliest expression of LNX is observed in the

embryonic brain and spinal cord – reaching peak levels at the early postnatal stage [25, 56]; it would prove interesting to determine if the reduced anxiety-like phenotype is as a result of abnormal neurodevelopment in the absence of LNX at these stages or due to its absence in adulthood, at the time of testing.

Role in social memory

Liu et al. [124] subsequently described social learning and behaviour deficits in their LNX1 KO mice – namely, deficits in social memory, decreased sociality and increased social avoidance in the three-chamber test paradigm. Importantly, social behaviour was not assessed in the behavioural battery described in this thesis. The authors attribute these deficits to the loss of LNX1 in the hippocampal CA3 region of their knockout line. Crucially, LNX2 is also expressed in the hippocampus [25], albeit its expression is not as specific to the CA3 region. Examination of social behavior in LNX2 single knockout and DKO lines – by conducting the same three-chamber test paradigm, may thus prove an interesting direction for future research. This will determine the effect, if any, of LNX2 knockout, either alone or in combination with LNX1, on social behaviour – deficits in which are linked to autism spectrum disorders.

Research to elucidate the mechanism by which LNX modulates anxiety-like behavior in adult mice continued after completion of this thesis work. With an extensive interactome of several hundred potentially interacting proteins [51, 59], including those described in Chapter 3 – at least twenty of which can be ubiquitinated by LNX – several other possible mechanisms may underlie this. LNX was so-named based on its initial discovery as a NUMB interacting protein [24]. NUMB interacts with and inhibits NOTCH receptor signaling. LNX has been shown to ubiquitinate NUMB, targeting it for proteasomal degradation [24-26, 28] – thus promoting

NOTCH signaling [26]. It therefore seemed probable that the behavioral changes noted in the DKO mice were due to LNX regulation of NUMB/NOTCH. Thus, primary investigations into the mechanism underlying the observed phenotype focused on NUMB. Levels of NUMB appeared unchanged in postnatal DKO whole brain lysates [56]. Furthermore, Wang et al. [42] attribute abnormal SVZ development in Gli3 knockout mice to a reduction in forebrain levels of NUMB as a result of LNX2 upregulation. Gli3 functions as a repressor in the sonic hedgehog signaling pathway and is critical for specifying cell-fate and for structural organization in the developing SVZ [42]. Importantly, the authors did not demonstrate a causal relationship between LNX2 and NUMB in these mice. Defective SVZ formation thus seemed possible in DKO mice and warranted investigation. SVZ formation and cell differentiation was however normal in DKO mice [56]. Future studies examining the spatial and temporal expression of NUMB in DKO mice may prove useful in determining the role – if any – played by NUMB. Bekri et al. [125] subsequently provided evidence in support of LNX1 regulation of NUMB/NOTCH - whereby glycine signalling suppression of *Lnx* was shown to stabilise NUMB, and thus modulate NOTCH activity. This seems worthy of future investigation as a potential mechanism underpinning the behaviour observed in DKO mice.

Other LNX-interacting proteins that could potentially mediate the reduced-anxiety related phenotype observed in DKO mice might include proteins that function in neuronal development and synaptic formation and function. Perhaps the most promising of these – in terms of physiological relevance, include the postsynaptic receptors EphB1, EphB2 and GluN2B. Liu et al. [126] recently described their novel interaction with and regulation by LNX1 *in vivo* – providing the first *in vivo* evidence of a LNX regulatory function. In this study, the authors report a reduction in levels of EphB1, EphB2 and GluN2B in the CA3 region of the hippocampus of their LNX1 KO mice – an area where LNX expression is normally relatively

high [25]. Seemingly, interaction of LNX1 with the postsynaptic receptors EphB1 and EphB2 in these CA3 cells prevents their targeting for proteasomal degradation, and is crucial for normal mossy fibre axon targeting and synaptic maturation [126, 127]. Furthermore, the authors attribute disruption of a LNX1-GluN2B-EphB2 ternary complex in their LNX1 KO to the social learning deficits described above. It seems probable that loss of such interactions could potentially underlie the reduced anxiety-like observed in DKO mice and warrant future investigation.

Connexin-36 (Cx36) represents another possible LNX-interacting protein candidate underlying the reduced anxiety-like behaviour in DKO mice. Lynn et al. [128] reported the novel interaction of Cx36 with LNX1 and LNX2 and regulation by LNX2 in cultured cells; LNX2 was shown to ubiquitinate and target Cx36 for lysosomal degradation, thus removing it from gap junctions. Cx36 is a major component of neuronal gap junctions, forming the majority of electrical synapses. Such synapses are crucial for synchronous neuronal activity. Loss of such interactions could thus result in gap junction deficits and abnormalities in synchronous neuronal activity. Gap junctions appeared normal in their LNX1 single knockout mice however [128] – possibly due to functional compensation by LNX2, but could potentially be altered in DKO described here and underpin the reduced anxiety-like phenotype observed in this study.

Other candidate proteins – that warrant future consideration as mediators of the behavioural changes in DKO mice – could include the presynaptic LNX-interacting proteins ERC/CAST [55] and LIPRIN-α proteins, and neuronal signaling molecules EPHA7, SYNGAP1, SRGAP2 and FCHSD2 – described in Chapter 3, to name but a few.

Other functions of LNX

One final report worth mentioning – in terms of the role of LNX in synaptic function – is a relatively recent study by De la Rocha-Munoz et al. [129] – describing a critical role for LNX as major regulators of the glycine transporter GlyT2. GlyT2 functions at glycinergic synapses in the brainstem, spinal cord and cerebellum – recapturing glycine into nerve terminals for synaptic vesicle refilling. In this study, LNX1 and LNX2 were shown to interact with and ubiquitinate GlyT2, and its ubiquitination by LNX2 in brainstem and spinal cord neurons resulted in decreased expression levels and thus impaired transporter activity. GlyT2 dysfunction causes Hyperekplexia, chronic pain and auditory processing [129]. No such phenotypes were apparent in DKO mice (Chapter 4) – however LNX as a regulator of GlyT2 has yet to be studied *in vivo* and may prove an interesting avenue for future research.

Bibliography

1. Kwon, Y.T. and A. Ciechanover, *The Ubiquitin Code in the Ubiquitin-Proteasome System and Autophagy.* Trends Biochem Sci, 2017. **42**(11): p. 873-886.

2. Jin, J., et al., *Dual E1 activation systems for ubiquitin differentially regulate E2 enzyme charging.* Nature, 2007. **447**(7148): p. 1135-8.

3. Stewart, M.D., et al., *E2 enzymes: more than just middle men.* Cell research, 2016. **26**(4): p. 423-440.

4. Callis, J., *The ubiquitination machinery of the ubiquitin system.* The arabidopsis book, 2014. **12**: p. e0174-e0174.

5. Talis, A.L., J.M. Huibregtse, and P.M. Howley, *The Role of E6AP in the Regulation of p53 Protein Levels in Human Papillomavirus (HPV)-positive and HPV-negative Cells*.* The Journal of Biological Chemistry, 1998. **273**: p. 6439 - 6445.

6. Huibregtse, J.M., et al., *A family of proteins structurally and functionally related to the E6-AP ubiquitin-protein ligase.* Proceedings of the National Academy of Sciences, 1995. **92**(7): p. 2563-2567.

7. Rotin, D. and S. Kumar, *Physiological functions of the HECT family of ubiquitin ligases.* Nature reviews Molecular cell biology, 2009. **10**(6): p. 398-409.

8. Huang, L., et al., *Structure of an E6AP-UbcH7 complex: insights into ubiquitination by the E2-E3 enzyme cascade.* Science, 1999. **286**(5443): p. 1321-1326.

9. Metzger, M.B., V.A. Hristova, and A.M. Weissman, *HECT and RING finger families of E3 ubiquitin ligases at a glance.* Journal of cell science, 2012. **125**(Pt 3): p. 531-537.

10. Li, W., et al., *Genome-wide and functional annotation of human E3 ubiquitin ligases identifies MULAN, a mitochondrial E3 that regulates the organelle's dynamics and signaling.* PloS one, 2008. **3**(1): p. e1487.

11. Deshaies, R.J. and C.A. Joazeiro, *RING domain E3 ubiquitin ligases.* Annu Rev Biochem, 2009. **78**: p. 399-434.

12. Coux, O., K. Tanaka, and A.L. Goldberg, *Structure and functions of the 20S and 26S proteasomes.* Annu Rev Biochem, 1996. **65**: p. 801-47.

13. Kish-Trier, E. and C.P. Hill, *Structural biology of the proteasome.* Annu Rev Biophys, 2013. **42**: p. 29-49.

14. Groll, M., et al., *A gated channel into the proteasome core particle.* Nature Structural Biology, 2000. **7**(11): p. 1062-1067.

15. Lander, G.C., et al., *Complete subunit architecture of the proteasome regulatory particle.* Nature, 2012. **482**(7384): p. 186-191.

16. Lowe, J., et al., *Crystal structure of the 20S proteasome from the archaeon T. acidophilum at 3.4 A resolution.* Science, 1995. **268**(5210): p. 533-539.

17. Yu, H. and A. Matouschek, *Recognition of Client Proteins by the Proteasome.* Annu Rev Biophys, 2017. **46**: p. 149-173.

18. Pan, T., et al., *The role of autophagy-lysosome pathway in neurodegeneration associated with Parkinson's disease.* Brain, 2008. **131**(8): p. 1969-1978.

19. Kirkin, V., et al., *A Role for Ubiquitin in Selective Autophagy.* Molecular Cell, 2009. **34**(3): p. 259-269.

20. Ghosh, R., et al., *Protein and Mitochondria Quality Control Mechanisms and Cardiac Aging.* Cells, 2020. **9**: p. 933.

21. Flynn, M., O. Saha, and P. Young, *Molecular evolution of the LNX gene family.* BMC Evol Biol, 2011. **11**: p. 235.

22. Young, P.W., *LNX1/LNX2 proteins: functions in neuronal signaling and beyond.* Neuronal Signaling, 2018. **2**(2): p. 1-20.

23. Duret, L., et al., *The Xist RNA gene evolved in eutherians by pseudogenization of a protein-coding gene.* Science, 2006. **312**(5780): p. 1653-5.

24. Dho, S.E., et al., *The mammalian numb phosphotyrosine-binding domain. Characterization of binding specificity and identification of a novel PDZ domain-containing numb binding protein, LNX.* J Biol Chem, 1998. **273**(15): p. 9179-87.

25. Rice, D.S., G.M. Northcutt, and C. Kurschner, *The Lnx family proteins function as molecular scaffolds for Numb family proteins.* Mol Cell Neurosci, 2001. **18**(5): p. 525-40.

26. Nie, J., et al., *LNX functions as a RING type E3 ubiquitin ligase that targets the cell fate determinant Numb for ubiquitin-dependent degradation.* EMBO J, 2002. **21**(1_2): p. 93-102.

27. Nayak, D. and J. Sivaraman, *Structural basis for the indispensable role of a unique zinc finger motif in LNX2 ubiquitination.* Oncotarget, 2015. **6**(33): p. 34342-57.

28. Won, M., H. Ro, and I.B. Dawid, *Lnx2 ubiquitin ligase is essential for exocrine cell differentiation in the early zebrafish pancreas.* Proc Natl Acad Sci U S A, 2015. **112**(40): p. 12426-31.

29. Nayak, D. and J. Sivaraman, *Structure of LNX1:Ubc13~Ubiquitin Complex Reveals the Role of Additional Motifs for the E3 Ligase Activity of LNX1.* J Mol Biol, 2018. **430**(8): p. 1173-1188.

30. Ro, H. and I.B. Dawid, *Organizer restriction through modulation of Bozozok stability by the E3 ubiquitin ligase Lnx-like.* Nat Cell Biol, 2009. **11**(9): p. 1121-7.

31. Ro, H. and I.B. Dawid, *Lnx-2b restricts gsc expression to the dorsal mesoderm by limiting Nodal and Bozozok activity.* Biochem Biophys Res Commun, 2010. **402**(4): p. 626-30.

32. Ro, H. and I.B. Dawid, *Modulation of Tcf3 repressor complex composition regulates cdx4 expression in zebrafish.* EMBO J, 2011. **30**(14): p. 2894-907.

33. Xie, Y., et al., *Identification of a human LNX protein containing multiple PDZ domains.* Biochem Genet, 2001. **39**(3-4): p. 117-26.

34. Bailey, M.J., et al., *Night/day changes in pineal expression of >600 genes: central role of adrenergic/cAMP signaling.* J Biol Chem, 2009. **284**(12): p. 7606-22.

35. Vriend, J., W. Liu, and R.J. Reiter, *The pineal gland: A model for adrenergic modulation of ubiquitin ligases.* PLoS One, 2017. **12**(2): p. e0172441.

36. Cahoy, J.D., et al., *A transcriptome database for astrocytes, neurons, and oligodendrocytes: a new resource for understanding brain development and function.* J Neurosci, 2008. **28**(1): p. 264-78.

37. Akinci, M.A., et al., *Differential gene expression in the pig limbal side population: implications for stem cell cycling, replication, and survival.* Invest Ophthalmol Vis Sci, 2009. **50**(12): p. 5630-8.

38. Pallafacchina, G., et al., *An adult tissue-specific stem cell in its niche: a gene profiling analysis of in vivo quiescent and activated muscle satellite cells.* Stem Cell Res, 2010. **4**(2): p. 77-91.

39. Mirza, M., et al., *The cell surface protein coxsackie- and adenovirus receptor (CAR) directly associates with the Ligand-of-Numb Protein-X2 (LNX2).* Exp Cell Res, 2005. **309**(1): p. 110-20.

40. Weiss, A., et al., *c-Src is a PDZ interaction partner and substrate of the E3 ubiquitin ligase Ligand-of-Numb protein X1.* FEBS Lett, 2007. **581**(26): p. 5131-6.

41. D'Agostino, M., et al., *Ligand of Numb proteins LNX1p80 and LNX2 interact with the human glycoprotein CD8alpha and promote its ubiquitylation and endocytosis.* J Cell Sci, 2011. **124**(Pt 21): p. 3545-56.

42. Wang, H., et al., *Gli3 repressor controls cell fates and cell adhesion for proper establishment of neurogenic niche.* Cell Rep, 2014. **8**(4): p. 1093-104.

43. Camps, J., et al., *Genetic Amplification of the NOTCH Modulator LNX2 Upregulates the WNT/beta-Catenin Pathway in Colorectal Cancer.* Cancer Res, 2013. **73**(3): p. 2003-2013.

44. Young, P., et al., *LNX1 is a perisynaptic Schwann cell specific E3 ubiquitin ligase that interacts with ErbB2.* Mol Cell Neurosci, 2005. **30**(2): p. 238-48.

45. Mirza, M., et al., *Coxsackievirus and adenovirus receptor (CAR) is expressed in male germ cells and forms a complex with the differentiation factor JAM-C in mouse testis.* Exp Cell Res, 2006. **312**(6): p. 817-30.

46. Nie, J., S.S. Li, and C.J. McGlade, *A novel PTB-PDZ domain interaction mediates isoform-specific ubiquitylation of mammalian Numb.* J Biol Chem, 2004. **279**(20): p. 20807-15.

47. Kandachar, V. and F. Roegiers, *Endocytosis and control of Notch signaling.* Curr Opin Cell Biol, 2012. **24**(4): p. 534-40.

48. Zhou, J., et al., *Ubiquitin E3 Ligase LNX2 is Critical for Osteoclastogenesis In Vitro by Regulating M-CSF/RANKL Signaling and Notch2.* Calcif Tissue Int, 2015. **96**(5): p. 465-75.

49. Li, L., et al., *Discovery of genetic biomarkers contributing to variation in drug response of cytidine analogues using human lymphoblastoid cell lines.* BMC Genomics, 2014. **15**: p. 93.

50. Yin, F.T., et al., *Caspr4 interaction with LNX2 modulates the proliferation and neuronal differentiation of mouse neural progenitor cells.* Stem Cells Dev, 2015. **24**(5): p. 640-52.

51. Guo, Z., et al., *Proteomics strategy to identify substrates of LNX, a PDZ domain-containing E3 ubiquitin ligase.* J Proteome Res, 2012. **11**(10): p. 4847-62.

52. Takahashi, S., et al., *The E3 ubiquitin ligase LNX1p80 promotes the removal of claudins from tight junctions in MDCK cells.* J Cell Sci, 2009. **122**(Pt 7): p. 985-94.

53. Kansaku, A., et al., *Ligand-of-Numb protein X is an endocytic scaffold for junctional adhesion molecule 4.* Oncogene, 2006. **25**(37): p. 5071-84.

54. Sollerbrant, K., et al., *The Coxsackievirus and adenovirus receptor (CAR) forms a complex with the PDZ domain-containing protein ligand-of-numb protein-X (LNX).* J Biol Chem, 2003. **278**(9): p. 7439-44.

55. Higa, S., et al., *The active zone protein CAST directly associates with Ligand-of-Numb protein X.* Biochem Biophys Res Commun, 2007. **354**(3): p. 686-92.

56. Lenihan, J.A., et al., *Decreased Anxiety-Related Behaviour but Apparently Unperturbed NUMB Function in Ligand of NUMB Protein-X (LNX) 1/2 Double Knockout Mice.* Mol Neurobiol, 2017. **54**(10): p. 8090-8109.

57. Lenihan, J.A., O. Saha, and P.W. Young, *Proteomic analysis reveals novel ligands and substrates for LNX1 E3 ubiquitin ligase.* PLoS One, 2017. **12**(11): p. e0187352.

58. Song, E., et al., *A high efficiency strategy for binding property characterization of peptide-binding domains.* Mol Cell Proteomics, 2006. **5**(8): p. 1368-81.

59. Wolting, C.D., et al., *Biochemical and computational analysis of LNX1 interacting proteins.* PLoS One, 2011. **6**(11): p. e26248.

60. Armbruester, V., et al., *Np9 protein of human endogenous retrovirus K interacts with ligand of numb protein X.* J Virol, 2004. **78**(19): p. 10310-9.

61. Chen, J., et al., *Characterization of human LNX, a novel ligand of Numb protein X that is downregulated in human gliomas.* Int J Biochem Cell Biol, 2005. **37**(11): p. 2273-83.

62. Lambert, B., et al., *Protein interactions of the transcription factor Hoxa1.* BMC Dev Biol, 2012. **12**: p. 29.

63. Zheng, D., et al., *LNX (Ligand of Numb-protein X) interacts with RhoC, both of which regulate AP-1-mediated transcriptional activation.* Mol Biol Rep, 2010. **37**(5): p. 2431-7.

64. Stiffler, M.A., et al., *PDZ domain binding selectivity is optimized across the mouse proteome.* Science, 2007. **317**(5836): p. 364-9.

65. Doyle, J.M., et al., *MAGE-RING protein complexes comprise a family of E3 ubiquitin ligases.* Mol Cell, 2010. **39**(6): p. 963-74.

66. Nandi, A.K., et al., *Attenuation of DNA damage checkpoint by PBK, a novel mitotic kinase, involves protein-protein interaction with tumor suppressor p53.* Biochem Biophys Res Commun, 2007. **358**(1): p. 181-8.

67. Abe, Y., et al., *Cloning and expression of a novel MAPKK-like protein kinase, lymphokine-activated killer T-cell-originated protein kinase, specifically expressed in the testis and activated lymphoid cells.* J Biol Chem, 2000. **275**(28): p. 21525-31.

68. Zhou, S., et al., *A Role for SKIP in EBNA2 Activation of CBF1-Repressed Promoters.* Journal of Virology, 2000. **74**(4): p. 1939-1947.

69. Vasquez-Del Carpio, R., et al., *Assembly of a Notch transcriptional activation complex requires multimerization.* Mol Cell Biol, 2011. **31**(7): p. 1396-408.

70. Burgner, D., et al., *A genome-wide association study identifies novel and functionally related susceptibility Loci for Kawasaki disease.* PLoS Genet, 2009. **5**(1): p. e1000319.

71. Mehraj, V., et al., *The ligands of Numb proteins X1 and X2 are specific markers for chronic Q fever.* FEMS Immunol Med Microbiol, 2011. **64**: p. 98-100.

72. Gulino, A., L. Di Marcotullio, and I. Screpanti, *The multiple functions of Numb.* Exp Cell Res, 2010. **316**(6): p. 900-6.

73. Blom, T., et al., *Mutation and copy number analysis of LNX1 and Numbl in nervous system tumors.* Cancer Genet Cytogenet, 2008. **186**(2): p. 103-9.

74. Holtkamp, N., et al., *Characterization of the amplicon on chromosomal segment 4q12 in glioblastoma multiforme.* Neuro Oncol, 2007. **9**(3): p. 291-7.

75. Ivanov, I.P., et al., *Initiation context modulates autoregulation of eukaryotic translation initiation factor 1 (eIF1).* Proc Natl Acad Sci U S A, 2010. **107**(42): p. 18056-60.

76. Tang, T., et al., *A mouse knockout library for secreted and transmembrane proteins.* Nat Biotechnol, 2010. **28**(7): p. 749-55.

77. Calvo, S.E., D.J. Pagliarini, and V.K. Mootha, *Upstream open reading frames cause widespread reduction of protein expression and are polymorphic among humans.* Proc Natl Acad Sci U S A, 2009. **106**(18): p. 7507-12.

78. de Bie, P. and A. Ciechanover, *Ubiquitination of E3 ligases: self-regulation of the ubiquitin system via proteolytic and non-proteolytic mechanisms.* Cell Death Differ, 2011. **18**(9): p. 1393-402.

79. Wethmar, K., J.J. Smink, and A. Leutz, *Upstream open reading frames: molecular switches in (patho)physiology.* Bioessays, 2010. **32**(10): p. 885-93.

80. Rogozin, I.B., et al., *Presence of ATG triplets in 5' untranslated regions of eukaryotic cDNAs correlates with a 'weak' context of the start codon.* Bioinformatics, 2001. **17**(10): p. 890-900.

81. Kozak, M., *Constraints on reinitiation of translation in mammals.* Nucleic Acids Res, 2001. **29**(24): p. 5226-32.

82. Schenborn, E.T. and V. Goiffon, *Calcium Phosphate Transfection of Mammalian Cultured Cells*, in *Transcription Factor Protocols*, M.J. Tymms, Editor. 2000, Humana Press: Totowa, NJ. p. 135-145.

83. Foley, K.S. and P.W. Young, *An analysis of splicing, actin-binding properties, heterodimerization and molecular interactions of the non-muscle alpha-actinins.* Biochem J, 2013. **452**(3): p. 477-88.

84. Saha, O., *Investigation of the function of the LNX family of E3 ubiquitin ligases in the nervous system.* . PhD Thesis, University College Cork. https://cora.ucc.ie/handle/10468/1195, 2013.

85. Bezprozvanny, I. and A. Maximov, *Classification of PDZ domains.* FEBS Lett, 2001. **509**(3): p. 457-62.

86. Tonikian, R., et al., *A specificity map for the PDZ domain family.* PLoS Biol, 2008. **6**(9): p. e239.

87. Short, K.M., et al., *MID1 and MID2 homo- and heterodimerise to tether the rapamycin-sensitive PP2A regulatory subunit, alpha 4, to microtubules: implications for the clinical variability of X-linked Opitz GBBB syndrome and other developmental disorders.* BMC Cell Biol, 2002. **3**: p. 1.

88. Kim, J., et al., *Rewiring of PDZ domain-ligand interaction network contributed to eukaryotic evolution.* PLoS Genet, 2012. **8**(2): p. e1002510.

89. Arroyo, J.D., G.M. Lee, and W.C. Hahn, *Liprin alpha1 interacts with PP2A B56gamma.* Cell Cycle, 2008. **7**(4): p. 525-32.

90. Liu, Y.C., et al., *The PPFIA1-PP2A protein complex promotes trafficking of Kif7 to the ciliary tip and Hedgehog signaling.* Sci Signal, 2014. **7**(355): p. ra117.

91. Sudhof, T.C., *The presynaptic active zone.* Neuron, 2012. **75**(1): p. 11-25.

92. Ko, J., et al., *Interaction of the ERC family of RIM-binding proteins with the liprin-alpha family of multidomain proteins.* J Biol Chem, 2003. **278**(43): p. 42377-85.

93. Nachat, R., et al., *KazrinE is a desmosome-associated liprin that colocalises with acetylated microtubules.* J Cell Sci, 2009. **122**(Pt 22): p. 4035-41.

94. Guerrier, S., et al., *The F-BAR domain of srGAP2 induces membrane protrusions required for neuronal migration and morphogenesis.* Cell, 2009. **138**(5): p. 990-1004.

95. Charrier, C., et al., *Inhibition of SRGAP2 function by its human-specific paralogs induces neoteny during spine maturation.* Cell, 2012. **149**(4): p. 923-35.

96. Dennis, M.Y., et al., *Evolution of human-specific neural SRGAP2 genes by incomplete segmental duplication.* Cell, 2012. **149**(4): p. 912-22.

97. Ma, Y., et al., *The inverse F-BAR domain protein srGAP2 acts through srGAP3 to modulate neuronal differentiation and neurite outgrowth of mouse neuroblastoma cells.* PLoS One, 2013. **8**(3): p. e57865.

98. Coyle, I.P., et al., *Nervous wreck, an SH3 adaptor protein that interacts with Wsp, regulates synaptic growth in Drosophila.* Neuron, 2004. **41**(4): p. 521-34.

99. Huang da, W., B.T. Sherman, and R.A. Lempicki, *Systematic and integrative analysis of large gene lists using DAVID bioinformatics resources.* Nat Protoc, 2009. **4**(1): p. 44-57.

100. Spangler, S.A. and C.C. Hoogenraad, *Liprin-alpha proteins: scaffold molecules for synapse maturation.* Biochem Soc Trans, 2007. **35**(Pt 5): p. 1278-82.

101. Rual, J.F., et al., *Towards a proteome-scale map of the human protein-protein interaction network.* Nature, 2005. **437**(7062): p. 1173-8.

102. Sardiello, M., et al., *Genomic analysis of the TRIM family reveals two groups of genes with distinct evolutionary properties.* BMC Evol Biol, 2008. **8**: p. 225.

103. Wang, Y., et al., *A family of RIM-binding proteins regulated by alternative splicing: Implications for the genesis of synaptic active zones.* Proc Natl Acad Sci U S A, 2002. **99**(22): p. 14464-9.

104. Dho, S.E., et al., *Characterization of four mammalian numb protein isoforms. Identification of cytoplasmic and membrane-associated variants of the phosphotyrosine binding domain.* J Biol Chem, 1999. **274**(46): p. 33097-104.

105. Lenihan, J.A., et al., *Decreased Anxiety-Related Behaviour but Apparently Unperturbed NUMB Function in Ligand of NUMB Protein-X (LNX) 1/2 Double Knockout Mice.* Mol Neurobiol, 2016: p. 1-20.

106. Endoh-Yamagami, S., et al., *The mammalian Cos2 homolog Kif7 plays an essential role in modulating Hh signal transduction during development.* Curr Biol, 2009. **19**(15): p. 1320-6.

107. Suzuki, M., et al., *MID1 and MID2 are required for Xenopus neural tube closure through the regulation of microtubule organization.* Development. **137**(14): p. 2329-39.

108. Heyer, M.P., et al., *Normal midbrain dopaminergic neuron development and function in miR-133b mutant mice.* J Neurosci, 2012. **32**(32): p. 10887-94.

109. Crawley, J.N., *Behavioral phenotyping strategies for mutant mice.* Neuron, 2008. **57**(6): p. 809-18.

110. Irwin, S., *Comprehensive observational assessment: Ia. A systematic, quantitative procedure for assessing the behavioral and physiologic state of the mouse.* Psychopharmacologia, 1968. **13**(3): p. 222-57.

111. Rogers, D.C., et al., *Behavioral and functional analysis of mouse phenotype: SHIRPA, a proposed protocol for comprehensive phenotype assessment.* Mamm Genome, 1997. **8**(10): p. 711-3.

112. Hughes, R.N., *The value of spontaneous alternation behavior (SAB) as a test of retention in pharmacological investigations of memory.* Neurosci Biobehav Rev, 2004. **28**(5): p. 497-505.

113. Cryan, J.F. and A. Holmes, *The ascent of mouse: advances in modelling human depression and anxiety.* Nat Rev Drug Discov, 2005. **4**(9): p. 775-90.

114. Bravo, J.A., et al., *Ingestion of Lactobacillus strain regulates emotional behavior and central GABA receptor expression in a mouse via the vagus nerve.* Proc Natl Acad Sci U S A, 2011. **108**(38): p. 16050-5.

115. Cryan, J.F. and C. Mombereau, *In search of a depressed mouse: utility of models for studying depression-related behavior in genetically modified mice.* Molecular Psychiatry, 2004. **9**(4): p. 326-357.

116. Riikonen, R., *Insulin-Like Growth Factors in the Pathogenesis of Neurological Diseases in Children.* International journal of molecular sciences, 2017. **18**(10): p. 2056.

117. Calhoon, G.G. and K.M. Tye, *Resolving the neural circuits of anxiety.* Nat Neurosci, 2015. **18**(10): p. 1394-404.

118. Butler, K., L.A. Martinez, and M.V. Tejada-Simon, *Impaired cognitive function and reduced anxiety-related behavior in a promyelocytic leukemia (PML) tumor suppressor protein-deficient mouse.* Genes Brain Behav, 2013. **12**(2): p. 189-202.

119. Semenova, S., et al., *Mice lacking the beta4 subunit of the nicotinic acetylcholine receptor show memory deficits, altered anxiety- and depression-like behavior, and diminished nicotine-induced analgesia.* Nicotine Tob Res, 2012. **14**(11): p. 1346-55.

120. Spampinato, D.A., P.A. Celnik, and J.C. Rothwell, *Cerebellar–Motor Cortex Connectivity: One or Two Different Networks?* The Journal of Neuroscience, 2020. **40**(21): p. 4230-4239.

121. O'Reilly, R.C. and K.A. Norman, *Hippocampal and neocortical contributions to memory: advances in the complementary learning systems framework.* Trends in Cognitive Sciences, 2002. **6**(12): p. 505-510.

122. Lee, S.J., et al., *Impaired Blastocyst Formation in Lnx2-Knockdown Mouse Embryos.* Int J Mol Sci, 2023. **24**(2).

123. Lenihan, J.A., et al., *Tight, cell type-specific control of LNX expression in the nervous system, at the level of transcription, translation and protein stability.* Gene, 2014. **552**(1): p. 39-50.

124. Liu, X.-D., et al., *Hippocampal Lnx1–NMDAR multiprotein complex mediates initial social memory.* Molecular Psychiatry, 2021. **26**(8): p. 3956-3969.

125. Bekri, A., M. Liao, and P. Drapeau, *Glycine Regulates Neural Stem Cell Proliferation During Development via Lnx1-Dependent Notch Signaling.* Front Mol Neurosci, 2019. **12**: p. 44.

126. Liu, X.D., et al., *Retrograde regulation of mossy fiber axon targeting and terminal maturation via postsynaptic Lnx1*. J Cell Biol, 2018. **217**(11): p. 4007-4024.

127. Li, N., et al., *Scaffold Protein Lnx1 Stabilizes EphB Receptor Kinases for Synaptogenesis.* Front Mol Neurosci, 2022. **15**: p. 861873.

128. Lynn, B.D., et al., *E3 ubiquitin ligases LNX1 and LNX2 localize at neuronal gap junctions formed by connexin36 in rodent brain and molecularly interact with connexin36.* Eur J Neurosci, 2018. **48**(9): p. 3062-3081.

129. de la Rocha-Muñoz, A., et al., *E3 ubiquitin ligases LNX1 and LNX2 are major regulators of the presynaptic glycine transporter GlyT2.* Scientific Reports, 2019. **9**(1): p. 14944.

Appendix A: Supplementary tables & figures

Table A1. Proteomic analysis of GFP-LNX1 interacting proteins purified from HEK 293 cells. Proteins are ranked by Mascot score. Previously known interactions are underlined, as are carboxyl-terminal cysteines.

Gene Symbol	Mascot Score	Name	Carboxyl terminus
PPFIA1	5644	Isoform 1 of Liprin-alpha-1	DSATVRTYSC
LNX1	3662	Isoform 1 of E3 ubiquitin-protein ligase LNX	TIVSWPGTFL
MID2	2641	Isoform 1 of probable E3 ubiquitin-protein ligase MID2	PYVSGMKTCH
USP9X	2229	Isoform 2 of probable ubiquitin carboxyl-terminal hydrolase FAF-X	EVSPPQTKDQ
MYCBP2	1995	Probable E3 ubiquitin-protein ligase MYCBP2	CGVCRNAHTF
KIF7	1131	Kinesin-like protein KIF7	GMIDVRKNPL
KLHL11	1056	Kelch-like protein 11	RRVPSSQIEC
MID1	1030	Isoform 1 of Midline-1	DHLDCTEQLP
IARS	1020	Isoleucyl-tRNAsynthetase, cytoplasmic	VSVLPTTADF
PPFIA3	791	Isoform 1 of Liprin-alpha-3	DGVSVRTYSC
KIF14	629	Kinesin-like protein KIF14	ECTPSRIQWV
AKAP13	510	Isoform 6 of A-kinase anchor protein 13	VSAEGEEIFC
PEX1	494	Peroxisome biogenesis factor 1	FRPGQKVTLA
NUMB	438	Isoform 1 of Protein numb homolog	DLQKTFEIEL
RPL4	391	60S ribosomal protein L4	PTTEEKKPAA
NUMBL	356	Numb-like protein	DLQKTFEIEL
AP2M1	352	Isoform 1 of AP-2 complex subunit mu	GRSGIYETRC
PLEK	341	Pleckstrin	AIQMASRTGK
PPP1CA	294	Serine/threonine-protein phosphatase PP1-alpha catalytic subunit isoform 3	PPRNSAKAKK
TRIM27	279	Isoform Alpha of Zinc finger protein RFP	NHGHSMETSP
DUSP14	265	Dual specificity protein phosphatase 14	SRHLMPYWGI
TMED10	253	Transmembrane emp24 domain-containing protein 10	RFFKAKKLIE
ZNF24	248	Isoform 1 of Zinc finger protein 24	AEKLLNVVKV
ZCRB1	247	Zinc finger CCHC-type and RNA-binding motif-containing protein 1	YFSDEEELSD
AP2A1	246	Isoform B of AP-2 complex subunit alpha-1	HLCELLAQQF
LARS	244	Leucyl-tRNAsynthetase, cytoplasmic	IGDTIIYLVH
IQGAP1	242	RasGTPase-activating-like protein IQGAP1	FLLNKKFYGK
RPS27L	237	40S ribosomal protein S27-like	
CHD2	234	Isoform 2 of Chromodomain-helicase-DNA-binding protein 2	PDYNWNVRKT
ERC2	226	ERC protein 2	DQDDEEGIWA
PPP2R1A	224	Serine/threonine-protein phosphatase 2A 65 kDa regulatory subunit A alpha isoform	QEALTVLSLA
CSNK1D	199	CSNK1D Isoform 1 of Casein kinase I isoform delta	SSGLQSVVHR
PEX6	199	PEX6 Peroxisome assembly factor 2	KRIQRKFAAC
TRAF4	185	TRAF4 Isoform 1 of TNF receptor-associated factor 4	AVELPRKILS
MED7	180	MED7 Mediator of RNA polymerase II transcription subunit 7	VLIDEMNERP

Table A1 continued.

Gene Symbol	Mascot Score	Name	Carboxyl terminus
NDEL1	177	NDEL1 nuclear distribution protein nudE-like 1 isoform A	PIESNTLQHN
FBXO11	176	FBXO11 F-box only protein 11	LLMAANFLDC
TCEB1	175	TCEB1 Transcription elongation factor B polypeptide 1	LLMAANFLDC
AGMAT	157	AGMAT Agmatinase, mitochondrial	LCALPKVTTV
PPP2CA	155	PPP2CA Serine/threonine-protein phosphatase 2A catalytic subunit alpha isoform	VTRRTPDYFL
MRPL4	153	MRPL4 Isoform 1 of 39S ribosomal protein L4, mitochondrial	QGPAATPYHC
C3orf26	149	C3orf26 Uncharacterized protein C3orf26	KSESLKLGLF
COPA	148	COPA Isoform 1 of Coatomer subunit alpha	GLRISPLQFR
LMAN2	145	LMAN2 Vesicular integral-membrane protein VIP36	KRQERNKRFY
PRKDC	143	PRKDC Isoform 1 of DNA-dependent protein kinase catalytic subunit	RTWEGWEPWM
EIF3H	135	EIF3H cDNA FLJ35809, clone TESTI2006016, highly similar to Eukaryotic translation initiation factor 3 subunit 3	MAQALQEYNN
ERC1	135	ERC1 Isoform 2 of ELKS/Rab6-interacting/CAST family member 1	QVVNALEESS
MYH9	134	MYH9 Isoform 1 of Myosin-9	ADGAEAKPAE
DYNLRB1	132	DYNLRB1 Isoform 1 of Dynein light chain roadblock-type 1	FLIVIQNPTE
IGLV2-14	132	IGLV2-14;IGLC2 IGL@ protein	CALWYSTHFV
PKP1	130	PKP1 Isoform 2 of Plakophilin-1	NSLRNFTSRF
CLK4	129	CLK4 Dual specificity protein kinase CLK4	KKRKGQVIQF
RPL36AL	129	RPL36AL 60S ribosomal protein L36a-like	SGEKSESISV
ZNF192	128	ZNF192 Zinc finger protein 192	ILFYGRFSSP
SERPINB3	124	SERPINB3 Isoform 1 of Serpin B3	KKSALKKEKK
DNAJC9	123	DNAJC9 DnaJ homolog subfamily C member 9	KDYSDITSSK
GTF2E2	122	GTF2E2 Transcription initiation factor IIE subunit beta	GHPSRQLPKI
DZIP3	120	DZIP3 Isoform 1 of E3 ubiquitin-protein ligase DZIP3	LIKKATGVQV
FLOT2	120	FLOT2 Flotillin-2	GFTIFRTISV
GRWD1	110	GRWD1 Glutamate-rich WD repeat-containing protein 1	CEAPMEGFQL
KPNA1	109	KPNA1 Importin subunit alpha-1	KRFFEVRRVV
TMED2	109	TMED2 Transmembrane emp24 domain-containing protein 2	AEAQDGPQEA
PIGR	108	PIGR Polymeric immunoglobulin receptor	VNKVWDQSSV
CIT	106	CIT Isoform 1 of Citron Rho-interacting kinase	LIVYVRFWWL
SEC22B	104	SEC22B Vesicle-trafficking protein SEC22b	KSFFEAKKLV
TMED9	103	TMED9 Transmembrane emp24 domain-containing protein 9	GPRKVKLTLL
RBM12B	96	RBM12B Uncharacterized protein	QVNHKPLRTA
FLOT1	94	FLOT1 Flotillin-1	PEAPKGKKKK
MARS	94	MARS Methionyl-tRNAsynthetase, cytoplasmic	PEAPKGKKKK
CDK13	91	CDK13 Isoform 2 of Cyclin-dependent kinase 13	GRGRGRGLPY
PCM1	91	PCM1 Isoform 1 of Pericentriolar material 1 protein	EPETVGAQSI

Table A1 continued.

Gene Symbol	Mascot Score	Name	Carboxyl terminus
SMC4	86	SMC4 Isoform 2 of Structural maintenance of chromosomes protein 4	PKEIASKGLC
IKBKAP	82	IKBKAP Elongator complex protein 1	RTQWKLSLLD
TMED5	76	TMED5 Transmembrane emp24 domain-containing protein 5	LFEDKRKSRT
TMED4	71	TMED4 Isoform 1 of Transmembrane emp24 domain-containing protein 4	KSFFEAKKLV

Table A2. Proteomic analysis of GST-LNX1-PDZ2 interacting proteins purified from brain lysates Previously known interactions are underlined, as are carboxyl-terminal cysteines. An asterisk indicates proteins identified as interacting with both LNX1 and LNX2 PDZ2 domains.

Gene Symbol	Mascot Score	Name	Carboxyl terminus
Erc1*	7959	Erc1 ELKS/Rab6-interacting/CAST family member 1	DQDEEEGIWA
Ppfia3	4094	Ppfia3 Liprin-alpha-3	DGVSVRTYSC
Erc2*	2235	Erc2 ELKS/Rab6-interacting/CAST family member 2	DQDDEEGIWA
Lrrc16a*	2180	Lrrc16a Leucine-rich repeat-containing protein 16A	EEAEKEFIFV
Fchsd2*	2109	Fchsd2 FCH and double SH3 domains protein 2	KMEDVEITLV
Ppfia4	1549	Ppfia4 liprin-alpha-4	EPSTVRTYSC
Fermt2*	1467	Fermt2 Fermitin family homolog 2	MFYKLTSGWV
Ppfia2	1441	Ppfia2 Liprin-alpha-2	DNSTVRTYSC
Ppfia1	1358	Ppfia1 Liprin-alpha-1	DSATVRTYSC
Ppp2r5d	968	Ppp2r5d Protein phosphatase 2A B56 delta subunit	TGSRNGREGK
Prkcc	843	Prkcc Protein kinase C gamma type	PTSPVPVPVM
Akap11*	792	Akap11 A-kinase anchor protein 11	ANRLQTSMLV
Ndrg3	749	Ndrg3 Protein NDRG3	DRHQTMEVSC
Ppp2r5c	724	Ppp2r5c Isoform 2 of Serine/threonine-protein phosphatase 2A 56 kDa regulatory subunit gamma isoform	ASELLSQDGR
Pafah1b1*	710	Pafah1b1 Isoform 1 of Platelet-activating factor acetylhydrolase IB subunit alpha	DQTVKVWECR
Ndel1*	668	Ndel1 Isoform 1 of Nuclear distribution protein nudE-like 1	SAPGMLPLSV
Sphkap*	656	Sphkap A-kinase anchor protein SPHKAP	EQKERTPSLF
Prkar1a*	592	Prkar1a cAMP-dependent protein kinase type I-alpha regulatory subunit	QYNSFVSLSV
Slc1a3	570	Slc1a3 Excitatory amino acid transporter 1	KPVADSETKM
Klhl11	567	Klhl11 Isoform 1 of Kelch-like protein 11	RRVPSSQIEC
Ppp3ca*	559	Ppp3ca Isoform 1 of Serine/threonine-protein phosphatase 2B catalytic subunit alpha isoform	SNGSNSSNIQ
Prkar1b*	518	Prkar1b cAMP-dependent protein kinase type I-beta regulatory subunit	RYNSFISLTV
Camk2d	449	Camk2d Isoform 1 of Calcium/calmodulin-dependent protein kinase type II subunit delta	SGGTSLWQNI
Ndrg2	422	Ndrg2 Isoform 1 of Protein NDRG2	PPGHTMEVSC
Trim9	418	Trim9 Isoform 2 of E3 ubiquitin-protein ligase TRIM9	AVKSPQAPAP
Cyfip1	384	Cyfip1 Isoform 1 of Cytoplasmic FMR1-interacting protein 1	PPIHQSLASS
Ywhag*	382	Ywhag 14-3-3 protein gamma	QDDDGGEGNN
9030409G11Rik*	320	9030409G11Rik Isoform 1 of Kazrin	GYGSLEVTNV
Atp2b3	305	Atp2b3 plasma membrane calcium ATPase 3	AGNPGGESIP
Iqsec1*	301	Iqsec1 IQ motif and SEC7 domain-containing protein 1 isoform b	QPPQPPVLCS
Wasf1	282	Wasf1 Wiskott-Aldrich syndrome protein family member 1	SEFDEVDWLE
Dgcr8	272	Dgcr8 Microprocessor complex subunit DGCR8	GGEPLCTVDV
Hspa1b	270	Hspa1b Heat shock 70 kDa protein 1B	GSGPTIEEVD
Clec16a	267	Clec16a Isoform 5 of Protein CLEC16A	NPEPAEPTEH

Table A2 continued.

Gene Symbol	Mascot Score	Name	Carboxyl terminus
Unc-13	265	- Unc-13 homolog B	SESRSTEEGS
Srgap1	254	Srgap1 SLIT-ROBO Rho GTPase-activating protein 1	QGPTDKSCTM
Hnrnph1	239	Hnrnph1 Heterogeneous nuclear ribonucleoprotein H	NSSDFQSNIA
Ctnnd2	238	Ctnnd2 Isoform 1 of Catenin delta-2	HYPASPDSWV
Mios	236	Mios WD repeat-containing protein mio	NLVPAETVQP
Tufm	230	Tufm Isoform 1 of Elongation factor Tu, mitochondrial	TEEDKNIKWS
Phldb1	219	Phldb1 Uncharacterized protein	GAEGYTQFMN
Ywhaz*	214	Ywhaz 14-3-3 protein zeta/delta	EAEAGEGGEN
Snap47	200	Snap47 Isoform 1 of Synaptosomal-associated protein 47	KQNRRMRKLM
Hspa4l	194	Hspa4l Isoform 1 of Heat shock 70 kDa protein 4L	DKKLPEMDID
Ywhab	185	Ywhab Isoform Long of 14-3-3 protein beta/alpha	DEGDAGEGEN
Krt15	183	Krt15 keratin, type I cytoskeletal 15	KVVSSRKREI
Cct2	180	Cct2 T-complex protein 1 subunit beta	IKRVPDHHPC
Srcin1	170	Srcin1 Uncharacterized protein	FGARNSSISF
Ywhaq*	166	Ywhaq;LOC100503129 Isoform 1 of 14-3-3 protein theta	ECDAAEGAEN
Krt13	162	Krt13 Isoform 1 of Keratin, type I cytoskeletal 13	NSGRPDFRKY
Tecpr1	158	Tecpr1 Isoform 1 of Tectonin beta-propeller repeat-containing protein 1	EARGPGPVCC
Hspa4	150	Hspa4 Heat shock 70 kDa protein 4	HTDSGEMEVD
Pfkl*	145	Pfkl 6-phosphofructokinase, liver type	TRRTLSIDKF
Hepacam	143	Hepacam Hepatocyte cell adhesion molecule	DESGQVEISA
Camsap1	141	Camsap1 Isoform 1 of Calmodulin-regulated spectrin-associated protein 1	TVPKKTQTRK
Vwa5a	140	Vwa5a von Willebrand factor A domain-containing protein 5A	LSVNPAVFGV
Add1	139	Add1 Isoform 1 of Alpha-adducin	LKKSKKKSDS
Ppfibp1	136	Ppfibp1 Isoform 3 of Liprin-beta-1	ASITDEDSNV
AW555464	128	AW555464 Isoform 1 of Protein KIAA0284	FLPDAERFLI
Wars	127	Wars Isoform 1 of Tryptophanyl-tRNA synthetase, cytoplasmic	FHFQCFCFDT
Ap1b1	123	Ap1b1 AP-1 complex subunit beta-1	YQAYETILKN
Ndrg1	119	Ndrg1 Protein NDRG1	AGPKSMEVSC
Dtna	118	Dtna Isoform 1 of Dystrobrevin alpha	DEAYQVSLQG
Ldb1*	116	Ldb1 Isoform 1 of LIM domain-binding protein 1	SENPTSQASQ
Gstm7	116	Gstm7 Glutathione S-transferase Mu 7	FTKMATWGSN
Ctnna2*	115	Ctnna2 Isoform 1 of Catenin alpha-2	LSEFKAMDSF
Tbce	113	Tbce Tubulin-specific chaperone E	ENGDCLLVRW
Atp4a	113	Atp4a Uncharacterized protein	GSWWDQDFYY
Atp12a	112	Atp12a Potassium-transporting ATPase alpha chain 2	GSWWDKNMYY
Cdk14	108	Cdk14 Isoform 1 of Cyclin-dependent kinase 14	YGKSLSNSKH
Entpd2	104	Entpd2 Isoform Long of Ectonucleoside triphosphate diphosphohydrolase 2	VRSAKSPGAL
Bcr	104	Bcr Breakpoint cluster region protein	RQSILFSTEV
Cttnbp2	103	Cttnbp2 Cttnbp2 protein	KHEQVEKPNK

Table A2 continued.

Gene Symbol	Mascot Score	Name	Carboxyl terminus
Nptn	103	Nptn Isoform 2 of Neuroplastin	DKNLRQRNTN
Slc6a1*	101	Slc6a1 Sodium- and chloride-dependent GABA transporter 1	GSSASKEAYI
Rpn1*	100	Rpn1 Dolichyl-diphosphooligosaccharide--protein glycosyltransferase subunit 1	TKIDHILDAL
Atl1	99	Atl1 Atlastin-1	MQTCKVLPLE
Ctnnb1*	96	Ctnnb1 Catenin beta-1	NQLAWFDTDL

Table A3. Proteomic analysis of GST-LNX2-PDZ2 interacting proteins purified from brain lysates Previously known interactions are underlined, as are carboxyl-terminal cysteines. An asterisk indicates proteins identified as interacting with both LNX1 and LNX2 PDZ2 domains.

Gene Symbol	Mascot Score	Name	Carboxyl terminus
Erc1*	3181	Erc1 ELKS/Rab6-interacting/CAST family member 1	DQDEEEGIWA
Sphkap*	2692	Sphkap A-kinase anchor protein SPHKAP	EQKERTPSLF
Lrrc16a*	2270	Lrrc16a Isoform 1 of Leucine-rich repeat-containing protein 16A	EEAEKEFIFV
Fchsd2*	1938	Fchsd2 Isoform 2 of FCH and double SH3 domains protein 2	KMEDVEITLV
Srgap2	1935	Srgap2 SLIT-ROBO Rho GTPase-activating protein 2	PQATDKSCTV
Akap11*	1576	Akap11 A-kinase anchor protein 11	ANRLQTSMLV
Fermt2*	1287	Fermt2 Fermitin family homolog 2	MFYKLTSGWV
Erc2*	1139	Erc2 ELKS/Rab6-interacting/CAST family member 2	DQDDEEGIWA
Atp2a2	1125	Atp2a2 Isoform SERCA2B of Sarcoplasmic/endoplasmic reticulum calcium ATPase 2	DTNFSDMFWS
Rrbp1	1059	Rrbp1 ribosome-binding protein 1 isoform a	GSSSKEGTSV
9030409G11Rik*	560	9030409G11Rik Isoform 1 of Kazrin	GYGSLEVTNV
Eml3	549	Eml3 Echinoderm microtubule-associated protein-like 3	SLSPASSLDV
Prkar1b*	507	Prkar1b cAMP-dependent protein kinase type I-beta regulatory subunit	RYNSFISLTV
Prkar1a*	504	Prkar1a cAMP-dependent protein kinase type I-alpha regulatory subunit	QYNSFVSLSV
Ktn1	500	Ktn1 Uncharacterized protein	EVNQQLTKET
Kcnj10	327	Kcnj10 ATP-sensitive inward rectifier potassium channel 10	SALSVRISNV
Slc4a4	322	Slc4a4 Isoform 1 of Electrogenic sodium bicarbonate cotransporter 1	STFLERHTSC
Ckap4	292	Ckap4 Cytoskeleton-associated protein 4	LKVEKIHEKI
Ndel1*	287	Ndel1 Isoform 1 of Nuclear distribution protein nudE-like 1	SAPGMLPLSV
Gria2	278	Gria2 Isoform 1 of Glutamate receptor 2	NVYGIESVKI
Ctnnd2*	272	Ctnnd2 Isoform 1 of Catenin delta-2	HYPASPDSWV
Kif5a	236	Kif5a Kinesin heavy chain isoform 5A	FPLHQETAAS
Exoc4	230	Exoc4 Exocyst complex component 4	ATKDKKITTV
Rpn1*	224	Rpn1 Dolichyl-diphosphooligosaccharide-protein glycosyltransferase subunit 1	TKIDHILDAL
Agap2	215	Agap2 Isoform 1 of Arf-GAP with GTPase, ANK repeat and PH domain-containing protein 2	GRVDTTIALV
Ywhag*	207	Ywhag 14-3-3 protein gamma	QDDDGGEGNN
Mtmr1	204	Mtmr1 Myotubularin-related protein 1	HSATPVHTSV
C2cd2l	197	C2cd2l C2 domain-containing protein 2-like	KANGNPSPQL
Ddost	185	Ddost Dolichyl-diphosphooligosaccharide--protein glycosyltransferase 48 kDa subunit	LHMKEKEKSD
Amigo1	176	Amigo1 Isoform 1 of Amphoterin-induced protein 1	SVFSDTPIVV
Exoc2	176	Exoc2 Exocyst complex component 2	QAASPAVMKT
C230096C10Rik	175	C230096C10Rik Isoform 1 of Uncharacterized protein KIAA0090	QVKLLNRAWR

Table A3 continued.

Gene Symbol	Mascot Score	Name	Carboxyl terminus
Rpn2	172	Rpn2 Dolichyl-diphosphooligosaccharide-protein glycosyltransferase subunit 2	AQHAVKRTAH
Sbf2	153	Sbf2 SET-binding factor 2	DRIQSCLSDA
Slc6a1*	153	Slc6a1 Sodium- and chloride-dependent GABA transporter 1	GSSASKEAYI
Nrxn1	150	Nrxn1 Uncharacterized protein	KKNKDKEYYV
Ppp3ca*	149	Ppp3ca Isoform 1 of Serine/threonine-protein phosphatase 2B catalytic subunit alpha isoform	SNGSNSSNIQ
Nomo1	144	Nomo1 Nodal modulator 1	QTKKQKTRRT
Cds2	144	Cds2 Phosphatidate cytidylyltransferase 2	GILTSALEDE
Srr	138	Srr Isoform 1 of Serine racemase	RPAPYQTVSV
Exoc1	136	Exoc1 Uncharacterized protein	DYCSSIAQSH
Slc25a12	131	Slc25a12 Calcium-binding mitochondrial carrier protein Aralar1	AQPKAAAAAQ
Ywhaz*	129	Ywhaz 14-3-3 protein zeta/delta	EAEAGEGGEN
Canx	129	Canx Calnexin	SPRNRKPRRE
Ywhaq*	129	Ywhaq;LOC100503129 Isoform 1 of 14-3-3 protein theta	ECDAAEGAEN
Iqsec1*	125	Iqsec1 IQ motif and SEC7 domain-containing protein 1 isoform b	QPPQPPVLCS
Ldb1*	124	Ldb1 Isoform 1 of LIM domain-binding protein 1	SENPTSQASQ
Ppp2r1b	123	Ppp2r1b serine/threonine-protein phosphatase 2A 65 kDa regulatory subunit A beta isoform isoform a	AQEAISVLAA
Stt3a	120	Stt3a Putative uncharacterized protein	DLDNRGLSRT
Ilvbl	117	Ilvbl Isoform 1 of Acetolactate synthase-like protein	TDFRDGSISV
Pfkl*	113	Pfkl 6-phosphofructokinase, liver type	TRRTLSIDKF
Myl1	113	Myl1 Isoform MLC1 of Myosin light chain 1/3, skeletal muscle isoform	EAFVKHIMSV
Snd1	110	Snd1 Staphylococcal nuclease domain-containing protein 1	DDADEFGYSR
Pafah1b1*	109	Pafah1b1 Isoform 1 of Platelet-activating factor acetylhydrolase IB subunit alpha	DQTVKVWECR
Prkacb	107	Prkacb Isoform 1 of cAMP-dependent protein kinase catalytic subunit beta	EKCGKEFCEF
Ssbp3	107	Ssbp3 Isoform 1 of Single-stranded DNA-binding protein 3	NYSPSMTMSV
Lamc1	103	Lamc1 Uncharacterized protein	CFNTPSIEKP
Ctnnb1*	102	Ctnnb1 Catenin beta-1	NQLAWFDTDL
Atp1b2	101	Atp1b2 Sodium/potassium-transporting ATPase subunit beta-2	VAFKLRINKT
Clptm1	100	Clptm1 Cleft lip and palate transmembrane protein 1 homolog	PKPAEDKKKD

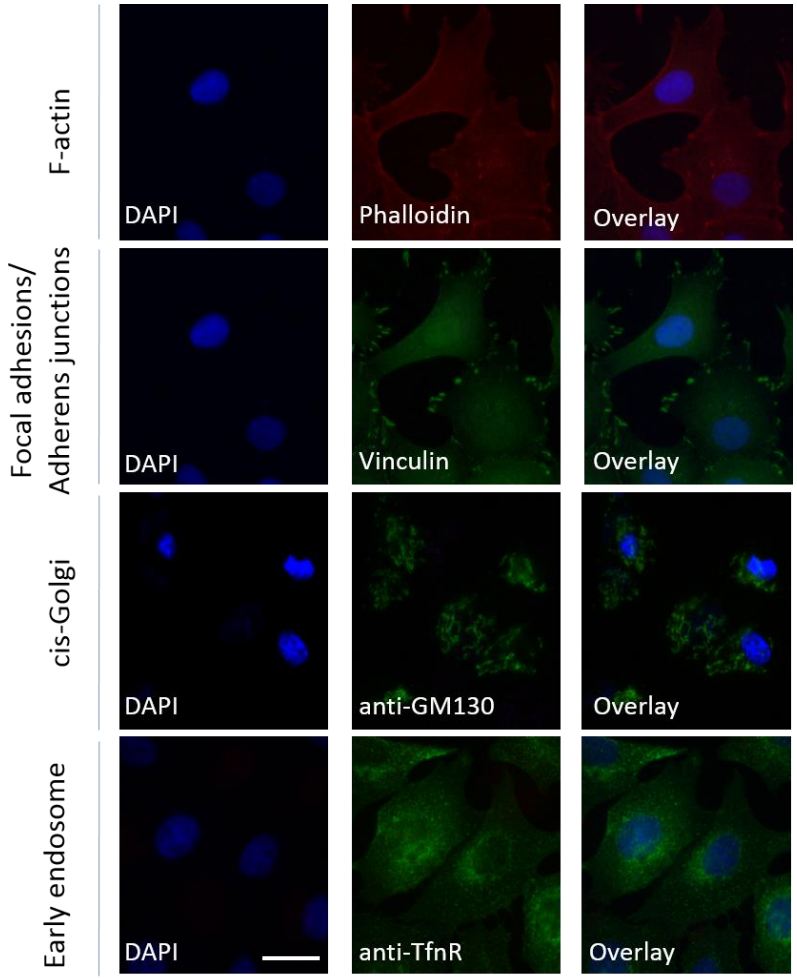

Figure A1: Representative fluorescence immunocytochemistry images examining localisation of the indicated cellular structures and organelles. Phalloidin (red), vinculin (green), anti-GM130 (green) and anti-TfnR (green) were used to visualise F-actin, focal adhesions, cis-Golgi and early endosomes respectively. Nuclei were stained with DAPI (blue). The different wavelengths were scanned individually and digitally merged. Scale bar indicated 10 µm. n = 1.

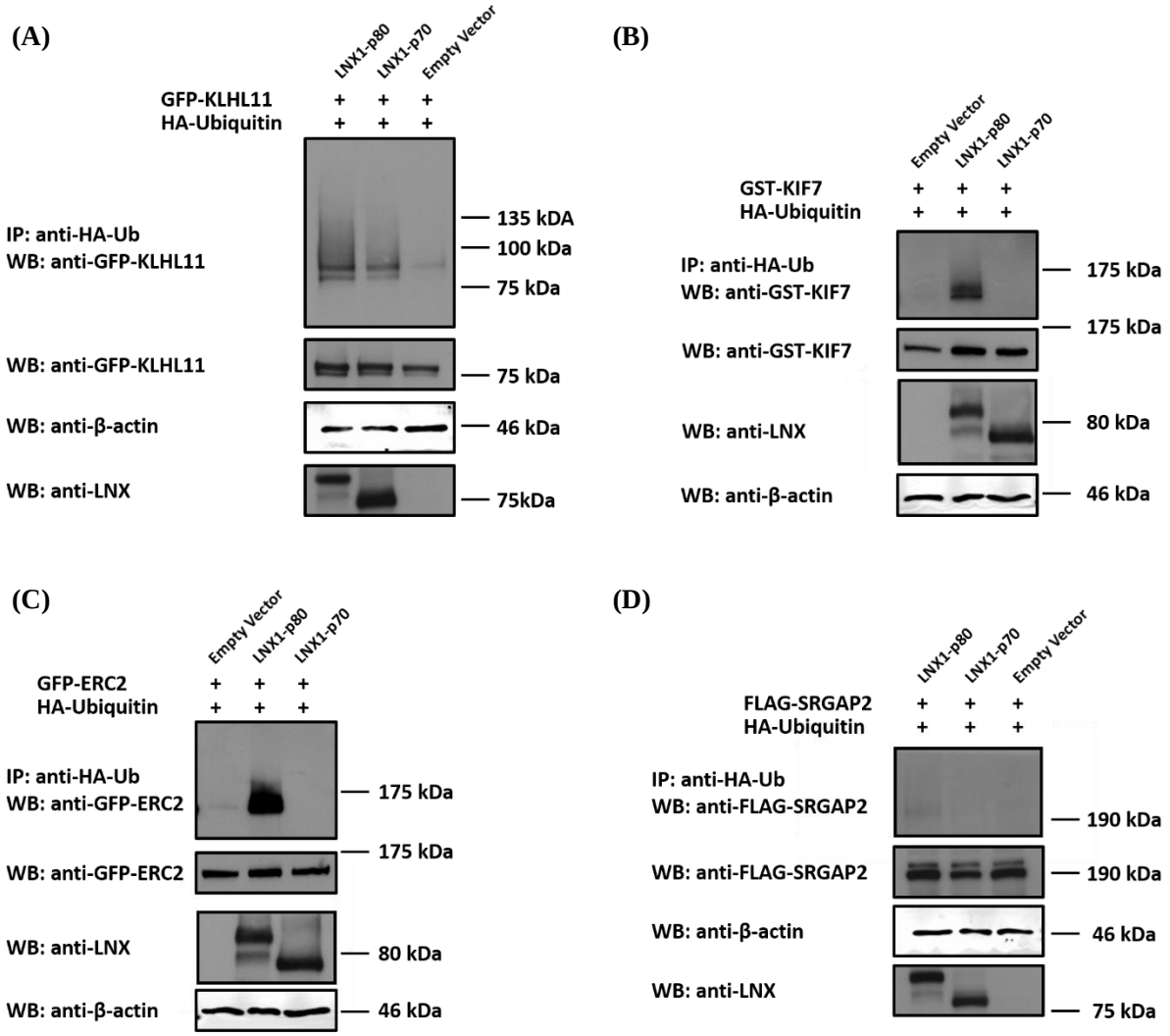

Figure A2: LNX mediates ubiquitination of a number of novel interacting proteins. HEK 293T cells were transiently transfected with the indicated constructs. 20 h post-transfection cells were treated with 10 μm of the proteosomal inhibitor MG132 for 6 h. Under stringent SDS-denaturing conditions, cell lysates were then prepared and ubiquitinated proteins were immunoprecipitated from cell lysates using an anti-HA antibody. The ubiquitination status of **(A)** KLHL11, **(B)** KIF7, **(C)** ERC2 and **(D)** SRGAP2 was then revealed by Western blot analysis using the indicated antibodies. Western blot of whole cell lysates confirmed expression of all constructs. n = 2.

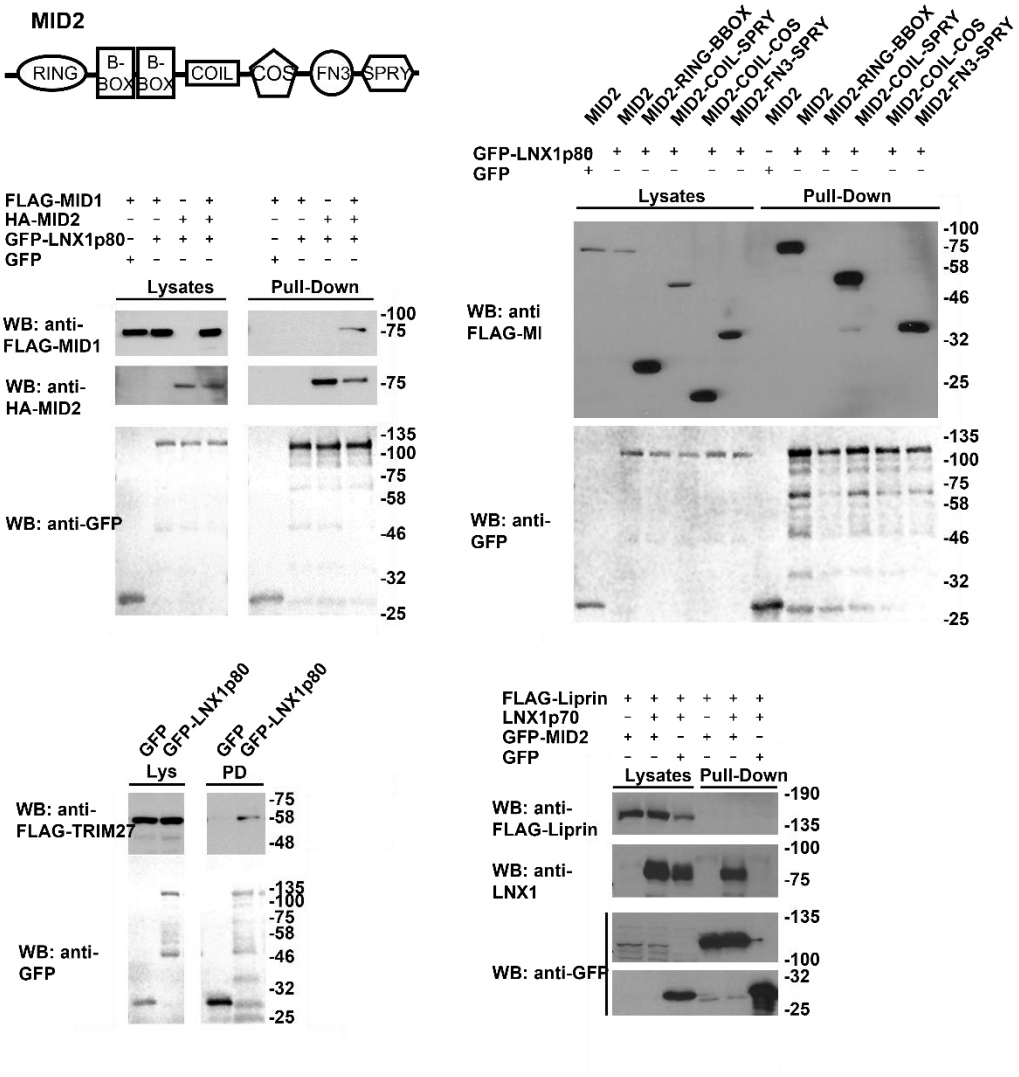

Figure A3. Interactions of LNX1 with the TRIM E3 ubiquitin ligase family. (A) Schematic diagram of the domain structure of MID2 showing the RING and B-BOX type zinc finger domains, the coiled-coil dimerization domain (COIL), the microtubule-binding COS (C-terminal subgroup one signature) domain, the fibronectin type III (FN3) domain and the SPRY (in splA kinase and ryanodine receptor) domain. MID1 shares a very similar domain organization, whereas TRIM27 lacks the COS and FN3 domains [102]. **(B)** Mapping of the LNX1 binding site on MID2. The ability of the indicated FLAG epitope tagged MID2 constructs to interact with GFP-tagged LNX1p80 was assessed following transfection into in HEK 293 cells by GFP "pull down" assays. Successful expression of constructs was verified by Western blotting of cell lysates and interactions detected in pull down samples. n = 2 **(C)** Analysis of LNX1 binding to MID1. The ability of FLAG epitope-tagged MID1 to interact with GFP-tagged LNX1p80 was assessed in the presence or absence of HA epitope-tagged MID2. n = 2 **(D)** Confirmation of TRIM27 interaction with LNX1 in a GFP "pull down" assay. n = 2 **(E)** Investigation of the ability of MID2, LNX1p70 and liprin-α1 to form a trimolecular complex. Interaction of untagged LNX1p70 and FLAG-tagged liprin-α1 with GFP-tagged MID2 was assessed in GFP "pull down" assays. n = 3.

Appendix A5

LNX1 p80 isoforms Clustal Alignment

```
[Homo           MNQP-ESANDPEP----LCAVCGQAHSLEENHFYSYPEEVDDDLICHICLQALLDPLDTP 55
[Macaca         MNQP-ESANDPEG----LCAVCGQAHSLEENHFYSYPEDVDDDLICHICLQALLDPLDTP 55
[Bos            MNQP-DPAEDPDPSPEPLCVVCGQAHSPEENHFYTYTEDVDDDLICHICLQALLDPLDTP 59
[Canis          MSQP-DPTCHPDPSPAPLCVVCGQAHSPEENHFYAYTEDVDDDLICHICLQALLDPLDTP 59
[Mus            MNQP-DLADDPDPSPEPLCIVCGQNHSPEENHFYTYTEDVDDDLICHICLQALLDPLDTP 59
[Rattus         MNQP-DLADDPDPSPEPLCVVCGQNHSPEENHFYTYTEDVDDDLVCHICLQALLDPLDTP 59
[Gallus         MEEN-SPA---------LCVTCGQAHLPEENHLYSYTEEVDDDLICHICLQPLLQPLDTL 50
[Danio          MPVCGATGVTPTAPPPDLCHICGQRHLQEENHEYTYKEDVDDDLMCHICLQPLIRPLDTP 60
                *                **  *** *  **** *:* *:*****:******.*: ****

[Homo           CGHTYCTLCLTNFLVEKDFCPMDRKPLVLQHCKKSSILVNKLLNKLLVTCPFREHCTQVL 115
[Macaca         CGHTYCTLCLTNFLVEKDFCPMDRKSLVLQHCKKSSILVNKLLNKLLVTCPFREHCTQVL 115
[Bos            CGHTYCTVCLTNFLVEKDFCPVDRKPLVLQHCKKSNILVNKLLNKLLVTCPFTEHCTEVL 119
[Canis          CGHTYCTLCLTNFLVEKDFCPVDRKLVVLQHCKKSSILVNKLLNKLMVTCPFSEYCAEVV 119
[Mus            CGHTYCTLCLTNFLVEKDFCPVDRKPVVLQHCKKSSILVNKLLNKLLVTCPFTEHCTEVL 119
[Rattus         CGHTYCTLCLTNFLVEKDFCPVDRKPVVLQHCKKSNILVNKLLNKLLVNCPFTEHCSEVL 119
[Gallus         CGHTFCTACLTNFLLEKDFCPMDRKLVALQNCRKSSILVNNLLDKLMVSCPFTEHCSEVV 110
[Danio          CGHTYCQECLTNFLLESDFCPVDRTPLMLQKCRKSSLLVHKLLDKLMVSCPFAEHCTEVM 120
                ****:*  ******:*.****:**. : **:*:**.:**::**:**:*.*** *:*::*:

[Homo           QRCDLEHHFQTSCKGASHYGLTKDRKRRSQDG-CPDGCASLTATAPSPEVSAAATISLMT 174
[Macaca         QRCDLEHHFQTSCKGASHYGLTKDRKRRSQDG-CPDGCASLTAMAPSPEVSAAATISLMT 174
[Bos            QRCDLEHHFQTSCKGASHYGLTKDRKRRSQDG-CPDGSTSLTATSLSPEISTVPTVSLMT 178
[Canis          QRCDLEQHFQTSCKGASHYGLTKDKKRRSQDG-CPDGCVSLTATALSPEVSATATVSLVT 178
[Mus            QRCDLQHHFQTSCKGASHYGLTKDRKRRSQDG-CPDGCASLMATTLSPEVSAAATISLMT 178
[Rattus         QRCNLQYHFQTSCKGASHYGLTKDRKRRSQDG-CPDGCASLTATTLSPEVSAAATISLMT 178
[Gallus         QRGHLEQHFQTRCKGASHYGLTKERKRRSQDC-SPDRSSSLAVAALGPELSAAAAIALMT 169
[Danio          PRGEMEGHIRCRCKGASHYGLSAERKRRSQEGDCTDSTSELTLAALPGEGCPSSAIALLS 180
                 * .:: *::  *********: ::*****:  ..*   .*   :   * .. .:::*::

[Homo           DEPGLDNPAYVSSAED-GQPAISPVDSGRSNRTRARPFERSTIRSRSFKKINRALSVLRR 233
[Macaca         DEPGLDNPAYVSSAED-GQPAVSPVDSGRSNRTRARPFERSTIRSRSFKKINRALSVLRR 233
[Bos            DEPGLDNPAYVSTAED-GQP-NSPLDSGRSNRTRARPFERSTIRSRSFKKINQALSVLRR 236
[Canis          NEPGLDNPAYVSTVED-GQPADSPLDSGRSNRTRARPFERSTIRSRSFKKINRALSVLRR 237
[Mus            DEPGLDNPAYVSSVED-GEPVANSSDSGRSNRTRARPFERSTMRSRSFKKINRALSALRR 237
[Rattus         DEPGLDNPAYTSSVED-GEPVTNPSDTGRSNRTRARPFERSTMRSRSFKKINRALSALRR 237
[Gallus         DEPGLVNPAFSPTSED-SQSGSGPRDLHCSNRNRTRHFERSTIRSRSFKKINKAFSVLRR 228
[Danio          DEPGLVNPAYEPSVEDNSQSGSTTSLAARSGSRKNRNFDRTSVRSRSFRRLNRAFSVLRR 240
                :**** ***: .: ** .:.   .     *.  : * *:*:::*****:::*:*:*.***

[Homo           TKSGSAVANHADQGRENSENTTAP-EVFPR--LYHLIPDGEITSIKINRVDPSESLSIRL 290
[Macaca         TKSGSAVANHADQGRENSENTTAP-EVFPR--LYHLIPDGEITSIKINRVDPSESLSIRL 290
[Bos            TKSGSTVVSQADQGREDSENTTVL-DVFPR--LYHLIPDGEITSIKINRTDPNENLSIRL 293
[Canis          TKSGSAVANQADQGRENSEDTTAP-EVFPR--LYHLIPDGEITSVKINRVDPNESLSIRL 294
[Mus            TKSGSVVANHVDQGRDNSENTTVP-EVFPR--LFHLIPDGEITSIKINRADPSESLSIRL 294
[Rattus         TKSGSAVANHADQGRDNSENDTVP-EVFPR--LFHLIPDGEITSIKINRVDPNESLSIRL 294
[Gallus         TKSGSAVSNQVDQEREAVGNSAAGEEGFPR--LYHLIPDGEITCIKINRTDPHENLAIRI 286
[Danio          TKSGTAVANDTTEERDNLRNANIPAEVFALPQLHHLIPDGEVTSIKITRADPCEPLAISI 300
                ****:.* ... : *:   :     : *.   *.*******:*.:**.*.** * *:* :

[Homo           VGGSETPLVHIIIQHIYRDGVIARDGRLLPGDIILKVNGMDISNVPHNYAVRLLRQPCQV 350
[Macaca         VGGSETPLVHIIIQHIYRDGVIARDGRLLPGDIILKVNGMDISNVPHNYAVRLLRQPCQV 350
[Bos            VGGSETPLVHIIVQHIYRDGVIARDGRLLPGDIILKVNGMDISNVRHNYALRLLRQPCQV 353
[Canis          VGGSETPLVHIIIQHIYRDGVIARDGRLLPGDIILKVNGMDISNVPHNYALHLLRQPCQV 354
[Mus            VGGSETPLVHIIIQHIYRDGVIARDGRLLPGDIILKVNGMDISNVPHNYAVRLLRQPCQV 354
[Rattus         VGGSETPLVHIIIQHIYRDGVIARDGRLLPGDIILKVNGMDISNVPHNYAVRLLRQPCQV 354
[Gallus         VGGSETPLVHIIIQHIYRDGVIARDGRLLPGDMILKVNGMDIKNVPHHYALSILKQPCHV 346
[Danio          VGGNETPLVRILIQDIYREGVIARDGRLLPGDMILKVNGIDISNVPHCYAVAALKQPCTL 360
                ***.*****:*::*.***:**************:******:**.** * **:  *:*** :

[Homo           LWLTVMREQKFRSRNNGQAPDAYRP------RDDSFHVILNKSSPEEQLGIKLVRKVDEP 404
[Macaca         LWLTVLREQKFRSRNNGQALDAYGS------RDDSFHVILNKSSPEEQLGIKLVRKVDEP 404
[Bos            LRLTVLREQKFRSRTDGQPLDTYGP------RDDSFHVILNKSSPEEQLGIKLVRKMDEP 407
[Canis          LRLTVLREQKFQSRSSGQALDAYGP------RSDTFHVILNKSSPEEQLGIKLVRRVDEP 408
[Mus            LRLTVLREQKFRSRSNAHVPDSYGP------RDDSFHVILNKSSPEEQLGIKLVRRVDEP 408
[Rattus         LRLTVLREQKFRSRSNAPAPDSYGP------RDDSFHVILNKSSPEEQLGIKLVRRVDEP 408
[Gallus         LRLTVLREQRYRCRSSGLSLDAHCS------RDDSFHVVLNKSSPDEQLGIKLVRRADEP 400
[Danio          LRLTVLREQRHRYRSHHHSPTEPFPAHTATIRDDSLHVVLVKRAPDEQLGIKLVRRPDEH 420
                * ***:***:.: *.          .      *.*::**:* * :*:*********: **
```

Appendix A5 (continued)

```
[Homo           GVFIFNVLDGGVAYRHGQLEENDRVLAINGHDLRYGSPESAAHLIQASERRVHLVVSRQV 464
[Macaca         GVFIFNVLDGGVADRHGQLEENDRVLAINGHDLRYGSPESAAHLIQASERRVHLIVSRQV 464
[Bos            GVFIFNVLDGGVADRHGQLEENDRVLAINGHDLRYGSPESAAHLIQASERRVHLVVSRQV 467
[Canis          GVYIFNVLDGGVADRHGQLEENDRVLAINGHDLRYGSPESAAHLIQASERRVHLVVSRQV 468
[Mus            GVFIFNVLNGGVADRHGQLEENDRVLAINGHDLRFGSPESAAHLIQASERRVHLVVSRQV 468
[Rattus         GVFIFNVLNGGVADRHGQLEENDRVLAINGHDLRFGSPESAAHLIQASERRVHLVVSRQV 468
[Gallus         GVFIFNLLDGGVAARDGQLQENDRVLAINGHDHRYGSPESAAQLIQASERHVHFVVSRQT 460
[Danio          GVFIFHLLEGGLAARDGRLRVDDRVLAINGHDLRYGAPEHAALLIQASEDRVHFIVSRQT 480
                **:**::*:**:* *.*:*. :********** *:*:** ** ****** :**::****.

[Homo           RQRSPDIFQEAGWNSNGSWSPGPGERSNTPKPLHPTITCHEKVVNIQKDPGESLGMTVAG 524
[Macaca         R-RSPDIFQEASWNSNGSWSPGPGERSNTPKPLHPKITCHEKVVNIQKDPGESLGMTVAG 523
[Bos            RRHSPDIFQEASWNSNGSQSPGSGDRSNTPKPLHPVVTCHEKVVSVRKDPGESLGMTVAG 527
[Canis          HLQSPDIFQEAGWNSDGSQSPGPGDRSSTPKPLHPVATCREKVVSVRKDPSESLGMTVAG 528
[Mus            RQSSPDIFQEAGWISNGQQSPGPGERNTASK---PAATCHEKVVSVWKDPSESLGMTVGG 525
[Rattus         RQPSPDIFQEAGCISNGQQSPVSGERSTSSK---PAATCHEKVVSVQKDPNESLGMTVGG 525
[Gallus         RQQPPDILQETGWSYSSSPQPCPAERINASKSTLHTVTCHEKVVAVRKDHTESLGMTVAG 520
[Danio          HIPAPDILQEAPWSMEGPPPYSPVDIEHTLLDSCQKPACYEKTVTLLKEPHDSLGMTVAG 540
                :  .***:**:    ..     . :   :        :* **.* : *:  :******.*

[Homo           GASHREWDLPIYVISVEPGGVISRDGRIKTGDILLNVDGVELTEVSRSEAVALLKRTSSS 584
[Macaca         GASHREWDLPIYVISVEPGGVISRDGRIKTGDILLNVDGVELTEVSRSEAVALLKRTSSS 583
[Bos            GASHTEWDLPIYVISVEPGGVISRDGRIKTGDILLNVNGIELTEVSRSEAVGLLKSTSSS 587
[Canis          GASHREWDLPIYVISVEPGGVISRDGRIKTGDILLNVNGIELTEVNRSEAVALLKSTSSL 588
[Mus            GASHREWDLPIYVISVEPGGVISRDGRIKTGDILLNVNGIELTEVSRTEAVAILKSAPSS 585
[Rattus         GASHREWDLPIYVISVEPGGVISRDGRIKTGDILLNVNGIELTEVSRTEAVAILKSTPSS 585
[Gallus         GATNREWDLPIYVISVEPGGVISRDSRIKTGDILLNVNGIDLTGVSRNEAVALLKNTSSS 580
[Danio          GMSSRGWDLPVYVTNVDPNGVVGQEGSIRKGDILLNVNGVDLTGVTRSEAVANLKNTSSP 600
                * :   ****:** .*:*.**:.::. *:.*******:*::** *.*.***. ** :.*

[Homo           IVLKALEVKEYEP---------QEDCSSPAALDSNHNMAPPSD-WSPSWVMWLELPRCLY 634
[Macaca         IVLKALEVKEYEP---------QEDCSSPAALDSNHNMAPPSD-WSPSWVMWLELPRCLY 633
[Bos            VVLKALEVKEYEP---------QEDDSSLAALDSDQDTAPPSD-WFPSWVMWLELPRYLY 637
[Canis          VVLKALEVEEHEP---------QEACSSPAALDSNHNMAPARD-WSPSWIMWLELPRYLY 638
[Mus            VVLKALEVKEQEA---------QEDCS-PAALDSNHNVTPPGD-WSPSWVMWLELPQYLC 634
[Rattus         VVLKALEVKEQET---------QEDCS-PAALDSNHNVTPPGD-WSPSWVMWLELPQYLY 634
[Gallus         VVLKALEMRTCDG---------RERSE----------AAEHSE-WSPSWVTWLGLPRYLY 620
[Danio          VVLQVLEMRPPNESSLDCMPPLHSPCALSPSSPGDVKLPPPNDDYAPLWVSWLQLPRHLY 660
                :**:.**:.  :          :.              .   : : * *: ** **: *

[Homo           NCKDIVLRRNTAGSLGFCIVGGYEEYNGNKPFFIKSIVEGTPAYNDGRIRCGDILLAVNG 694
[Macaca         NCKDIILRRNTAGSLGFCIVGGYEEYNGNKPFFIKSIVEGTPAYNDGRIRCGDILLAVNG 693
[Bos            NCKDVILRRNTAGSLGFCIVGGYEEYNGNKPFFIKSIVEGTPAYNDGRIRCGDILLAVNG 697
[Canis          NCKDVILRRNTAGSLGFCIVGGYEEYNGNKPFFIKSIVEGTPAYNDGRIRCGDILLAVNG 698
[Mus            NCKDVILRRNTAGSLGFCIVGGYEEYSGNKPFFIKSIVEGTPAYNDGRIRCGDILLAVNG 694
[Rattus         NCKDVILRRNTAGSLGFCIVGGYEEYSGNQPFFIKSIVEGTPAYNDGRIRCGDILLAVNG 694
[Gallus         SCKEIVLRRNTSGSLGFSIVGGYEEHTGNKPFFIKSIVGGTPAYNDGRIRCGDILLAVNG 680
[Danio          CCKDIVFRRSTSGSLGFSIVGGQEELNCNQSFFIRSIVEGTPAYNDGRIRCGDILLEVNG 720
                 **::::**.*:*****.**** ** . *:.***:*** ***************** ***

[Homo           RSTSGMIHACLARLLKELKGRITLTIVSWPGTFL 728
[Macaca         RSTSGMIHACLARLLKELKGRITLTIVSWPGTFL 727
[Bos            RSTTGMIHACLARMLKELKGKITLTIASWPGTFL 731
[Canis          RSTSGMIHACLARMLKELKGKITLTIVSWPGTFL 732
[Mus            RSTSGMIHACLARMLKELKGRITLTIASWPGTFL 728
[Rattus         RSTSGMMHACLARMLKELKGKITLTIASWPGTFL 728
[Gallus         RNTSGMMHACLARMLKELKGKITLTIVSWPGTFL 714
[Danio          KSTWGMTHTALVRLLKELRGRITLTIVSWPGSLL 754
                :.* ** *:.*.*:****:*:*****.****::*
```

p70 isoforms Clustal alignment

```
[Mus            MKALLLLVLPWLSPANYIDNVGNLHFLYSELCKGASHYGLTKDRKRRSQDGCPDGCASLM 60
[Rattus         MKALLLLVLPWLSPANYIDNVGNLHFLYSELCKGASHYGLTKDRKRRSQDGCPDGCASLT 60
[Homo           MKALLLLVLPWLSPANYIDNVGNLHFLYSELCKGASHYGLTKDRKRRSQDGCPDGCASLT 60
[Canis          MKALLLLVLPWLSPANYIDNVGNLHFLYSELCKGASHYGLTKDKKRRSQDGCPDGCVSLT 60
[Bos            MKALLLLILPWLSPANYVDNVGNLHFLYSELCKGASHYGLTKDRKRRSQDGCPDGSTSLT 60
[Gallus         MKALLLLVLPWLSPANYIDNVGNLHLLYSELCKGASHYGLTKERKRRSQDCSPDRSSSLA 60
                *******:*********:*******:****************::****** .** . **
```

Appendix A5 (continued)

LNX2 Clustal alignment

```
[Canis            MGTTSDEMVSVEQTSS-SSFNPLCFECGQQHWTRENHLYNYQNEVDDDLVCHICLQPLLQ 59
[Bos              MGTTSDEMGSVEQTLS-SSFNPLCFECGQQHWTRENHLYNYQDEVDDDLVCHICLQPLLQ 59
[Homo             MGTTSDEMVSVEQTSS-SSLNPLCFECGQQHWTRENHLYNYQNEVDDDLVCHICLQPLLQ 59
[Mus              MGTTSDEMVPVEQASSTSSLDPLCFECGQQHWARENHLYNYQGEVDDDLVCHICLQPLLQ 60
[Rattus           MGTTSDEMVPVQQASSASSLDPLCFECGQQHWARENHLYNYQGEVDDDLVCHICLQPLLQ 60
[Monodelphis      MGTTNDEIVSMEQNSS---LNPLCFECGQQHWTRENHLYNYQNEVDDDLVCHICLQPLLQ 57
[Gallus           MGTTGDDMALAEQNAS---LNPLCFECGQQHWTRENHLYNYQNEVDDDLVCHICLQPLLQ 57
[Xenopus          MTATTEELVLMEDDTS---LNPLCFECGQQHWTRENHLYNYQNEVDDDLVCHICLQPLLQ 57
[Danio            -------------MVSEALLEALCSECGQIHRTWENHLYNYRLEVDDDLVCHICLQPLVQ 47
                              *   ::.** **** * : *******: ***************:*

[Canis            PLDTPCGHTFCCKCLRNFLQEKDFCPLDRKRLHFKLCKKSSILVHKLLDKLLVLCPFSSV 119
[Bos              PLDTPCGHTFCCKCLRNFLQEKDFCPLDRKKLHFKSCKKSSILVHKLLDKLLISCPFSSV 119
[Homo             PLDTPCGHTFCYKCLRNFLQEKDFCPLDRKRLHFKLCKKSSILVHKLLDKLLVLCPFSSV 119
[Mus              PLDTPCGHTFCHKCLRNFLQEKDFCPLDRKRLHFKLCKKSSILVHKLLDKLLVLCPFSPV 120
[Rattus           PLDTPCGHTFCHKCLRNFLQEKDFCPLDRKRLHFKLCKKSSILVHKLLDKLLVLCPFSSV 120
[Monodelphis      PLDTPCGHTFCYKCLRNFLQEKDFCPLDRKRLHFKLCKKSSILVHKLLDKLLVLCPFSSV 117
[Gallus           PLDTPCGHTFCYKCLRNFLQEKDFCPLDRKRLHFKLCKKSSILVHKLLDKLLVLCPFSSV 117
[Xenopus          PLDTPCGHTFCFKCLRNFLQEKDFCPLDRKRLHFKLCKKSSILVHKLLDKLVVSCPYSAA 117
[Danio            PLDTPCGHTFCARCLRSFLQERDFCPLDRAHLQLQVCRRSSILVHKLLDKLSVTCPLTPS 107
                  *********** :***.****:******* :*::: *::************ : ** :.

[Canis            CQDVMQRCDLEAHLKNRCPGASHRRLALERRKTGKAQTEIENENGTTIIDLPGTLSPETD 179
[Bos              CHDVMQRCDLEGHLKNRCPGASHRRAALEKRKTSKTQMEIENENGTTVTDLPAALSPETD 179
[Homo             CKDVMQRCDLEAHLKNRCPGASHRRVALERRKTSRTQAEIENENGPTLLDPAGTLSPEAD 179
[Mus              CQDVMQRCDLEAHLKNRCPGASHRRVDLERRKTSQTQTQIEGETGSTVIDPPGTLPPETD 180
[Rattus           CQDVMQRCDLEAHLKNRCLGASHRRVDLERRKTSQAHTQIEGETGSTVIDPPGPSPPETD 180
[Monodelphis      CQDVMQRCDLEAHLKNRCPGASGRRVALERRKTSKLKTEIENENGSNVIDHPGTLSPDNA 177
[Gallus           CQEVMQRCDLAAHLKNRCPGASHRRVALERRRASKLQAEAEGEAGPGGPEHPNSVSVDAE 177
[Xenopus          CKETMQRCDMEAHLKNRCPGASHRRELLNQHRASKLQIEIEGENGSVLIDHQGPVSPESD 177
[Danio            CSLSMPRCDLEAHLKHRCPGTQSQRTKLER-------TQMEGSEDRVTATNP-PKSPQTE 159
                  *   * ***: .***:** *:. :*  *::        : *.. .        . . :

[Canis            CSGTGTAPAERNLPSASLPAWTEEPGLDNPAFEENTATDTTQ------------------ 221
[Bos              CSG-------RTLTSASLPSWTEEPGLDNPAFEESPAGDTTP------------------ 214
[Homo             CLGTGAVPVERHLTSASLSTWSEEPGLDNPAFEESAGADTTQ------------------ 221
[Mus              CSG--TVPGERNLTPASLPVWTEEPGLDNPAFEESAAADSVQ------------------ 220
[Rattus           CLG--TVPGERNSTPAPLPVWTEDPGLDNPAFEESAAADSVQ------------------ 220
[Monodelphis      GTG--TVPAERNLTSTSLPMWTDEPGLDNPAFEETTVADTSQ------------------ 217
[Gallus           QSI---VPAEQSFTPA-LPAWADEPGIDNPPFEENTGADTNQ------------------ 215
[Xenopus          KTRSGSALPERNVTPSVMPAWMEEHGFDNPAFEESTVADATH------------------ 219
[Danio            IKEDTPSPPAGSNACNNVPTWTEEPGIDNPAFEESTEEDSVHGLECALPRVKRPLSNPCI 219
                              .   :. * :: *:***.***..  *:

[Canis            ----------------------------QPLSLPEGEITTIEIHRSNPYIQLGISIVGGN 253
[Bos              ----------------------------QPLSLPEGEITTIEIHRSNPFIRLGISIVGGN 246
[Homo             ----------------------------QPLSLPEGEITTIEIHRSNPYIQLGISIVGGN 253
[Mus              ----------------------------QPLSLPEGEITTIEIHRSNPYIQLGISIVGGN 252
[Rattus           ----------------------------QPLSLPEGEITTIEIHRTNPYIQLGISIVGGN 252
[Monodelphis      ----------------------------PPPSLPEGEITTIEIHRSNPYIELGISIVGGN 249
[Gallus           ----------------------------QPPTLPEGEITTIEIHRSNPYIELGISIVGGN 247
[Xenopus          ----------------------------PPPSLPEGEITTIEIHRSNPYIELGISIVGGN 251
[Danio            HLLRTGSSASSGWDFVETLPLSAEEGCVKLPSLPEGEITTIEVHRTNPYSEMGISIVGGN 279
                                             :**********:**:**: .:********

[Canis            ETPLINIVIQEVYRDGIIAKDGRLLAGDQILQVNNCNISNVSHNYARAVLSQPCSTLHLT 313
[Bos              ETPLINIVIQEVYRDGVIAKDGRLLAGDQILQVNNYNISSVSHNYARAVLSQPCSTLQLT 306
[Homo             ETPLINIVIQEVYRDGVIARDGRLLAGDQILQVNNYNISNVSHNYARAVLSQPCNTLHLT 313
[Mus              ETPLINIVIQEVYRDGVIARDGRLLAGDQILQVNNYDISNVSHNHARAVLSQPCSTLQLT 312
[Rattus           ETPLINIVIQEVYRDGAIARDGRLLAGDQILQVNNCDISNVSHNYARAVLSQPCSTLHLT 312
[Monodelphis      ETPLINIVIQEVYRDGIIARDGRLLAGDQILQVNNFDISNVSHNYARAVLSQPCSVLYLT 309
[Gallus           ETPLINIVIQEVYRDGIIARDGRLLAGDQILQVNSFDISNVSHNHARAVLSQPCTVLHLT 307
[Xenopus          ETPLINVVIQEIYRDGVIARDGRLLAGDQILQVNNFDISNVSHNYARWVLSQPCTVLHLT 311
[Danio            ETPLINVVIQEVYRDGVIARDGRLLAGDQILQVNNVDISNVPHNFARSTLARPCATLQLT 339
                  ******:****:**** **:**************. :**.*.**.** .*::** .* **
```

Appendix A5 (continued)

```
[Canis          VLRERRFGNRTNSHSD-------SSSPREDIFHVVLHKRDSGEQLGIKLVRRTDEPGVFI 366
[Bos            VLRERRFGSRAHGHPE-------GGSPREEVFPVVLHKRDSAEQLGIKLVRRTDEPGVFI 359
[Homo           VLRERRFGNRAHNHSD-------SNSPREEIFQVALHKRDSGEQLGIKLVRRTDEPGVFI 366
[Mus            VLRERRFGSRANSHAD-------GSAPRDEVFQVLLHKRDSTEQLGIKLVRRTDEPGVFI 365
[Rattus         VLRERRFGSRANNHAD-------GSAPRDEVFQVLLHKRDSAEQLGIKLVRRTDEPGVFI 365
[Monodelphis    VLRERRFGSRTYSHSD-------NNSLREESFHVILHKRDSNEQLGIKLVRRTDEPGVFI 362
[Gallus         VLRERRFGSRTHGHTDTTTTTTTSSSSRDDSFQVTLHKRDSSEQLGIKLVRRTDEPGVFI 367
[Xenopus        VLRERRFGSRAHGHGD-------GGSQRDESFHITLNKRGSNEQLGIKLVRRTDESGVFI 364
[Danio          VLRERRCSARPPAATA-------SPKGSPASIRITLHKRESSEQLGIKLVRRTDEAGVFI 392
                ****** . *.            .       : : *:** * *************.****

[Canis          LDLLEGGLAAQDGRLSSNDRVLAINGHDLKHGTPELAAQIIQASGERVDLTIARQGK--- 423
[Bos            LDLLEGGLAAQDGRLSSNDRVLAINGHDLKHGTPELAAQIIQASGERVSLTIARPGK--- 416
[Homo           LDLLEGGLAAQDGRLSSNDRVLAINGHDLKYGTPELAAQIIQASGERVNLTIARPGK--- 423
[Mus            LDLLEGGLAAQDGRLNSNDRVLAINGHDLKHGTPELAAQIIQASGERVNLTIARPGK--- 422
[Rattus         LDLLEGGLAAQDGRLSSNDRVLAINGHDLKQGTPELAAHIIQASGERVNLTIARPGK--- 422
[Monodelphis    LDLLEGGLAAQDGRLSSNDRVLAINGHDLKHGTPELAAQIIQASGERVNLTIARPGK--- 419
[Gallus         LDLLEGGLAAQDGRLCSNDRVLAINGHDLKHGTPELAAQVIQASGERVNLIISRPMK--- 424
[Xenopus        LDLLEGGLAAQDGRLHSNDRVLAINGLDLKHGTPELAAQIIQGSGERVNLTVSRPGK--- 421
[Danio          LDLLEGGLAAKDGRLCSNDRVLAVNEHDLRHGTPELAAQIIQASGERVNLLISRSSKQTM 452
                **********:**** *******:*  **: *******::**.*****.* ::*  *

[Canis          --SQPGNSVRDTGAQSSS--------QHHAQPLYHNRPSSHKDLTQCVTCQEKHITVKKE 473
[Bos            --PQPGSTVREAGTQSSS--------QHHTQTLPYNRPSSHKDLAQCVTCQEKHITIKKE 466
[Homo           --PQPGNTIREAGNHSSSS-------QHHTPPPYYSRPSSHKDLTQCVTCQEKHITVKKE 474
[Mus            --PQPSNGSREAGAHSSS---------NHAQPPSHSRPGSHKDLTRCVTCQEKHITVKKE 471
[Rattus         --PQPSNGSREAGAHSS----------NHAQPPSHSRPSSHKDLTRCVTCQEKHITVKKE 470
[Monodelphis    --PQTTNTNREPGTHNSG--------QHQAQQLYHSRPSSHKDLSQCVTCQEKHITVKKE 469
[Gallus         --SQTVSIIRDTGTHNSNP------HQHQSQQLFHCRPNSHKDLSQCVTCQEKHITVKKE 476
[Xenopus        --HQPGNITRDLGMNQPH---------HHTQQVYHHRPSAHKDLAQCVKCQEKHITVKKE 470
[Danio          AVHTGSTLTRDIWSHDHIPPPLPSTATPSPVPSLHLARSSTQRDLSQCVNCKEKHITVKKE 512
                      .  *:   :.                    *..:::**::**.*:*****:***

[Canis          PHESLGMTVAGGRGSKSGELPIFVTSVPPHGCLARDGRIKRGDILLNINGIDLTNLSHSE 533
[Bos            PHESLGMTVAGGRGSKSGELPIFVTSVPPHGCLARDGRIKRGDILLNINGIDLTNLSHSE 526
[Homo           PHESLGMTVAGGRGSKSGELPIFVTSVPPHGCLARDGRIKRGDVLLNINGIDLTNLSHSE 534
[Mus            PHESLGMTVAGGRGSKSGELPIFVTSVPPHGCLARDGRIKRGDVLLNINGIDLTNLSHSE 531
[Rattus         PHESLGMTVAGGRGSKSGELPIFVTSVPPHGCLARDGRIKRGDVLLNINGIDLTNLSHSE 530
[Monodelphis    PHESLGMTVAGGRGSKSGELPIFVTSVPPHGCLARDGRIKRGDVLLNINGIDLTDLSHSE 529
[Gallus         PHESLGMTVAGGRGSKSGELPIFVTSVQPHGCLARDGRIKRGDVLLNINGIDLTNLSHSE 536
[Xenopus        PQESLGMTVAGGRGSKSGELPIFVTSVQPHGCLARDSRIKRGDVLLSINGIDLTNLSHSE 530
[Danio          PHESLGMTVAGGRGSKSGELPIFVTSVQPHGCLSRDGRIKRGDVLLSINGQDLTYLSHSE 572
                *:************************ *****:**.******:**.*** *** *****

[Canis          AVAMLKASAASPAVVLKALEVQIVEEATQATEEQLSTFSENEYDASWSPSWVMWLGLPSA 593
[Bos            AVAMLKASATSPTVALKALEVQVVEEAAQGLDEPLSAVSENEYDASWSPSWVMWLGLPSA 586
[Homo           AVAMLKASAASPAVALKALEVQIVEEATQNAEEQPSTFSENEYDASWSPSWVMWLGLPST 594
[Mus            AVAMLKASAASPAVILKALEVQIAEEAAQATEEQPSAFSENEYDASWSPSWVMWLGLPSA 591
[Rattus         AVAMLKASAASPAVILKALEVQIAEEAAQATEEQPGAFSENEYDASWSPSWVMWLGLPSA 590
[Monodelphis    AVAVLKASAASSAVTLKALEVQIVEEQTQVNEEQPSTISENEYDASWSPSWIMWLGLPSV 589
[Gallus         AVAMLKASAASSVVALKALEVQIVEEQPQANEEQLSTISENEYDASWSPSWVMWLGLPSC 596
[Xenopus        AVAMLKASATSSVVSLKAIEVEVIEEQTPGKEE-MSTVSENEYDASWSPSWVMWLGLPSC 589
[Danio          AVGTLKSSATSCSVQLKALEVTMVEE--PGLDEELLPPHENDYDASWSPSWVLWLGLPSY 630
                **. **:**:*  * ***:** : **     :*   .  **:*********::******

[Canis          LHSCHDIVLRRSYLGSWGFSIVGGYEENHTNQPFFIKTIVLGTPAYYDGRLKCGDMIVAV 653
[Bos            LHSCHDIVLRRSYLGSWGFSIVGGYEENHTNQPFFIKTIVLGTPAYYDGRLKCGDMIVAV 646
[Homo           LHSCHDIVLRRSYLGSWGFSIVGGYEENHTNQPFFIKTIVLGTPAYYDGRLKCGDMIVAV 654
[Mus            LHSCHDIVLRRSYLGSWGFSIVGGYEENHTNQPFFIKTIVLGTPAYYDGRLKCGDMIVAV 651
[Rattus         LHSCHDIVLRRSYLGSWGFSIVGGYEENHSNQPFFIKTIVLGTPAYYDGRLKCGDMIVAV 650
[Monodelphis    LHSFHDVVLRRSNLGSWGFSIVGGYEENHTNQPFFIKTIVLGTPAYYDGRLKCGDMIIAV 649
[Gallus         LHSCHDVVLRRSNLGSWGFSIVGGYEENHTNQPFFIKTIVLGTPAYFDGRLKCGDMIVAV 656
[Xenopus        LHSCHDVVLRRSSLGSWGFSIVGGYEENHTNQPFFIKTIVLGTPAYYDGRLKCGDMIIAV 649
[Danio          LHSSHEIVLRRSHPGSWGFSIVGGYEENHSNQAFFIKTIVLGTPAYYDGRLKCGDMIVAV 690
                *** *::*****  ***************:**.*************:**********:**

[Canis          NGLSTVGMSHSALVPMLKEQRNKVTLTVICWPGSLV 689
[Bos            NGLSTVGMSHSALVPMLKEQRNKVTLTVICWPGSLV 682
[Homo           NGLSTVGMSHSALVPMLKEQRNKVTLTVICWPGSLV 690
[Mus            NGLSTVGMSHSALVPMLKEQRNKVTLTVICWPGSLV 687
[Rattus         NGLSTVGMSHSALVPMLKEQRNKVTLTVVCWPGSLV 686
[Monodelphis    NGLSTLGMSHSALVPMLKEQRNKVTLTVICWPGSLV 685
[Gallus         NGLSTVGMSHSALVPMLKEQRNKVTLTVICWPGSLI 692
[Xenopus        NGLSTVGMSHSALVPMLKEQRNKVTLSVISWPGSLV 685
```

Appendix A5 (continued)

```
[Danio            NGLSTAGMSHSALVPMLKEQRSRVALTVVSWPGSLI 726
                  ***** ***************.:*:*:*:.*****:
```

Appendix B: Publications

Gene 552 (2014) 39–50

Contents lists available at ScienceDirect

Gene

journal homepage: www.elsevier.com/locate/gene

Regular research article

Tight, cell type-specific control of LNX expression in the nervous system, at the level of transcription, translation and protein stability

Joan A. Lenihan [1], Orthis Saha [1], Louise M. Mansfield, Paul W. Young *

School of Biochemistry and Cell Biology, University College Cork, Cork, Ireland

ARTICLE INFO

Article history:
Received 19 April 2014
Received in revised form 1 September 2014
Accepted 4 September 2014
Available online 6 September 2014

Keywords:
LNX
LNX1
LNX2
PDZRN
Translational control
Upstream open reading frame (uORF)

ABSTRACT

LNX1 and LNX2 are E3 ubiquitin ligases that can interact with Numb — a key regulator of neurogenesis and neuronal differentiation. LNX1 can target Numb for proteasomal degradation, and *Lnx* mRNAs are prominently expressed in the nervous system, suggesting that LNX proteins play a role in neural development. This hypothesis remains unproven, however, largely because LNX proteins are present at very low levels *in vivo*. Here, we demonstrate expression of both LNX1 and LNX2 proteins in the brain for the first time. We clarify the cell-type specific expression of LNX isoforms in both the CNS and PNS, and identify a novel LNX1 isoform. Using luciferase reporter assays, we show that the 5′ untranslated region of the *Lnx1_variant 2* mRNA, that generates the LNX1p70 isoform, strongly suppresses protein production. This effect is mediated in part by the presence of upstream open reading frames (uORFs), but also by a sequence element that decreases both mRNA levels and translational efficiency. By contrast, uORFs do not negatively regulate LNX1p80 or LNX2 expression. Instead, we find some evidence that protein turnover via proteasomal degradation may influence LNX1p80 levels in cells. These observations provide plausible explanations for the low levels of LNX1 proteins detected *in vivo*.

© 2014 Elsevier B.V. All rights reserved.

1. Introduction

Ligand of NUMB protein X1 (LNX1) and LNX2 are closely related proteins that share an identical domain structure consisting of one amino-terminal RING (Really Interesting New Gene) and four PDZ (PSD-95, DlgA, ZO-1) domains (Rice et al., 2001). LNX proteins were originally described as ligands of Numb and its paralog Numb-like (Dho et al., 1998; Rice et al., 2001), and LNX1 has been shown to ubiquitinate and target specific Numb isoforms for proteasomal degradation (Nie et al., 2002, 2004). Numb is a key protein involved in the specification of cell fates during development. In the nervous system, Numb functions in maintaining neural progenitors at early developmental stages while later, it promotes neuronal differentiation and maturation (Gulino et al., 2010). The combination of RING and PDZ domains in LNX proteins suggests that their ubiquitin ligase activity may be targeted to specific substrate proteins, by PDZ domain-mediated interactions (Flynn et al., 2011). Indeed, a large number of other LNX-interacting proteins have also been identified, and several of these are substrates for ubiquitination (Guo et al., 2012; Wolting et al., 2011). LNX substrates include the proto-oncogenes, cSrc and BCR, the cell junction-associated molecule Claudin-1, the T-cell co-receptor CD8α and the protein kinase PBK (D'Agostino et al., 2011; Guo et al., 2012; Takahashi et al., 2009; Weiss et al., 2007). However, the *in vivo* relevance of these interactions, including the interactions with Numb proteins, remains unclear. Zebrafish have an additional *Lnx* paralog, *Lnx2b*, that has been well-characterized *in vivo* as a modulator of transcription factors involved in dorso-ventral and antero-posterior axis specification during embryogenesis (Ro and Dawid, 2009, 2010, 2011). However, these functions may be unique to Lnx2b, which is not present in mammals. LNX1 and LNX2 functions have not been thoroughly explored *in vivo* in any model organism and all studies of LNX1 and LNX2, to date, have relied heavily on exogenously expressed LNX proteins.

Studies of *Lnx* expression showed a widespread distribution of *Lnx1* and *Lnx2* mRNAs in several adult tissues, with the earliest embryonic expression of both genes being observed in the CNS (Dho et al., 1998; Rice et al., 2001). By contrast, the expression patterns of LNX1 and LNX2 proteins remain poorly characterized. Expression of endogenous LNX1 protein was first reported in perisynaptic Schwann cells, at neuromuscular junctions (NMJs) (Young et al., 2005). Both LNX1 and LNX2 proteins, on the other hand, were detected in the acrosome of spermatozoa, while LNX2 expression was reported in a subset of blood vessels (Mirza et al., 2005, 2006). Detection of LNX proteins by western blotting generally requires prior immunoprecipitation from tissue lysates (Mirza et al., 2005; Weiss et al., 2007; Young et al., 2005), indicating that

Abbreviations: BCA, Bicinchoninic acid; BCIP, 5-bromo-4-chloro-3-indolyl phosphate; BSA, bovine serum albumin; CNS, central nervous system; DAB, 3, 3′-diaminobenzidine; DIG, Digoxigenin; LNX, ligand of NUMB protein X1; NBT, 4-nitro-blue-tetracolium-chloride; NGS, normal goat serum; NMJ, neuromuscular junction; OPC, oligodendrocyte precursor cells; PBS, phosphate buffered saline; PDZ, PSD-95, DlgA, ZO-1; PNS, peripheral nervous system; RING, Really Interesting New Gene; UTR, untranslated region.

* Corresponding author.
E-mail address: p.young@ucc.ie (P.W. Young).

[1] These authors contributed equally to this work.

http://dx.doi.org/10.1016/j.gene.2014.09.011
0378-1119/© 2014 Elsevier B.V. All rights reserved.

despite widespread mRNA expression, LNX1 and LNX2 proteins are present at extremely low levels *in vivo*.

The early expression of *Lnx1* and *Lnx2* in the embryonic brain and spinal cord (Rice et al., 2001) hints at potential functions in neural development, possibly through regulation of Numb proteins. However, there is a lack of data about the cell-type specific expression of the mRNA for the *Lnx* genes in the CNS that would provide clues about the functions of these genes. An isoform of LNX1 (LNX1p70), lacking the amino terminal RING domain, is expressed in the CNS using an alternate promoter to the one that drives expression of the longer, RING domain-containing, LNX1p80 isoform, which is expressed in other tissues ((Dho et al., 1998), Fig. 1A, B). This suggests that the functions of LNX1 in the brain, in contrast to LNX2, may be independent of the ubiquitin ligase activity of its RING domain. Amplification of the *Lnx1* and *Lnx2* genes has been reported in brain tumors and colorectal cancer respectively (Blom et al., 2008; Camps et al., 2013; Holtkamp et al., 2007), while alterations of *Lnx1* mRNA levels were associated with gliomas, Kawasaki disease and chronic Q fever (Burgner et al., 2009; Chen et al., 2005; Mehraj et al., 2011). In the case of colorectal cancer in particular, a plausible role for *Lnx2* overexpression in activating signaling pathways that drive tumor progression was established (Camps et al., 2013). A better understanding of *Lnx* mRNA expression patterns, and how these relate to protein levels, will facilitate the elucidation of the physiological functions of LNX proteins, as well as their proposed roles in disease states.

To address these issues, we have examined *Lnx* mRNA and LNX protein expression, focusing especially on the CNS. We find both LNX1 and LNX2 to be predominantly expressed in neurons, and describe a novel LNX1 protein isoform in the brain. We find that the presence of uORFs and other sequence elements in the 5′ untranslated region (5′ UTR) of neuronal *Lnx1* mRNA transcripts attenuate LNX1p70 protein production. We also examine the stability and proteasomal degradation of LNX1p80. Our findings provide a plausible explanation for the lack of correlation between *Lnx1* mRNA and protein levels *in vivo*, and have significant implications for understanding LNX protein function, their roles in disease, and the physiological relevance of the many interactions of LNX proteins that have been identified to date.

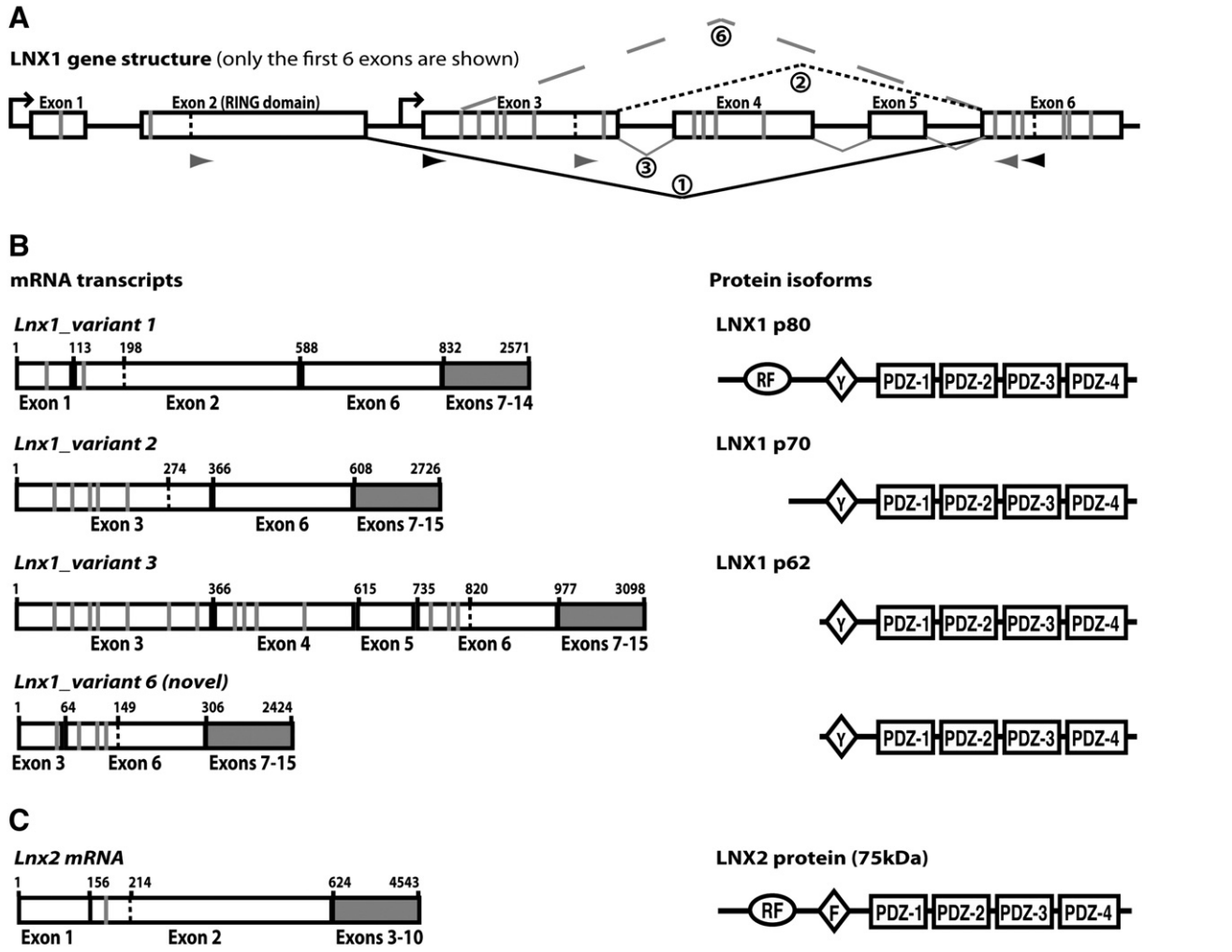

Fig. 1. Schematic diagrams of *Lnx1* and *Lnx2* genes, mRNA transcripts and proteins. (A) *Lnx1* gene structure showing the first 6 exons only (rectangles). Two alternate promoters (arrows) generate transcripts that start with either exon 1 or exon 3. The splicing events that generate *Lnx1* transcript variants 1, 2, 3 and 6 are numbered (in circles) and indicated by the black, black-dotted, gray and gray-dashed lines respectively. Vertical gray lines within the exons indicate non-initiation AUG codons, while the initiation codons for the main *Lnx1* coding sequences are shown as vertical dashed black lines. Arrowheads indicate the positions of primers used for reverse transcriptase PCR (see Fig. 3). (B) *Lnx1* mRNA transcript variants 1, 2, 3 and a novel variant that we term transcript variant 6 are depicted on the left, with the corresponding predicted protein products on the right. *Lnx1_variant 1* contains exon 2 that codes for the RING finger domain (RF) while the other variants, expressed from the alternate promoter, start with exon 3 and lack the RING domain. The NPAY motif (Y) that binds Numb and the four PDZ domains are common to all isoforms and are encoded by exon 6 and downstream exons (indicated by the gray box). Upstream AUG (uAUG) and initiation AUG codons for each transcript are indicated by vertical gray and dashed lines respectively. Nucleotide positions of splice junctions and the initiation AUG are indicated above each mRNA. *Lnx1_variant 6* is generated by splicing from an internal site within exon 3 to exon 6 and is predicted to give rise to the same 62 kDa protein product as *Lnx1_variant 3*. (C) The first two exons of the *Lnx2* mRNA transcript are depicted on the left with AUG codons and downstream exons indicated as in B (above). LNX2 protein (right) has an identical domain structure to LNX1p80 except that it has an NPAF (F) rather than an NPAY motif.

2. Materials and methods

2.1. Animals and animal procedures

Lnx1$^{exon3-/-}$ mice, originally generated by Lexicon pharmaceuticals, were obtained from the Mutant Mouse Regional Resource Center, University of California, Davis (Stock No: 032436-UCD; Strain Name: B6;129S5-Lnx1<tm1Lex>/Mmcd) and were maintained on a C57BL/6J genetic background. *Lnx2*$^{-/-}$ mice were generated recently in our laboratory and will be described in detail elsewhere. All animal experiments were performed as per institutional guidelines set by the University College Cork, Ethics Committee and conducted under license (No: B100/3814) issued by the Department of Health and Children.

2.2. In situ probes, antibodies and reagents

To generate in situ hybridization probes, partial *Lnx1*, *Lnx2*, and *Plp* cDNAs were cloned into the pBluescript II KS(+) vector (Agilent Technologies) and used as template for *in vitro* transcription to generate Digoxigenin (DIG)-labeled or fluorescein-labeled antisense and sense riboprobes that were detected using alkaline phosphatase-conjugated anti-DIG, and horse radish peroxidase conjugated anti-fluorescein antibodies (all reagents from Roche Applied Sciences). Probes correspond to nucleotides 1–557, 1–646 and 1–833 of the *Lnx1_variant 2*, *Lnx2* and *Plp* coding sequences respectively. The *Lnx1* probe is complementary to exons 6 and 7 and parts of exons 3 and 8, and is thus expected to hybridize to all known *Lnx1* isoforms. Sources and catalog numbers for commercial antibodies used were: anti-GFAP, anti-OLIG2, and anti-NeuN (Millipore; MAB3402, AB9610 and MAB377 respectively), anti-FLAG M2, anti-β-tubulin and anti-β-actin (Sigma-Aldrich; F3165, T4026 and A5441 respectively), and anti-HA (catalog number MMS-101R, Covance). The guinea pig polyclonal anti-LNX antibodies, that are either LNX1-specific (anti-LNX1-PDZ3/4), or that recognize both LNX1 and LNX2 (anti-LNX1/2-PDZ3/4) (Young et al., 2005), and the rabbit polyclonal anti-LNX antibody (anti-LNX1/2-RING/NPAY), that recognizes both LNX1 and LNX2 (Dho et al., 1998), have been described previously. The guinea pig and rabbit antibodies that recognize both LNX1 and LNX2 were used for immunoprecipitation and immunoblotting respectively, while the LNX1-specific guinea pig antibody was used for immunostaining of NMJs. Secondary antibodies were from Jackson ImmunoResearch Laboratories and LI-COR, Biosciences, and Alexa-647 conjugated α-bungarotoxin from Molecular Probes. All chemicals and other reagents were purchased from Sigma-Aldrich unless otherwise stated.

2.3. Plasmids, primers, cDNA constructs and bioinformatic analysis

Lnx cDNA constructs were based on the following GenBank sequences: NM_001159577.1 for *Lnx1_variant 1*, NM_010727 for *Lnx1_variant 2*, NM_001159578 for *Lnx1_variant 3* and AF401681.1 for *Lnx2*. The *Lnx1_variant 6* sequence described here, has been deposited in GenBank, with the accession number KJ418422. For luciferase reporter assays, 5′ UTR constructs were either amplified by PCR, or synthesized as gBlock™ Gene fragments (Integrated DNA Technologies), and cloned into the HindIII and BamHI sites of the p2luc vector (Grentzmann et al., 1998), replacing the *Renilla* luciferase sequence in this vector and placing the *Lnx* sequence upstream of the Firefly luciferase coding sequence that lacks its own initiation AUG codon. A vector that expresses *Renilla* luciferase (pDluc-*Renilla*) was cotransfected with the p2luc-*Lnx* constructs, to control for transfection efficiency. For LNX1 protein stability studies, the coding sequences for LNX1p80 or LNX1p80 C48A were cloned into an expression vector (pCMV-N-FLAG) that drives expression of these proteins with an N-terminal FLAG epitope tag. An expression plasmid encoding HA-ubiquitin was a generous gift from Dr. J. McCarthy (University College Cork, Cork, Ireland). The sequences of primers used for reverse transcriptase PCR were as follows. For detection of *Lnx1 variant_1* and *variant_2* (Fig. 3B, left panel) the forward primers Lnx1v1-F (ATGAACCAACCGGACCTTG) and Lnx1v2-F (ATGAAGGCGCTGCTGCTTCTGG) respectively, were used in combination with the reverse primer Lnx1-R1 (CGCTCTCAAGATGGCTGTCCTG) for PCR amplification from cDNA prepared from adult mouse tissues. For detection and cloning of *Lnx1 variants_2 and 6*, the primers Lnx1v2-5UTR-F-HindIII (5′-TTTAAGCTTCCATCCCTCTCCCAGGCATTCATCAGCC-3′) and Lnx1v3-5UTR-R-BamHI (5′-TTTGGATCCTGCCATGAGGCTGGCGCAACCATC-3′) were used for PCR amplification from P3 mouse spinal cord and P8 brain cDNA, prepared as previously described (Foley and Young, 2013). For quantification of mRNAs for firefly and *Renilla* luciferase, the primers Fluc-F (5′-GACCAACGCCTTGATTGACA-3′), Fluc-R (5′-GGGCCACCTGATATCCTTTG-3′), Rluc-F (5′-CCCTGATCAAGAGCGAAGAG-3′) and Rluc-R (5′-GTCTAACCTCGCCCTTCTCC-3′) were used. For bioinformatic analysis of *Lnx* 5′ UTRs, *Lnx* sequences with well-annotated 5′ UTRs were retrieved from the GenBank database and uAUGs were counted using Lasergene software (DNAstar). Expected AUG frequencies were calculated as described by Rogozin et al. (2001).

2.4. In situ hybridization and immunohistochemistry

In situ hybridization was performed on frozen tissue sections of 20 μm thickness that were fixed post sectioning with 4% paraformaldehyde/PBS. Following acetylation and pre-hybridization, probes were added at a final concentration of 30 ng/μl in hybridization solution (50% deionized formamide, 5× SSC buffer, 5× Denhardt's solution, 250 μg/ml yeast tRNA, 500 μg/ml denatured salmon sperm DNA, and 50 μg/ml heparin) and incubated for 12–16 h at 68 °C. Post-hybridization washes were performed in 0.2% SSC buffer for a total duration of 3–4 h. Incubation with anti-DIG antibodies was performed according to the supplier's instructions. Signal of DIG-labeled riboprobes was then detected with 5-bromo-4-chloro-3-indolyl phosphate (BCIP) and 4-nitro-blue-tetracolium-chloride (NBT), as the chromogenic substrate of alkaline phosphatase. For double-in situ hybridization, sections were subsequently re-blocked, probed with peroxidase-conjugated anti-fluorescein antibodies and the signal detected using DAB ((3, 3′-diaminobenzidine); Vector Laboratories Ltd., Peterborough, UK) as substrate. For combined in situ/immunostaining, in situ detection with NBT/BCIP was performed first. For immunostaining, sections were blocked with immunostaining blocking solution (2% bovine serum albumin (BSA), 5% normal goat serum (NGS) and 0.2% Triton X-100 diluted in PBS). Antibody incubations were performed at 4 °C overnight in blocking solution lacking Triton X-100. Sections were mounted with Fluoromount mounting solution and imaged on a Leica DMI 3000 microscope. Whole mount staining of P14 diaphragm muscle from *LNX1*$^{exon3-/-}$ mice and heterozygous littermate control animals was performed in a similar manner using the LNX1-specific guinea pig anti-LNX1-PDZ3/4 antibody.

2.5. Immunoprecipitation of endogenous LNX proteins

Three P14 whole mouse brains were homogenized using a Dounce homogenizer in a volume of lysis buffer (20 mM, pH 7.5, 10 mM NaCl, 1% NP40, 0.1% sodium deoxycholate, 1 mM EDTA and 1× Complete protease inhibitors (Roche Applied Sciences)) which was 10 times the weight of the tissue. Following centrifugation at 16,000 *g* for 30 min at 4 °C immunoprecipitation was performed by addition of 10 μl guinea pig anti-LNX1/2-PDZ3/4 serum (Young et al., 2005) for 4 h and 50 μl Protein A sepharose beads (Thermo Scientific Pierce) for 2 h at 4 °C. Following 5 × 5 minute washes in lysis buffer, immunoprecipitated proteins were eluted by boiling in 2× SDS-PAGE gel loading buffer. Western blotting was performed using rabbit anti-LNX1/2-RING/NPAY antibody and enhanced chemiluminescent detection (Thermo Scientific Pierce, Rockford, IL, USA).

2.6. Cell culture and transfection

HEK293T cells (ATCC) were maintained in Dulbecco's Modified Eagle's Medium supplemented with 10% fetal bovine serum, 2 mM

L-glutamine and antibiotics, at 37 °C, 100% humidity and 5% CO_2. For dual-luciferase assays performed without RNA quantification, 8×10^4 HEK293T cells in 100 μl of growth media without antibiotics were transfected per well in a 96-well plate, using 40 ng of p2-luc luciferase reporter plasmid construct, 10 ng of pDluc-*Renilla* vector and 0.4 μl lipofectamine 2000 in 50 μl Optimem I media (Invitrogen). Transfections for dual-luciferase assays and parallel RNA isolation were performed in a 6-well dish with 1 μg of DNA (0.8 μg of p2-luc luciferase reporter plasmid constructs, 0.2 μg of pRL-SV40 *Renilla* vector) using a calcium phosphate based method (Schenborn and Goiffon, 2000). Cells were harvested 40 h after transfection and divided for dual-luciferase assays and RNA isolation. To study LNX1 levels following proteosomal inhibition 3×10^6 HEK293T cells were seeded on a 10 cm diameter plate and transfected the following day with 4 μg of DNA constructs using calcium phosphate precipitation. Media was changed 18 hour post-transfection and cells were sub-cultured onto a 6-well plate for MG132 treatment. For ubiquitination assays, and to study LNX1 stability following inhibition of translation, 7.5×10^5 HEK293T cells were seeded per well of a 6-well plate and transfected the following day with 2 μg of DNA constructs using calcium phosphate precipitation. Media was changed 20 hour post-transfection for MG132 or cycloheximide treatment.

2.7. Dual luciferase assays

Transfected cells were washed once with PBS followed by lysis in 25 μl 1× passive lysis buffer (Promega). 12.5 μl of cell extract was assayed for Firefly and *Renilla* luciferase activities using the Dual-Luciferase assay kit (Promega) and a Veritas Microplate Luminometer (Turner Biosystems) as described (Ivanov et al., 2010). The relative level of reporter gene expression was calculated as the ratio of firefly luciferase activity to co-transfected control plasmid expressing *Renilla* luciferase.

2.8. RNA isolation and real time qPCR analysis

Total RNAs were isolated using TriPure Isolation Reagent (Roche Applied Sciences). Following quantification by spectroscopy, 5.5 μg of total RNA was treated using 1 unit of DNAseI (New England Biolabs). One step quantitative reverse transcriptase PCR (qRT-PCR) reactions were carried out in a Opticon DNA Engine thermocycler (MJ Research) using 10 ng of DNAseI treated total RNA, 2× SensiFAST™SYBR No-ROX one-Step reagent (Bioline, UK), and 400 nM of each primer. The thermocycling conditions were as follows: 10 min at 45 °C (reverse transcription), 2 min at 95 °C (polymerase activation), 30 cycles of 5 s at 95 °C, 10 s at 60 °C and 5 s at 72 °C. Fluorescent signal was recorded during the 60 °C step. The baseline fluorescence was set as the mean fluorescence for cycles 3–10 and a threshold of 10 standard deviations above the mean baseline fluorescence was set to determine the cycle threshold (C_t) values. A standard curve was constructed using 4-fold serial dilutions of total RNA, (spanning 100 ng to 0.1 ng), assayed in duplicate with mean C_t values plotted versus the log [RNA]. Curve fitting was performed using KaleidaGraph software (Synergy Software). Relative values for [firefly mRNA] were divided by [*Renilla* mRNA] to control for differences in transfection efficiency. The mean of these normalized values were plotted for each construct. A minimum of three biological and three technical replicates were tested for each sample. To correct relative luciferase activity values for mRNA levels, the mean relative luciferase activity for a given sample was divided by the mean relative mRNA levels for that same sample.

2.9. Analysis of LNX1 protein stability

To assess proteasomal dependent degradation of LNX1, cells that had been transfected with FLAG epitope-tagged LNX1 constructs were treated with 10 μM MG132 for 6 h (n = 6). For this an MG132 stock solution at a concentration of 10 mM in DMSO was diluted 1 to 1000 in culture media and added to cells by changing the media. The control groups were treated with media containing an equal volume of DMSO only. To examine LNX1 turnover rates, cells were treated with cycloheximide in ethanol (100 μg/ml) at time-points up to 10 h (n = 3). A solution of 20 mg/ml cycloheximide in ethanol was diluted 1 in 200 with media prior to addition to cells. The control groups were treated with media containing an equal volume of ethanol only. Following drug treatment, cells were washed in PBS, pelleted by centrifugation, lysed in 150 μl of lysis buffer (20 mM Tris/Cl^- pH 7.5, 150 mM NaCl, 1 mM EDTA, 1% NP-40, plus protease inhibitors) on ice for 20 min and centrifuged at 4 °C for 20 min at 13,000 rpm. Protein concentrations of cleared lysates were determined using a Bicinchoninic acid (BCA) protein assay kit (Thermo Scientific Pierce). Equivalent amounts of protein lysate were analyzed by SDS gel electrophoresis and western blotting, and detected with the Odyssey Infrared Imaging System (LI-COR Biosciences). Immunoblots were quantified using Image Studio Lite software, version 2.1.

2.10. Ubiquitination assay

Twenty-four hours after transfection, cells were incubated in fresh medium containing either 10 μM MG132 (Merck Millipore) or vehicle only for 6 h. Cells were then washed twice with ice-cold PBS, and pelleted by centrifugation at 4000 rpm for 3 min at 4 °C. Pellets were resuspended in 100 μl 1% (w/v) Sodium Dodecyl Sulfate (SDS) supplemented with 15 mM *N*-ethylmaleimide (NEM) and 1× Complete protease inhibitors (Roche Applied Sciences), and boiled for 5 min. Following cooling on ice, samples were diluted with 900 μl of ice cold buffer that contained 50 mM Tris (pH 8.0), 150 mM NaCl, 1% Triton, 0.5% sodium deoxycholate, 50 mM sodium fluoride, 0.1 mM sodium orthovanadate and 1× Complete protease inhibitors (Roche Applied Science). Lysates were cleared by centrifugation at 13,000 rpm for 30 min at 4 °C. The supernatant was collected and protein concentrations were determined. Equivalent amounts (800 μg) of lysates were immunoprecipitated overnight at 4 °C, with rotation, using 0.5 μg of the indicated antibody, followed by incubation with 20 μl Protein A/G agarose beads (Thermo Scientific Pierce) for 4 h. Protein A/G agarose beads were washed three times in the dilution buffer. Proteins were eluted by boiling the Protein A/G agarose in 2× SDS PAGE sample buffer for 5 min and then analyzed by western blotting.

2.11. Statistical analysis

Microsoft Excel software was used to perform two tailed Student's *T*-tests to evaluate changes in luciferase activities for constructs lacking uORFs (Fig. 4A) and changes in LNX protein levels following proteasomal inhibition. To test the significance of changes in luciferase and mRNA levels in Fig. 4(C–E) a one-way ANOVA was performed using SPSS software (IBM). ANOVA revealed significant differences between groups in all cases. A Dunnett T3 post hoc test was chosen since the assumption of homogeneity of variances was violated. Similar results were obtained using a Games–Howell post hoc test.

3. Results

3.1. Characterization of cell-type specific expression Lnx1 and Lnx2 mRNA in the CNS

While the gross patterns of *Lnx1* and *Lnx2* mRNA expression in the mammalian brain were previously described, the issue of which CNS cell types express *Lnx* mRNAs has not been examined in detail (Rice et al., 2001). To address this important question, we employed in situ hybridization for *Lnx* mRNAs in combination with either immunohistochemistry, or in situ hybridization for cell-type specific markers. We focused initially on the postnatal spinal cord, which had not been examined by Rice et al. (2001). In the postnatal day 17 (P17) spinal cord,

antisense riboprobes specifically detected *Lnx1* and *Lnx2* throughout the gray matter, with little signal in the white matter (Fig. 2A, B). *Lnx1* in situ signal was not present in GFAP positive ($GFAP^+$) astrocytes, in Plp^+ or in $OLIG2^+$ oligodendrocytes, but was co-localized with $NeuN^+$ neurons (Fig. 2D–F). *Lnx2* expression patterns in the spinal cord were essentially the same as for *Lnx1*, with mRNA for both genes found exclusively in neurons throughout the gray matter, including large motor neurons in ventral regions (Fig. 2G–H).

To examine cell-type specific expression of *Lnx* genes in the brain, we focused on the cerebellum, which has the most prominent *Lnx1*,

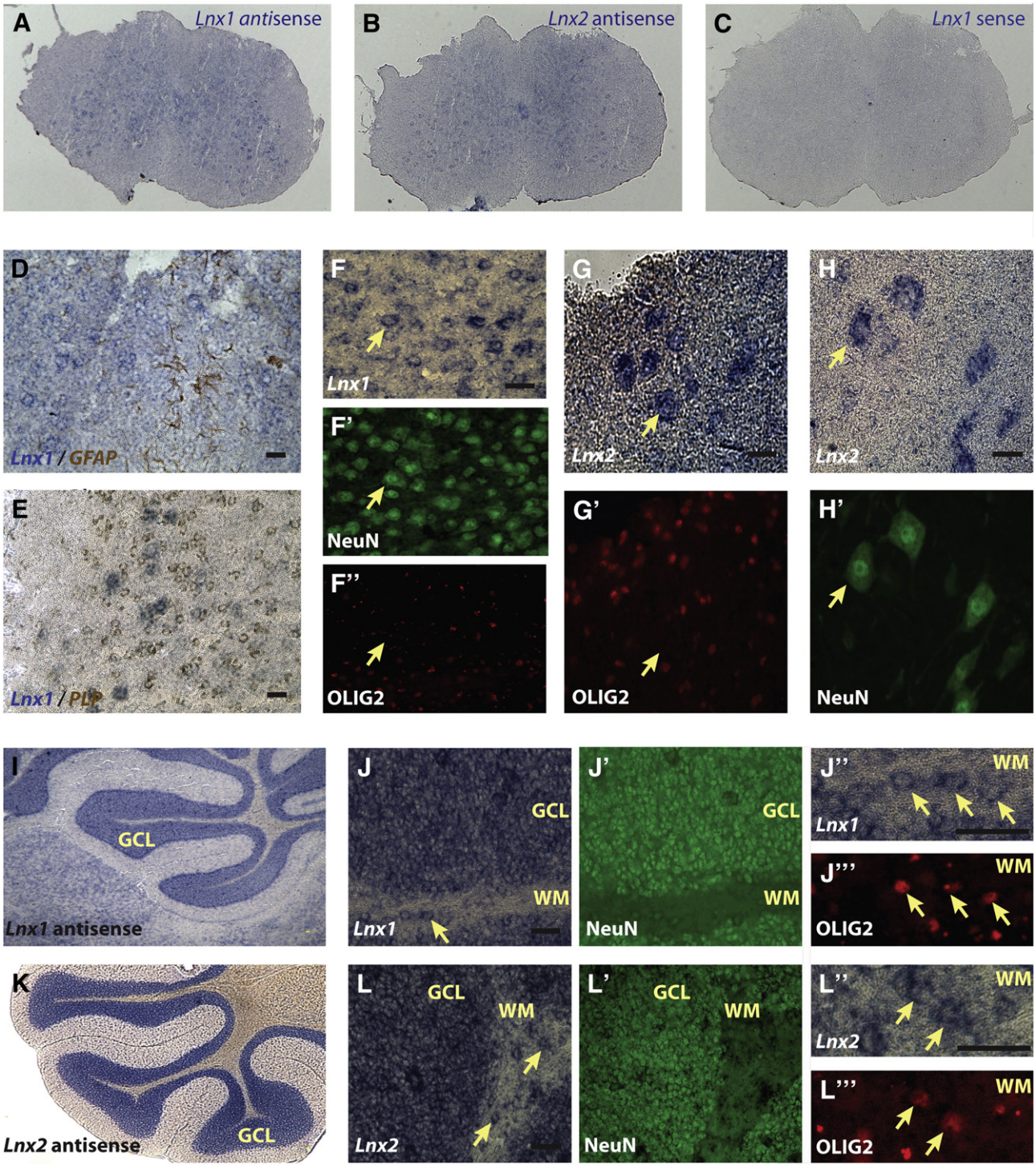

Fig. 2. Expression of *Lnx1* and *Lnx2* mRNAs in the postnatal murine spinal cord and cerebellum. (A–C) Low magnification views of *Lnx1* (A) and *Lnx2* (B) mRNA (in blue) in the spinal cord cross sections detected with antisense riboprobes in comparison to a section probed with a sense *Lnx1* riboprobe as a control (C). (D–H) Double and triple labeling of spinal cord sections for *Lnx1* (D–F) or *Lnx2* (G,H) mRNA in blue, with the indicated markers for the following cell-types: $GFAP^+$ astrocytes (stained brown in D); Plp^+ myelinating oligodendrocytes (stained brown in E); $NeuN^+$ neurons (stained green in F′ and H′); $OLIG2^+$ oligodendrocytes (stained red in F″ and G′). *Lnx1* and *Lnx2* expression is observed in $NeuN^+$ neurons (arrows) but not in other cell types. (I–L) *Lnx1* and *Lnx2* mRNA expression in the cerebellum. Low magnification view of prominent *Lnx1* and *Lnx2* mRNA expression in the granule cell layer (GCL) of the cerebellum (I, K). Labeling for cell-type markers confirms that *Lnx1* and *Lnx2* are predominantly expressed in $NeuN^+$ granule cells in the GCL (J, J′ and L, L′), but some expression is also evident in cells within the white matter (WM) (arrows in J and L). A higher magnification view of these white matter cells and co-labeling for OLIG2, indicates that they are $OLIG2^+$ oligodendrocytes (J″, J‴ and L″, L‴). Scale bars = 50 μm.

and especially *Lnx2*, expression as previously reported (Rice et al., 2001). We observed complete co-localization of *Lnx1* and *Lnx2* in situ signal with NeuN$^+$ neurons in the granule cell layer of the P17 murine cerebellum (Fig. 2I–L). Some *Lnx1*- and *Lnx2*-expressing cells were observed in the cerebellar white matter (arrows in Fig. 2J, L), and at least some of these were OLIG2$^+$ oligodendrocytes (Fig. 2J″, J‴ and L″, L‴). Overall though, expression of *Lnx1* and *Lnx2* in the cerebellum, and other brain regions (not shown), is overwhelmingly found in neurons, with *Lnx* mRNA detected in only a very small proportion of oligodendrocytes.

3.2. Examination of LNX protein expression in the nervous system

Despite clear mRNA expression, endogenous LNX2 protein has not been detected in the nervous system and LNX1 protein has only been detected following immunoprecipitation from brain lysates (Weiss et al., 2007). Using antibodies that recognize both LNX1 and LNX2, we detect 3 LNX bands by western blotting following immunoprecipitation from brain lysates (Fig. 3A). None of these bands are directly detected in brain lysates, in agreement with the notion of endogenous LNX proteins being present at very low levels. To examine the identity of these bands, we took advantage of the availability of a mouse line in which *Lnx1* exon 3 has been deleted (Tang et al., 2010). We refer to these mice as *Lnx1*$^{exon3-/-}$. Exon 3 is the first exon of *Lnx1_variant 2* mRNA (Fig. 1B), that gives rise to the p70 LNX1 protein, and so these mice should lack this isoform. However, the absence of LNX protein in these mice was never confirmed, and no obvious phenotype was reported for this line (https://www.mmrrc.org/). The middle and lower bands, observed by western blotting, are absent in immunoprecipitates from *Lnx1*$^{exon3-/-}$ brains (Fig. 3A, left panel), confirming that they both correspond to LNX1 isoforms, probably arising from transcripts that contain exon 3. The middle band corresponds to the size of the brain-specific LNX1p70 isoform, while the identity of the lower band, at approx 60 kDa, is unclear. The top band, migrates at approximately the molecular weight of LNX2 (75 kDa), and is absent in immunoprecipitates from *Lnx2*$^{-/-}$ mice, identifying it as corresponding to LNX2 protein (Fig. 3A, right panel).

The lower molecular weight LNX1 protein identified above may represent a novel LNX1 isoform arising from alternative splicing of a transcript that contains exon 3. The GenBank sequence database lists three *Lnx1* transcript variants, in addition to *Lnx1 variants 1* and *2* that generate the well-characterized p80 and p70 protein isoforms respectively. *Lnx1_variant 3* contains exon 3 and two additional exons (exons 4 and 5) that are not present in *variants 1* and *2* (Fig. 1B). This transcript is predicted to produce a protein of 62 kDa, though there has been no experimental evidence for the existence of this protein isoform to date. We expressed the predicted LNX1p62 isoform in HEK293 cells. This protein migrates at the same molecular weight as the lower band that we observed in anti-LNX immunoprecipitates from brain tissue (Fig. 3A, middle panel), strongly suggesting that this band corresponds to LNX1p62.

We next wanted to examine which *Lnx1 mRNA* transcripts are expressed in the CNS and identify transcripts that could give rise to the novel LNX1p62 protein. We first performed rtPCR using primers designed to detect the well-characterized transcript *variants_1* and *2* (Fig. 3B, left panel). In line with previous reports (Dho et al., 1998), *Lnx1 variant_1* was readily detected in non-neuronal tissues (liver and muscle) but was not detected in the spinal cord and only just detectable in the brain, whereas *Lnx1 variant_2* expression was specific to the CNS tissues. To examine if *Lnx1 variant_3*, or other exon 3-containing variants distinct from *variant_2*, are expressed in the brain, we performed rtPCR using a primer at the 5′ end of exon 3 in combination with a primer within exon 6. The major product obtained corresponds to *Lnx1_variant 2*. No product of the size expected for *Lnx1_variant 3* was obtained, but instead, a minor product of much smaller size was present (Fig. 3B, right panel). Sequencing identified this as a novel transcript variant, in which splicing occurs between an internal site within exon 3 and exon 6 (Fig. 1B). This transcript, which we call *Lnx1_variant 6*, is predicted to give rise to the same 62 kDa protein product as *Lnx1_variant 3*, but has a much shorter 5′ UTR. Thus, this novel *Lnx1_variant 6* mRNA could give rise to the lower band detected by western blotting in the region of 60 kDa. While *Lnx1_variant 6* seems to be much less abundant than *Lnx1_variant 2* in the brain, our PCR results suggest that its expression, relative to *Lnx1_variant 2*, is somewhat higher in the spinal cord (Fig. 3B, right panel). These observations provide evidence at both the mRNA and protein levels for a novel LNX1 p62 isoform in the CNS.

We have previously reported LNX1 protein expression in the perisynaptic glial cells at the NMJ by immunofluorescent staining using several anti-LNX1 antibodies (Young et al., 2005). However, we had not established the identity of the LNX1 isoform expressed in these cells (Young et al., 2005). Immunofluorescence staining of NMJs, from *Lnx1*$^{exon3-/-}$ mice, shows that the LNX1 staining is still present (Fig. 3C,D). This indicates that it is, in fact, the p80 isoform, rather than the p70 isoform, of LNX1 that is expressed in perisynaptic glial cells at the NMJ. We also performed immunohistochemistry with anti-LNX antibodies on brain sections, but this did not reveal any specific staining pattern, indicating perhaps that the low levels of LNX proteins in the brain cannot be detected by immunostaining. Overall, these observations suggest that LNX1 and LNX2 proteins are both expressed in the brain, albeit at low levels. In addition, the absence of LNX1 and LNX2 protein expression in the brains of *Lnx1*$^{exon3-/-}$ and *Lnx2*$^{-/-}$ mice validates them as models to study the function of LNX proteins in the central nervous system.

3.3. uORFs attenuate translation of LNX1p70 but not LNX1p80 or LNX2

The miniscule levels of endogenous LNX proteins that we detect, despite relatively widespread expression of *Lnx* mRNA (Rice et al., 2001), suggest that LNX protein synthesis is tightly regulated. The presence of uORFs in the 5′-UTR of genes has been shown to be a common mechanism to inhibit translation of the main coding sequence (Calvo et al., 2009). To see whether this mechanism might regulate LNX protein expression, we examined the 5′-UTRs of *Lnx1p80*, *Lnx1p70* and *Lnx2* transcripts from ten diverse vertebrate species (Table 1). We found at least one upstream initiation codon (uAUG) in virtually every transcript examined for both *Lnx1* and *Lnx2*, suggesting that uORFs could play an evolutionarily conserved role in regulating translation of LNX proteins.

To test this hypothesis, we employed dual luciferase reporter assays. *Lnx* 5′-UTRs, and the first two codons of the murine *Lnx* coding sequences, were cloned upstream and in frame with a firefly luciferase coding sequence that lacked its own initiation AUG codon. Reporter constructs containing wild type 5′-UTRs, as well as 5′-UTRs in which the uAUGs had been mutated to AAA, were prepared and co-transfected into HEK293T cells, along with a vector encoding *Renilla* luciferase that acted as a control for transfection efficiency. Normalized firefly/*Renilla* luciferase activity was measured to assess protein production. For *Lnx2*, the wild type 5′ UTR construct exhibited relatively high luciferase activity, and mutation of the single uAUG had no effect (Fig. 4A). Surprisingly, for *Lnx1_ variant 1*, mutation of two uAUGs to AAA decreased protein production. By contrast, the wild type *Lnx1_variant 2 5′ UTR* construct, which contains 5 uAUGs, exhibited relatively low luciferase activity, that was increased approximately 2-fold when these uAUGs were mutated to AAA (Fig. 4A). This indicates that the presence of uORFs may negatively regulate the efficiency of correct translation initiation for *Lnx1_variant 2*, but not for *Lnx1_variant 1* or *Lnx2*.

3.4. Additional 5′ UTR elements regulate LNX1 p70 protein expression

The relative luciferase activity observed for the wild-type *Lnx1_variant 2* 5′ UTR was very low compared to *Lnx1_variant 1* and *Lnx2* (12 and 36-fold less respectively). Even after mutation of all five uAUGs, the 5′ UTR of *Lnx1_variant 2* does not support protein expression levels comparable to the other 5′ UTRs (Fig. 4A). This suggested to us that there might be other inhibitory elements in the 5′ UTR of the *Lnx1_variant 2* mRNA. We

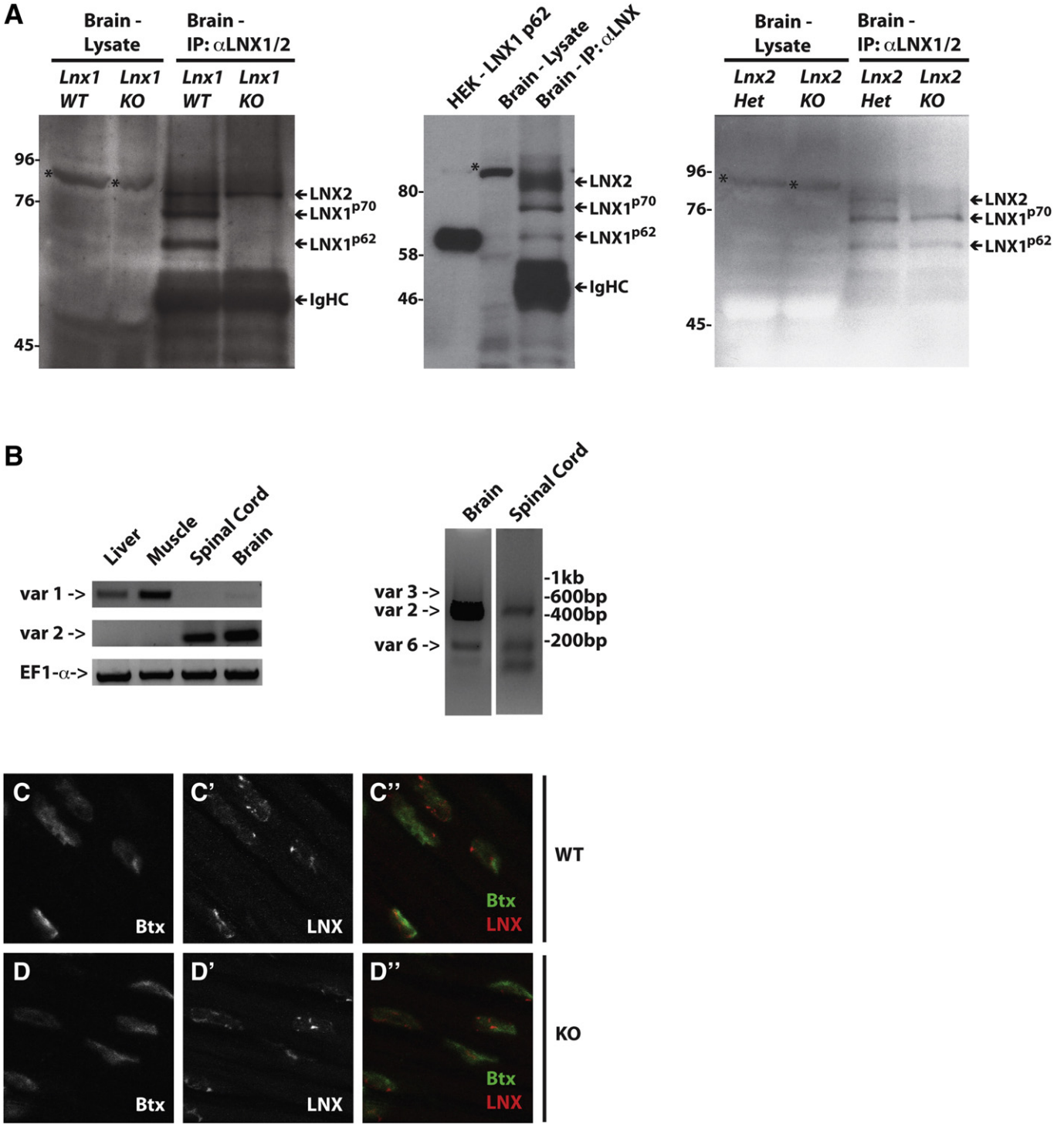

Fig. 3. LNX protein and mRNA expression in the nervous system examined using LNX1$^{exon3-/-}$ mice. (A) LNX protein expression in the brain was examined by western blotting of lysates and immunoprecipitates (IP) from P17 mouse brain. Immunoprecipitation and immunoblotting were performed with guinea pig anti-LNX1/2-PDZ3/4 and rabbit anti-LNX1/2-RING/NPAY antibodies respectively, that recognize both LNX1 and LNX2. Left panel shows immunoprecipitations from LNX1$^{+/+}$ (WT) and LNX1$^{exon3-/-}$ (KO) tissues. Middle panel shows immunoprecipitates from wild-type mice run side-by-side with lysate from HEK cells overexpressing LNX1p62 (left lane). Right panel shows immunoprecipitations from LNX2$^{+/-}$ (Het) and LNX2$^{-/-}$ (KO) mice. * = non-specific band detected in brain lysates, IgHC = immunoglobulin heavy chains from the antibody used for immunoprecipitation. (B) Reverse transcriptase PCR of *Lnx1* mRNA transcripts expressed in neuronal and non-neuronal tissues analyzed by gel electrophoresis. In the left panel, primers designed to detect *Lnx1_variants 1* and *2* were employed (indicated by gray arrowheads in Fig. 1A). In the right panel, primers designed to detect any exon 3-containing transcripts were used (indicated by black arrowheads in Fig. 1A). Expected positions of products corresponding to *Lnx1_variants 2*, *3* and *6* are indicated on the left. (C and D) Immunofluorescent staining of neuromuscular junctions in P14 diaphragm muscle from wild type (C–C″) and LNX1$^{exon3-/-}$ (D–D″) mice. LNX1 protein is detected in perisynaptic Schwann cells using an anti-LNX1 specific antibody that does not recognize LNX2 (C′,D′). α-Bungarotoxin (Btx) was used to stain acetylcholine receptors at the neuromuscular junctions (C,D). Merged images are shown in panels C″ and D″ with α-bungarotoxin in green and anti-LNX staining in red.

generated a number of 5′ and 3′ deletion constructs to explore this possibility (Fig. 4B). Luciferase activity for a construct containing nucleotides 1–192 was similar to the wild type 273 nucleotide 5′ UTR (Fig. 4C). Mutation of the four uAUGs in this truncation construct increased luciferase activity approximately 5-fold. However, a construct containing nucleotides 187–273, or this construct with its one uAUG mutated to AAA,

Table 1
Analysis of uAUG codons in *Lnx1* and *Lnx2* 5′ UTRs. 5′ UTR length and number of uAUG codons are presented for a diverse selection of vertebrate Lnx transcripts. n/a = sequence not available or 5′ UTR not annotated. Bt = *Bos taurus* (cattle); Dr = *Danio rerio* (zebrafish); Gg = *Gallus gallus* (chicken); Hs = *Homo sapiens* (human); Mm = *Mus musculus* (house mouse); Ol = *Oryzias latipes* (Japanese medaka) Oo = *Orcinus orca* (killer whale); Or = *Odobenus rosmarus divergens* (Pacific walrus); Rn = *Rattus norvegicus* (Norway rat); Xt = *Xenopus tropicalis* (western clawed frog); Fa = *Ficedula albicollis* (collared flycatcher); Cc = *Condylura cristata* (star-nosed mole).

Species	Lnx1_variant 1		Lnx1_variant 2		Lnx2	
	Length (ntd)	# uAUG	Length (ntd)	# uAUG	Length (ntd)	# uAUG
Bt	228	1	225	3	281	1
Dr	359	3	n/a	n/a	243	5
Gg	111	1	376	5	255	4
Hs	285	4	304	1	309	1
Mm	197	2	273	5	213	1
Ol	n/a	n/a	483	4	n/a	n/a
Oo	268	2	246	4	n/a	n/a
Or	263	3	306	2	317	1
Rn	190	2	201	3	197	1
Xt	195	2	315	7	116	1
Fa	74	0	138	1	162	5
Cc	n/a	n/a	n/a	n/a	105	1
Average	217	2	287	3.5	220	2.1
uAUG frequency/1000 ntd						
Observed:		9.2		12.2		9.6
Expected:		13.9		14.7		13.7

exhibited 23-fold and 30-fold increased activities respectively, compared to the wild type 5′ UTR. Luciferase activity for a construct containing nucleotides 1–80, with a single uAUG, was 8-fold higher than the wild type. To rule out the possibility that these observations were just a consequence of shorter 5′ UTR length of the truncated constructs, we randomized the *Lnx1_variant 2* 5′ UTR sequence to generate a construct of the same length, and similar nucleotide composition as the wild-type 5′ UTR (but lacking uAUGs). Luciferase activity for this construct was 22-fold higher than the wild-type 5′ UTR and 8-fold higher than the full length UTR lacking uAUGs (Fig. 4C). Taken together, these observations indicate the presence of a sequence-specific element in the region between nucleotides 80 and 192 of the *Lnx1_variant 2* 5′ UTR, that has a significant negative impact on protein expression, additional to the effect of uAUGs.

To examine the mechanism by which this element suppresses protein production, we measured relative luciferase mRNA levels for the various constructs (Fig. 4D). We observed a very consistent 3–4 fold increase in mRNA levels for constructs that lack the nucleotide 80–192 region of the 5′ UTR. This strongly suggests that this region either inhibits mRNA transcription, or increases mRNA degradation. To ask whether these effects on mRNA expression account for the large differences in luciferase activity that we observed, we normalized the luciferase activities for mRNA levels (Fig. 4E). Even correcting for mRNA levels, luciferase activity for the nucleotide 187–273 construct, lacking uAUGs, is significantly higher than the wild type 5′ UTR, or the 5′ UTR lacking uAUGs. The corrected activity for the nucleotides 1–80 and randomized constructs is also higher, though it does not reach statistical significance. This indicates that, in addition to decreasing mRNA levels, the nucleotide 80–192 region of the *Lnx1_variant 2* 5′ UTR inhibits protein translation, by some mechanism other than through the presence of uORFs. Interestingly, the novel splicing of *Lnx1_variant 6* that we describe in Section 3.2 above, skips this inhibitory region and joins nucleotides 1–63 of exon 3 directly to exon 6. Thus, a reporter construct containing the 5′ UTR of *Lnx1_variant 6* exhibits higher luciferase activity than *Lnx1_variant 2* (Fig. 4B, C). This difference can be accounted for by higher mRNA levels, that are similar to other constructs lacking the inhibitory region of exon 3 (Fig. 4D). *Lnx1_variant 6* contains 4 uAUGs that may modulate translational efficiency, though we have not examined their effect. Overall, these findings demonstrate that the expression of the CNS-specific LNX1 protein isoforms is tightly regulated, both at the level of mRNA transcription/stability, and translation by elements within the 5′ UTR. This regulation is likely to contribute significantly to the low levels of LNX1 protein that are observed in the CNS *in vivo*.

3.5. Proteasomal degradation and turnover of LNX1p80 protein

The *Lnx1_variant 1* mRNA, that codes for the RING finger domain-containing p80 protein isoform, is expressed widely in non-neuronal tissues (Dho et al., 1998; Rice et al., 2001), but endogenous LNX1 p80 protein is not readily detected, except in perisynaptic Schwann cells. One possible explanation for the low levels of LNX proteins *in vivo* is that the protein is intrinsically unstable, or is turned over at a high rate. The stability of several ubiquitin ligases is known to be regulated by ubiquitination and proteasomal degradation (de Bie and Ciechanover, 2011). To examine whether LNX1 is regulated in this manner, we examined levels of exogenously-expressed LNX1p80 in cultured cells following a 6 hour treatment with the proteasomal inhibitor MG-132 (Fig. 5A, B). Wild type LNX1p80 levels were increased by close to 100% under these conditions. Proteasomal targeting of LNX1p80 could occur through either auto-ubiquitination, or ubiquitination mediated by a distinct E3 ubiquitin ligase (de Bie and Ciechanover, 2011). We found that a mutant LNX1 protein, lacking ubiquitin ligase activity (LNX1p80-C48A (Nie et al., 2002)), was stabilized to a similar extent following proteasomal inhibition as wild type LNX1, indicating that proteasomal degradation of LNX1 is probably not a consequence of auto-ubiquitination. To directly demonstrate ubiquitination of LNX1p80, we co-expressed LNX1p80 constructs with HA epitope-tagged ubiquitin and immunoprecipitated ubiquitinated proteins from cell lysates that had been boiled in the presence of SDS to disrupt protein–protein interactions. Ubiquitinated LNX1p80 and LNX1p80-C48A are both detected and accumulate in the presence of proteasomal inhibitor (Fig. 5C). To examine the turnover rate of LNX1, we performed a "cycloheximide chase" experiment in which we monitored levels of transfected FLAG epitope-tagged LNX1p80 in HEK293 cells following inhibition of protein synthesis (Fig. 5D). A clear decline in LNX1p80 levels was seen at 8 and 10 hour post-cycloheximide treatment (100 μg/ml). This observation indicates that LNX1p80 is turned over at an appreciable rate in cells, although deterioration of the health of the cycloheximide-treated cells prevented us from extending this time-course beyond 10 h.

4. Discussion

A detailed understanding of the cell-type specific expression of *Lnx* mRNA, and more importantly LNX proteins, is a prerequisite to elucidating their physiological functions and the *in vivo* significance of their interactions with Numb and other proteins. We have previously reported the first *in vivo* localization of LNX1 protein in perisynaptic glial cells, at neuromuscular synapses (Young et al., 2005). Here we show that immunostaining for LNX1 at the NMJ persists in $Lnx1^{exon3-/-}$ knockout mice, and thus, it is likely to be Lnx1 variant_1 (coding for LNX1p80 protein) that is expressed in perisynaptic glial cells of the PNS. In the CNS, in situ hybridization showed widespread expression of both *Lnx1* and *Lnx2* (Rice et al., 2001), while a microarray analysis reported enhanced expression of *Lnx1* in oligodendrocyte precursor cells (OPCs), compared to other neural cell types (Cahoy et al., 2008). In the present study we have examined the cell type-specific expression of *Lnx* mRNAs in detail by in situ hybridization and find that *Lnx1* and *Lnx2* mRNAs are predominantly expressed in neurons, rather than astrocytes or oligodendrocytes, in both the spinal cord and cerebellum. We saw *Lnx* expression in only a small proportion of oligodendrocytes in the white matter of the cerebellum and we did not see prominent expression of *Lnx1* in cells of the spinal cord that are positive for NG2 — an OPC marker (data not shown). Thus in contrast to the PNS, the expression of *Lnx* genes in the CNS is mainly neuronal. This suggests that interactions of LNX proteins with neuronal proteins, such as the presynaptic component Erc2/CAST (Higa et al., 2007), may be physiologically relevant.

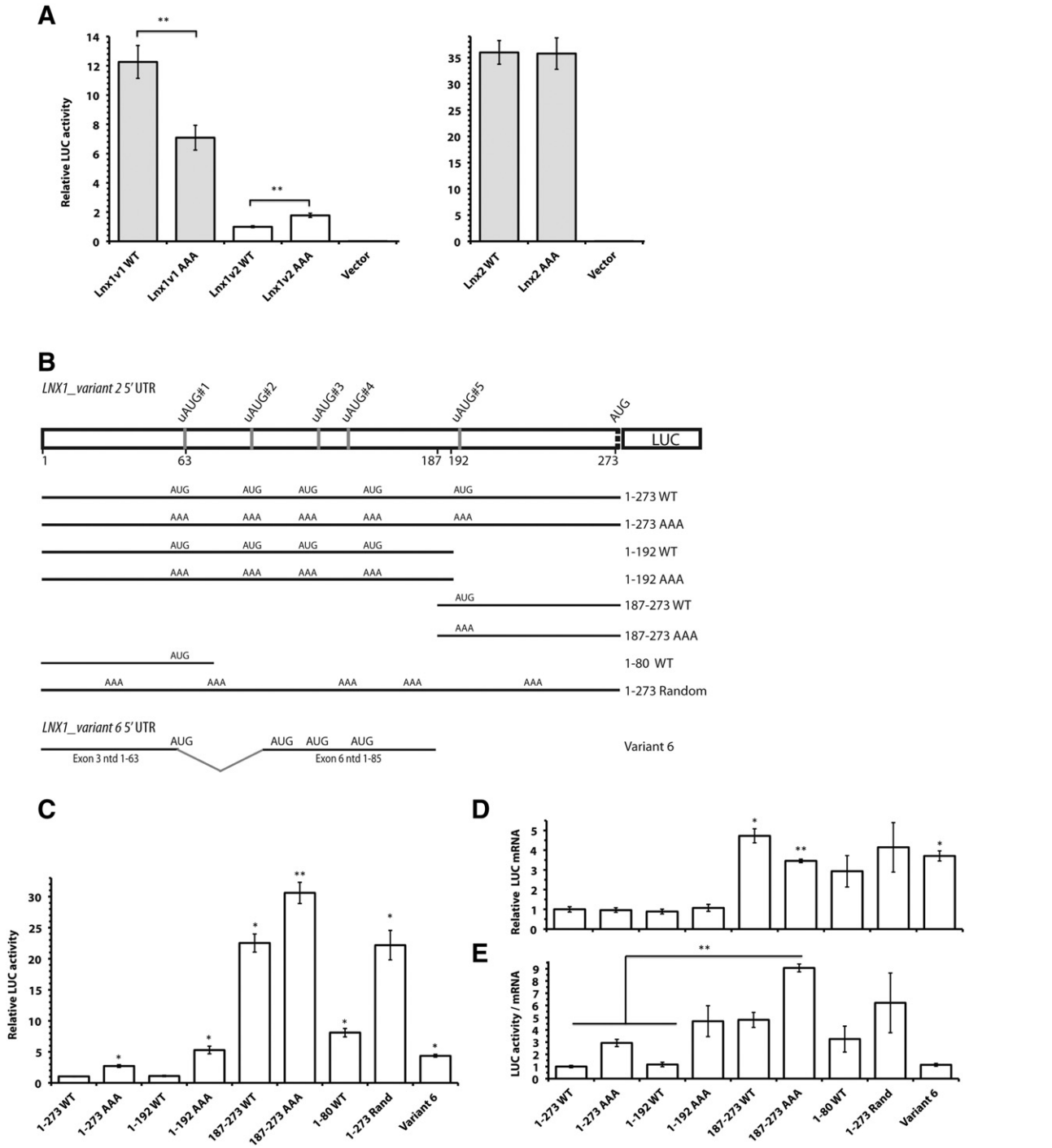

Fig. 4. Expression and translation of *Lnx1_variant 2* mRNA are controlled by uORFs and other regulatory elements in the 5′ UTR. (A) The effects of uORFs on translation of *Lnx* mRNAs were assessed using a dual luciferase reporter assay. Relative luciferase activity for either wild type (WT) 5′ UTRs or 5′ UTR constructs in which all uAUGs have been mutated to AAA (AAA) is plotted for *Lnx1_variant 1* (*Lnx1v1*; light gray bars), *LNX1_variant 2* (*Lnx1v2*; white bars) and *Lnx2*. Data for *Lnx1* and *Lnx2* are from the same experiment that can be directly compared, but are shown with different y-axis scales for clarity. **P < 0.01 Student's *T*-test, Error bars represent S.E.M. N = 5. (B) Schematic representation of luciferase reporter constructs used in C–E below. The *Lnx1*_variant 2 5′ UTR consists of 273 nucleotides and contains five uAUGs as shown on top. Truncated constructs and those with uAUGs mutated to AAA are depicted below. In the construct designated 1–273 Random, the wild type 5′ UTR sequence has been randomized and any AUG codons changed to AAA. The 5′ UTR of *Lnx1_variant 6* containing part of exon 3 spliced into exon 6 is depicted at the bottom and contains four uAUGs. (C–E) Relative luciferase activity (C), mRNA levels (D) and luciferase activity corrected for mRNA levels (E) are shown for the constructs described in (B) above. In all graphs the values for the 1–273 WT is arbitrarily set to one for ease of comparison of fold changes in luciferase or mRNA levels. In (C) and (D) statistical significance of differences in luciferase activity or mRNA levels relative to the 1–273 WT construct as determined using the Dunnett T3 posthoc test are indicated; *P < 0.05, **P < 0.01. In (E) statistically significant differences are similarly indicated. Error bars represent S.E.M. N = 4 for (C) and N = 3 for (D) and (E).

The lack of any overt phenotype in Lnx1$^{exon3-/-}$ or Lnx2$^{-/-}$ mice hints at functional compensation, in agreement with the observation that both genes are co-expressed in overlapping populations of neurons.

A surprising observation, when we immunoprecipitated LNX proteins from brain lysates, was the detection of two LNX1 bands by western blotting, both of which were absent from immunoprecipitates from the brains of LNX1$^{exon3-/-}$ mice (Fig. 3A). The upper band corresponds to LNX1p70 while the lower band migrates with a molecular weight of approximately 60 kDa. The *Lnx1_variant 3* mRNA transcript, annotated in sequence databases, is predicted to produce a protein of

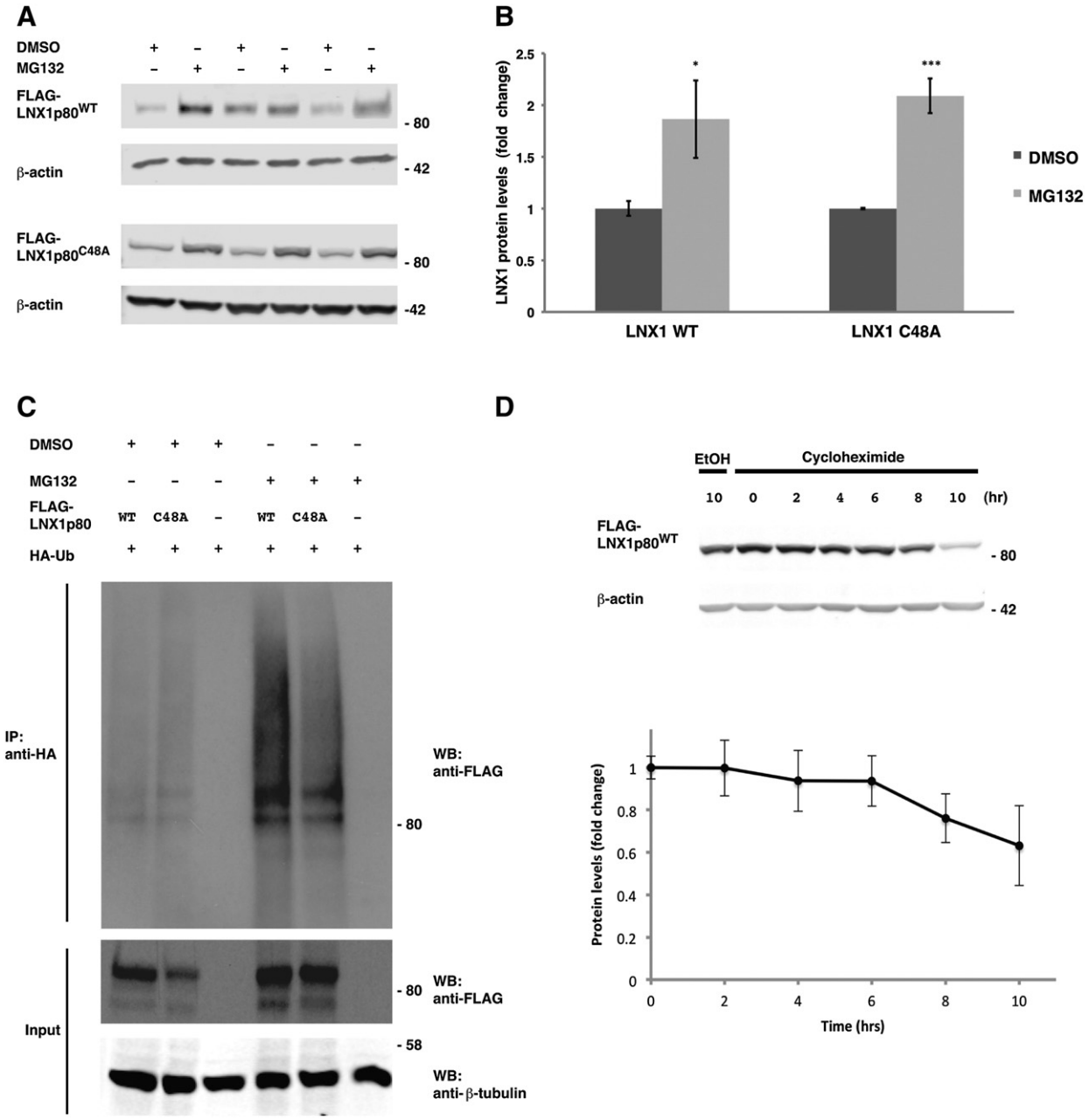

Fig. 5. Stability and turnover of LNX1 protein. (A, B) Proteasomal inhibition increases LNX1 protein levels. HEK293T cells were transfected with FLAG-tagged LNX1p80 or a mutant (LNX1 p80^{C48A}) lacking ubiquitin ligase activity and treated for 6 h with either 10 μM of the proteasomal inhibitor MG132 or vehicle only (DMSO). LNX1 protein was detected by immunoblotting using an anti-FLAG antibody (A). LNX1 protein levels were quantified and normalized against β-actin levels (B). (n = 6, *P < 0.05, ***P < 0.001 Student's *T*-test). (C) Ubiquitination of LNX1p80 and LNX1p80^{C48A} assessed by immunoprecipitation (IP) following co-expression with HA-tagged ubiquitin (HA-Ub). The indicated constructs were expressed in HEK293T cells, that were treated with either the proteasomal inhibitor MG132 or vehicle only (DMSO) for 6 h. Ubiquitinated proteins were immunoprecipitated from cell lysates (Input) using an anti-HA antibody. A high molecular weight smear corresponding to ubiquitinated LNX1 is detected by western blot (WB) for both the wild type and mutant proteins and accumulates in the presence of MG132. (D) LNX1 protein levels decrease following inhibition of protein synthesis. HEK293T cells transfected with LNX1p80 were treated with 100 μg/ml cycloheximide or vehicle only (EtOH) and harvested at the indicated time point post-treatment. LNX1 protein levels were detected as described above, quantified and plotted versus time after treatment (n = 3). Error bars represent S.E.M.

62 kDa. This transcript has two additional exons, exons 4 and 5, compared to *Lnx_variant 2*, generating an 820 nucleotide 5′ UTR, with 13 uORFs prior to the predicted start codon. We have also detected a novel transcript, *Lnx1_variant 6*, in both the brain and spinal cord, that is predicted to produce the same 62 kDa product as *Lnx1_variant 3*, but has a 150 bp 5′ UTR with 4 uORFs. Reverse transcriptase PCR, with flanking primers that should amplify all three transcripts, only yields a product for transcript *variants 2* and *6*, but not *3*. *Lnx1_variant 3*-specific primers, located in exons 4 and 5, do amplify a product from brain cDNA (data not shown), suggesting that this variant is expressed in the brain. However, it would not appear to be very abundant, and given the presence of so many (13) uORFs in this transcript, it seems more likely that the novel *Lnx1_variant 6* transcript may give rise to the 62 kDa protein detected by western blotting.

As reported previously (Weiss et al., 2007), we find that LNX1 can only be detected in brain tissue following immunoprecipitation. Here, using the same approach, we demonstrate LNX2 protein expression in the brain for the first time. Detection of either protein required immunoprecipitation from a large volume of brain lysate. The presence of LNX protein at very low levels *in vivo*, despite the mRNA for these

genes being readily detectable, suggests that protein expression is tightly regulated post-transcriptionally. One mechanism that has emerged for translational regulation is the presence of uORFs in the 5′-UTR of gene transcripts, which divert the translation machinery away from translation of the main coding sequence (Wethmar et al., 2010). The degree to which uORFs affect translation of the main coding sequence is variable, and factors that seem to contribute to this include the context (Kozak sequence) of the uAUG codon, the presence of multiple uORFs, and distance of the uORF from the 5′ cap of the transcript. Overlap between the uORF and main coding sequence, proximity of the uORF to the main coding sequence and uORF length may also be important factors in some cases (Calvo et al., 2009; Wethmar et al., 2010).

Examining sequences from diverse species, *Lnx* 5′ UTRs are longer than average (Table 1). In addition, uAUGs are found virtually in every *Lnx* sequence examined and uAUG frequency is higher than values previously reported for large gene sets (Calvo et al., 2009; Rogozin et al., 2001). This is noteworthy given that over half of all genes lack uAUGs in most vertebrate species. The above points are especially true of *Lnx1_variant 2* mRNAs, which have longer 5′ UTRs and more uAUGs than *LNX1_variant 1* or *LNX2* transcripts. Generally, uAUGs in 5′ UTRs occur at significantly lower frequency than would be expected by chance (Rogozin et al., 2001), but for *Lnx1_variant 2* the uAUG frequency is closer to that expected by chance, based on 5′ UTR nucleotide composition (Table 1). Thus the bioinformatic evidence points toward an evolutionarily conserved regulatory role for uORFs in *Lnx* transcripts, particularly *Lnx1_variant 2*. In agreement with this, our luciferase reporter assays indicate that the presence of uORFs in *Lnx1_variant 2* serves to negatively regulate translation. Thus luciferase activity is 2–3 fold higher, when the five uAUGs in the LNX1p70 encoding *Lnx1_variant 2* 5′ UTR are mutated to AAA. These uAUGs are not very close to the AUG of the LNX1p70 coding sequence and the predicted uORFs do not overlap the main ORF. The 1st uORF, at 25 codons, is significantly longer than the others, a factor that is thought to prevent ribosome reinitiation (Kozak, 2001). In addition, the 1st uAUG has a strong Kozak consensus sequence, suggesting that the 1st uORF may contribute significantly to the observed inhibition of translation, but this needs to be tested experimentally. The presence of a uORF in the *Lnx2* 5′ UTR doesn't appear to affect translation. Strangely, mutation of two uAUGs in the *Lnx1_variant 1* 5′ UTR seemed to decrease protein production somewhat, a result that we are at a loss to explain, at present.

In addition to identifying a role for uORFs in suppressing translation of *Lnx1_variant 2*, we also found evidence for an element within the 5′ UTR of *Lnx1_variant 2* that decreases mRNA levels and also seems to suppress translation by a mechanism independent of uORFs. At present, we do not know the underlying mechanisms of these effects, but it is clear that expression of LNX1p70 protein is tightly regulated by sequences present in the 5′ UTR of the *Lnx1_variant 2 mRNA*. Our assays did not reveal such inhibitory effects for the 5′ UTR of *Lnx1_variant 1* or *Lnx2*, suggesting that other mechanisms operating at the level of protein translation may contribute to the low endogenous levels of these proteins. Possible regulatory mechanisms could include microRNAs, or natural antisense transcripts that may cause repression of translation.

Another explanation for low levels of LNX1 p80 and LNX2 protein could be that LNX proteins have a short half-life. Proteasomal degradation is a likely pathway for LNX1p80 and LNX2 turnover, since they contain a RING domain that, at least for LNX1, has been shown to have ubiquitin ligase activity. We find that LNX1p80 levels double in 6 h following proteasomal inhibition, suggesting that there is significant, ongoing, proteasomal degradation of LNX1. However, similar results for a mutant LNX1, that lacks ubiquitin ligase activity, implicate ubiquitination by another E3 enzyme, rather than LNX auto-ubiquitination in this process. One caveat to this observation is that proteasomal degradation of transiently transfected LNX in these experiments may be elevated, compared to that of endogenous protein. A decline in LNX1p80 levels within 8 h following cycloheximide treatment also indicates that LNX1p80 is turned over at an appreciable rate. Protein turnover, mediated at least in part by proteasomal degradation, may thus contribute to the very low levels of endogenous LNX1 proteins that are observed *in vivo*.

The low expression levels of LNX1 and LNX2 proteins, and the identification of mechanisms that negatively regulate LNX1p70 protein expression, have implications for understanding LNX protein function. It may be that LNX proteins have a very general function in the many tissues for which *Lnx* mRNA expression has been reported, but that they are only required at extremely low levels, and that excess LNX protein expression may be deleterious. Alternatively, synthesis of LNX proteins may simply be suppressed and be non-essential under most circumstances, in order to allow them to play a very specific role in certain cell types or scenarios, when inhibition of LNX protein production is relieved. One may speculate that some such mechanism may exist to overcome the effects of uORFs, or other inhibitory elements in cells that exhibit significant levels of LNX proteins, such as perisynaptic Schwann cells (LNX1p80) and spermatozoa (LNX1 and LNX2). Notably, amplification of the *Lnx1* and *Lnx2* genes has been reported in gliomas and colorectal cancer respectively. Any transcriptional or post-transcriptional inhibition of protein synthesis would also have to be overcome if amplification of *Lnx* genes is to result in LNX protein overexpression in these cancers. Overall, the identification of mechanisms that regulate LNX protein expression is a significant step toward understanding the physiological functions of these enigmatic proteins and their postulated roles in diseases such as glioma, colorectal cancer, Kawasaki disease and Q fever (Blom et al., 2008; Burgner et al., 2009; Camps et al., 2013; Chen et al., 2005; Holtkamp et al., 2007; Mehraj et al., 2011).

Acknowledgments

We thank Jane McGlade (University of Toronto) for providing the rabbit anti LNX-RING/NPAY antibody. We are grateful to Gary Loughran (University College Cork) for providing the p2luc and pDluc-*Renilla* plasmids and for his advice and help with luciferase assays and for reading the manuscript. This work was supported by a Research Frontiers Programme grant from the Science Foundation Ireland (08/RFP/NSC1382), and an Irish Research Council EMBARK Postgraduate Research Scholarship to Joan Lenihan.

References

Blom, T., Roselli, A., Tanner, M., Nupponen, N.N., 2008. Mutation and copy number analysis of LNX1 and Numbl in nervous system tumors. Cancer Genet. Cytogenet. 186, 103–109.

Burgner, D., Davila, S., Breunis, W.B., Ng, S.B., Li, Y., Bonnard, C., Ling, L., Wright, V.J., Thalamuthu, A., Odam, M., Shimizu, C., Burns, J.C., Levin, M., Kuijpers, T.W., Hibberd, M.L., 2009. A genome-wide association study identifies novel and functionally related susceptibility Loci for Kawasaki disease. PLoS Genet. 5, e1000319.

Cahoy, J.D., Emery, B., Kaushal, A., Foo, L.C., Zamanian, J.L., Christopherson, K.S., Xing, Y., Lubischer, J.L., Krieg, P.A., Krupenko, S.A., Thompson, W.J., Barres, B.A., 2008. A transcriptome database for astrocytes, neurons, and oligodendrocytes: a new resource for understanding brain development and function. J. Neurosci. 28, 264–278.

Calvo, S.E., Pagliarini, D.J., Mootha, V.K., 2009. Upstream open reading frames cause widespread reduction of protein expression and are polymorphic among humans. Proc. Natl. Acad. Sci. U. S. A. 106, 7507–7512.

Camps, J., Pitt, J.J., Emons, G., Hummon, A.B., Case, C.M., Grade, M., Jones, T.L., Nguyen, Q.T., Ghadimi, B.M., Beissbarth, T., Difilippantonio, M.J., Caplen, N.J., Ried, T., 2013. Genetic amplification of the NOTCH modulator LNX2 upregulates the WNT/beta-catenin pathway in colorectal cancer. Cancer Res. 73, 2003–2013.

Chen, J., Xu, J., Zhao, W., Hu, G., Cheng, H., Kang, Y., Xie, Y., Lu, Y., 2005. Characterization of human LNX, a novel ligand of Numb protein X that is downregulated in human gliomas. Int. J. Biochem. Cell Biol. 37, 2273–2283.

D'Agostino, M., Tornillo, G., Caporaso, M.G., Barone, M.V., Ghigo, E., Bonatti, S., Mottola, G., 2011. Ligand of Numb proteins LNX1p80 and LNX2 interact with the human glycoprotein CD8alpha and promote its ubiquitylation and endocytosis. J. Cell Sci. 124, 3545–3556.

de Bie, P., Ciechanover, A., 2011. Ubiquitination of E3 ligases: self-regulation of the ubiquitin system via proteolytic and non-proteolytic mechanisms. Cell Death Differ. 18, 1393–1402.

Dho, S.E., Jacob, S., Wolting, C.D., French, M.B., Rohrschneider, L.R., McGlade, C.J., 1998. The mammalian numb phosphotyrosine-binding domain. Characterization of binding specificity and identification of a novel PDZ domain-containing numb binding protein, LNX. J. Biol. Chem. 273, 9179–9187.

Flynn, M., Saha, O., Young, P., 2011. Molecular evolution of the LNX gene family. BMC Evol. Biol. 11, 235.
Foley, K.S., Young, P.W., 2013. An analysis of splicing, actin-binding properties, heterodimerization and molecular interactions of the non-muscle alpha-actinins. Biochem. J. 452, 477–488.
Grentzmann, G., Ingram, J.A., Kelly, P.J., Gesteland, R.F., Atkins, J.F., 1998. A dual-luciferase reporter system for studying recoding signals. RNA 4, 479–486.
Gulino, A., Di Marcotullio, L., Screpanti, I., 2010. The multiple functions of Numb. Exp. Cell Res. 316, 900–906.
Guo, Z., Song, E., Ma, S., Wang, X., Gao, S., Shao, C., Hu, S., Jia, L., Tian, R., Xu, T., Gao, Y., 2012. Proteomics strategy to identify substrates of LNX, a PDZ domain-containing E3 ubiquitin ligase. J. Proteome Res. 11, 4847–4862.
Higa, S., Tokoro, T., Inoue, E., Kitajima, I., Ohtsuka, T., 2007. The active zone protein CAST directly associates with Ligand-of-Numb protein X. Biochem. Biophys. Res. Commun. 354, 686–692.
Holtkamp, N., Ziegenhagen, N., Malzer, E., Hartmann, C., Giese, A., von Deimling, A., 2007. Characterization of the amplicon on chromosomal segment 4q12 in glioblastoma multiforme. Neuro-Oncol. 9, 291–297.
Ivanov, I.P., Loughran, G., Sachs, M.S., Atkins, J.F., 2010. Initiation context modulates autoregulation of eukaryotic translation initiation factor 1 (eIF1). Proc. Natl. Acad. Sci. U. S. A. 107, 18056–18060.
Kozak, M., 2001. Constraints on reinitiation of translation in mammals. Nucleic Acids Res. 29, 5226–5232.
Mehraj, V., Boucherit, N., Amara, A.B., Capo, C., Bonatti, S., Mege, J.L., Mottola, G., Ghigo, E., 2011. The ligands of Numb proteins X1 and X2 are specific markers for chronic Q fever. FEMS Immunol. Med. Microbiol. 64, 98–100.
Mirza, M., Raschperger, E., Philipson, L., Pettersson, R.F., Sollerbrant, K., 2005. The cell surface protein coxsackie- and adenovirus receptor (CAR) directly associates with the Ligand-of-Numb Protein-X2 (LNX2). Exp. Cell Res. 309, 110–120.
Mirza, M., Hreinsson, J., Strand, M.L., Hovatta, O., Soder, O., Philipson, L., Pettersson, R.F., Sollerbrant, K., 2006. Coxsackievirus and adenovirus receptor (CAR) is expressed in male germ cells and forms a complex with the differentiation factor JAM-C in mouse testis. Exp. Cell Res. 312, 817–830.
Nie, J., McGill, M.A., Dermer, M., Dho, S.E., Wolting, C.D., McGlade, C.J., 2002. LNX functions as a RING type E3 ubiquitin ligase that targets the cell fate determinant Numb for ubiquitin-dependent degradation. EMBO J. 21, 93–102.
Nie, J., Li, S.S., McGlade, C.J., 2004. A novel PTB–PDZ domain interaction mediates isoform-specific ubiquitylation of mammalian Numb. J. Biol. Chem. 279, 20807–20815.
Rice, D.S., Northcutt, G.M., Kurschner, C., 2001. The Lnx family proteins function as molecular scaffolds for Numb family proteins. Mol. Cell. Neurosci. 18, 525–540.
Ro, H., Dawid, I.B., 2009. Organizer restriction through modulation of Bozozok stability by the E3 ubiquitin ligase Lnx-like. Nat. Cell Biol. 11, 1121–1127.
Ro, H., Dawid, I.B., 2010. Lnx-2b restricts gsc expression to the dorsal mesoderm by limiting Nodal and Bozozok activity. Biochem. Biophys. Res. Commun. 402, 626–630.
Ro, H., Dawid, I.B., 2011. Modulation of Tcf3 repressor complex composition regulates cdx4 expression in zebrafish. EMBO J. 30, 2894–2907.
Rogozin, I.B., Kochetov, A.V., Kondrashov, F.A., Koonin, E.V., Milanesi, L., 2001. Presence of ATG triplets in 5′ untranslated regions of eukaryotic cDNAs correlates with a 'weak' context of the start codon. Bioinformatics 17, 890–900.
Schenborn, E.T., Goiffon, V., 2000. Calcium phosphate transfection of mammalian cultured cells. Methods Mol. Biol. 130, 135–145.
Takahashi, S., Iwamoto, N., Sasaki, H., Ohashi, M., Oda, Y., Tsukita, S., Furuse, M., 2009. The E3 ubiquitin ligase LNX1p80 promotes the removal of claudins from tight junctions in MDCK cells. J. Cell Sci. 122, 985–994.
Tang, T., Li, L., Tang, J., Li, Y., Lin, W.Y., Martin, F., Grant, D., Solloway, M., Parker, L., Ye, W., Forrest, W., Ghilardi, N., Oravecz, T., Platt, K.A., Rice, D.S., Hansen, G.M., Abuin, A., Eberhart, D.E., Godowski, P., Holt, K.H., Peterson, A., Zambrowicz, B.P., de Sauvage, F.J., 2010. A mouse knockout library for secreted and transmembrane proteins. Nat. Biotechnol. 28, 749–755.
Weiss, A., Baumgartner, M., Radziwill, G., Dennler, J., Moelling, K., 2007. c-Src is a PDZ interaction partner and substrate of the E3 ubiquitin ligase Ligand-of-Numb protein X1. FEBS Lett. 581, 5131–5136.
Wethmar, K., Smink, J.J., Leutz, A., 2010. Upstream open reading frames: molecular switches in (patho) physiology. Bioessays 32, 885–893.
Wolting, C.D., Griffiths, E.K., Sarao, R., Prevost, B.C., Wybenga-Groot, L.E., McGlade, C.J., 2011. Biochemical and computational analysis of LNX1 interacting proteins. PLoS One 6, e26248.
Young, P., Nie, J., Wang, X., McGlade, C.J., Rich, M.M., Feng, G., 2005. LNX1 is a perisynaptic Schwann cell specific E3 ubiquitin ligase that interacts with ErbB2. Mol. Cell. Neurosci. 30, 238–248.

Mol Neurobiol
DOI 10.1007/s12035-016-0261-0

Decreased Anxiety-Related Behaviour but Apparently Unperturbed NUMB Function in Ligand of NUMB Protein-X (LNX) 1/2 Double Knockout Mice

Joan A. Lenihan[1] · Orthis Saha[1,2] · Victoria Heimer-McGinn[1,3] · John F. Cryan[4,5,6] · Guoping Feng[7,8,9] · Paul W. Young[1,6]

Received: 23 August 2016 / Accepted: 25 October 2016
© Springer Science+Business Media New York 2016

Abstract NUMB is a key regulator of neurogenesis and neuronal differentiation that can be ubiquitinated and targeted for proteasomal degradation by ligand of numb protein-X (LNX) family E3 ubiquitin ligases. However, our understanding of LNX protein function in vivo is very limited. To examine the role of LNX proteins in regulating NUMB function in vivo, we generated mice lacking both LNX1 and LNX2 expression in the brain. Surprisingly, these mice are healthy, exhibit unaltered levels of NUMB protein and do not display any neuroanatomical defects indicative of aberrant NUMB function. Behavioural analysis of LNX1/LNX2 double knockout mice revealed decreased anxiety-related behaviour, as assessed in the open field and elevated plus maze paradigms. By contrast, no major defects in learning, motor or sensory function were observed. Given the apparent absence of major NUMB dysfunction in LNX null animals, we performed a proteomic analysis to identify neuronal LNX-interacting proteins other than NUMB that might contribute to the anxiolytic phenotype observed. We identified and/or confirmed interactions of LNX1 and LNX2 with proteins known to have presynaptic and neuronal signalling functions, including the presynaptic active zone constituents ERC1, ERC2 and LIPRIN-αs (PPFIA1, PPFIA3), as well as the F-BAR domain proteins FCHSD2 (nervous wreck homologue) and SRGAP2. These and other novel LNX-interacting proteins identified are promising candidates to mediate LNX functions in the central nervous system, including their role in modulating anxiety-related behaviour.

Keywords LNX1 · LNX2 · LIPRIN/PPFIA · ERC1/ERC2 · NUMB · Anxiety

Electronic supplementary material The online version of this article (doi:10.1007/s12035-016-0261-0) contains supplementary material, which is available to authorized users.

✉ Paul W. Young
p.young@ucc.ie

[1] School of Biochemistry and Cell Biology, University College Cork, Cork, Ireland

[2] Present address: Institut de Biologie de l'ENS (IBENS), INSERM, CNRS, École Normale Supérieure, PSL Research University, 75005 Paris, France

[3] Present address: Department of Cognitive, Linguistic and Psychological Sciences, Brown University, Providence, RI, USA

[4] Department of Anatomy and Neuroscience, University College Cork, Cork, Ireland

[5] Alimentary Pharmabiotic Centre, University College Cork, Cork, Ireland

[6] Cork Neuroscience Centre, University College Cork, Cork, Ireland

[7] McGovern Institute for Brain Research, Department of Brain and Cognitive Sciences, Massachusetts Institute of Technology, Cambridge, MA 02139, USA

[8] Key Laboratory of Brain Functional Genomics (Ministry of Education and Science and Technology Commission of Shanghai Municipality), Institute of Cognitive Neuroscience, School of Psychology and Cognitive Science, East China Normal University, Shanghai 200062, China

[9] Stanley Center for Psychiatric Research, Broad Institute of Massachusetts Institute of Technology and Harvard, Cambridge, MA 02142, USA

Published online: 26 November 2016

Abbreviations

PDZ	PSD-95
DlgA	ZO-1
RING	Really Interesting New Gene
LNX	Ligand of numb protein X
CNS	Central nervous system
ERC	ELKS/Rab6-interacting/CAST
SVZ	Subventricular zone
PBK	PDZ-binding kinase
DKO	$Lnx1^{exon3-/-}$;$Lnx2^{-/-}$ double knockout
DHET	$Lnx1^{exon3+/-}$;$Lnx2^{+/-}$ double heterozygous knockout
GFP	Green fluorescent protein
GST	Glutathione S-transferase
PCR	Polymerase chain reaction
PTB	Phosphotyrosine-binding domain

Introduction

Ligand of NUMB protein X (LNX) proteins were first characterized based on their ability to bind to NUMB and NUMBLIKE [1, 2]. LNX1 and LNX2 are closely related E3 ubiquitin ligases that can ubiquitinate specific isoforms of NUMB, and LNX-mediated ubiquitination, at least in the case of LNX1, has been shown to target NUMB for proteasomal degradation [3–5]. NUMB is a negative regulator of Notch signalling, and degradation of NUMB upon LNX1 overexpression was shown to moderately enhance Notch signalling in cultured cells [4]. However, LNX2 knockdown in colorectal cancer cell lines caused a decrease in NUMB levels, a result that does not fit with the notion of LNX2 targeting NUMB for degradation [6]. Developmentally, expression of both *Lnx*1 and *Lnx2* messenger RNA (mRNA) is prominent in the embryonic and adult central nervous system (CNS) [1, 2]. This observation suggests a possible role for LNX1 and LNX2 in modulating neural development through their interaction with NUMB and/or its paralogue NUMBLIKE—key regulators of mammalian neurogenesis and neuronal differentiation [7]. However, LNX proteins are present at very low levels in the brain, despite the presence of *Lnx* mRNAs [8], and the regulation of NUMB by endogenous levels of LNX proteins has not been definitively demonstrated. One of many aspects of neural development regulated by NUMB/NUMBLIKE is the development of the neurogenic subventricular zone (SVZ) [9]. A recent study has reported an upregulation of LNX2 within the SVZ of mice lacking the *Gli3* transcriptional repressor and demonstrated that these mice have lower levels of NUMB protein [10]. However, a causal relationship between these two observations was not proven and the question of whether NUMB is modulated by endogenous levels of LNX proteins in the SVZ has not been addressed. There have not been any in vivo *Lnx* loss-of-function studies in a mammalian context, and hence, the physiological significance of the LNX–NUMB interaction remains unclear.

LNX1 and LNX2 have the same domain structure, comprising an amino-terminal Really Interesting New Gene (RING) domain, a NUMB-binding motif (NPAY or NPAF) and four carboxyl-terminal PSD-95, DlgA and ZO-1 (PDZ) domains (Fig. 1). The RING domain harbours the catalytic E3 ubiquitin ligase activity, but notably, the shorter LNX1 p70 and p62 isoforms that are expressed in the brain lack the RING domain, suggesting that they might have functions that are independent of ubiquitination [1, 11]. No such alternative splicing of *Lnx2* has been reported. The combination of a RING and one or more PDZ domains is unique to the LNX family [12]. PDZ domains function as protein–protein interaction modules, most commonly binding to the carboxyl-termini of other proteins. Wolting et al. [13] catalogued around 220 LNX-interacting proteins both from their own work and the published literature, while a subsequent study by Guo et al. [14] added approximately 30 additional proteins to this list. Most of these interactions are PDZ domain-mediated and were identified using either yeast two-hybrid assays or arrays of PDZ domains and PDZ-binding motifs. To date, only a small number of the described LNX-interacting proteins have been shown to be substrates for ubiquitination by LNX. For example, ubiquitination of c-Src and PDZ-binding kinase (PBK) by LNX1 targets them for proteasomal degradation [8, 14], while LNX-mediated ubiquitination of CLAUDINS and CD-8α appears to cause their internalization from the cell surface, via endocytic pathways [15, 16]. Nevertheless, these examples indicate that the ubiquitin ligase activity of LNX proteins can be targeted to specific substrates via PDZ-mediated interactions. Thus, we need to consider interacting proteins beyond NUMB and NUMBLIKE that may be substrates for ubiquitination by LNX proteins or that may mediate E3 ligase-independent LNX functions. Given the low and potentially cell type-restricted expression patterns of LNX proteins [8, 11, 17], the identification of physiologically relevant interacting proteins and substrates will be key to elucidating the in vivo functions of LNX proteins.

To explore the neuronal functions of LNX proteins in vivo, we generated double knockout mice that lack LNX protein expression in the CNS. These mice exhibit decreased anxiety-related behaviours, in the apparent absence of any sensory, motor or learning deficits. However, we do not find evidence to support the hypothesis that LNX proteins are major regulators of NUMB/NUMBLIKE function during CNS development. To identify other proteins that may mediate LNX functions in the CNS, we characterized brain proteins that bind LNX1 and LNX2 PDZ domains using affinity purification and mass spectrometry. This approach revealed interactions of LNX1 and LNX2 with proteins that have established synaptic or neuronal functions, including ERC1/ERC2, LIPRIN-αs, FCHSD2 and SRGAP2—providing candidates, in addition to NUMB, that may play a role in the altered anxiety-related behaviour in LNX-deficient mice.

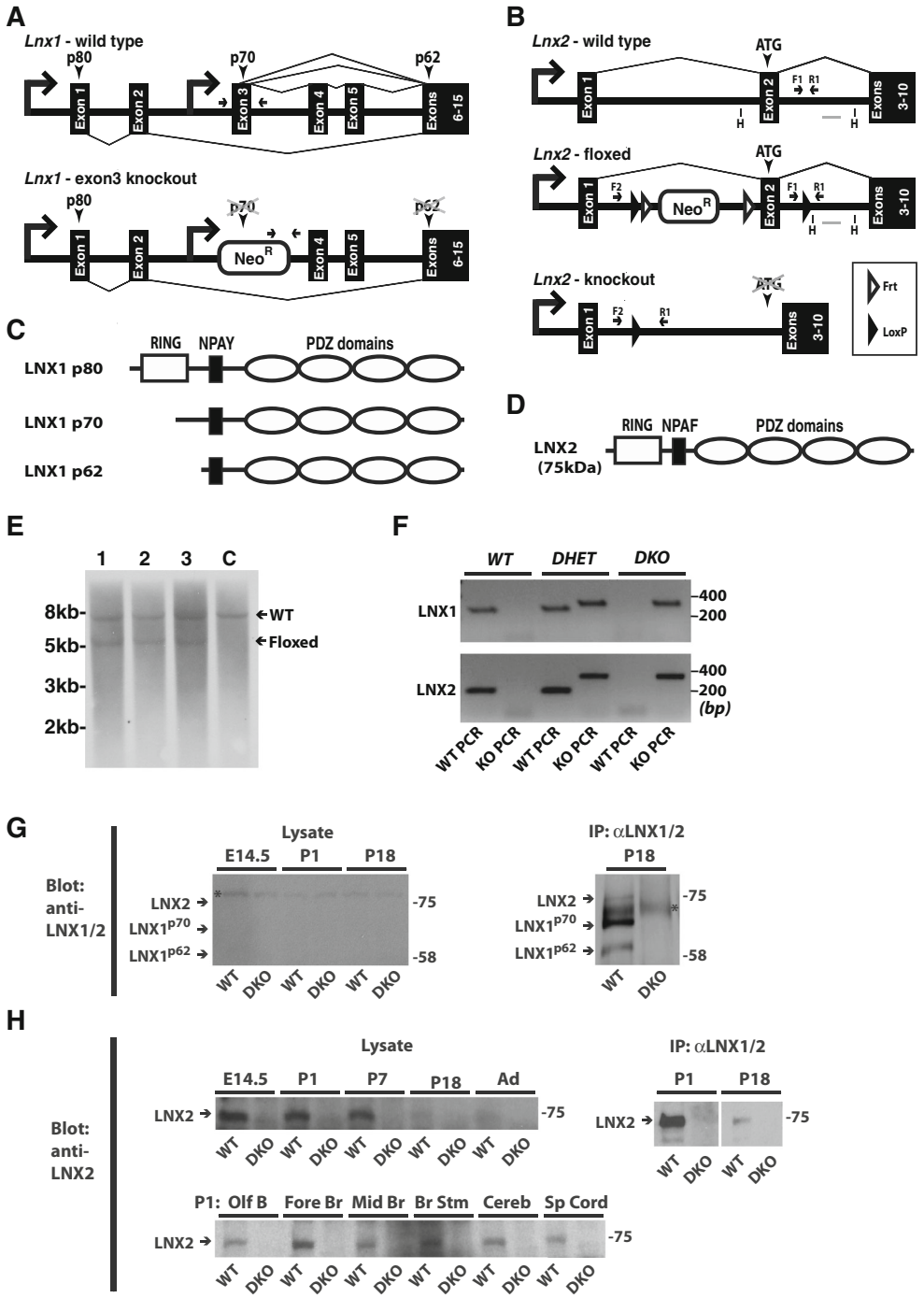

Materials and Methods

Animals

Lnx1$^{exon3-/-}$ knockout mice (originally made by Lexicon Pharmaceuticals, Inc.) were obtained through the Mutant Mouse Regional Resource Center (MMRRC, www.mmrrc.org) at University of California, Davis, CA, USA (stock no. 032436-UCD; strain name: B6;129S5-Lnx1<tm1 Lex>/Mmcd). In these mice, exon 3, which is the first exon of the transcripts that codes for the p70 and p62 neuronal isoforms of LNX1, is replaced by a neomycin resistance gene (Fig. 1a). This is expected to abolish transcription of these neuronal isoforms, but should not affect the expression of the non-neuronal LNX1 p80 isoform that is transcribed from a different upstream promoter [11].

Lnx2 conditional knockout mice were generated through homologous recombination in mouse R1 embryonic stem (ES) cells by using standard procedures as previously described [18]. These *Lnx2* conditional knockout mice were

◀ **Fig. 1** Generation of *Lnx1*$^{exon\ 3}$*;Lnx2* double knockout (DKO) mice. **a** Schematic of *Lnx1* gene structure showing the alternative promoters (*large arrows*) and splicing events (*thin lines*) that generate the non-neuronal p80 and the neuronal p70 and p62 protein isoforms. In the knockout allele, exon 3, the first exon of all the neuronal transcripts, is deleted and replaced by a neomycin resistance cassette. *Arrowheads* show the locations of translation initiation ATG codons for the indicated protein isoforms. *Small arrows* in **a**, **b** indicate positions of genotyping primers. **b** Schematic of *Lnx2* wild-type, floxed and knockout alleles. Exon 2, which contains the ATG codon for the initiation of LNX2 translation, was first flanked by *loxP* sites and then deleted through Cre-mediated recombination to generate the knockout allele used in this study. HindIII restriction sites are indicated by the letter *H*, and the *grey bar* indicates the probe used for southern blotting (not to scale). **c**, **d** Domain structures of LNX1 and LNX2 proteins. The LNX1 p70 and p62 isoforms that lack the catalytic RING domain are expressed in the central nervous system. The NPAY and NPAF motifs in LNX1 and LNX2 respectively are involved in binding NUMB while both proteins contain four PDZ domains. **e** Southern blot verifying correct *Lnx2* gene targeting. A HindIII restriction site in the targeting construct results in a shorter 5.5-kb fragment being generated upon HindIII digestion of genomic DNA from three correctly targeted ES cell clones (*1*, *2*, *3*), compared to the parental ES cells (*C*). **f** PCR-based genotyping of wild-type (*WT*), *Lnx1*$^{exon3+/-}$*/Lnx2*$^{+/-}$ (*DHET*) and *Lnx1*$^{exon3-/-}$*/Lnx2*$^{-/-}$ (*DKO*) mice analysed by agarose gel electrophoresis. Using the primer pairs indicated in **a**, **b** above, *Lnx1* and *Lnx2* WT and KO alleles were detected in separate PCR reactions. **g**, **h** Elimination of LNX1 and LNX2 proteins from the brains of *Lnx1/Lnx2* DKO mice confirmed by western blotting of brain lysates (*left panels*) and immunoprecipitates (*right panels*) from WT and DKO mice. Immunoprecipitation was performed using an antibody that recognizes both LNX1 and LNX2. **g** Immunoblotting using an anti-LNX1 antibody that cross reacts with LNX2 does not detect LNX proteins directly in brain lysates at any of the indicated developmental stages. However, following immunoprecipitation, neuronal LNX1p70 and p62 isoforms, as well as LNX2 (75 kDa), are all detected in WT, but not DKO, P18 brains. **h** Immunoblotting using a LNX2-specific antibody directly detects LNX2 in WT, but not DKO, E14.5, P1 and P7 brain lysates. LNX2 cannot be clearly detected by immunoblotting at P18 or adult (P42) stages without prior immunoprecipitation. In P1 mice, LNX2 is present across multiple brain regions. The positions (or expected positions) of LNX proteins (*arrows*) as well as molecular weight markers (kDa) are indicated. *Asterisks* (*) indicate non-specific bands. *Ad* adult, *Olf B* olfactory bulb, *Fore Br* forebrain, *Mid Br* Midbrain, *Br Stm* brain stem, *Cereb* cerebellum, *Sp Cord* Spinal Cord

designed so that a neomycin resistance gene, used as a selectable marker, and the adjacent exon 2 of the *Lnx2* gene are flanked by *loxP* sites (Fig. 1b). Exon 2 and the neomycin resistance gene were deleted by crossing these mice to a Cre recombinase-expressing transgenic mouse line from the Jackson Laboratory, Bar Harbor, ME, USA (strain name: B6.C-Tg(CMV-cre)1Cgn/J; stock no. 006054). The heterozygote (*Lnx2*$^{+/-}$) mice, so obtained, were then crossed with each other to obtain knockout (*Lnx2*$^{-/-}$) mice. Removal of exon 2 deletes the ATG start codon and the coding region for the RING finger domain. If, following deletion of exon 2, exon 1 were to splice into exon 3 or a downstream exon, and the first available in-frame ATG (in exon 7) was used to initiate translation, a protein of 211 amino acids in length could theoretically be produced. However, several out-of-frame ATGs in exons 3–6 would likely attenuate translation of any such product. Thus, deletion of exon 2 in *Lnx2* is likely to result in the production of at most very small quantities of a severely truncated LNX2 polypeptide lacking E3 ligase activity and is highly likely to be a null or severely hypomorphic allele.

Lnx2$^{-/-}$ mice were crossed to *Lnx1*$^{exon3-/-}$ mice. Compound heterozygous mice *Lnx1*$^{exon3+/-}$ and *Lnx2*$^{+/-}$ were obtained and back-crossed for at least eight generations to the C57/BL6J strain to ensure a uniform C57/BL6J genetic background. After back-crossing, double knockout (DKO) mice (*Lnx1*$^{exon3-/-}$*;Lnx2*$^{-/-}$) and the other genotypes required were bred for the experiments described hereafter. All animal experiments were approved by the Animal Experimentation Ethics Committee of University College Cork (No: 2013/028) and were conducted under licence (No: AE19130/P013) issued by the Health Products Regulatory Authority of Ireland, in accordance with the European Union Directive 2010/63/EU for animals used for scientific purposes.

Genotyping

Tail biopsies were digested with Proteinase K as described previously [19]. PCR genotyping was performed using the following cycling conditions: 96 °C—3 min, 40 cycles [96 °C—40 s, 60 °C—40 s, 68 °C—1 min 30 s] and 68 °C—10 min. Primer pairs and sizes of PCR products were as follows:

- *Lnx1* WT PCR—DNA274-3 [5′-TGCCTTAATCTACAGGCTCC-3′] and DNA274-4 [5′-GAGTTGTGGGCACTGAGAG-3′], 253 bp
- *Lnx1* KO PCR—Neo3a 5′ [5′-GCAGCGCATCGCCTTCTATC-3′] and DNA274-7 5′ [5′-GTCACAAAGCACTAAGCGTG-3′], 298 bp
- *Lnx2* WT/FLOX PCR—*Lnx2*GENO-F1 [5′-CGCAGCCTTAGGCATGGTTGG-3′] and *Lnx2*GENO-R1 [5′-CTGACTGTGGGTTACAGTTCTGG], 210 /252 bp
- *Lnx2* KO PCR—*Lnx2*GENO-F2 [CCCCATCATGCAGAGCAAAGTC] and *Lnx2*GENO-R1, 368 bp

Antibodies and cDNA Constructs

The coding sequences of mouse *Lnx1* (p80 isoform) and *Lnx2* were cloned into the pEGFP-C2 vector (Clontech, Mountain View, CA, USA). Empty pEGFP-C2 vector was used to express EGFP alone. Constructs encoding the second PDZ domains of LNX1 and LNX2, corresponding to aa377–470 and aa330–423 respectively, were cloned into the vector pET24d-GST to produce glutathione S-transferase (GST)-tagged proteins. Coding sequences for LNX-interacting proteins were cloned into the vector pCMV-N-FLAG to produce proteins with amino-terminal FLAG epitope tag. The following commercially

available antibodies were used at the indicated dilutions: anti-green fluorescent protein (GFP, catalogue number ab290, Abcam, 1:3000 dilution), anti-FLAG (catalogue number F3165, Sigma-Aldrich, 1:2000 dilution), anti-LIPRIN-α3 (catalogue number 169102, Synaptic Systems, 1:1000 dilution), anti-NUMB (catalogue number NB500-178, Novus Biologicals, 1:7000 dilution), anti-FOXJ1 (catalogue number 14-9965, e-Bioscience, 1:400 dilution), anti-glial fibrillary acidic protein (GFAP, catalogue number ab7260, Abcam, 1:1000 dilution) and anti-VINCULIN (catalogue number V9131, Sigma-Aldrich, 1:1000 dilution). The guinea pig polyclonal anti-LNX1/2 antibody (anti-LNX1/2-PDZ3/4), rabbit anti-LNX2 antibody (used at 1:500 dilution) [17] and the rabbit polyclonal anti-LNX1/2 antibody (anti-LNX1/2-RING/NPAY, used at 1:3000 dilution) [1] have been described previously. Secondary antibodies were from Jackson ImmunoResearch Laboratories (West Grove, PA, USA) and LI-COR Biosciences (Cambridge, UK). All reagents were from Sigma-Aldrich (Arklow, Ireland) unless stated otherwise.

Western Blotting and Immunoprecipitation

Brain tissues from wild-type (WT) and DKO mice were homogenized on ice using a Dounce homogenizer in a volume of lysis buffer (20 mM, pH 7.5, 10 mM NaCl, 1% NP40, 0.1% sodium deoxycholate, 1 mM EDTA and protease inhibitors (Roche Applied Sciences)) which was 10 times the weight of the tissue. Following centrifugation at 16,000×*g* for 30 min at 4 °C, the supernatants were used directly either for western blotting (to detect NUMB or LNX proteins) or for immunoprecipitation of LNX proteins. Immunoprecipitation was performed on lysates prepared from approximately 0.4 g of brain tissue, by addition of 10 μl guinea pig anti-LNX1/2-PDZ3/4 serum [17] for 4 h and 50 μl Protein A sepharose beads (Thermo Scientific Pierce) for 2 h with mixing at 4 °C. Following 5 × 5 min washes in lysis buffer, immunoprecipitated proteins were eluted by boiling in 2× SDS-PAGE gel loading buffer. Western blotting for LNX proteins was performed using rabbit anti-LNX1/2-RING/NPAY or anti-LNX2 antibody and enhanced chemiluminescent detection (Thermo Scientific Pierce, Rockford, IL, USA). For NUMB quantification, total protein concentration of lysates was calculated using a BCA assay (Thermo Scientific Pierce) and NUMB detection was performed using Odyssey V2.1 software (LI-COR Biosciences, Cambridge, UK).

Histology and Immunofluorescence Staining

Mice to be used for histology and immunofluorescence were anesthetized by isofluorane inhalation and perfused transcardially with phosphate-buffered saline (PBS) followed by 4% paraformaldehyde dissolved in PBS. To examine gross brain anatomy, 66-μm-thick sagittal brain sections were cut using a vibratome and stained with DAPI dissolved in PBS in a 24-well plate with rocking, washed three times for 10 min in PBS, prior to mounting with Fluoromount mounting solution. Images were captured and montages of entire sections created using an EVOS FL Cell Imaging System microscope and associated software (Thermo Scientific Pierce). Brain regions were identified with the aid of the Allen Brain Atlas (http://mouse.brain-map.org) and quantified using ImageJ software [20]. For immunofluorescence staining, fixed tissues were cryoprotected in sucrose before embedding and freezing in OCT compound (Tissue-Tek, Torrance, CA, USA). Twenty-micrometre cryostat sections were fixed post sectioning with 4% paraformaldehyde/PBS for an additional 5 min, rinsed extensively with PBS and then blocked with blocking solution (2% bovine serum albumin (BSA), 5% normal goat serum (NGS) and 0.2% Triton X-100 diluted in PBS). Antibody incubations were performed at 4 °C overnight in blocking solution lacking Triton X-100. Sections were mounted with Fluoromount mounting solution and imaged on a Leica DM 6000 microscope. For FOXJ1 staining, antigen retrieval was performed in 10 mM Na citrate buffer (pH 6) for 20 min at 90–100 °C prior to the blocking step.

Phenotypic Characterization of Lnx DKO Mice

Mice were bred to obtain WT, double heterozygote (DHET) and DKO genotypes. Fathers were removed before parturition after which mothers were singly housed with their pups. Pups were weaned at 3 weeks of age, housed in groups of two to four mice of mixed genotype and fed *ad libitum*. Body weight was measured on a weekly basis to the nearest 0.1 g, beginning at 1 week of age. Cages contained minimally enriched living conditions, and mice were maintained on a 12-h light/dark cycle (lights on at 07:30), with temperature- (22 ± 1 °C) and humidity-controlled conditions. At adulthood (8 weeks old), mice underwent a battery of behavioural tests. Each cohort of mice, of a given sex and genotype, was made up of animals from at least three different litters. Tests were conducted in sequence from the least to the most stressful test, over a period of 5 weeks (Fig. 4a). There was a minimum rest period of at least 24 h between each test. For all procedures, animals were brought to the room at least 30 min prior to testing. All experiments were conducted during the light phase of the day. All apparatus were cleaned between animals with 70% ethanol to remove odours. Genotypes were blinded for the duration of the behavioural battery and for subsequent scoring.

Primary Observation, Grip Strength and Hotplate Tests

A primary observational assessment following a modified SHIRPA protocol was performed for male and female mice

of each genotype [21–23]. In total, 36 observations were quantified, including spontaneous activity, respiration rate, fur, skin and whisker condition, tremor, body position, palpebral closure, piloerection, gait, pelvic elevation, tail elevation, touch escape, positional passivity, transfer arousal, trunk curl, limb grasping, body tone, pinna reflex, corneal reflex, tail pinch reflex, skin colour, heart rate, limb tone, abdominal tone, lacrimation, provoked biting, righting reflex and negative geotaxis. In addition, muscle strength was assessed using a grip strength meter (Ugo Basile, Varese, Italy). Mice were held by the tail and allowed to grasp the grid with their front paws and were gently pulled back until they released their grip. The apparatus registered the peak strength for that trial. Each animal had five trials, with an inter-trial interval of 15–30 s. Mice were tested for analgesia-related responses using a hotplate apparatus preheated to 55 °C (Columbus Instruments, Columbus, OH, USA). Mice were placed onto the hotplate, and the time to first show a hind limb response was recorded. Typical responses are licking or shaking the hindpaw, or jumping. Mice were immediately removed after showing a response. The test was terminated at 30 s in the absence of a response.

Open Field

Spontaneous locomotor activity and anxiety-like behaviour were assessed in the open field task. This paradigm is based on the idea that mice will naturally prefer to be near a protective wall rather than being exposed to danger out in the open [21]. The apparatus was a grey, plastic, open box without any bedding (40 cm × 32 cm × 25 cm, $L \times W \times H$). The experiment was performed under a low light level (circa 100 lx). After 30 min habituation to the testing room, animals were placed individually in the middle of the arena and allowed 10 min free exploration. Each mouse was video-recorded for the duration of the test, and the researcher left the room after the start of the trial. Total distance travelled, time spent and number of entries into the centre and the four corner areas of the arena were measured post-test using a video-tracking system (EthoVision software, Noldus, The Netherlands). The total distance travelled served as an index of locomotor activity. Time spent and number of entries into the centre and corners zones were considered an inverse score for anxiety-like behaviour.

Elevated Plus Maze

The elevated plus maze protocol is designed to test levels of passive anxiety-like behaviour, based on the conflict between the exploratory instinct of mice and their aversion for the elevated, exposed open arms of the maze [24]. The elevated plus maze consisted of four arms, forming the shape of a plus, elevated 91 cm above the floor. Two opposing arms were enclosed by walls; the other two arms were open. All four arms were connected by a centre area. The experiment was performed under dim light (circa 30 lx). Each mouse was placed gently on the centre of the maze facing an open arm and allowed to freely explore the maze for 6 min. Each mouse was video-recorded for the duration of the test, and the researcher left the room after the start of the trial. Variables measured manually post-test were the time spent and percentage of entries into the open and closed arms of the maze, as indices of anxiety-like behaviour. Total arm entries were analysed as an index of general locomotor activity. An animal was adjudged to have entered an arm of the maze only when all four paws were inside the arm in question.

Light–Dark Box Test

The light–dark box test assessed levels of unconditioned anxiety in rodents based on levels of passive avoidance behaviour [24]. The apparatus was a plexiglas enclosure (44 cm × 21 cm × 21 cm, $L \times W \times H$) divided unequally into two chambers by a black partition containing a small opening (10 cm × 5 cm). The larger chamber was approximately twice the size of the smaller chamber, had clear walls and an open top, and was brightly illuminated (1000 lx) to generate aversive conditions. The small chamber (14 cm length) was enclosed on all sides by black walls except for the small opening between the chambers. Mice were individually placed into the illuminated side facing away from the dark compartment and were allowed to freely explore the apparatus for 10 min. During this period, the behaviour of the animals was recorded. Mice were manually scored post-test for their initial latency to enter the dark compartment, the time spent in the light compartment and the number of transitions between the two compartments, using the recorded videos. An animal was adjudged to have entered a compartment when all four paws had crossed the threshold.

Y-Maze

Spontaneous alternation behaviour in the Y-maze is used to assess spatial memory [25]. The maze consisted of a black plastic three-arm Y-maze (15 cm × 5 cm × 10 cm, $L \times W \times H$). Mice were individually placed in one of the three arms and allowed 5 min free exploration. The sequence of visited arms was recorded. At the end of the test, mice were returned to their home cage. Parameters measured included the number of entries, as an index of locomotor activity, and the percentage alternation as a measure of spatial memory.

Rotarod Test

Motor coordination and skill learning were assessed using a rotarod apparatus (UGO Basile, Varese, Italy) [21]. The

rotarod task was first introduced to animals by a 5-min trial at a constant speed of 4 rpm. During this initial training phase, mice were placed back on the rod immediately after falling, allowing them to become familiar with the test. Thereafter, mice were placed on the rotating drum, which accelerated from 4 to 40 r.p.m. over a 5-min period. Time spent walking on top of the rod before falling was recorded. Mice were given three trials on three consecutive days for a maximum time of 300 s (5 min) per trial. An interval of 30 min was given between trials.

Other Behavioural Tests

As indicated in Fig. 4a, a number of additional behavioural tests were performed, the results of which are not presented here. Gait was monitored by analysis of paw print patterns, the acquisition and extinction of contextual and auditory cued fear was assessed in a fear conditioning paradigm and the forced swim test was performed as a measure of behavioural despair. No significant phenotypes were observed in these tests; however, for the latter two tests, which were performed at the end of the overall testing sequence, the possibility that the animals have become overly experienced to testing needs to be considered. The novel object recognition test was also performed; however, the data from this test could not be analysed because mice of all genotypes failed to preferentially explore the 'novel' objects used.

Purification of LNX1-PDZ2- and LNX2-PDZ2-Interacting Proteins from Brain Lysates

To prepare brain lysates, 0.8 g of brain tissue from P16 mice was resuspended in 2.5 volumes (*w*/*v*) of lysis buffer (10 mM Tris/Cl, pH 7.5, 150 mM NaCl, 0.5 mM EDTA, 0.5% NP-40 and protease inhibitors (Roche Applied Sciences)). After homogenization using a Dounce homogenizer, the samples were incubated on ice for 30 min with frequent agitation. Samples were then clarified by centrifugation at 16 000×*g* for 30 min at 4 °C. The supernatant was collected and diluted to a final volume that was 10 times the weight of the tissue in lysis buffer lacking NP-40. GST, GST-LNX1-PDZ2 and GST-LNX2-PDZ2 recombinant proteins were produced in *Escherichia coli* BL21 cells and purified with glutathione-sepharose 4B beads (GE Healthcare) as previously described [26]. Proteins were dialysed into binding buffer (20 mM Tris, pH 7.5, 50 mM NaCl, 5 mM β-mercaptoethanol), and 300 μl of GST or GST fusion protein, at a concentration of 58 μM, was added to 1 ml of brain lysate and incubated with mixing for 90 min at 4 °C. 40 μl of glutathione-sepharose beads was added, incubated for 10 min at 4 °C with rotation and washed three times in binding buffer for 5 min each at 4 °C. Bound proteins were eluted in 10 mM glutathione and 50 mM Tris/Cl, pH 8. Purified samples were prepared for mass spectrometry analysis as previously described [27].

Protein Identification by Mass Spectrometry

Protein digestion, nano-liquid chromatography and MS/MS mass spectrometric analysis were performed at the FingerPrints Proteomics Facility at University of Dundee, Scotland, UK. Proteins were identified by searching against the IPI protein database, and data analysis was performed as previously described [27]. Briefly, proteins identified in LNX complexes, but not in the control samples, were ranked according to Mascot protein scores and listed using gene symbols as identifiers. A Mascot protein score of 100 was then applied as a cut-off value to limit results to proteins that have been reliably identified, and probable environmental contaminants or false positives were eliminated as previously described [27].

Characterization of Interactions by GFP Pull-Down Assays

Expression vectors encoding GFP-tagged LNX1 or LNX2 constructs were transfected into HEK 293 cells, either alone or together with constructs encoding FLAG epitope-tagged LNX-interacting protein. Cultures were harvested 24–48 h post-transfection, and GFP affinity was purification performed using 10 μl GFP-Trap_M beads according to the manufacturer's protocol (ChromoTek GmbH, Planegg-Martinsried, Germany). In some cases, the wash conditions were made more stringent by increasing the NaCl concentration in the standard wash buffer up to 500 mM. Proteins were eluted by boiling in 2× SDS sample buffer and analysed by western blotting.

Statistical Analysis

The normal distribution of behavioural data was assessed using the D'Agostino–Pearson test. Two-way repeated measures analysis of variance (rANOVA) was carried out to investigate the overall effect of genotype and age on body weight profile and rotarod, followed by Bonferroni post hoc test where appropriate. Data from all other paradigms were analysed by one-way ANOVA, followed by Bonferroni post hoc test where appropriate. Statistical analyses were performed using GraphPad Prism v.6.0 (La Jolla, CA, USA). Two-tailed Student *t* tests were performed using Microsoft Excel software. *P* values of less than 0.05 were considered significant. Unless stated otherwise, all data are presented as mean ± SEM.

Results

Generation of Lnx 1/2 Double Knockout Mice

Considering the high degree of sequence and functional similarity between LNX1 and LNX2, we decided to make *Lnx 1/2* DKO mice in order to study neuronal functions of LNX proteins in vivo. To this end, we first obtained a mouse line in which exon3 of the Lnx1 gene has been deleted (Fig. 1a). We have previously shown that this line, which we refer to as $Lnx1^{exon3-/-}$, lacks expression of the neuronally expressed LNX1 p70 and p62 protein isoforms (Fig. 1c) [11]. Comprehensive phenotyping of this line, which included some basic neurological and behavioural tests, did not reveal any significant findings apart from an increased percentage of B1-like B cells in peritoneal lavage (https://www.mmrrc.org/catalog/sds.php?mmrrc_id=32436). Next, we generated a *Lnx2* conditional knockout line in which exon 2 is flanked by *loxP* sites (Fig. 1b, e). Following deletion of exon 2 through Cre-mediated recombination, homozygous *Lnx2* knockout mice ($Lnx2^{-/-}$) were generated. These mice displayed no obvious abnormalities, and no phenotype has been reported for a different *Lnx2* KO line that was generated and phenotyped as part of the knockout mouse project (KOMP) (http://www.mousephenotype.org/data/genes/MGI:2155959).

$Lnx1^{exon3-/-}$ mice were then crossed to $Lnx2^{-/-}$ animals in order to generate $Lnx1^{exon3-/-}$; $Lnx2^{-/-}$ mice (DKO mice) [28]. Genotyping was performed by PCR (Fig. 1f). Similar to $Lnx1^{exon3}$ and *Lnx2* single knockouts, *Lnx* DKO mice were born at expected Mendelian frequencies, were healthy and displayed no overt phenotype. Immunoblotting was employed to characterize LNX protein expression in the murine brain and verify the absence of LNX proteins in DKO mice (Fig. 1g, h). Due to its low level of expression, LNX1 is not detectable directly in brain lysates from E14.5, P1 or P18 mice (Fig. 1g). However, immunoprecipitation of P18 brain lysates and subsequent immunoblotting using antibodies raised against LNX1 reveal the presence of the LNX1p70 and p62 isoforms in WT but not DKO P18 brain lysates. These antibodies cross react with LNX2, which is weakly detected in WT but not DKO immunoprecipitates. No compensatory upregulation of the non-neuronal LNX1p80 isoform, which would run just above LNX2, was observed in DKO animals. Using a LNX2-specific antibody, LNX2 can be detected directly in brain lysates from WT, but not DKO, E14.5, P1 and P7 mice (Fig. 1h). By contrast, LNX2 expression is barely detectable or undetectable in P18 or adult whole brain lysates. This downregulation of LNX2 protein in the early postnatal period is also apparent in immunoprecipitates from P1 and P18 animals, with LNX2 detected at P18 but at a much lower level than P1. The embryonic/early postnatal expression of LNX2 protein seems to be widespread within the CNS, with LNX2 detected in multiple brain regions, as well as the spinal cord of WT but not DKO P1 animals (Fig. 1h; lower panel). This analysis provides new information regarding LNX protein expression patterns and also validates the DKO mice as a suitable model to study the function of LNX proteins in the CNS.

Normal Gross Neuroanatomy in Lnx DKO Mice

To assess whether *Lnx1/Lnx2* deletion affects gross brain structure, we compared brain morphology in DAPI-stained sagittal sections from WT and DKO mice. Gross neuroanatomy was indistinguishable between genotypes (Fig. 2a). All major brain structures are present in DKO mice, and the cross-sectional area of major brain regions is not significantly different from WT animals (Fig. 2b). No significant differences in ventricular size were noted, and DKO brains exhibited normal lamination of neocortical and hippocampal regions. Since *Lnx1* and *2* mRNAs are prominently expressed in the cerebellum, we examined the areas of the cerebellar molecular and granule cell layers as well as the white matter and cerebellar nuclei (Fig. 2c). Again, no significant difference between genotypes was observed. These observations suggest that gross brain development proceeds normally in *Lnx* DKO mice.

Unaltered NUMB Levels and Subventricular Zone Development in Lnx DKO Mice

LNX1-mediated ubiquitination targets NUMB for proteasomal degradation [4]. LNX2 can also ubiquitinate NUMB, and it was recently proposed that LNX2 upregulation may cause the dramatic decrease in NUMB protein levels observed in $Gli3^{-/-}$ mice, thereby contributing to abnormalities in the development of the SVZ in these animals [5, 10]. To examine whether LNX proteins regulate NUMB levels under normal circumstances, we detected NUMB by western blotting of forebrain lysates from P1 WT and *Lnx* DKO mice—a developmental stage at which we observed relatively strong LNX2 protein expression. Three bands, which we interpret as representing three of the four known NUMB isoforms, were quantified individually (Fig. 3a). No significant differences in the levels of any NUMB isoforms were observed (Fig. 3b). Quantification of total NUMB protein at E14.5 and P18 also failed to reveal any significant alteration in NUMB levels (data not shown).

We next examined the SVZ in *Lnx* DKO mice, given that its development is abnormal in $Gli3^{-/-}$ mice that have elevated levels of LNX2 protein [10]. We specifically examined the differentiation of the ependymal cells, a process that proceeds abnormally in $Gli3^{-/-}$ animals. Immunostaining of the SVZ at P8 for the ependymal cell marker FOXJ1 reveals normal ependymal cell maturation, with a single line of $FOXJ1^{+}$ cells lining each ventricular wall (Fig. 3c, d). To assess cell fate specification, we co-stained for GFAP as a marker of neural

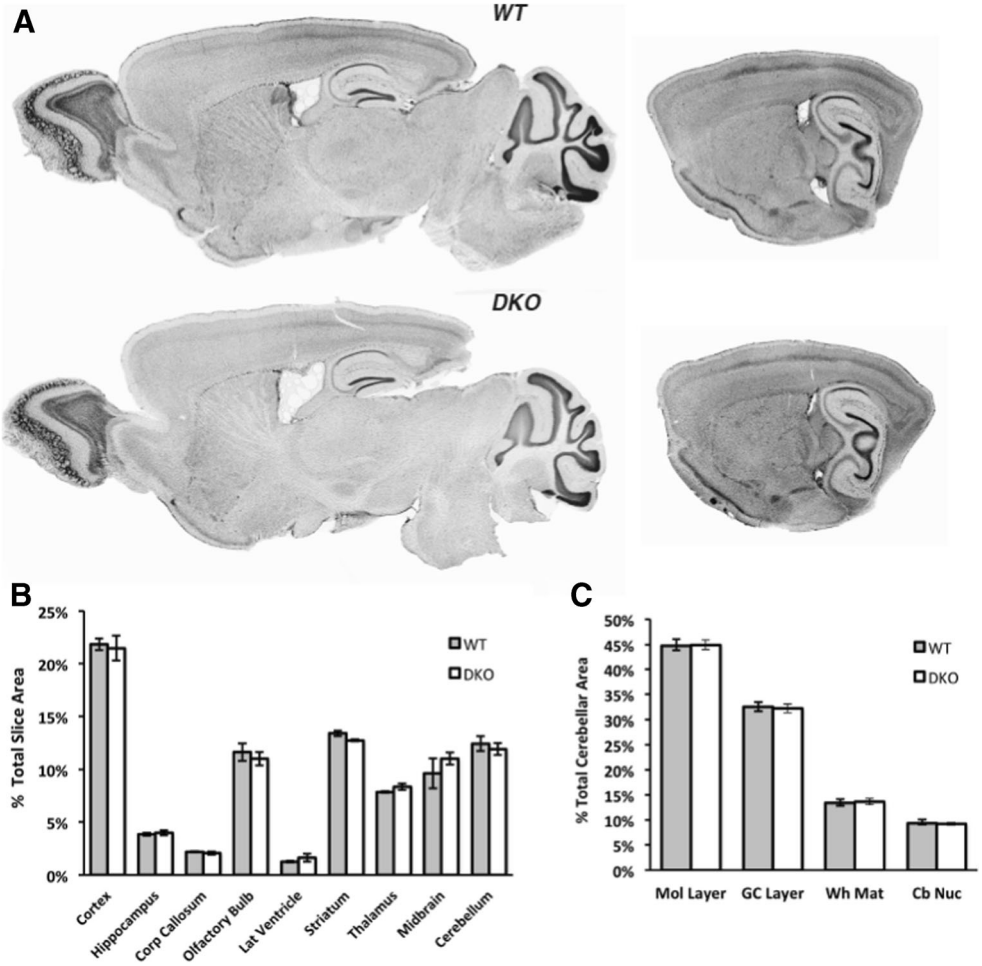

Fig. 2 Gross neuroanatomy of *Lnx* DKO mice is normal. **a** DAPI staining of medial (*left*) and lateral (*right*) sagittal sections from WT and *Lnx* DKO mice. **b** Measurements of the area of major brain regions from equivalent medial sagittal sections expressed as a percentage of total slice area. $n = 4$. **c** Measurements of the area of subregions of the cerebellum (molecular layer, granule cell layer, white matter and cerebellar nuclei) expressed as a percentage of total cerebellar area. $n = 4$

stem cells and quantified the proportion of $GFAP^+/FOXJ1^+$ double-positive cells—a parameter that is dramatically elevated in $Gli3^{-/-}$ mice (Fig. 3d). We observed no difference in this parameter between *Lnx* WT and DKO mice, with a low proportion of $GFAP^+/FOXJ1^+$ cells detected, indicative of normal cell fate specification of ependymal cells (Fig. 3e). Finally, immunostaining of P4 SVZ of *Lnx* WT and DKO mice did not reveal a specific staining pattern for LNX2 protein that differed between these genotypes (Fig. 3f). This staining was performed using the same antibody that detects LNX2 in forebrain lysates by western blotting. The lack of a specific staining pattern suggests that LNX2 expression in the SVZ, as in other brain regions of WT mice, is below the limit of detection by immunohistochemistry.

Behavioural Phenotyping of Lnx DKO Mice

Body Weight and Basic Sensory/Motor Function

Given the absence of gross neuroanatomical defects or obvious dysregulation of NUMB, we decided to subject *Lnx* DKO mice to a series of behavioural tests to reveal possible unanticipated physiological functions of LNX proteins in the CNS (Fig. 4a). For these analyses, both male and female WT, DHET and DKO mice were tested. Body weight was monitored weekly from 1 week of age through to the end of the testing period (Fig. 4b). For males and females, growth curves for the three genotypes started to diverge significantly at 5 and 3 weeks after birth respectively. Male DKO mice gained less weight than their WT and DHET counterparts. A similar pattern was initially observed for DKO females, though by 11 weeks female DHET mice also weighed significantly less than their WT counterparts. For males, there was a significant effect of week ($F_{12,336} = 1564$, $p < 0.0001$), genotype ($F_{2,28} = 5.098$, $p = 0.0129$) and interaction between week and genotype ($F_{24,336} = 2.653$, $p < 0.0001$) in the overall rANOVA. Similarly, for females there was also a significant effect of week ($F_{12,324} = 1351$, $p < 0.0001$), genotype ($F_{2,27} = 7.213$, $p = 0.0031$) and interaction between week and genotype ($F_{24,324} = 2.130$, $p = 0.0019$). In general, the differences in weight established during adolescence were stably maintained into adulthood and throughout the period of behavioural analysis. At 12 weeks of age, male DKO animals weighed on average 11.2 and 8.3% less than WT animals and DHET mice respectively, while female DKO and DHET mice weighed 13.2 and 10.2% less than WT mice respectively.

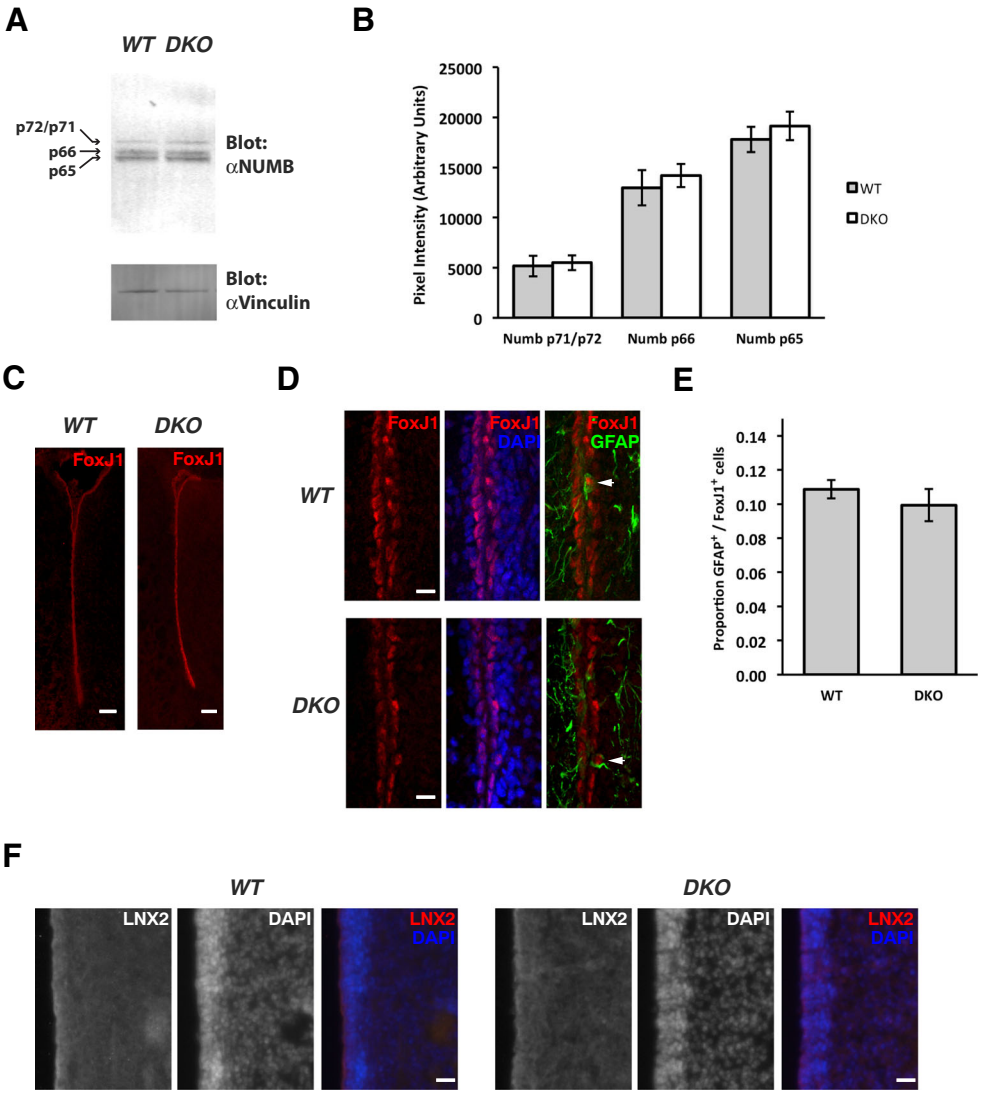

Fig. 3 Unaltered NUMB levels and normal subventricular zone (SVZ) development in *Lnx* DKO mice. **a** Protein levels of NUMB isoforms in brain lysates prepared from P1 WT and DKO mice were analysed by western blot. Blotting for vinculin verified equal protein loading in each lane. **b** Quantification of the levels of individual NUMB isoforms. No significant changes in NUMB protein levels in DKO mice were detected for any isoform, as assessed by Student's *t* test. $n = 4$. **c** *Low-magnification view* of the SVZ of P8 WT and DKO mice stained for the ependymal cell marker FOXJ1. *Scale bar* = 100 μm. **d** Co-staining of P8 WT and DKO SVZ for FOXJ1, DAPI and GFAP. *Arrowheads* indicate examples of $FOXJ1^+/GFAP^+$ double-labelled cells. *Scale bar* = 10 μm. **e** Quantification of the proportion of $FOXJ1^+$ ependymal cells that are also $GFAP^+$. There are no significant differences between WT and DKO mice as assessed by Student's *t* test. $n = 3$. **f** Co-staining of P4 WT and DKO SVZ for LNX2 and DAPI. Any staining observed with a LNX2-specific antibody is indistinguishable between WT and DKO mice. *Scale bar* = 20 μm

Despite these weight differences, no mice of any genotype showed signs of ill health. Extensive primary observational testing following a modified SHIRPA protocol, as well as grip strength and hotplate tests, did not reveal significant differences between genotypes for any of 36 parameters assessed (see "Materials and Methods" section). While the weight differences between genotypes must be borne in mind, they should not preclude interpretation of other behavioural tests described below, given the absence of any other physical abnormalities or ill health in *Lnx* DKO mice.

Open Field Test

The exploratory and locomotor activity of WT, DHET and DKO mice was examined by monitoring mice in an open field (Fig. 5). In male mice, no overall effect of genotype was found in total distance travelled ($F_{2,31} = 1.322$, $p = 0.2813$; Fig. 5a) or average speed of movement ($F_{2,31} = 1.255$, $p = 0.2993$; Fig. 5b). However, one-way ANOVA indicated a significant overall effect of genotype on the number of entries into ($F_{2,31} = 5.681$, $p = 0.0079$; Fig. 5c) and time spent in the centre area of the open field arena ($F_{2,31} = 8.910$, $p = 0.0009$; Fig. 5d). Bonferroni post hoc analysis revealed that DKO mice entered the centre area of the arena more frequently than their WT and DHET counterparts and spent significantly more time there ($p < 0.01$). Furthermore, one-way ANOVA indicated a significant overall effect of genotype for the time spent in the corners of the arena ($F_{2,31} = 4.694$, $p = 0.0166$; Fig. 5f). Bonferroni post hoc test revealed that DKO spent significantly less time in the corners than either WT or DHET mice ($p < 0.05$). No difference in the number of corner entries was observed ($F_{2,31} = 0.1019$, $p = 0.9034$; Fig. 5e).

With regard to females, significant overall differences between genotypes were observed in the total distance travelled ($F_{2,31} = 9.402$, $p = 0.0006$; Fig. 5a) in the open field arena, as revealed by one-way ANOVA. Bonferroni post hoc test indicated that DHET and DKO mice travelled significantly less ($p < 0.001$ and $p < 0.05$ respectively) and, in the case of

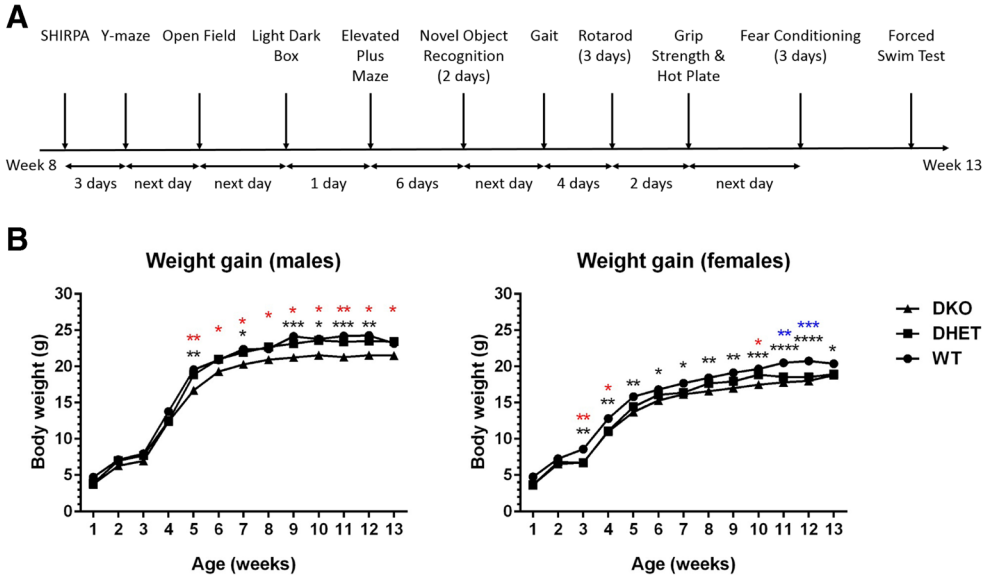

Fig. 4 Timeline of behavioural testing and body weight analysis. **a** Timeline illustrating the sequence of behavioural testing and intervals between tests for both male and female mice. **b** Effect of LNX1/LNX2 genotype on body weight gain during postnatal development. Body weights of mice were recorded weekly for the duration of the study. Initially, body weights were not different between genotypes of either sex. However, from 5 and 3 weeks of age respectively, DKO male (*left*) and female (*right*) mice weighed significantly less than their WT and DHET counterparts, and this difference in body weight persisted for the indicated period of analysis. n = 7–12/group. *$p < 0.05$, **$p < 0.01$, ***$p < 0.001$, ****$p < 0.0001$; two-way repeated measures ANOVA followed by Bonferroni post hoc test (*black* WT versus DKO, *red* DHET versus DKO, *blue* WT versus DHET)

DHET, at a significantly slower average speed ($p < 0.05$) than WT controls, reflecting hypoactivity. No significant difference in the number of centre entries was detected among genotypes ($F_{2,31} = 0.2967$, $p = 0.7453$; Fig. 5c). Although DHET and

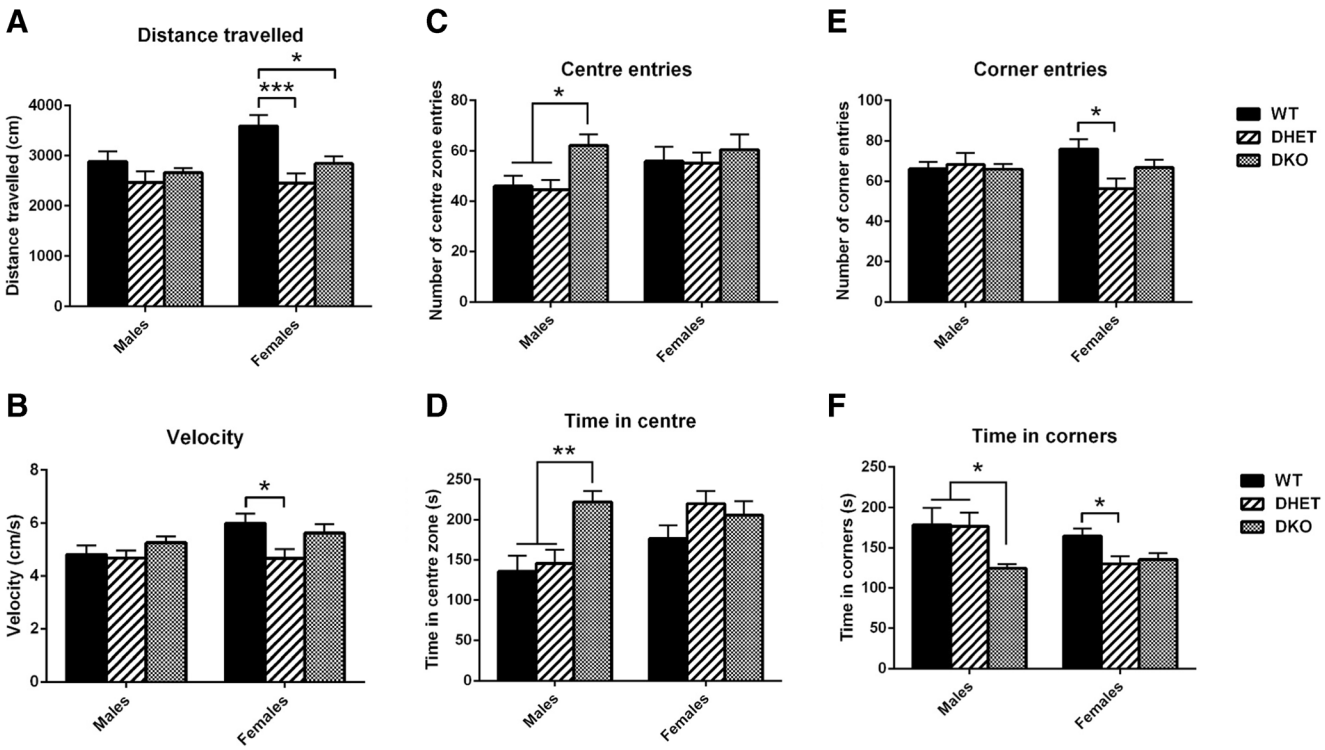

Fig. 5 Effect of *Lnx* genotype on spontaneous locomotor activity and anxiety-related behaviour in the open field task. Mice of the indicated genotypes were placed in the centre of the arena and allowed to move freely for 10 min. Distance travelled (**a**) and velocity (**b**) were analysed as indices of general locomotor activity. The number of entries into, and amount of time spent in, the centre (**c**, **d**) versus the corners (**e**, **f**) of the open field arena were monitored as indicators of differences in anxiety-like behaviour. n = 10–13/group. *$p < 0.05$, **$p < 0.01$, ***$p < 0.001$; one-way ANOVA followed by Bonferroni post hoc test

DKO mice tended to spend an increased amount of time in the centre area compared to WT controls, the effect of genotype was not significant ($F_{2,31}$ = 1.745, p = 0.1913; Fig. 5d). A significant overall effect of genotype was detected in the number of corner entries ($F_{2,31}$ = 4.262, p = 0.0232; Fig. 5e) and time spent in the corners of the arena ($F_{2,31}$ = 4.283, p = 0.0228; Fig. 5f), as indicated by one-way ANOVA. Post hoc analysis revealed that DHET mice entered the corners of the arena less frequently ($p < 0.05$) and spent less time there ($p < 0.05$) than WT controls. A similar trend, though not statistically significant, was observed for DKO mice. Overall, the observation that DKO male mice spend more time in the centre and less time in the corners of the open field arena is indicative of reduced anxiety-like behaviour. Interpretation of similar trends that were seen for female DHET and DKO mice is complicated by the reduced overall locomotor activity of females of these genotypes in the open field test. Nevertheless, it is interesting to look at other tests that relate to anxiety.

Elevated Plus Maze Test

The elevated plus maze is used to analyse anxiety-related behaviour based on a preference for rodents to explore and spend time in the 'safer' environment of the closed versus the open arms of the maze [24]. For male mice, a significant effect of genotype was detected for the percentage of entries into ($F_{2,31}$ = 8.891, p = 0.0009; Fig. 6a) and the time spent in the open arms ($F_{2,31}$ = 21.03, $p \leq 0.0001$; one-way ANOVA; Fig. 6d). Bonferroni post hoc analysis revealed that DKO mice entered the open arms more frequently ($p < 0.001$ and $p < 0.05$) and spent significantly more time in the open arms ($p < 0.0001$ and $p < 0.001$) when compared to WT and DHET counterparts respectively, consistent with a phenotype characterized by a reduced anxiety-like behaviour. Conversely, significant effects of genotype on the percentage of entries into ($F_{2,31}$ = 8.891, p = 0.0009; Fig. 6b) and the time spent in the closed arms ($F_{2,31}$ = 13.77, p = <0.0001; Fig. 6e) were observed, with DKO mice displaying a significantly lower percentage of closed arm entries ($p < 0.001$ and $p < 0.05$) and significantly less time spent in the closed arms ($p < 0.001$) compared to WT and DHET mice respectively. One-way ANOVA indicated a significant overall effect of genotype on total number of arm entries ($F_{2,31}$ = 6.407, p = 0.0047; Fig. 6c). Bonferroni post hoc test revealed that DHET mice exhibited a significantly lower number of total entries in comparison to WT and DKO counterparts ($p < 0.05$ and $p < 0.01$ respectively). No difference in the total number of arm entries was

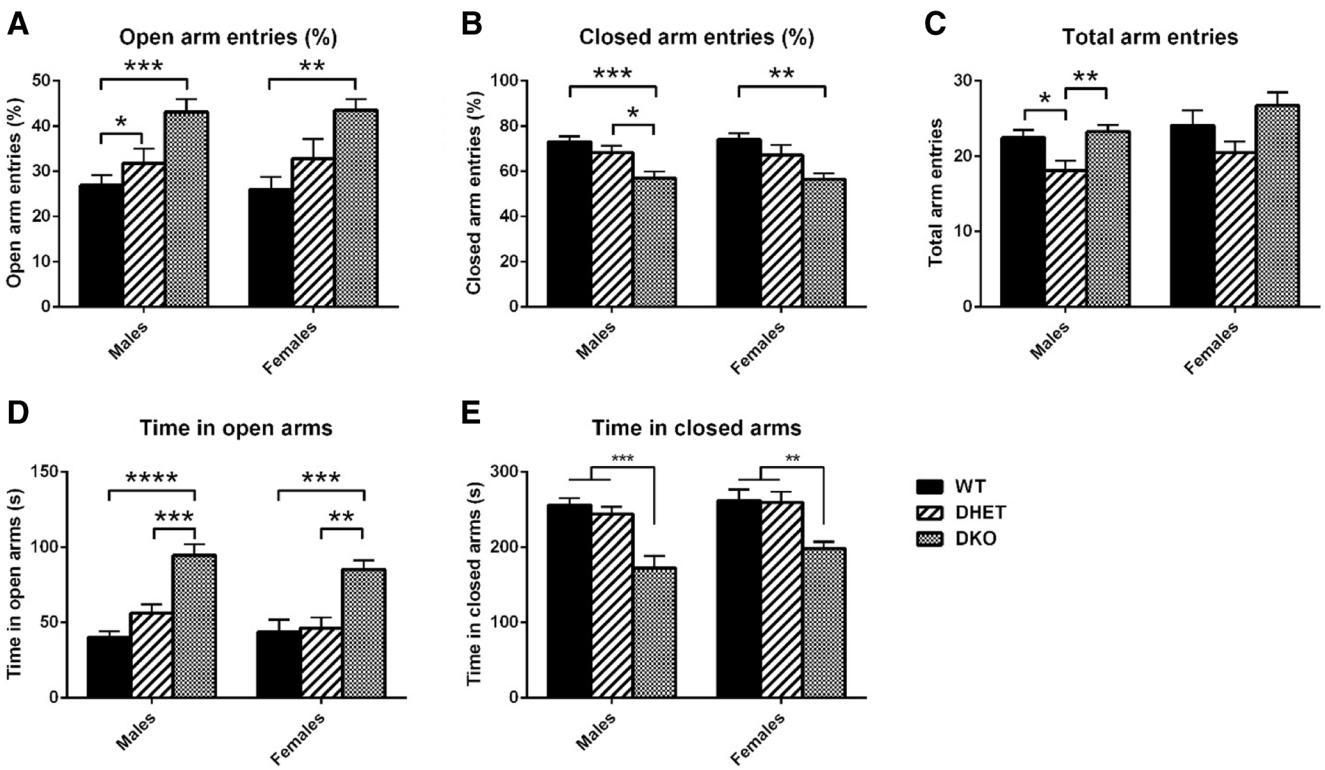

Fig. 6 Effect of *Lnx* genotype on anxiety-related behaviour in the elevated plus maze. Mice of all genotypes were tested for 6 min on the elevated plus maze. **a** Percentage of entries into the open arms, **b** percentage of entries into the closed arms, **c** total arm entries, **d** time spent in the open arms and **e** time spent in the closed arms are shown. Increased entries into, and time spent in the open versus the closed arms are indicative of reduced anxiety-like behaviour. The total number of entries is an index of general locomotor activity during the task. n = 10–13/group. *$p < 0.05$, **$p < 0.01$, ***$p < 0.001$, ****$p < 0.0001$; one-way ANOVA followed by Bonferroni post hoc test

observed between WT and DKO mice, however, confirming that the behavioural variability between these genotypes was not as a result of differences in their locomotor activity.

With regard to female mice, significant overall differences in the percentage of entries ($F_{2,31} = 7.362$, $p = 0.0024$; Fig. 6a) and time spent in the open arms ($F_{2,31} = 10.70$, $p = 0.0003$; Fig. 6d) of the elevated plus maze were also observed, as indicated by one-way ANOVA. Bonferroni post hoc analysis revealed that DKO mice showed a significant increase in the percentage of entries into the open arms compared to WT controls ($p < 0.01$) and an increase in the time spent in the open arms compared to WT and DHET counterparts respectively ($p < 0.001$ and $p < 0.01$). Furthermore, no differences in the total number of entries were observed ($F_{2,31} = 3.284$, $p < 0.0509$; Fig. 6c). One-way ANOVA revealed a significant effect of genotype on the percentage of entries into ($F_{2,31} = 7.362$, $p = 0.0024$; Fig. 6b) and the time spent ($F_{2,31} = 8.137$, $p = 0.0014$; Fig. 6e) in the closed arms of the elevated plus maze. The post hoc test indicated that DKO mice entered the closed arms less often than WT mice ($p < 0.01$) and spent less time there ($p < 0.01$) than either WT or DHET mice.

Light–Dark Box Test

The light–dark box exploration paradigm, which is based on the innate aversion of rodents to brightly illuminated areas and their spontaneous exploratory behaviour, is used primarily to detect anxiogenic behaviour [24]. In this test, there were no significant overall differences between male genotypes in latency to first enter the dark compartment ($F_{2,32} = 0.07835$, $p = 0.9248$; Fig. 7a), number of light–dark transitions ($F_{2,32} = 2.501$, $p = 0.0979$; Fig. 7c) or total time spent in the light compartment ($F_{2,32} = 0.2197$, $p = 0.8040$; Fig. 7b), as revealed by one-way ANOVA. There were also no significant effects of genotype among females on latency to first enter the dark chamber ($F_{2,31} = 0.9406$, $p = 0.4012$; Fig. 7a) or total number of light–dark transitions ($F_{2,31} = 0.7211$, $p = 0.4947$; Fig. 7c). Female DKO mice did however tend to spend more time in the light compartment when compared to WT and DHET counterparts, but this difference was only marginally significant ($F_{2,31} = 3.250$, $p = 0.0533$; Fig. 7b), as revealed by one-way ANOVA.

Rotarod Test

Motor coordination and skill learning were evaluated in an accelerating rotarod test. As seen in Fig. 8a, the performance of both male and female mice of all genotypes improved on the second and third days of testing, with mice remaining on the rotarod for longer durations compared to the first day of testing ($F_{2,72} = 24.74$, $p = <0.0001$ and $F_{2,58} = 9.850$, $p = 0.0002$ for males and females respectively in the overall rANOVA). Bonferroni post hoc tests revealed that the improved performance of males from day 1 to day 3 was significant for all genotypes, while those from day 1 to day 2 were significant for DKO and DHET but not WT animals ($p < 0.05$). Rotarod performance on day 1 was much better for females compared to males, and improvements across testing days was

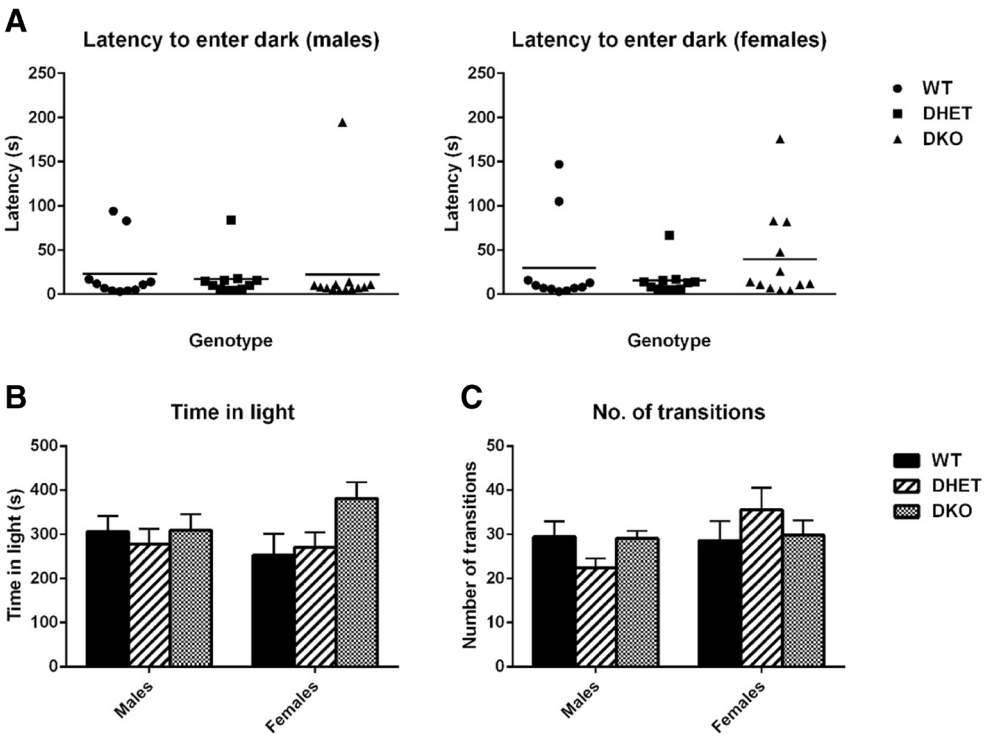

Fig. 7 Effect of *Lnx* genotype on anxiety-related behaviour in the light/dark box. Mice were placed in the lighted compartment of the light–dark box apparatus, and latency to enter the dark compartment (**a**), time in light compartment (**b**) and the number of transitions between the light and dark compartments (**c**) were recorded for mice of the indicated genotypes and sex. Data are displayed in **a** as mean with individual data points. Analysis by one-way ANOVA did not reveal any significant effects of genotype on the parameters measured. $n = 10–13$/group

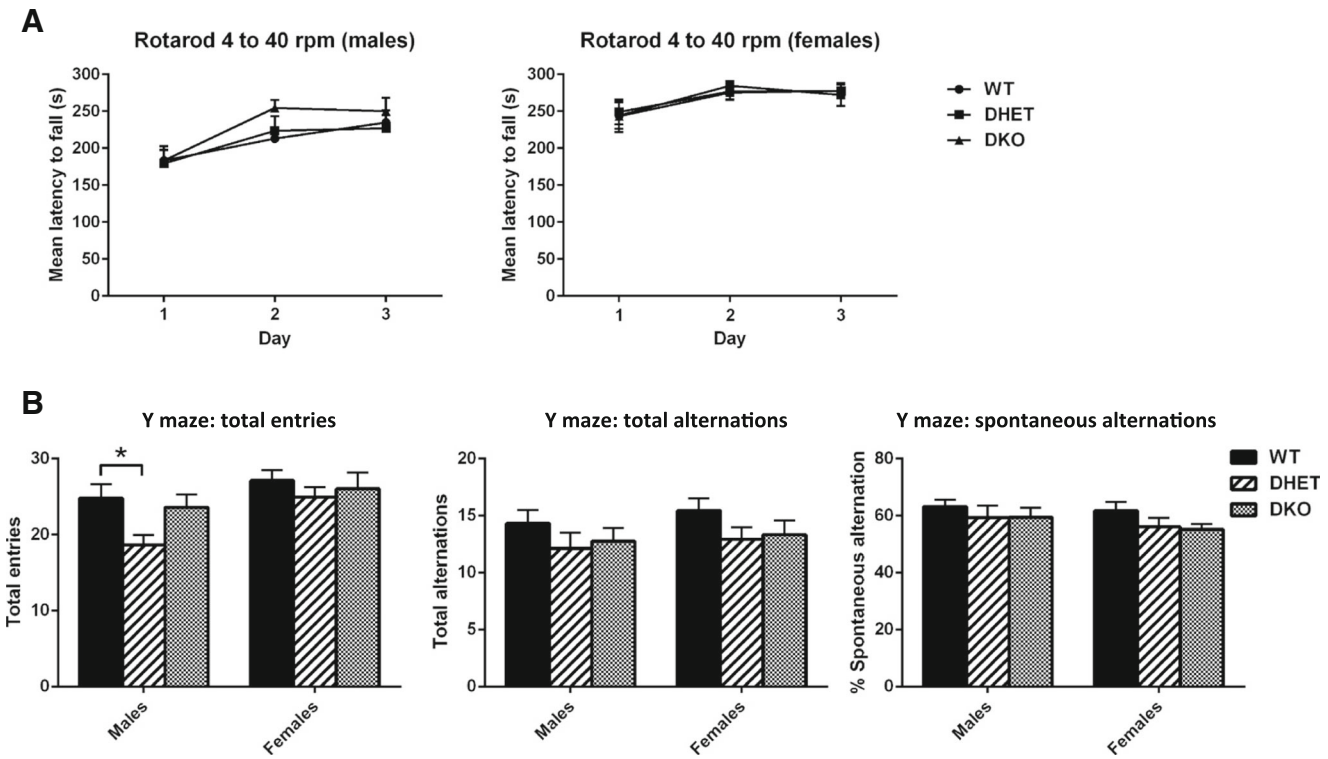

Fig. 8 Effect of *Lnx* genotype on learning, memory and motor coordination. **a** Analysis of motor skill learning and coordination in the accelerating rotarod test. Male (*left*) and female (*right*) mice of the indicated genotypes were placed onto an accelerating rotarod, and their latency to fall was measured in three trials per day, for three consecutive days. There were no significant differences between genotypes for either sex on any of the days as assessed by repeated measures two-way ANOVA. Improved performance on days 2 and 3 is indicative of normal motor skill learning in the task (see text). n = 9–13/group. **b** Analysis of spontaneous alternation behaviour in the Y-maze. Total entries into the arms of the maze were measured as an index of locomotor activity in the task. The number and percentage of alternations—instances where the mouse visits all three arms in sequence—were monitored as a measure of short-term spatial working memory. n = 10–13/group. *$p < 0.05$; one-way ANOVA followed by Bonferroni post hoc test

significant only for WT mice from day 1 to day 2 and DKO mice from day 1 to day 3 ($p < 0.05$). There was no overall difference between genotypes, however ($F_{2,36} = 0.9243$, $p = 0.4060$ and $F_{2,29} = 0.01303$, $p = 0.9871$ for males and females respectively), and no significant genotype by day interaction on latency to fall from the apparatus ($F_{4,72} = 0.7746$, $p = 0.5453$ and $F_{4,58} = 0.1860$, $p = 0.9448$ for males and females respectively). These observations indicate that both motor coordination and motor skill learning, as assessed by performance on the rotarod, are intact in all genotypes for both male and female mice. In agreement with this, paw print analysis did not reveal any major defects in gait (data not shown).

Y-Maze Test

Short-term spatial working memory was examined by monitoring spontaneous alternation behaviour in the Y-maze, a hippocampus-dependent learning task (Fig. 8b). This test relies on the inherent tendency of mice to enter a less recently visited arm of the Y-maze. If working memory is impaired, mice will fail to remember the positions of the arms just visited and the number of alternations will be reduced [25]. Total arm entries serve as a measure of overall exploratory activity in this task. A significant overall difference between genotypes was observed in total arm entries in male mice ($F_{2,30} = 3.689$, $p = 0.0370$; Fig. 8b, left panel), with DHET mice displaying significantly less arm entries when compared to WT controls ($p < 0.05$). However, no differences in total arm entries were observed between male WT and DKO mice, indicating comparable exploratory activities between these two groups. No effect of genotype was detected in total alternations for male mice ($F_{2,30} = 0.7880$, $p = 0.4642$; Fig. 8b, middle panel). There were no overall differences between genotypes in the percentage of spontaneous alternations ($F_{2,30} = 0.4270$, $p = 0.6564$; Fig. 8b, right panel). With regard to females, there was no significant overall effect of genotype on the total number of arm entries ($F_{2,29} = 0.3615$, $p = 0.6997$; Fig. 8b, left panel), indicating comparable exploratory activity across groups. Again, no significant overall differences in total alternations ($F_{2,29} = 1.294$, $p = 0.2896$; Fig. 8b, middle panel) or in alternation percentage ($F_{2,29} = 1.559$, $p = 0.2275$; Fig. 8b, right panel) were detected. Alternation performances across genotypes were well above the random performance level of 50% for both sexes. These results indicate that there is no effect of *Lnx* genotype on spatial working memory in this task for either male or female mice.

Identification of Novel Neuronal LNX1- and LNX2-Interacting Proteins

We next sought to identify LNX-interacting proteins other than NUMB that may mediate the neuronal functions of LNX1 and LNX2, including the altered anxiety-like behaviours noted above. While many LNX-interacting proteins are known, most were found by yeast two-hybrid assays and protein/peptide arrays, and only a minority of these have been confirmed in mammalian cells using full-length proteins. Noting that a large proportion of previously reported LNX1 and LNX2 interactions involve their second PDZ domain [13, 14], we reasoned that analysis of PDZ2 may thus be sufficient to capture a significant fraction of all LNX1- and LNX2-interacting proteins. To compare the range of ligands that bind LNX1 and LNX2 PDZ2 in a neural context, we purified recombinant GST-tagged PDZ2 domains and used these proteins to 'pull down' interacting proteins from mouse brain lysates. Proteins identified by mass spectrometry as interacting with the PDZ domains, but not the GST tag alone, are listed in Table 1 (full lists available online in Supp. Tables 1 and 2). The known LNX-interacting proteins ERC1 and ERC2 were abundant components of both LNX1 and LNX2 complexes, as were several novel proteins such as

Table 1 Proteomic analysis of LNX1 and LNX2 PDZ2 domain interactomes

Gene symbol	Mascot score	Gene name	Carboxyl terminus
A. GST-LNX1-PDZ2-interacting proteins purified from mouse brain lysates			
Erc1[a]	7959	ELKS/Rab6-interacting/CAST family member 1	DQDEEEGIWA
Ppfia3	4094	Liprin-alpha-3	DGVSVRTYSC
Erc2[a]	2235	ELKS/Rab6-interacting/CAST family member 2	DQDDEEGIWA
Lrrc16a[a]	2180	Leucine-rich repeat-containing protein 16A	EEAEKEFIFV
Fchsd2[a]	2109	FCH and double SH3 domains protein 2	KMEDVEITLV
Ppfia4	1549	Liprin-alpha-4	EPSTVRTYSC
Fermt2[a]	1467	Fermitin family homologue 2	MFYKLTSGWV
Ppfia2	1441	Liprin-alpha-2	DNSTVRTYSC
Ppfia1	1358	Liprin-alpha-1	DSATVRTYSC
Ppp2r5d	968	Protein phosphatase 2A B56 delta subunit	TGSRNGREGK
Prkcc	843	Protein kinase C gamma type	PTSPVPVPVM
Akap11[a]	792	A-kinase anchor protein 11	ANRLQTSMLV
Ndrg3	749	N-myc downstream regulated gene NDRG3	DRHQTMEVSC
Ppp2r5c	724	Serine/threonine-protein phosphatase 2A 56 kDa regulatory subunit gamma isoform	ASELLSQDGR
Pafah1b1[a]	710	Platelet-activating factor acetylhydrolase IB subunit alpha	DQTVKVWECR
B. GST-LNX2-PDZ2-interacting proteins purified from mouse brain lysates			
Erc1[a]	3181	ELKS/Rab6-interacting/CAST family member 1	DQDEEEGIWA
Sphkap[a]	2692	A-kinase anchor protein SPHKAP	EQKERTPSLF
Lrrc16a[a]	2270	Leucine-rich repeat-containing protein 16A	EEAEKEFIFV
Fchsd2[a]	1938	FCH and double SH3 domains protein 2	KMEDVEITLV
Srgap2	1935	SLIT-ROBO Rho GTPase-activating protein 2	PQATDKSCTV
Akap11[a]	1576	A-kinase anchor protein 11	ANRLQTSMLV
Fermt2[a]	1287	Fermitin family homologue 2	MFYKLTSGWV
Erc2[a]	1139	ELKS/Rab6-interacting/CAST family member 2	DQDDEEGIWA
Atp2a2	1125	SERCA2B of sarcoplasmic/endoplasmic reticulum Ca^{++} ATPase2	DTNFSDMFWS
Rrbp1	1059	Rrbp1 ribosome-binding protein 1 isoform a	GSSSKEGTSV
Kazn[a]	560	Isoform 1 of Kazrin	GYGSLEVTNV
Eml3	549	Eml3 echinoderm microtubule-associated protein-like 3	SLSPASSLDV
Prkar1b[a]	507	cAMP-dependent protein kinase type I-beta regulatory subunit	RYNSFISLTV
Prkar1a[a]	504	cAMP-dependent protein kinase type I-alpha regulatory subunit	QYNSFVSLSV
Ktn1	500	Ktn1 uncharacterized protein	EVNQQLTKET

Selected proteins, ranked by Mascot score, are shown for each experiment. Full tables are available as supplementary material. Previously known interactions are underlined, as are carboxyl-terminal cysteines

[a] A protein identified as interacting with both LNX1 and LNX2 PDZ2 domains

LRRC16A, FCHSD2, FERMT2, SHPKAP and AKAP11. LIPRIN-α proteins (PPFIA1, PPFIA3 and PPFIA4) were identified as LNX1-PDZ2-specific interacting proteins. Putative LNX2-PDZ2-specific interactions included SRGAP2, ATP2A2 and EML3.

We next assessed the ability of a selection of these proteins to interact with full-length LNX1 and LNX2 proteins using GFP pull-down assays, employing GFP-tagged LNX proteins expressed in cultured cells (Fig. 9). LIPRIN-α proteins again bound specifically to LNX1 in this assay, while FCHSD2, SRGAP2, ERC1 and ERC2 interacted with both full-length LNX1 and LNX2. Notably, SRGAP2 was able to interact with full-length LNX1, even though it was only detected in LNX2–PDZ2 and not LNX1–PDZ2 complexes from brain lysates. By contrast, the FERMT2 interaction could not be confirmed with full-length LNX1 or LNX2 proteins. Overall, our GST pull-down analysis of LNX PDZ2 domains identified 58 putative LNX1-specific, 39 putative LNX2-specific and 26 apparently common interactions (Supp. Tables 1 and 2). However, verification of these interactions and their specificity using full-length LNX1 and LNX2 proteins is clearly necessary.

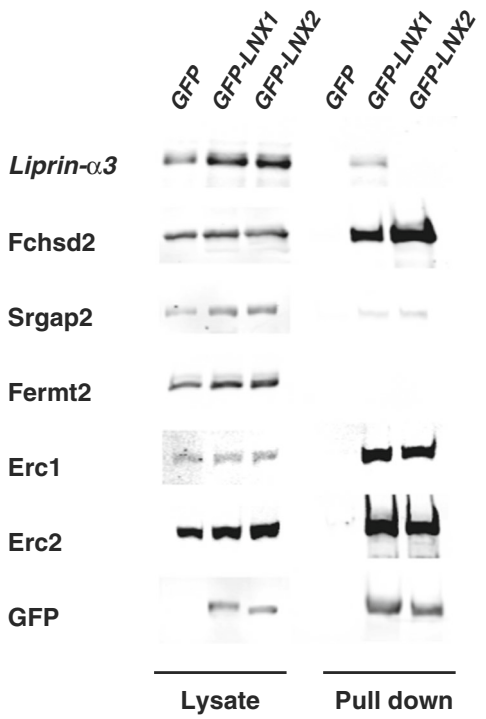

Fig. 9 Verification of the ability of candidate interacting proteins to bind full-length LNX1 and/or LNX2. Selected proteins that co-purified with either LNX1-PDZ2 or LNX2-PDZ2 from brain lysates were tested for their ability to interact with full-length, GFP-tagged LNX1 and/or LNX2 constructs following co-transfection into HEK293 cells. Following a GFP 'pull-down' assay, LNX-interacting proteins were detected by western blotting via either a FLAG epitope tag or using an antibody to detect endogenous protein in the case of LIPRIN-α3. GFP alone was used as a negative control (not visible on blots due to its low molecular weight)

Discussion

The function of LNX proteins in vivo remains unknown, largely because LNX proteins are present at exceedingly low levels in most adult tissues. *Lnx1* and *Lnx2* mRNAs are expressed prominently in the CNS during embryonic development, with strong *Lnx2* mRNA expression in the forebrain being particularly noteworthy [2]. Here, we show that both LNX1 and LNX2 proteins are present in the juvenile murine brain, albeit at low levels. LNX2 protein is detectable at embryonic and early postnatal stages, but decreases dramatically thereafter. Given that *Lnx2* mRNA expression persists into adulthood, the downregulation of LNX2 expression seems to be occurring post-transcriptionally, possibly at the level of translation as has been described for LNX1 [2, 11], although a high protein turnover rate may also contribute to the low levels of LNX proteins observed in vivo.

Since LNX proteins interact with and can ubiquitinate and promote the proteasomal degradation of the key cell fate-determinant protein NUMB [2–5], we hypothesized that they may play a role in regulating neuronal development or function in some way. Here, we sought to test this hypothesis by generating *Lnx* DKO mice, in which expression of all CNS LNX protein isoforms is eliminated. In these mice, LNX2 is expected to be eliminated globally in all tissues, while the loss of LNX1 is expected to be restricted to the exon 3-containing, CNS-specific LNX1 p70 and p62 isoforms. In agreement with this, we previously noted intact immunostaining for what is presumed to be the LNX1 p80 isoform in perisynaptic Schwann cells in the PNS of these $Lnx1^{exon3-/-}$ mice [11, 17]. *Lnx* DKO mice are viable and fertile and display no overt phenotype, apart from weighing approximately 10% less than WT animals by adulthood. This weight difference only became noticeable at, or soon after, weaning age and could be a consequence of some function of LNX2 outside the CNS. Tooth development appeared to be normal, and DKO animals showed no difficulty eating, so perhaps a role for LNX2 in the gut or in regulating some aspect of metabolism could be responsible. However, DKO mice seem completely healthy despite their slightly lower body weight and thus represent a valid model to examine neuronal functions of LNX proteins.

NUMB and NUMBLIKE regulate multiple aspects of neural development, from early embryonic through postnatal stages. During early mouse cortical neurogenesis, asymmetric localization of NUMB in dividing ventricular cells promotes an undifferentiated progenitor cell fate [29, 30], but at later developmental stages or in other cellular contexts, NUMB has been shown to promote neuronal differentiation [31–33]. While NUMB and NUMBLIKE have a well-established role as negative regulators of Notch signalling, some aspects of their neuronal functions are thought to be Notch-independent, mediated via regulation of hedgehog signalling and cadherin-based cell adhesion [7]. NUMB knockout in mice causes a

failure of neural tube closure and is lethal by E11.5, while NUMB/NUMBLIKE double knockout embryos are more severely affected and die by E9.5 [29, 33, 34]. Various studies employing conditional knockout of NUMB, often in a NUMBLIKE null background, have highlighted essential roles for NUMB/NUMBLIKE in regulating neural progenitor cell maintenance, cortical development, organization and lamination, ventricular size, cerebellar granule cell maturation and migration and SVZ formation [9, 29, 31, 35–37]. *Lnx2* mRNA is expressed as early as E11.5 in the neuroepithelium [2], and we have shown here that LNX2 protein is expressed in the brain from E14.5 to P7. A role for LNX2 in negatively regulating NUMB levels during the later stages of cortical neurogenesis thus seems plausible. However, we do not observe any defects in gross neuroanatomy in DKO mice and cortical organization and lamination appear normal. Similarly, we did not note any malformation of cell layers in the cerebellum, another region with strong *Lnx1* and *Lnx2* mRNA expression and one where NUMB has been shown to regulate granule cell maturation and migration [2, 31].

We also examined the development of the neurogenic SVZ—an early postnatal NUMB-dependent process [9]. Conditional NUMB/NUMBLIKE knockout mice show severe damage to, and enlargement of, the lateral ventricles, and a recent report has implicated LNX2 in regulating NUMB levels in the SVZ in the context of *Gli3* knockout mice [9, 10]. The Gli3 transcriptional repressor is a sonic hedgehog signalling component that was shown to be required for cell-type specification and structural organization in the developing SVZ, phenocopying to a degree, NUMB loss-of-function mutants. Indeed, $Gli3^{-/-}$ mice were reported to have dramatically reduced forebrain NUMB protein levels [10]. This finding was attributed to upregulation of LNX2 in the SVZ of these mice; however, a causal relationship between LNX2 and NUMB levels in $Gli3^{-/-}$ mice remains to be established. In any case, our data suggest that SVZ zone formation and ependymal cell differentiation proceed normally in *Lnx* DKO mice and that LNX2 at normal expression levels is not affecting NUMB function in SVZ formation. These findings are in agreement with the observation of unaltered levels of any NUMB protein isoforms in *Lnx* DKO mice. It has been found that while LNX1 is able to interact with all four NUMB isoforms, only those containing a short sequence insertion in the PTB domain (p66 and p72) are ubiquitinated by LNX1 [3]. Thus, we would not necessarily expect LNX to regulate levels of NUMB p65 or p71, assuming that the same specificity with regard to NUMB ubiquitination applies to LNX2. However, even the levels of NUMB p66, which should be prone to LNX-mediated ubiquitination, are unaltered in DKO mice. This suggests that endogenous LNX2 expression levels are not sufficient to promote ubiquitin-mediated degradation of NUMB or that LNX2 and NUMB are not widely co-expressed in the same cells in vivo. We cannot rule out however that some LNX-mediated degradation of NUMB may occur in a temporally or spatially restricted manner. Unfortunately, we could not detect LNX2 by immunostaining to address this issue. Overall though, our analysis of *Lnx* DKO animals does not provide any direct evidence that LNX proteins are major regulators of NUMB in vivo, since no obvious defects in NUMB-dependent processes are observed.

Given this lack of evidence for NUMB dysregulation, we proceeded to conduct behavioural phenotyping of *Lnx* DKO mice. Since there are few clues in the literature regarding neuronal functions of LNX proteins in vivo, we performed a battery of tests to screen for a broad range of potential phenotypes. The main phenotype identified was one of reduced anxiety-like behaviour. This was assessed in three approach-avoidance paradigms: the open field test, the light–dark box test and the elevated plus maze. These tests are based on the conflict between the innate exploratory behaviour of rodents and their aversion towards open, bright or elevated spaces, which carry an associated risk of predation [24]. The anxiolytic phenotype was very robust in the elevated plus maze, with DKO mice of both sexes exhibiting increased entries into, and time spent in, the open arms of the maze. Male DKO animals also spent more time exploring the centre versus the corners of the arena in the open field test. A similar trend was observed for females in the open field, but this data was confounded by the fact that DHET and DKO females showed less overall locomotor activity in this task. By contrast, no effect of *Lnx* genotype was seen for either sex in latency to enter the dark compartment, the number of transitions between light and dark sides or time spent in the light compartment in the light–dark box test. While obtaining consistent findings across multiple tests is generally strong evidence for a particular phenotype, it is recognized that various tests of anxiety in rodents do not measure exactly the same psychological phenomenon. Rather, each test can be regarded as measuring overlapping, but partially distinct, aspects of anxiety-related behaviour [24]. Thus, knockout models with both anxiogenic and anxiolytic phenotypes that are specific to particular tests have previously been reported [21, 38]. Overall, reports on transgenic and knockout mice with reduced anxiety-like behaviour are not uncommon in the literature, though anxiolytic indications are sometimes found in combination with other behavioural deficits [39]. *Lnx* DKO mice did not show any deficiencies in basic motor function, or in motor coordination or motor skill learning as assessed by the rotarod test, despite the fact that *Lnx1* and *Lnx2* mRNAs are expressed in the motor cortex, spinal cord and cerebellum [2, 11] and the observation that Numb can influence these behaviours [40]. Sensory function and spatial working memory, as measured by spontaneous alternation in the Y-maze, were also unaffected. Thus, the reduced anxiety-like behaviour observed for DKO mice seems to be a very specific phenotype that is restricted to a subset of anxiety-related testing paradigms.

The anxiolytic phenotype reported here for *Lnx* DKO mice clearly merits further investigation. Genetic analyses will determine if either *Lnx1* or *Lnx2* single knockout animals display the same phenotype or whether the simultaneous loss of both genes is responsible. The use of conditional approaches to spatially restrict knockout of one or both genes should allow the brain region(s) responsible for the phenotype to be identified. Temporally restricted *Lnx* knockout could address the question of whether the phenotype arises from a developmental defect or from the absence of LNX proteins from the adult brain at the time of behavioural testing. It will also be interesting to subject *Lnx* DKO mice to a wider array of behavioural tests that may be able, for example, to dissociate decreased anxiety-related behaviour from any increased novelty seeking or impulsivity that could contribute to increased time spent in novel, aversive areas in the open field and elevated plus maze paradigms [24]. More extensive testing may also reveal phenotypes beyond the decreased anxiety-related behaviour described here. Finally, examining the effects of known anxiogenic or anxiolytic pharmacological agents in *Lnx* DKO mice might identify neurotransmitter systems or signalling pathways responsible for the reduced anxiety-like phenotype. Studies of the type outlined above should determine whether LNX proteins could represent novel drug targets, whereby selective blockade of LNX function or expression would have therapeutic potential in anxiety disorders.

It is important to elucidate the neurobiological circuits and pathways that are altered by ablation of *Lnx1* and *Lnx2* in DKO mice, generating the anxiolytic-like phenotype. Although we found no change in NUMB levels in DKO mice, we cannot rule out that this phenotype may be attributed to the interaction of LNX proteins with NUMB. For example, LNX could regulate NUMB by mechanisms other than promoting its proteasomal degradation, such as altering its subcellular localization. Indeed, the absence of the RING domain from neuronal LNX1 isoforms suggests ubiquitination-independent functions [1, 11]. Nevertheless, given the absence of obvious NUMB-related abnormalities in DKO mice, the possibility that LNX functions in the CNS are mediated by interacting proteins other than NUMB needs to be considered. Many LNX1-interacting proteins have been identified [13, 14]. Most of these are PDZ domain ligands, with the second PDZ domain mediating a large proportion of these interactions. However, the physiological relevance of the vast majority of these reported interactions is unclear. Fewer LNX2-interacting proteins have been reported, and the LNX1 and LNX2 interactomes have never been systematically compared. To address these issues, we used an affinity purification/mass spectrometry-based approach to isolate and identify proteins from P16 mouse brain lysates that bind the second PDZ domain of each protein. Five out of six interactions tested could be confirmed with full-length LNX proteins, validating the approach of using a single PDZ domain as a bait to isolate meaningful interactions.

These proteomic results provide confirmation of just four of the approximately 250 previously reported LNX interactions (BCR, CTNND2, ERC2, KRT15) [13, 14]. This partly reflects our focus on just the second PDZ domain and the fact that previously reported proteins may not be expressed in P16 mouse brain tissue. However, it may be that some interaction pairs that have been identified by yeast two-hybrid or protein/peptide arrays are not significant in a physiological context, in which many potential ligands can bind competitively to LNX proteins. Many of the proteins we identified have carboxyl terminal sequences that fit consensus sequences previously identified for LNX1 and LNX2 PDZ2 [14], suggesting that they interact with LNX proteins directly. The identification of putative LNX1 PDZ2-interacting proteins with carboxyl terminal cysteines is particularly noteworthy, with ten such proteins found in LNX1 complexes as compared to just one for LNX2 PDZ2. Notable LNX1-specific interactors with carboxyl terminal cysteines are members of the LIPRIN-α (PPFIA1, PPFIA2, PPFIA3, PPFIA4) and N-myc downstream-regulated gene (NDRG1, NDRG2, NDRG3) families. The LNX1-specific interaction of LIPRIN-α3 was confirmed in assays using full-length LNX proteins. In addition, some indirect interactions are likely to have been detected by our affinity purification approach, which may partly explain the lack of overlap with LNX ligands previously identified using methods that favoured detection of direct interactions. For example, the protein phosphatase 2A regulatory subunits (PPP2R5C and PPP2R5D) lack a carboxyl terminal PDZ-binding consensus sequence but are known to interact with LIPRIN-αs [41, 42]. This suggests that their specific co-purification with LNX1 PDZ2 may be due to an indirect interaction mediated by LIPRIN-α. In any case, such isoform-specific interactions, whether direct or indirect, provide clues regarding differential functions of LNX1 and LNX2—an area that has not previously been explored.

Comparing the lists of 84 LNX1- and 65 LNX2-interacting proteins (Supp. Tables 1 and 2), there is considerable overlap (26 proteins). Notable interactions common to PDZ2 of both LNX1 and LNX2 are the ELKS/Rab6-interacting/CAST family members ERC1 and ERC2. LNX1 is known to interact with ERC2 [43]. Our data confirm this and indicate that this ability is shared by LNX2. Interestingly, ERC and liprin-α proteins interact with each other and are evolutionarily conserved core components of the presynaptic active zone complex that underpins synapse formation and maturation, as well as neurotransmitter release [44, 45]. ERC1/2 and liprin-αs are likely to bind competitively to LNX1–PDZ2; however, LNX1 is known to dimerise [2], and so a LNX1 dimer could potentially form a tripartite complex binding both ERC and liprin-α proteins simultaneously. Higa et al. [43] reported that LNX1 and ERC2 co-localize at nerve terminals in cultured neurons. Our findings that LNX2 also binds ERC1/2 and that LNX1 binds liprin-α now provide further support for a potential function for LNX

proteins at the active zone. While probably not abundant enough to play a structural role, they might regulate some aspect of active zone formation or plasticity. Kazrin (KAZN) was another interaction shared by LNX1 and LNX2 and interestingly has been described as belonging to the LIPRIN protein family [46]. The SLIT-ROBO Rho GTPase-activating proteins, SRGAP1 and SRGAP2, were co-purified with LNX1 and LNX2 PDZ2 domains respectively. However, in confirmatory assays using full-length LNX proteins, SRGAP2 bound both LNX1 and LNX2 and so was not isoform-specific in its interaction. SRGAP2 acts as a regulator of neuronal migration, neurite outgrowth and dendritic spine formation and plays important roles in cortical development, with human-specific duplications of SRGAP2 hypothesized to have played a role in the evolution of the human neocortex [47–50]. FCHSD2, which we identified as binding to both LNX1 and LNX2 via PDZ2, is evolutionarily related to the SRGAP proteins, having in common the presence of an F-BAR and SH3 domains in its domain structure, but lacking the GTPase-activating domain. FCHSD2 is a mammalian homologue of *nervous wreck* (*nwk*)—a regulator of synaptic growth in *Drosophila* [51]. Other putative LNX1- and LNX2-interacting proteins identified include regulatory subunits of protein kinase A (PRKAR1A and PRKAR1B) and a GABA neurotransmitter transporter (SLC6A1). Overall, this analysis confirms the propensity of LNX proteins to interact with a large number of ligands via their PDZ domains and provides a catalogue of putative interacting partners that will be a valuable resource in exploring the molecular mechanism of LNX function in the CNS. Subject to further validation, this brain-specific interactome identifies many plausible candidates that could mediate neuronal functions of LNX proteins in the CNS, including their role in modulating anxiety-related behaviour.

In summary, this is the first study of the in vivo functions of LNX1 and LNX2 in a mammalian context. Zebrafish have an additional LNX paralogue—LNX2b—which has been studied extensively and found to modulate transcription factors involved in dorso-ventral and antero-posterior axis specification during embryogenesis [52–54]. The relatively mild phenotype of *Lnx* DKO mice suggests that mammalian LNX proteins do not have analogous functions to fish LNX2b. While our findings do not provide evidence of a major role for LNX in regulating NUMB during mammalian CNS development, we cannot exclude a subtle role. An unexpected function for LNX proteins in the regulation of anxiety-related behaviour has been revealed. However, the molecular mechanisms and the brain regions underlying this behavioural phenotype need further investigation in order to gain a more complete understanding of LNX protein function in vivo.

Acknowledgements We are extremely grateful to Pat Fitzgerald and James O'Leary for their generous assistance and advice regarding behavioural experiments. We thank Mary McCaffrey (University College Cork) for access to her Science Foundation Ireland-funded confocal microscope and Jane McGlade (University of Toronto) for providing the rabbit anti-LNX1/2-RING/NPAY antibody. This work was supported by a Research Frontiers Programme grant from Science Foundation Ireland (08/RFP/NSC1382) and an Irish Research Council EMBARK Postgraduate Research Scholarship to Joan Lenihan. We thank Tom Moore for access to the EVOS FL Cell Imaging System.

Compliance with Ethical Standards All animal experiments were approved by the Animal Experimentation Ethics Committee of University College Cork (No: 2013/028) and were conducted under licence (No: AE19130/P013) issued by the Health Products Regulatory Authority of Ireland, in accordance with the European Union Directive 2010/63/EU for animals used for scientific purposes.

Conflict of Interest The authors declare that they have no conflict of interest.

References

1. Dho SE, Jacob S, Wolting CD, French MB, Rohrschneider LR, McGlade CJ (1998) The mammalian numb phosphotyrosine-binding domain. Characterization of binding specificity and identification of a novel PDZ domain-containing numb binding protein, LNX. J Biol Chem 273:9179–9187
2. Rice DS, Northcutt GM, Kurschner C (2001) The Lnx family proteins function as molecular scaffolds for Numb family proteins. Mol Cell Neurosci 18:525–540
3. Nie J, Li SS, McGlade CJ (2004) A novel PTB-PDZ domain interaction mediates isoform-specific ubiquitylation of mammalian Numb. J Biol Chem 279:20807–20815
4. Nie J, McGill MA, Dermer M, Dho SE, Wolting CD, McGlade CJ (2002) LNX functions as a RING type E3 ubiquitin ligase that targets the cell fate determinant Numb for ubiquitin-dependent degradation. EMBO J 21:93–102
5. Nayak D, Sivaraman J (2015) Structural basis for the indispensable role of a unique zinc finger motif in LNX2 ubiquitination. Oncotarget 6:34342–34357
6. Camps J et al. (2013) Genetic amplification of the NOTCH modulator LNX2 upregulates the WNT/beta-catenin pathway in colorectal cancer. Cancer Res
7. Gulino A, Di Marcotullio L, Screpanti I (2010) The multiple functions of Numb. Exp Cell Res 316:900–906
8. Weiss A, Baumgartner M, Radziwill G, Dennler J, Moelling K (2007) C-Src is a PDZ interaction partner and substrate of the E3 ubiquitin ligase ligand-of-Numb protein X1. FEBS Lett 581:5131–5136
9. Kuo CT et al (2006) Postnatal deletion of Numb/Numblike reveals repair and remodeling capacity in the subventricular neurogenic niche. Cell 127:1253–1264
10. Wang H, Kane AW, Lee C, Ahn S (2014) Gli3 repressor controls cell fates and cell adhesion for proper establishment of neurogenic niche. Cell Rep 8:1093–1104
11. Lenihan JA, Saha O, Mansfield LM, Young PW (2014) Tight, cell type-specific control of LNX expression in the nervous system, at the level of transcription, translation and protein stability. Gene 552:39–50
12. Flynn M, Saha O, Young P (2011) Molecular evolution of the LNX gene family. BMC Evol Biol 11:235
13. Wolting CD, Griffiths EK, Sarao R, Prevost BC, Wybenga-Groot LE, McGlade CJ (2011) Biochemical and computational analysis of LNX1 interacting proteins. PLoS One 6:e26248

14. Guo Z et al (2012) Proteomics strategy to identify substrates of LNX, a PDZ domain-containing E3 ubiquitin ligase. J Proteome Res 11:4847–4862
15. D'Agostino M, Tornillo G, Caporaso MG, Barone MV, Ghigo E, Bonatti S, Mottola G (2011) Ligand of Numb proteins LNX1p80 and LNX2 interact with the human glycoprotein CD8alpha and promote its ubiquitylation and endocytosis. J Cell Sci 124:3545–3556
16. Takahashi S, Iwamoto N, Sasaki H, Ohashi M, Oda Y, Tsukita S, Furuse M (2009) The E3 ubiquitin ligase LNX1p80 promotes the removal of claudins from tight junctions in MDCK cells. J Cell Sci 122:985–994
17. Young P, Nie J, Wang X, McGlade CJ, Rich MM, Feng G (2005) LNX1 is a perisynaptic Schwann cell specific E3 ubiquitin ligase that interacts with ErbB2. Mol Cell Neurosci 30:238–248
18. Heyer MP, Pani AK, Smeyne RJ, Kenny PJ, Feng G (2012) Normal midbrain dopaminergic neuron development and function in miR-133b mutant mice. J Neurosci 32:10887–10894
19. Heimer-McGinn V, Young P (2011) Efficient inducible Pan-neuronal cre-mediated recombination in SLICK-H transgenic mice. Genesis 49:942–949
20. Schneider CA, Rasband WS, Eliceiri KW (2012) NIH image to ImageJ: 25 years of image analysis. Nat Methods 9:671–675
21. Crawley JN (2008) Behavioral phenotyping strategies for mutant mice. Neuron 57:809–818
22. Irwin S (1968) Comprehensive observational assessment: Ia. A systematic, quantitative procedure for assessing the behavioral and physiologic state of the mouse. Psychopharmacologia 13: 222–257
23. Rogers DC, Fisher EM, Brown SD, Peters J, Hunter AJ, Martin JE (1997) Behavioral and functional analysis of mouse phenotype: SHIRPA, a proposed protocol for comprehensive phenotype assessment. Mamm Genome 8:711–713
24. Cryan JF, Holmes A (2005) The ascent of mouse: advances in modelling human depression and anxiety. Nat Rev Drug Discov 4:775–790
25. Hughes RN (2004) The value of spontaneous alternation behavior (SAB) as a test of retention in pharmacological investigations of memory. Neurosci Biobehav Rev 28:497–505
26. Murphy AC, Lindsay AJ, McCaffrey MW, Djinovic-Carugo K, Young PW (2016) Congenital macrothrombocytopenia-linked mutations in the actin-binding domain of alpha-actinin-1 enhance F-actin association. FEBS Lett 590:685–695
27. Foley KS, Young PW (2013) An analysis of splicing, actin-binding properties, heterodimerization and molecular interactions of the non-muscle alpha-actinins. Biochem J 452:477–488
28. Saha O (2013) Investigation of the function of the LNX family of E3 ubiquitin ligases in the nervous system. PhD Thesis, University College Cork. https://cora.ucc.ie/handle/10468/1195
29. Petersen PH, Zou K, Hwang JK, Jan YN, Zhong W (2002) Progenitor cell maintenance requires numb and numblike during mouse neurogenesis. Nature 419:929–934
30. Zhong W, Feder JN, Jiang MM, Jan LY, Jan YN (1996) Asymmetric localization of a mammalian numb homolog during mouse cortical neurogenesis. Neuron 17:43–53
31. Klein AL, Zilian O, Suter U, Taylor V (2004) Murine numb regulates granule cell maturation in the cerebellum. Dev Biol 266:161–177
32. Shen Q, Zhong W, Jan YN, Temple S (2002) Asymmetric Numb distribution is critical for asymmetric cell division of mouse cerebral cortical stem cells and neuroblasts. Development 129: 4843–4853
33. Zilian O, Saner C, Hagedorn L, Lee HY, Sauberli E, Suter U, Sommer L, Aguet M (2001) Multiple roles of mouse Numb in tuning developmental cell fates. Curr Biol 11:494–501
34. Zhong W, Jiang MM, Schonemann MD, Meneses JJ, Pedersen RA, Jan LY, Jan YN (2000) Mouse numb is an essential gene involved in cortical neurogenesis. Proc Natl Acad Sci U S A 97:6844–6849
35. Li HS et al (2003) Inactivation of Numb and Numblike in embryonic dorsal forebrain impairs neurogenesis and disrupts cortical morphogenesis. Neuron 40:1105–1118
36. Petersen PH, Zou K, Krauss S, Zhong W (2004) Continuing role for mouse Numb and Numbl in maintaining progenitor cells during cortical neurogenesis. Nat Neurosci 7:803–811
37. Rasin MR et al (2007) Numb and Numbl are required for maintenance of cadherin-based adhesion and polarity of neural progenitors. Nat Neurosci 10:819–827
38. Butler K, Martinez LA, Tejada-Simon MV (2013) Impaired cognitive function and reduced anxiety-related behavior in a promyelocytic leukemia (PML) tumor suppressor protein-deficient mouse. Genes Brain Behav 12:189–202
39. Semenova S, Contet C, Roberts AJ, Markou A (2012) Mice lacking the beta4 subunit of the nicotinic acetylcholine receptor show memory deficits, altered anxiety- and depression-like behavior, and diminished nicotine-induced analgesia. Nicotine Tob Res 14:1346–1355
40. Zhou L et al (2015) Numb deficiency in cerebellar Purkinje cells impairs synaptic expression of metabotropic glutamate receptor and motor coordination. Proc Natl Acad Sci U S A 112:15474–15479
41. Arroyo JD, Lee GM, Hahn WC (2008) Liprin alpha1 interacts with PP2A B56gamma. Cell Cycle 7:525–532
42. Liu YC et al (2014) The PPFIA1-PP2A protein complex promotes trafficking of Kif7 to the ciliary tip and Hedgehog signaling. Sci Signal 7:ra117
43. Higa S, Tokoro T, Inoue E, Kitajima I, Ohtsuka T (2007) The active zone protein CAST directly associates with Ligand-of-Numb protein X. Biochem Biophys Res Commun 354:686–692
44. Sudhof TC (2012) The presynaptic active zone. Neuron 75:11–25
45. Ko J, Na M, Kim S, Lee JR, Kim E (2003) Interaction of the ERC family of RIM-binding proteins with the liprin-alpha family of multidomain proteins. J Biol Chem 278:42377–42385
46. Nachat R, Cipolat S, Sevilla LM, Chhatriwala M, Groot KR, Watt FM (2009) KazrinE is a desmosome-associated liprin that colocalises with acetylated microtubules. J Cell Sci 122:4035–4041
47. Guerrier S et al (2009) The F-BAR domain of srGAP2 induces membrane protrusions required for neuronal migration and morphogenesis. Cell 138:990–1004
48. Charrier C et al (2012) Inhibition of SRGAP2 function by its human-specific paralogs induces neoteny during spine maturation. Cell 149:923–935
49. Dennis MY et al (2012) Evolution of human-specific neural SRGAP2 genes by incomplete segmental duplication. Cell 149: 912–922
50. Ma Y, Mi YJ, Dai YK, Fu HL, Cui DX, Jin WL (2013) The inverse F-BAR domain protein srGAP2 acts through srGAP3 to modulate neuronal differentiation and neurite outgrowth of mouse neuroblastoma cells. PLoS One 8:e57865
51. Coyle IP, Koh YH, Lee WC, Slind J, Fergestad T, Littleton JT, Ganetzky B (2004) Nervous wreck, an SH3 adaptor protein that interacts with Wsp, regulates synaptic growth in Drosophila. Neuron 41:521–534
52. Ro H, Dawid IB (2009) Organizer restriction through modulation of Bozozok stability by the E3 ubiquitin ligase Lnx-like. Nat Cell Biol 11:1121–1127
53. Ro H, Dawid IB (2010) Lnx-2b restricts gsc expression to the dorsal mesoderm by limiting nodal and Bozozok activity. Biochem Biophys Res Commun 402:626–630
54. Ro H, Dawid IB (2011) Modulation of Tcf3 repressor complex composition regulates cdx4 expression in zebrafish. EMBO J 30: 2894–2907

PLOS ONE

RESEARCH ARTICLE

Proteomic analysis reveals novel ligands and substrates for LNX1 E3 ubiquitin ligase

Joan A. Lenihan, Orthis Saha¤, Paul W. Young*

School of Biochemistry and Cell Biology, University College Cork, Cork, Ireland

¤ Current address: Institut de Biologie de l'Ecole Normale Supérieure, Paris, France
* p.young@ucc.ie

Check for updates

OPEN ACCESS

Citation: Lenihan JA, Saha O, Young PW (2017) Proteomic analysis reveals novel ligands and substrates for LNX1 E3 ubiquitin ligase. PLoS ONE 12(11): e0187352. https://doi.org/10.1371/journal.pone.0187352

Editor: Chunhong Yan, Augusta University, UNITED STATES

Received: July 4, 2017

Accepted: October 18, 2017

Published: November 9, 2017

Copyright: © 2017 Lenihan et al. This is an open access article distributed under the terms of the Creative Commons Attribution License, which permits unrestricted use, distribution, and reproduction in any medium, provided the original author and source are credited.

Data Availability Statement: All relevant data are within the paper and its Supporting Information files.

Funding: This work was supported by Science Foundation Ireland Research Frontiers Programme (08/RFP/NSC1382); Irish Research Council EMBARK Postgraduate Research Scholarship.

Competing interests: The authors have declared that no competing interests exist.

Abbreviations: PDZ, PSD-95, DlgA, ZO-1; RING, Really Interesting New Gene; LNX, Ligand of

Abstract

Ligand of Numb protein X1 (LNX1) is an E3 ubiquitin ligase that contains a catalytic RING (Really Interesting New Gene) domain and four PDZ (PSD-95, DlgA, ZO-1) domains. LNX1 can ubiquitinate Numb, as well as a number of other ligands. However, the physiological relevance of these interactions *in vivo* remain unclear. To gain functional insights into the LNX family, we have characterised the LNX1 interactome using affinity purification and mass spectrometry. This approach identified a large number of novel LNX1-interacting proteins, as well as confirming known interactions with NUMB and ERC2. Many of the novel interactions mapped to the LNX PDZ domains, particularly PDZ2, and many showed specificity for LNX1 over the closely related LNX2. We show that PPFIA1 (liprin-α1), KLHL11, KIF7 and ERC2 are substrates for ubiquitination by LNX1. LNX1 ubiquitination of liprin-α1 is dependent on a PDZ binding motif containing a carboxyl terminal cysteine that binds LNX1 PDZ2. Surprisingly, the neuronally-expressed LNX1p70 isoform, that lacks the RING domain, was found to promote ubiquitination of PPFIA1 and KLHL11, albeit to a lesser extent than the longer RING-containing LNX1p80 isoform. Of several E3-ligases identified in the LNX1 interactome we confirm interactions of LNX1 with MID2/TRIM1 and TRIM27. On this basis we propose a model whereby LNX1p70, despite lacking a catalytic RING domain, may function as a scaffold to promote ubiquitination of its ligands through recruitment of other E3-ligases. These findings provide functional insights into the LNX protein family, particularly the neuronal LNX1p70 isoform.

Introduction

Ligand of Numb protein X1 (LNX1) was first characterised based on its ability to bind to the cell fate determinant protein, NUMB [1]. This ability is shared by the closely related LNX2 protein [2]. LNX1 and LNX2 have the same domain structure, comprising an amino-terminal RING (Really Interesting New Gene) domain, a NUMB-binding motif (NPAY or NPAF) and four carboxyl-terminal PDZ (PSD-95, DlgA, ZO-1) domains (Fig 1A). Three major isoforms of LNX1 have been described; the non-neuronal LNX1p80 isoform and two shorter, brain-specific, isoforms, LNX1p70 and LNX1p62, that lack the RING domain but contain the NPAY motif. LNX1p80, through its RING domain, can ubiquitinate specific isoforms of NUMB,

NUMB protein X; CNS, Central Nervous System; ERC, ELKS/Rab6-interacting/CAST; SPRY, (in splA kinase and ryanodine receptor); TRIM, tripartite motif; FN3, fibronectin type III; COS, C-terminal subgroup one signature.

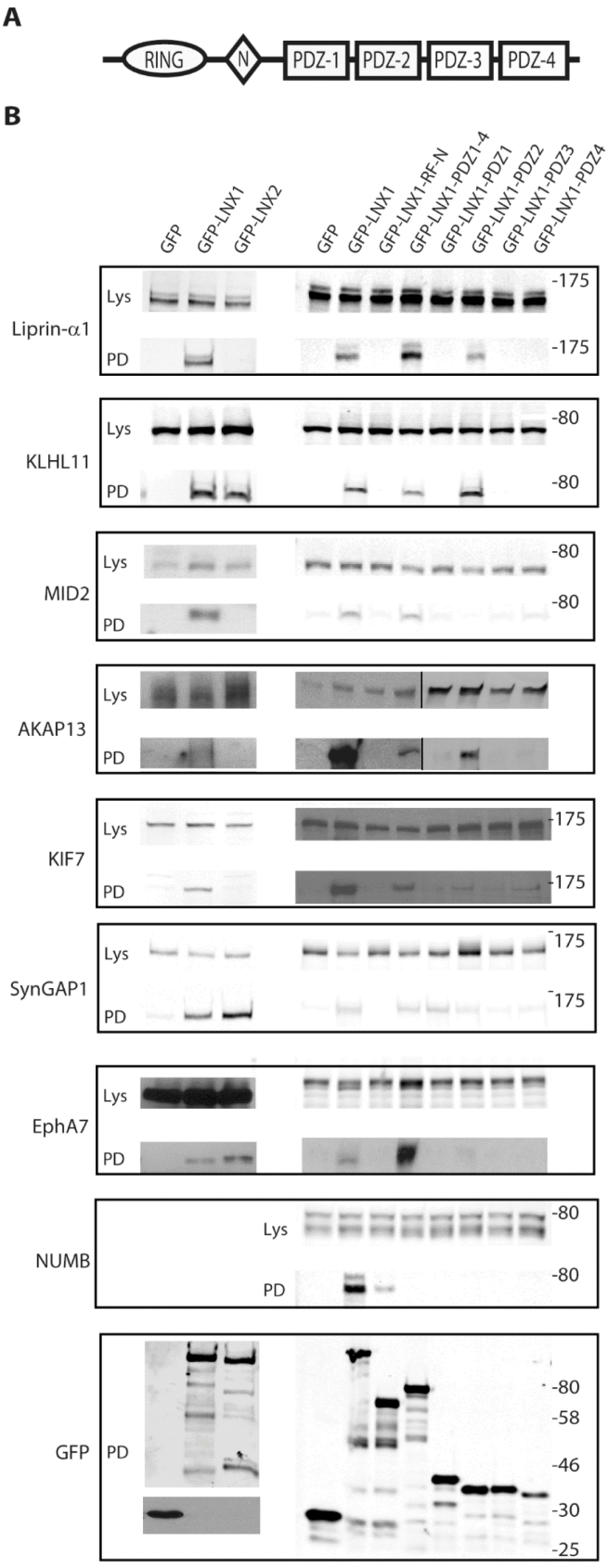

Fig 1. Characterisation of LNX1 interacting proteins. (A) Schematic diagram of the domain structure of LNX1p80 and LNX2 showing the RING and four PDZ domains. N represents the NUMB-binding NPAY/NPAF motif. **(B)** The ability of the indicated proteins to interact with transfected GFP-tagged LNX constructs was assessed in HEK 293 cells. For each interacting protein, top panels show western blots of cell lysates (Lys), while the bottom panels show the output of a GFP "pull down" assay (PD). In the panels on the left, the specificity of interactions for LNX1 versus LNX2 was assessed, while on the right the interaction site on LNX1 was mapped to individual protein domains. Binding of endogenous proteins to LNX was assessed for liprinα-1, KIF7 and NUMB. For the other proteins, interactions of transfected HA or GST epitope-tagged proteins were assessed. For AKAP13, the mapping to LNX domains was performed in two separate experiments. Successful expression and pull down of GFP-tagged LNX proteins was verified in all assays and representative "pull down" blots probed for GFP are shown. n = 2–3.

https://doi.org/10.1371/journal.pone.0187352.g001

thereby targeting NUMB for proteasomal degradation [3, 4]. While *Lnx*1 and *Lnx2* mRNAs are widely expressed in several adult tissues, the earliest embryonic expression of both genes is observed in the central nervous system (CNS) [1, 2, 5]. Two recent studies have proposed a role for LNX2 in modulating neurogenesis in the sub-ventricular zone of the developing brain [6, 7]. In agreement with a role for LNX proteins in regulating neural development, double knockout mice lacking both LNX1 and LNX2 in the central nervous system exhibit reduced anxiety-related behaviour [8]. The molecular basis for this phenotype is unclear however, and notably no alterations in NUMB levels were seen in these mice. Other studies suggest roles for LNX proteins in cancer, immune function and bone homeostasis [9–11], and in zebra fish LNX2 is important for exocrine cell differentiation in the pancreas [12]. However our understanding of such putative functions of mammalian LNX1 and LNX2 proteins *in vivo* is very incomplete.

The combination of a RING and one or more PDZ domains is a unique feature of the LNX family [13]. PDZ domains function as protein-protein interaction modules, most commonly binding to the carboxyl-termini of other proteins. Wolting *et al.* [14] compiled a list of 220 LNX-interacting proteins both from their own work and the published literature, while a subsequent study by Guo *et al.* [15] identified a further 30 LNX-interacting proteins. Most studies of LNX interacting proteins to date have employed either yeast-two hybrid assays or arrays of PDZ domains and PDZ-binding motifs. The vast majority of interactions identified involve the LNX PDZ domains. Apart from NUMB [4], only a small number of the other described LNX-interacting proteins have been shown to be substrates for ubiquitination by LNX. For example, overexpression of LNX1 was shown to cause ubiquitination and proteasomal degradation of c-Src and PBK (PDZ binding kinase) [15, 16], while LNX-mediated ubiquitination of claudins and CD-8α triggers endocytosis of these transmembrane proteins from the cell surface [10, 17]. These examples demonstrate that the ubiquitin ligase activity of LNX RING domains can be directed towards specific substrates via PDZ-mediated interactions. Given the low and potentially cell-type restricted expression patterns of LNX proteins [16, 18], it is important to identify physiologically relevant interacting proteins and substrates in order to elucidate the *in vivo* functions of mammalian LNX proteins.

To gain further insights into the poorly understood LNX proteins, we sought to examine the molecular interactions of the full length LNX1 protein in mammalian cells under conditions that are more physiologically relevant than previous studies. To that end, we have characterised the LNX1 interactome using affinity purification and mass spectrometry. Our results validate some known LNX interactions and identify a significant number of new ones. We show that several of these novel ligands co-localize with LNX1 in cultured cells and are substrates for ubiquitination by LNX1. In addition, we provide evidence that the neuronal LNX1p70 isoform that lacks the RING domain, may nevertheless promote ubiquitination of interacting proteins possibly through recruitment of other E3 ligases into multi-protein complexes. This proteomic analysis thus provides novel insights into LNX1 protein function.

Materials and methods

Antibodies and cDNA constructs

The coding sequences of mouse *Lnx1* (p80 isoform) and *Lnx2* were cloned into the pEGFP-C2 vector (Clontech). Empty pEGFP-C2 vector was used to express EGFP alone. LNX1 sequences in pEGFP-C2, for mapping interactions, encoded the following amino acids (aa) based on the LNX1p80 protein sequence: RING-NPAY motif, aa1-277; PDZ1-4, aa268-728; PDZ1, aa271-384; PDZ2, aa377-470; PDZ3, aa500-598; PDZ4, aa630-725. MID2 constructs based on transcript variant 2 of human MID2 (NM_052817) encoded the following amino acids: full length MID2, aa 1–705; RING domain—BBOX type Zinc finger-2, aa 1–235; Coiled coil–SPRY domain, aa 222–705; Coiled coil-COS domain, aa 222–406; FN3 domain—SPRY domain, aa 395–705. MID1 and TRIM 27 constructs encoded aa 1–667 of human MID1 (NM_000381) and aa 1–513 of human TRIM27 (NM_006510) respectively. Coding sequences for LNX interacting proteins were cloned into the vectors pCMV-N-HA, pCMV-N-FLAG or pDEST27 to produce proteins with amino-terminal HA, FLAG and GST tags respectively. The following antibodies were used: anti-GFP (Green Fluorescent Protein, catalogue number ab290, Abcam), anti-HA (catalogue number MMS-101R, Covance), anti-GST (Glutathione-S-Transferase, catalogue number G1160, Sigma-Aldrich), anti-FLAG (catalogue number F3165, Sigma-Aldrich), anti-liprin-α1 (catalogue number ab26192, Abcam), anti-liprin-α3 (catalogue number 169102, Synaptic Systems), anti-KIF7 (catalogue number ab95854, Abcam), anti-NUMB (catalogue number NB500-178, Novus Biologicals), anti-AKAP13 (catalogue number NB100-68214, Novus Biologicals). Horse radish peroxidase, Dylight 488 and Cy3 conjugated secondary antibodies were purchased from Jackson ImmunoResearch, while IR_{700} and IR_{800} conjugated secondary antibodies were from Li-Cor Biosciences. All other reagents were from Sigma-Aldrich unless stated otherwise.

Purification of LNX1 complexes from stably-transfected cells

HEK (Human Embryonic Kidney) 293 cells (ATTC), cultured under standard conditions, were transfected with GFP and GFP-LNX1 expression constructs using calcium phosphate precipitation, and stable cell pools were selected using G418 antibiotic. To purify GFP-LNX1 and GFP protein complexes, ten confluent 15 cm dishes of cells were harvested and GFP affinity purifications performed using magnetic GFP-Trap® beads, as per manufacturer's instructions (ChromoTek). Purified complexes were separated by gel electrophoresis and stained using GelCode Blue Protein Stain (Thermo Scientific Pierce). Each lane was cut into slices for mass spectrometry analysis.

Protein identification by mass spectrometry

Protein digestion, nano-liquid chromatography and MS/MS mass spectrometric analysis was performed at the Fingerprints Proteomics facility at University of Dundee, Scotland, UK. Proteins were identified by searching against the IPI protein database and data analysis was performed as previously described [8, 19]. Briefly, proteins identified in LNX complexes, but not in the control samples, were ranked according to Mascot protein scores and listed using protein symbols as identifiers. A Mascot protein score of 70 was then applied as a cut-off value to limit results to proteins that have been reliably identified, and probable environmental contaminants or false positives were eliminated as previously described [19].

Characterisation of interactions by GFP pull-down assays

Expression vectors encoding GFP-tagged LNX1 or LNX2 constructs were transfected into HEK 293 cells, either alone or together with constructs encoding a LNX-interacting protein as

previously described [8]. Briefly, cultures were harvested 24–48 hours post-transfection, and GFP affinity purification performed using 10ul GFP-Trap_M beads according to the manufacturer's protocol. In some cases, the stringency of the wash conditions were increased by increasing the NaCl concentration in the standard wash buffer up to 500mM. Proteins were eluted by boiling in 2X SDS sample buffer and analysed by western blotting.

Immunofluorescence staining

MCF7 cells (ATTC) were chosen for these experiments because of their flat morphology and good adherence to coverslips during the immunostaining procedure. They were grown under standard conditions on poly-D-lysine coated glass coverslips in a 6 well plate, were transfected with 2 μg of DNA using a calcium phosphate precipitation protocol. 24 hrs post transfection cells were washed with PBS and fixed with 4% PFA for 10 minutes at 4˚C. Cells were incubated in blocking buffer (0.1% triton X-100, 5% goat serum and 2% bovine serum in PBS) prior to antibody incubation. All antibodies were diluted in 5% goat serum and 2% bovine serum in PBS (as described [20]). Cells were washed three times in PBS following each antibody incubation and coverslips were mounted onto glass slides using Fluoromount mounting media.

Ubiquitination assays

Expression vectors encoding LNX proteins, LNX-interacting proteins and a HA epitope-tagged ubiquitin construct were co-transfected into HEK293 cells. Twenty hours after transfection, cells were incubated in fresh medium containing 10 μM MG132 (Merck Millipore). Cells were lysed in 100 μl 1% (w/v) Sodium Dodecyl Sulphate (SDS) supplemented with 15 mM *N*-Ethylmaleimide (NEM) and 1x Complete protease inhibitors (Roche Applied Sciences), and boiled for 5 min. Following cooling on ice, samples were diluted with 900 μl of ice cold buffer that contained 50 mM Tris (pH 8.0), 150 mM NaCl, 1% Triton, 0.5% sodium deoxycholate, 50 mM sodium fluoride, 0.1 mM sodium orthovanadate and protease inhibitors. Lysates were cleared by centrifugation at 13,000 rpm for 30 min at 4˚C. Ubiquitinated proteins were immunoprecipitated overnight at 4˚C from cell lysates using an anti-HA antibody. The ubiquitination status of substrate proteins was then revealed by Western blot analysis.

Analysis of functional associations of LNX-interacting proteins

To compare interactions identified here with those from previous studies, lists of interacting proteins were taken from Wolting *et al.* [14], Guo *et al.* [15] and Lenihan *et al.* [8] and gene identifiers converted to gene symbols. These lists were combined and compared to the proteins identified here using Excel software (S2 Table). For analysis of functional associations, lists of gene symbols were submitted to the functional annotation tool in DAVID (Database for Annotation, Visualisation and Integrated Discovery; http://david.abcc.ncifcrf.gov/) using default settings [21].

Statistical analysis

Two tailed Student *t* tests were performed using Microsoft Excel software. Where appropriate, data were analysed by one-way ANOVA, followed by Bonferroni post-hoc test using GraphPad Prism v.6.0 (La Jolla, CA, USA). *P* values of less than 0.05 were considered significant. Unless stated otherwise, all data are presented as mean ± SEM.

Results

Affinity purification and identification of LNX1 interacting proteins

The majority of LNX-interacting proteins have been identified by yeast-two hybrid assays and protein/peptide arrays [14, 15]. Only a minority of these have been confirmed in mammalian cells using full-length proteins that are targeted to their normal subcellular location. To directly identify interactions of LNX1 in a physiologically relevant context, we established stably-transfected HEK cells expressing GFP-tagged LNX1p80. We then affinity purified LNX1-containing protein complexes from these cells using GFP-Trap® magnetic beads. Cells expressing GFP alone were used as a negative control for non-specific binding to either the beads or GFP tag. Purified proteins from both samples were identified by mass spectrometry. Non-specific interactions present in control GFP complexes, and likely false positives or environmental contaminants, were eliminated to generate a list of over 70 proteins specifically identified in affinity purified GFP-LNX1 complexes. The top 30 proteins ranked according to Mascot scores are shown in Table 1 and the full list is available as supplemental material online (S1 Table). The

Table 1. Proteomic analysis of GFP-LNX1 interacting proteins purified from HEK293 cells. The top 30 proteins identified, as ranked by Mascot score, are shown. The full table is available as supplementary material. Previously known interactions are underlined, as are carboxyl-terminal cysteine residues.

Gene Symbol	Mascot Score	Name	Carboxyl terminus
PPFIA1	5644	Isoform 1 of Liprin-alpha-1	DSATVRTYSC
LNX1	3662	Isoform 1 of E3 ubiquitin-protein ligase LNX	TIVSWPGTFL
MID2	2641	Isoform 1 of probable E3 ubiquitin-protein ligase MID2	PYVSGMKTCH
USP9X	2229	Isoform 2 of probable ubiquitin carboxyl-terminal hydrolase FAF-X	EVSPPQTKDQ
MYCBP2	1995	Probable E3 ubiquitin-protein ligase MYCBP2	CGVCRNAHTF
KIF7	1131	Kinesin-like protein KIF7	GMIDVRKNPL
KLHL11	1056	Kelch-like protein 11	RRVPSSQIEC
MID1	1030	Isoform 1 of Midline-1	DHLDCTEQLP
IARS	1020	Isoleucyl-tRNAsynthetase, cytoplasmic	VSVLPTTADF
PPFIA3	791	Isoform 1 of Liprin-alpha-3	DGVSVRTYSC
KIF14	629	Kinesin-like protein KIF14	ECTPSRIQWV
AKAP13	510	Isoform 6 of A-kinase anchor protein 13	VSAEGEEIFC
PEX1	494	Peroxisome biogenesis factor 1	FRPGQKVTLA
NUMB	438	Isoform 1 of Protein numb homolog	DLQKTFEIEL
RPL4	391	60S ribosomal protein L4	PTTEEKKPAA
NUMBL	356	Numb-like protein	DLQKTFEIEL
AP2M1	352	Isoform 1 of AP-2 complex subunit mu	GRSGIYETRC
PLEK	341	Pleckstrin	AIQMASRTGK
PPP1CA	294	Serine/threonine-protein phosphatase PP1-alpha catalytic subunit isoform 3	PPRNSAKAKK
TRIM27	279	Isoform Alpha of Zinc finger protein RFP	NHGHSMETSP
DUSP14	265	Dual specificity protein phosphatase 14	SRHLMPYWGI
TMED10	253	Transmembrane emp24 domain-containing protein 10	RFFKAKKLIE
ZNF24	248	Isoform 1 of Zinc finger protein 24	AEKLLNVVKV
ZCRB1	247	Zinc finger CCHC-type and RNA-binding motif-containing protein 1	YFSDEEELSD
AP2A1	246	Isoform B of AP-2 complex subunit alpha-1	HLCELLAQQF
LARS	244	Leucyl-tRNAsynthetase, cytoplasmic	IGDTIIYLVH
IQGAP1	242	RasGTPase-activating-like protein IQGAP1	FLLNKKFYGK
RPS27L	237	40S ribosomal protein S27-like	EGCSFRRKQH
CHD2	234	Isoform 2 of Chromodomain-helicase-DNA-binding protein 2	PDYNWNVRKT
ERC2	226	ERC protein 2	DQDDEEGIWA

https://doi.org/10.1371/journal.pone.0187352.t001

well-characterised LNX1-interacting proteins NUMB, NUMB-like and ERC2/CAST1 were specifically identified in GFP-LNX1 complexes–validating the overall approach. Examination of the carboxyl-terminal sequence of proteins that we identified indicates that many of them potentially contain PDZ binding motifs. Particularly noteworthy were proteins containing a putative PDZ-binding motif with a carboxyl-terminal cysteine.

Confirmation and characterisation of LNX1 interactions

We chose five of the most reliably identified novel GFP-LNX1 interacting proteins from our proteomics study for further confirmation and analysis (liprinα1, MID2, KIF7, KLHL11 and AKAP13). The choice of these particular proteins was based on our ability to obtain cDNAs to make expression constructs or antibodies to detect them. We also examined two proteins (EphA7 and SynGAP1) that we previously demonstrated to interact with both LNX1 and LNX2 in yeast two-hybrid assays [13]. We first assessed the specificity of the interaction of these proteins with LNX1 and LNX2 by western blotting after "pull down" of GFP-tagged LNX proteins (Fig 1B). As expected from previous yeast two-hybrid data, SynGAP1 and EphA7 were able to bind both LNX1 and LNX2 in a GFP pull down assay, as was KLHL11. By contrast, liprin-α1, MID2, KIF7 and AKAP13 interacted specifically with LNX1 but not LNX2.

We then attempted to map these interactions to particular regions or individual domains of LNX1. We used amino-terminal (RING-NPAY motif) and carboxyl-terminal (PDZ1-PDZ4) fragments of LNX1, as well as constructs encoding the individual LNX1 PDZ domains, to map these interactions within LNX1 (Fig 1B). All the novel interactions mapped to the C-terminal PDZ domain region. As expected, NUMB was seen to bind the N-terminal fragment containing the NPAY motif, which serves as a positive control to show that this construct was fully functional in our assay. Interactions with individual PDZ domains were generally less prominent than with the full-length or PDZ1-PDZ4 constructs, despite equivalent amounts of GFP-tagged LNX constructs being expressed and pulled down in the assays. Nevertheless, the interactions of liprin-α1, KLHL11 and AKAP13 could be clearly mapped to LNX1 PDZ2, whereas KIF7 seemed to bind PDZ2 and PDZ4. SynGAP1 showed interactions with PDZ1, and to a somewhat lesser extent PDZ2, while the MID2 and EphA7 interactions could not be mapped clearly to any individual PDZ domain.

Co-localisation between LNX and novel interacting proteins

To further evaluate the relevance of these interactions we sought to assess potential co-localisation of LNX1 with some of these interacting proteins in a cellular context. LNX1p80 was co-expressed with either HA- or FLAG-epitope-tagged interacting proteins in MCF-7 cells and detected by immunofluorescence microscopy. In this analysis we observe partial co-localisation of liprin-α1 with LNX1 in the cytoplasm, particularly in structures in the perinuclear region of co-expressing cells (Fig 2B). This staining pattern is in contrast to the relatively diffuse localization of LNX1 in both the cytosol and nucleus when expressed alone (Fig 2A). KLHL11 shows a striking punctate cytoplasmic staining pattern and LNX1 redistributes to these structures when co-expressed with KLHL11, demonstrating clear co-localization (Fig 2C). Erc2 exhibits a diffuse cytoplasmic localization pattern but with some small punctate structures discernible in which co-staining for LNX1 is observed (Fig 2D). MID2 has a diffuse cytoplasmic localization similar to LNX1, but no clear co-localization in discrete structures was observed (Fig 2E). EphA7 localized exhibited a perinuclear staining which possibly represents localization of this transmembrane protein in the endoplasmic reticulum and/or Golgi, but LNX1 remained diffusely distributed in co-expressing cells and did not prominently co-localize with EphA7, suggesting that they do not interact extensively in this cellular context

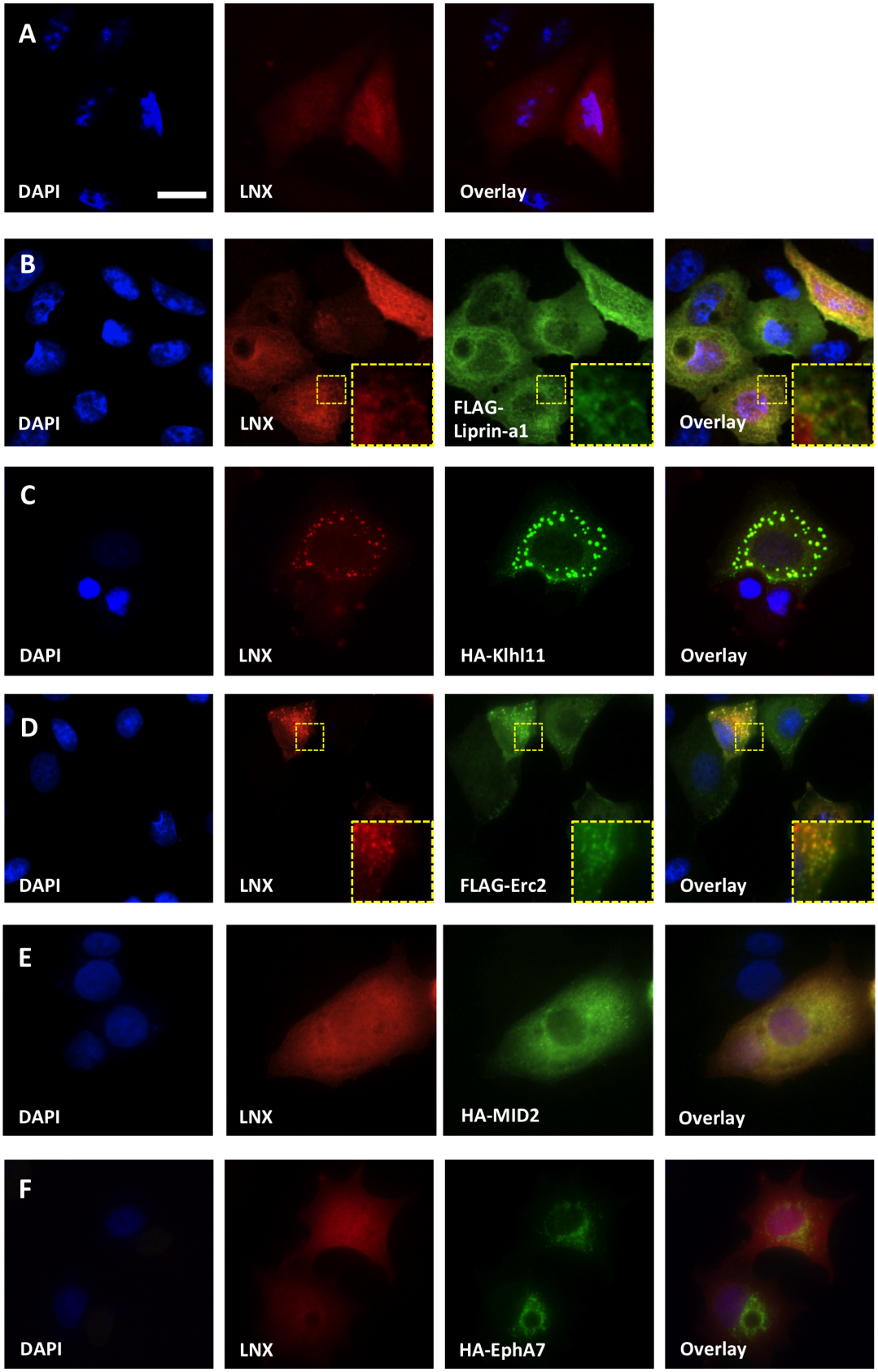
A
DAPI
LNX
Overlay
B
DAPI
LNX
FLAG-
Liprin-a1
Overlay
C
DAPI
LNX
HA-Klhl11
Overlay
D
DAPI
LNX
FLAG-Erc2
Overlay
E
DAPI
LNX
HA-MID2
Overlay
F
DAPI
LNX
HA-EphA7
Overlay

Fig 2. Representative fluorescence immunocytochemistry images examining localisation of the LNX1 and interacting proteins following transient expression in MCF-7 cells. (A) LNX1p80 transfected alone **(B)-(F)** LNX1p80 transfected in combination with the indicated interacting proteins that had been tagged with either HA or FLAG epitope tags. Anti-FLAG (green), anti-HA (green) and anti-LNX (red) were used to visualize the proteins of interest. Nuclei were stained with DAPI (blue). The different wavelengths were scanned individually and digitally merged (*overlay*). The regions highlighted by the small dashed boxes in B and D are shown enlarged in the bottom right corners of these images. Scale bar indicates 20 μm.

https://doi.org/10.1371/journal.pone.0187352.g002

(Fig 2F). In summary then this analysis provides direct evidence for the co-localization of LNX1 with liprin-α1, KLHL11 and ERC2, while the diffuse cytoplasmic localization of both LNX1 and MID2 is at least compatible with their interaction in a cellular context.

LNX1 binds the carboxyl-terminus of liprin-α1 and promotes its ubiquitination in both a RING domain dependent and independent manner

Many PDZ domains bind to carboxyl terminal motifs of their interaction partners, with the amino acids at positions 0 and -2 relative to the carboxyl terminus being particularly crucial for recognition by PDZ domains [22]. Liprin-α1 is one of several proteins in our proteomic analysis that contains a putative PDZ binding motif with a cysteine at its C-terminus (Table 1; S1 Table). To test if this motif was indeed required for binding to LNX1, a mutant of liprin-α1 was generated in which the carboxyl-terminal sequence YSC* was changed to DSE*. This mutation was found to abolish the binding of liprin-α1 to both full length LNX1 and also to LNX1 PDZ2, as assessed by GFP-Trap pull-down assays (Fig 3A). These results strongly indicate that liprin-α1 binds directly to the second PDZ domain of LNX1 through its carboxyl-terminal PDZ-binding motif.

We next assessed the ability of LNX proteins to ubiquitinate liprin-α1. For this purpose, liprin-α1, HA-tagged ubiquitin and various LNX proteins were co-expressed in HEK 293T cells in the presence of the proteasome inhibitor, MG132. Ubiquitinated proteins were specifically immunoprecipitated using an anti-HA antibody and detected by western blotting. Liprin-α1 ubiquitination was detected as a high molecular smear above the position of the main liprin-α1 band and quantified by densitometry analysis (Fig 3B). One-way ANOVA revealed significant differences in the ubiquitination status of liprin-α1 in the presence of LNX ($p < 0.0001$, $F_{4,15} = 17.15$). Ubiquitination in immunoprecipitates from cells expressing LNX1p80 was significantly stronger than in those from cells transfected with the control vector ($p < 0.0001$), as revealed by Bonferroni post-hoc test, indicating that LNX1p80 strongly promotes ubiquitination of liprin-α1. Surprisingly, cells expressing LNX1p80 containing the catalytically inactive RING-finger domain, (LNX1p80C48A) [4], also exhibited increased ubiquitination compared to the control vector, though not to the level observed for the wild type protein. This increase did not quite reach statistical significance but statistically significant increases in ubiquitination of liprin-α1 were observed in immunoprecipitates from cells transfected with the neuronal LNX1p70 isoform ($p < 0.05$), which lacks the RING finger domain required for ubiquitination, and LNX2 ($p < 0.05$), compared to the control vector (Fig 3B, upper graph). These increases in ubiquitination were of a similar magnitude to those seen for samples transfected with the catalytically inactive RING-finger domain mutant LNX1p80C48A. We next tested a LNX1 construct consisting of just the four PDZ domains and saw that this region of LNX1 was sufficient to promote liprin-α1 ubiquitination to a similar extent as LNX1p70 (Fig 3B, lower graph). These observations suggest that in addition to directly ubiquitinating liprin-α1 in a RING-domain dependent manner, LNX1 can promote liprin-α1 ubiquitination indirectly. Both of these effects are dependent on the LNX1: liprin-α1 interaction, since the ubiquitination

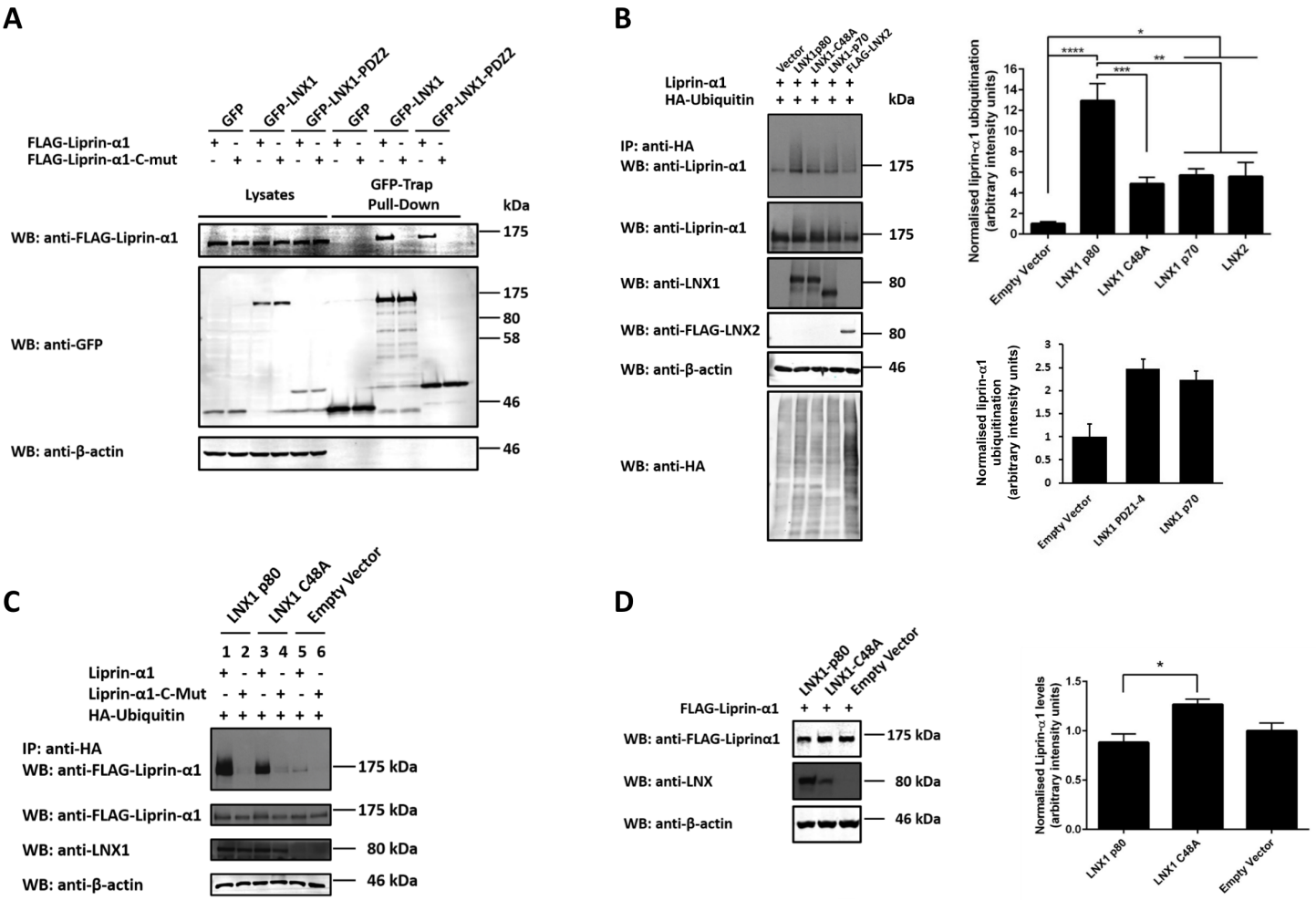

Fig 3. Liprin-α1 interacts with LNX1 via its C-terminus and is a substrate for LNX-mediated ubiquitination. (A) GFP pull-down assays performed on HEK 293T cells transiently transfected with either wild-type FLAG-liprin-α1 or a similar liprin-α1 construct with a carboxyl-terminal YSC* to DSE* mutation (FLAG-liprin-α1-C-mut) and either GFP-LNX1, GFP-LNX1-PDZ2 or GFP. Cell lysates and purified proteins were subjected to western blotting (WB) with the indicated antibodies. n = 2. **(B)** Ubiquitination of liprin-α1 assessed in a cell based assay. HEK 293T cells were co-transfected with the indicated LNX and liprin-α1 expression constructs as well with a construct encoding HA epitope-tagged ubiquitin. Ubiquitinated proteins were immunoprecipitated from cell lysates using an anti-HA antibody. Western blotting of immunoprecipitates for liprin- α1 revealed its ubiquitination as a high molecular weight smear. Western blot of whole cell lysates confirmed expression of all constructs. Levels of ubiquitinated liprin-α1 were quantified by densitometry and normalised for liprin-α1 expression in whole cell lysates. Data in the upper graph are expressed as mean ± SEM. n = 4. $*p < 0.05$, $**p < 0.01$, $***p < 0.001$, $****p < 0.0001$; one-way ANOVA followed by Bonferroni post-hoc test. Data from a separate experiment are shown in the lower graph as mean ± SEM. n = 3. **(C)** Ubiquitination of wild-type FLAG-liprin-α1 or FLAG-liprin-α1-C-mut in the presence of the indicated LNX1 constructs was assessed as in (B) above. An obvious high molecular weight smear corresponding to ubiquitinated wild-type liprin-α1, but not liprin-α1-C-mut with a carboxyl-terminal mutation, was detected for both wild-type LNX1p80 and the catalytically inactive LNXp80-C48A mutant. **(D)** Liprin-α1 protein levels assessed in the presence of either wild-type LNX1p80 or the LNXp80-C48A mutant. Whole cell lysates were analysed by Western blot using anti-FLAG, anti-LNX1/2-PDZ3/4 and anti-β-actin antibodies. Liprin-α1 protein levels were quantified, normalised to β-actin levels and subjected to one-way ANOVA followed by Bonferroni post-hoc test. Data are expressed as mean ± SEM. n = 4. $*p < 0.05$.

https://doi.org/10.1371/journal.pone.0187352.g003

of liprin-α1 induced by both LNX1p80 and LNX1p80C48A is abrogated when the liprin-α1 carboxyl terminal PDZ binding motif is mutated (Fig 3C).

We next assessed whether the ubiquitination of liprin-α1 induced by LNX1 promotes its degradation by the proteasome or other mechanisms. FLAG-liprin-α1, HA-ubiquitin and LNX1p80, LNX1p80C48A or vector only were co-transfected into HEK 293T cells. Quantitative western blot analysis of liprin-α1 in total cell lysates followed by one-way ANOVA

indicated a significant effect of LNX on the levels of liprin-α1 in transfected cell lysates ($p = 0.0134$, $F_{2,9} = 7.236$; Fig 3D). Bonferroni post-hoc analysis, however, did not reveal a significant reduction of liprin-α1 in wild-type LNX1p80 or mutant LNX1p80C48A transfected cell lysates, compared to the control vector. Instead liprin levels were significantly increased when co-transfected with the ubiquitination deficient LNX1p80C48A mutant compared to the wild type LNX1p80. These results suggest that the strong ubiquitination of liprin-α1 by LNX1p80 wild type does not target liprin-α1 for proteasomal degradation and that LNX1p80C48A, despite also promoting a degree of ubiquitination, has a slight stabilizing effect on liprin-α1 levels.

KLHL11, KIF7 and ERC2 are substrates for LNX-mediated ubiquitination substrates

Having shown that liprin-α1 is ubiquitinated by LNX, we next investigated whether a number of the other LNX1 interacting proteins identified were also LNX1 substrates in similar cell-based ubiquitination assays. HEK 293T cells were transiently transfected with GFP-KLHL11, GST-KIF7, GFP-ERC2, or FLAG-SRGAP2, HA-Ubiquitin and LNX1p80, LNX1p70 or vector only. LNX1p80 increased ubiquitination of KLHL11, KIF-7, ERC2 and possibly SRGAP2 to a much lesser extent (Fig 4A, 4B, 4C and 4D respectively). As was the case for liprin-α1, expression of LNX1p70 increased ubiquitination of KLHL11 (Fig 4A), but appeared to have no effect on KIF7, ERC2 or SRGAP2 (Fig 4B, 4C and 4D respectively). These results underline the ability of LNX1p80 to ubiquitinate its interacting proteins via its p80 RING domain, but also further support a RING domain-independent function for LNX1p70 in enhancing ubiquitination of certain ligand proteins.

Interaction of LNX1 with members of the TRIM E3 ubiquitin ligase family

We hypothesized that LNXp70 might act as a scaffold to recruit other E3 ubiquitin ligases to substrates that bind to its PDZ domains. Since six E3 ubiquitin ligases (MID1, MID2, MycBP2, TRIM27, TRAF4 and DZIP3) were identified in the LNX1 interactome we sought to further characterize some of these interactions (Table 1). We focused on the three members of the tripartite motif (TRIM) family identified in our mass spectrometry data—MID1/TRIM18, MID2/TRIM1 and TRIM27. We had already seen that transfected, epitope-tagged MID2 interacted with the PDZ domain region of LNX1, but that this interaction could not be mapped to an individual PDZ domain (Fig 1B). Furthermore the histidine residue present at the carboxyl terminus of MID2 (Table 1) does not fit with consensus sequences for PDZ binding motifs [15, 23]. These observations suggest that MID2 does not bind LNX via a typical carboxyl terminal: PDZ domain interaction. We therefore investigated which part of MID2 mediates this interaction (Fig 5A and 5B). We found that a region containing the FN3 and SPRY domains of MID2 is necessary and sufficient to bind LNX1, with no interaction being observed for constructs containing the RING, B-BOX, coiled-coil or microtubule binding COS domains.

We next sought to confirm the interaction of LNX1 with MID1 and TRIM27. Surprisingly, no interaction with LNX1p80 was seen for transfected epitope-tagged MID1 under the same experimental conditions for which MID2 binding was observed (Fig 5C). However, when MID1 and MID2 were co-transfected with LNX1, MID1 did co-purify with LNX1, suggesting that MID1 interacts indirectly with LNX1 because of its ability to heterdimerize with MID2 via the coiled coil regions of both proteins [25]. By contrast, we were able to observe the interaction of transfected epitope-tagged TRIM27 with LNX1 without having to co-transfect MID2, confirming this interaction and suggesting that it is direct rather than mediated by heterodimerization with MID2 (Fig 5D).

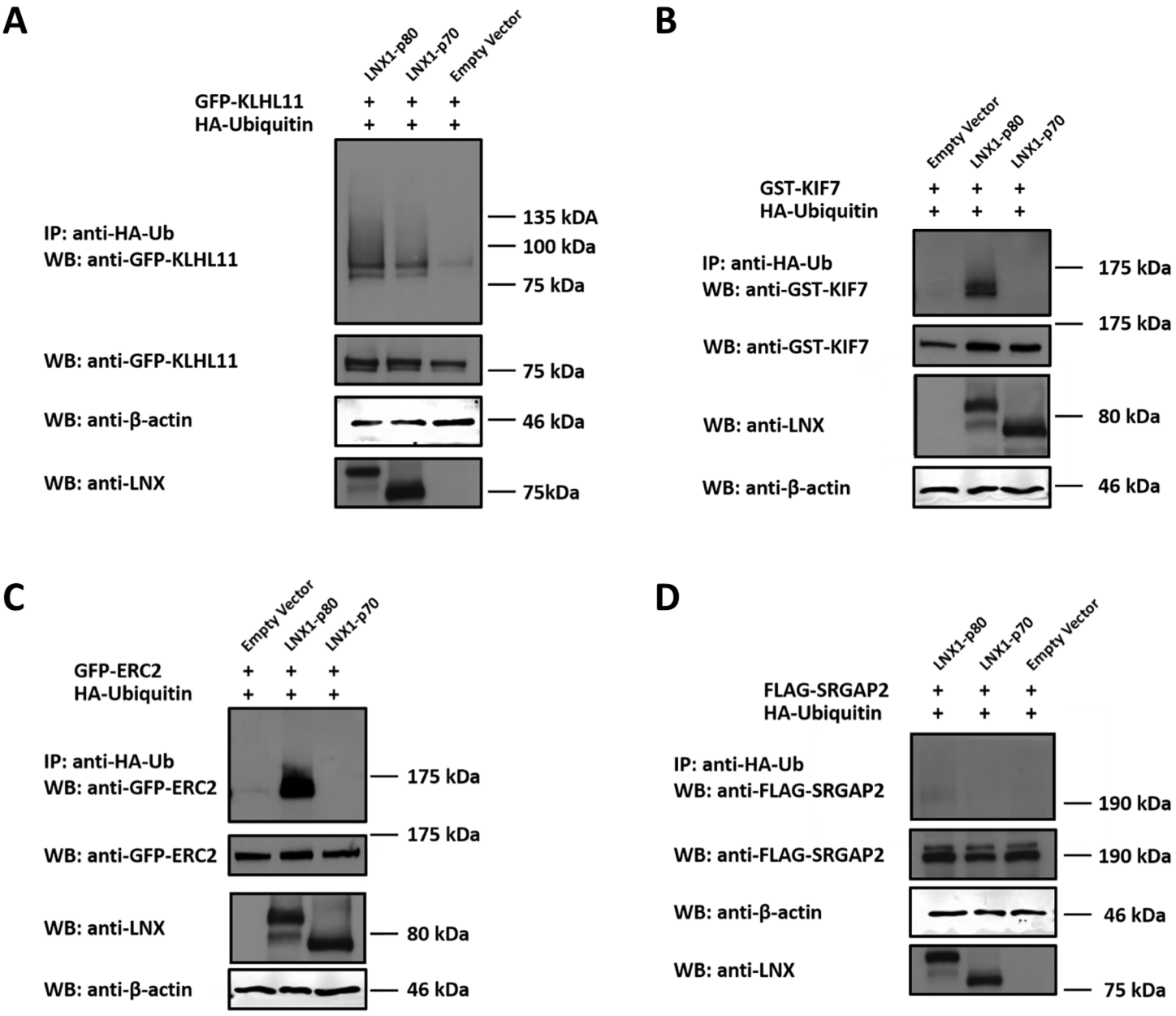

Fig 4. LNX1 mediated ubiquitination of KLHL11, KIF7 and ERC2. HEK 293T cells were transiently transfected with the indicated constructs and ubiquitinated proteins detected as in Fig 3B above. The ubiquitination status of **(A)** KLHL11, **(B)** KIF7, **(C)** ERC2 and **(D)** SRGAP2 was then revealed by Western blot analysis using the indicated antibodies. Western blot of whole cell lysates confirmed expression of all constructs. n = 2.

https://doi.org/10.1371/journal.pone.0187352.g004

Given the robust interaction of MID2 with the LNX1 PDZ domains we sought to test the idea that the LNX1p70 isoform, while lacking its own RING domain, might target the ubiquitin ligase activity of the MID2 RING domain to proteins that bind the LNX1 PDZ domains. To do this we examined whether MID2, LNX1p70 and the LNX1 ligand liprin-α1 could form a ternary complex (Fig 5D). While LNX1p70 was seen to interact strongly with GFP-tagged MID2, we could not observe co-purification of liprin-α1 with LNX1p70 and MID2. It is thus unlikely that the recruitment of MID2 E3 ligase activity by LNX1p70 could explain the ability of LNX1p70 to promote liprin-α1 ubiquitination. However, confirmation of the ability of

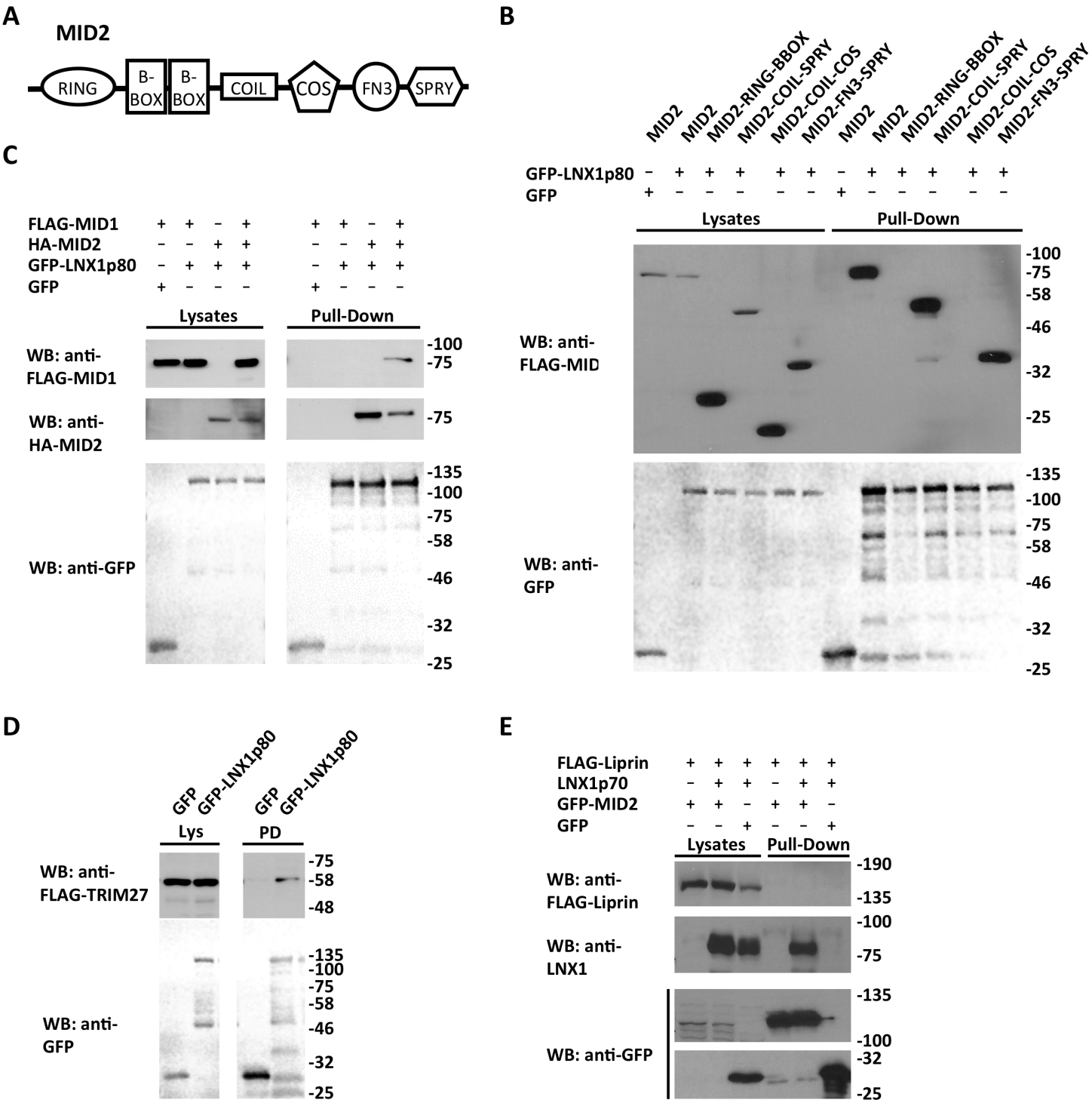

Fig 5. Interactions of LNX1 with the TRIM E3 ubiquitin ligase family. A, Schematic diagram of the domain structure of MID2 showing the RING and B-BOX type zinc finger domains, the coiled-coil dimerization domain (COIL), the microtubule-binding COS (C-terminal subgroup one signature) domain, the fibronectin type III (FN3) domain and the SPRY (in splA kinase and ryanodine receptor) domain. MID1 shares a very similar domain organization, whereas TRIM27 lacks the COS and FN3 domains [24]. B, Mapping of the LNX1 binding site on MID2. The ability of the indicated FLAG epitope tagged MID2 constructs to interact with GFP-tagged LNX1p80 was assessed following transfection into in HEK 293 cells by GFP "pull down" assays. Successful expression of constructs was verified by western blotting of cell lysates and interactions detected in pull down samples. n = 2. C, Analysis of LNX1 binding to MID1. The ability of FLAG epitope-tagged MID1 to interact with GFP-tagged LNX1p80 was assessed in the presence or absence of HA epitope-tagged MID2. n = 2 D, Confirmation of TRIM27 interaction with LNX1 in a GFP "pull down" assay. n = 2. E, Investigation of the ability of MID2, LNX1p70 and liprin-α1 to form a trimolecular complex. Interaction of untagged LNX1p70 and FLAG-tagged liprin-α1 with GFP-tagged MID2 was assessed in GFP "pull down" assays. n = 3.

https://doi.org/10.1371/journal.pone.0187352.g005

LNX1p70 to bind strongly to MID2 indicates that LNX1p70 might recruit MID2 to mediate ubiquitination of other LNX1 interacting proteins.

Discussion

In an analysis of the human PDZ domain-ligand interactions network (PDZNet), LNX1 ranked third in terms of total number of interactions [26]. The large number of interactions that have been reported for LNX1 is remarkable, given that it is not a well-studied protein. Considering that LNX protein levels are tightly regulated [5, 8, 18], establishing which LNX interactions are physiologically relevant is a key challenge. To complement previous approaches, we have carried out the first affinity purification/mass spectrometry-based analysis of the LNX1 interactome in the context of mammalian cells. Our results provide confirmation of just 10 of the approximately 400 previously reported LNX interactions [8, 14, 15] (S2 Table). The identification of well-characterised interaction partners, such as NUMB and ERC2, validates our methodology, and supports the veracity of these interactions. The failure to confirm more previously reported interactions may simply be because these proteins are not expressed in HEK cells. However, this seems unlikely to be true in all cases, and it may be that some previously reported LNX binding protein were not detected in our study because, (1) they do not interact with full-length LNX proteins, (2) they are localised in a different subcellular compartment from LNX, or (3) they are out-competed by ligands present in HEK cell lysates that have a higher affinity. Thus, some interaction pairs that have been identified by yeast-two-hybrid or protein/peptide arrays may not be significant in a mammalian cellular context in which many potential ligands are binding competitively to LNX proteins. In addition, indirect interactions detected by our affinity purification approach may partly explain the lack of overlap with previously identified LNX ligands. For example, KIF7 lacks a strong carboxyl terminal PDZ-binding consensus sequence, but is known to interact with liprin-α1 [27], suggesting that the interaction of KIF7 with LNX1 could be mediated by liprin-α1. Overall though, our data confirm the propensity of LNX proteins to interact with a large number of ligands and may highlight those interactions that are physiologically relevant.

Our goal in characterising the LNX1 interactome was to gain insights into potential functions of LNX proteins and to identify differential functions of LNX1 and LNX2. We used the DAVID Bioinformatics Resource [21] to identify significant biological associations of proteins present in LNX1 complexes. Functional annotation terms that are enriched in the LNX1 interactome include: ATP/nucleotide binding, microtubule cytoskeleton/microtubule-based process, translation/protein biosynthesis, ER-Golgi intermediate compartment, protein transport/localisation, peroxisome membrane, protein kinases, protein phosphatases, cell projection morphogenesis/organisation, synaptosome, regulation of synaptic transmission, ubiquitin conjugation pathway, cell division, zinc/RING finger domain-containing and emp24 domain-containing. Examination of the proteins identified, also reveals several incidences of multiple members of a protein family being identified. These families (with family members identified in parentheses) include: NUMB (NUMB, NUMBL), Midline probable E3 ligases (MID1, MID2), peroxisome biogenesis/assembly factors (PEX1, PEX6), tRNA synthetases (IARS, LARS, MARS), ELKS/Rab6-interacting/CAST family (ERC1, ERC2), Flotillin (FLOT1, FLOT2), Kinesin-like proteins (KIF7, KIF14), liprin-α proteins (PPFIA1, PPFIA3) and Transmembrane emp24 domain-containing proteins (TMED2, TMED4, TMED5, TMED9, TMED10). While the liprin, NUMB and ERC family members have conserved carboxyl-terminal PDZ-binding consensus motifs, the other families do not have conserved carboxyl-termini that would explain their interaction with LNX PDZ domains. Nevertheless, these novel associations represent valuable clues regarding putative functions of LNX1 and merit further investigation.

The *Lnx1* and *Lnx2* genes arose by gene duplication early in the vertebrate lineage [13]. The invertebrate *Lnx1/2-like* gene is more similar to *Lnx2*, indicating that *Lnx1* may have may have undergone neofunctionalisation following the gene duplication[13]. We identified several LNX1-specific interactions (liprin-α1, MID2, AKAP13 and KIF7) that could mediate functions that are unique to LNX1. Liprin-α1 and AKAP13 have putative PDZ binding motifs with a carboxyl-terminal cysteine, and interact specifically with LNX1 via PDZ2, indicating that LNX1-PDZ2 seems to have a preference for ligands with carboxyl-terminal cysteines compared to LNX2-PDZ2. This would agree with previous reports [8, 15]. The molecular basis for the specificity of these interactions with LNX1 versus LNX2 is not obvious however, as key residues involved in ligand recognition are conserved between the PDZ2 domains of LNX1 and LNX2 [13] and some interacting proteins with a carboxyl-terminal cysteine such as KLHL11, seem to interact equally well with both LNX1 and LNX2.

We have characterised the interaction with liprin-α1 in more detail by verifying that the interaction is dependent on the carboxyl-terminal–YSC* motif and showing that liprin-α1 is a substrate for ubiquitination by LNX1p80. However, ubiquitination of liprin-α1 by LNX1 did not significantly alter liprin-α1 protein levels. This suggests that LNX1-mediated ubiquitination does not target liprin-α1 for proteasomal (or lysosomal) degradation, but perhaps affects some other aspect of liprin-α1 function. While liprin-α1 is widely expressed in many tissues, liprin-αs are best characterised as a component of the presynaptic cytomatrix of the active zone (CAZ) complex, that is involved in synapse maturation in neurons [28]. While LNX1p80 could ubiquitinate liprin-α1 in non-neuronal tissues, neurons are thought to exclusively express the LNX1p70 and LNX1p62 isoforms that lack the catalytic RING domain. Surprisingly, we found that LNX1p70 was able to promote ubiquitination of liprin-α1, albeit to a lesser extent than LNX1p80. A similar effect was observed for ubiquitination of KLHL11.

These findings suggest that the neuronal LNX1p70 isoform may be able to recruit other E3 ligases to mediate ubiquitination of substrates that bind to its PDZ domains. Notably we identified six E3-ubiquitin ligases in our LNX1 interactome (MID1, MID2, MYCBP2, TRIM27, TRAF4 and DZIP3) and some were identified in previous studies [29]. MID1/TRIM18, MID2/TRIM1 and TRIM27 are members of the large TRIM family of E3-ubiquitin ligases [24]. We could confirm the interaction of MID2 and TRIM27 with LNX1, while MID1 seemed to require the co-expression of MID2 to interact with LNX1, suggesting its interaction is indirect and mediated by its known ability to heterodimerize with MID2 [25]. The MID2 interaction mapped to the PDZ region of LNX1, though not clearly to any one PDZ domain, while the FN3 and SPRY domains of MID2 are required for the interaction. The carboxyl terminal sequences of MID2 and TRIM27 are not closely related and don't match consensus PDZ binding motifs (Table 1), arguing against a canonical carboxyl terminal: PDZ domain mode of binding. Since TRIM27 lacks an FN3 domain it may be the SPRY that mediates the interaction of LNX with MID2 and TRIM27. However there is evidence in the IntAct database (http://www.ebi.ac.uk/intact/) that MID2 can dimerize with TRIM27, and so we cannot completely rule out the possibility that the interaction of TRIM27 with LNX1 might be mediated by endogenous MID2 in our experiments.

To explore whether MID2 might be responsible for the ability of LNX1p70 to promote ubiquitination of liprin-α1 we tested the ability of these three proteins to form a ternary complex. Robust binding of LNX1p70 to GFP-tagged MID2 was observed, but co-purification of liprin-α1 was not observed in this experimental setup. It may be that binding of MID2 and liprin-α1 to LNX1 is competitive, or that the formation of a ternary complex is very transient. While we were not able to obtain direct evidence for LNX1p70 acting to scaffold an interaction of MID2 with liprin-α1 in this case, it will be interesting to test this hypothesis for other combinations of LNX1-interacting E3 ligases and substrates including TRIM27 and KLHL11. Such a

mechanism, if proven, could explain the existence and conservation of the LNX1p70 isoform in diverse vertebrate species despite its lack of catalytic activity [13].

Another component of the presynaptic CAZ complex that we identified is the known LNX1 interacting protein ERC2/CAST1. ERC2 was previously shown to bind to LNX1-PDZ2 via a carboxyl terminal IWA* motif and to co-localise with LNX1 in neurons [30]. We show here for the first time that LNX1p80 but not LNX1p70 causes ubiquitination of ERC2. However this may not be so relevant *in vivo* since ERC2 (and the isoform of ERC1 that has the IWA* motif) are exclusively expressed in the brain [31], whereas LNX1p80 is expressed in non-neuronal tissues [32]. Instead LNX2, which can also interact with ERC1 and ERC2 [8], is perhaps more likely to promote their ubiquitination in neurons *in vivo*. Mice lacking LNX2 as well as the neuronal LNX1p70 and p62 isoforms have recently been shown to exhibit decreased anxiety-related behaviour [8]. Notably these mice don't show observable differences in levels of NUMB proteins. The ability of LNX proteins to bind to, and potentially promote ubiquitination of the prominent presynaptic CAZ complex components liprin-α1, liprin-α3, ERC1 and ERC2 provides a putative mechanism whereby loss of LNX proteins might cause an anxiety related phenotype through altered synaptic function. In addition, we have identified many other proteins with well-established functions in neuronal development and synapse formation in the LNX1 interactome. For example, KIF7, a kinesin motor protein involved in Hedgehog signalling, and MID2, an E3 ubiquitin ligase, both function in neural development [33, 34], as does SRGAP2[35], while MYCBP2 (Pam/highwire/rpm-1) is a well-known regulator of synapse formation. Overall, the LNX1 interacting proteins and substrates identified and characterised here are plausible candidates that may, in addition to NUMB, mediate physiological functions of LNX proteins in the CNS as well as other tissues.

Supporting information

S1 Table. Proteomic analysis of GFP-LNX1 interacting proteins purified from HEK293 cells.
(DOC)

S2 Table. Comparison of LNX1-interacting proteins identified here with those identified in previous studies.
(XLSX)

Acknowledgments

We are grateful to Colin Kenny, Kate Barry and Daniel Nyhan for their contributions to various aspects of the project.

Author Contributions

Conceptualization: Orthis Saha, Paul W. Young.

Data curation: Joan A. Lenihan, Orthis Saha.

Formal analysis: Joan A. Lenihan, Orthis Saha.

Funding acquisition: Paul W. Young.

Investigation: Joan A. Lenihan, Orthis Saha.

Methodology: Joan A. Lenihan, Orthis Saha, Paul W. Young.

Supervision: Paul W. Young.

Writing – original draft: Joan A. Lenihan, Paul W. Young.

Writing – review & editing: Joan A. Lenihan, Orthis Saha, Paul W. Young.

References

1. Dho SE, Jacob S, Wolting CD, French MB, Rohrschneider LR, McGlade CJ. The mammalian numb phosphotyrosine-binding domain. Characterization of binding specificity and identification of a novel PDZ domain-containing numb binding protein, LNX. J Biol Chem. 1998; 273(15):9179–87. PMID: 9535908.
2. Rice DS, Northcutt GM, Kurschner C. The Lnx family proteins function as molecular scaffolds for Numb family proteins. Mol Cell Neurosci. 2001; 18(5):525–40. Epub 2002/04/02. S1044-7431(01)91024-3 [pii] https://doi.org/10.1006/mcne.2001.1024 PMID: 11922143.
3. Nie J, Li SS, McGlade CJ. A novel PTB-PDZ domain interaction mediates isoform-specific ubiquitylation of mammalian Numb. J Biol Chem. 2004; 279(20):20807–15. Epub 2004/03/03. https://doi.org/10.1074/jbc.M311396200 [pii]. PMID: 14990566.
4. Nie J, McGill MA, Dermer M, Dho SE, Wolting CD, McGlade CJ. LNX functions as a RING type E3 ubiquitin ligase that targets the cell fate determinant Numb for ubiquitin-dependent degradation. EMBO J. 2002; 21(1_2):93–102. https://doi.org/10.1093/emboj/21.1.93 PMID: 11782429.
5. Lenihan JA, Saha O, Mansfield LM, Young PW. Tight, cell type-specific control of LNX expression in the nervous system, at the level of transcription, translation and protein stability. Gene. 2014; 552(1):39–50. Epub 2014/09/10. S0378-1119(14)01037-3 [pii] https://doi.org/10.1016/j.gene.2014.09.011 PMID: 25200495.
6. Wang H, Kane AW, Lee C, Ahn S. Gli3 repressor controls cell fates and cell adhesion for proper establishment of neurogenic niche. Cell Rep. 2014; 8(4):1093–104. Epub 2014/08/16. S2211-1247(14)00573-7 [pii] https://doi.org/10.1016/j.celrep.2014.07.006 PMID: 25127137.
7. Yin FT, Futagawa T, Li D, Ma YX, Lu MH, Lu L, et al. Caspr4 interaction with LNX2 modulates the proliferation and neuronal differentiation of mouse neural progenitor cells. Stem Cells Dev. 2015; 24(5):640–52. https://doi.org/10.1089/scd.2014.0261 PMID: 25279559; PubMed Central PMCID: PMCPMC4501688.
8. Lenihan JA, Saha O, Heimer-McGinn V, Cryan JF, Feng G, Young PW. Decreased Anxiety-Related Behaviour but Apparently Unperturbed NUMB Function in Ligand of NUMB Protein-X (LNX) 1/2 Double Knockout Mice. Mol Neurobiol. 2016:1–20. https://doi.org/10.1007/s12035-014-8981-5 PMID: 27889896.
9. Camps J, Pitt JJ, Emons G, Hummon AB, Case CM, Grade M, et al. Genetic Amplification of the NOTCH Modulator LNX2 Upregulates the WNT/beta-Catenin Pathway in Colorectal Cancer. Cancer Res. 2013. Epub 2013/01/16. 0008-5472.CAN-12-3159 [pii] https://doi.org/10.1158/0008-5472.CAN-12-3159 PMID: 23319804.
10. D'Agostino M, Tornillo G, Caporaso MG, Barone MV, Ghigo E, Bonatti S, et al. Ligand of Numb proteins LNX1p80 and LNX2 interact with the human glycoprotein CD8alpha and promote its ubiquitylation and endocytosis. J Cell Sci. 2011; 124(Pt 21):3545–56. Epub 2011/11/03. jcs.081224 [pii] https://doi.org/10.1242/jcs.081224 PMID: 22045731.
11. Zhou J, Fujiwara T, Ye S, Li X, Zhao H. Ubiquitin E3 Ligase LNX2 is Critical for Osteoclastogenesis In Vitro by Regulating M-CSF/RANKL Signaling and Notch2. Calcif Tissue Int. 2015; 96(5):465–75. https://doi.org/10.1007/s00223-015-9967-7 PMID: 25712254; PubMed Central PMCID: PMCPMC4730947.
12. Won M, Ro H, Dawid IB. Lnx2 ubiquitin ligase is essential for exocrine cell differentiation in the early zebrafish pancreas. Proc Natl Acad Sci U S A. 2015; 112(40):12426–31. https://doi.org/10.1073/pnas.1517033112 PMID: 26392552; PubMed Central PMCID: PMCPMC4603503.
13. Flynn M, Saha O, Young P. Molecular evolution of the LNX gene family. BMC Evol Biol. 2011; 11:235. Epub 2011/08/11. 1471-2148-11-235 [pii] https://doi.org/10.1186/1471-2148-11-235 PMID: 21827680.
14. Wolting CD, Griffiths EK, Sarao R, Prevost BC, Wybenga-Groot LE, McGlade CJ. Biochemical and computational analysis of LNX1 interacting proteins. PLoS One. 2011; 6(11):e26248. Epub 2011/11/17. https://doi.org/10.1371/journal.pone.0026248 [pii]. PMID: 22087225.
15. Guo Z, Song E, Ma S, Wang X, Gao S, Shao C, et al. Proteomics strategy to identify substrates of LNX, a PDZ domain-containing E3 ubiquitin ligase. J Proteome Res. 2012; 11(10):4847–62. Epub 2012/08/15. https://doi.org/10.1021/pr300674c PMID: 22889411.
16. Weiss A, Baumgartner M, Radziwill G, Dennler J, Moelling K. c-Src is a PDZ interaction partner and substrate of the E3 ubiquitin ligase Ligand-of-Numb protein X1. FEBS Lett. 2007; 581(26):5131–6. https://doi.org/10.1016/j.febslet.2007.09.062 PMID: 17936276.

17. Takahashi S, Iwamoto N, Sasaki H, Ohashi M, Oda Y, Tsukita S, et al. The E3 ubiquitin ligase LNX1p80 promotes the removal of claudins from tight junctions in MDCK cells. J Cell Sci. 2009; 122(Pt 7):985–94. Epub 2009/03/20. 122/7/985 [pii] https://doi.org/10.1242/jcs.040055 PMID: 19295125.

18. Young P, Nie J, Wang X, McGlade CJ, Rich MM, Feng G. LNX1 is a perisynaptic Schwann cell specific E3 ubiquitin ligase that interacts with ErbB2. Mol Cell Neurosci. 2005; 30(2):238–48. Epub 2005/08/27. S1044-7431(05)00170-3 [pii] https://doi.org/10.1016/j.mcn.2005.07.015 PMID: 16122940.

19. Foley KS, Young PW. An analysis of splicing, actin-binding properties, heterodimerization and molecular interactions of the non-muscle alpha-actinins. Biochem J. 2013; 452(3):477–88. Epub 2013/04/06. BJ20121824 [pii] https://doi.org/10.1042/BJ20121824 PMID: 23557398.

20. Murphy AC, Lindsay AJ, McCaffrey MW, Djinovic-Carugo K, Young PW. Congenital macrothrombocytopenia-linked mutations in the actin-binding domain of alpha-actinin-1 enhance F-actin association. FEBS Lett. 2016; 590(6):685–95. Epub 2016/02/18. https://doi.org/10.1002/1873-3468.12101 PMID: 26879394.

21. Huang da W, Sherman BT, Lempicki RA. Systematic and integrative analysis of large gene lists using DAVID bioinformatics resources. Nat Protoc. 2009; 4(1):44–57. Epub 2009/01/10. nprot.2008.211 [pii] https://doi.org/10.1038/nprot.2008.211 PMID: 19131956.

22. Bezprozvanny I, Maximov A. Classification of PDZ domains. FEBS Lett. 2001; 509(3):457–62. PMID: 11749973.

23. Tonikian R, Zhang Y, Sazinsky SL, Currell B, Yeh JH, Reva B, et al. A specificity map for the PDZ domain family. PLoS Biol. 2008; 6(9):e239. https://doi.org/10.1371/journal.pbio.0060239 PMID: 18828675; PubMed Central PMCID: PMCPMC2553845.

24. Sardiello M, Cairo S, Fontanella B, Ballabio A, Meroni G. Genomic analysis of the TRIM family reveals two groups of genes with distinct evolutionary properties. BMC Evol Biol. 2008; 8:225. https://doi.org/10.1186/1471-2148-8-225 PMID: 18673550; PubMed Central PMCID: PMCPMC2533329.

25. Short KM, Hopwood B, Yi Z, Cox TC. MID1 and MID2 homo- and heterodimerise to tether the rapamycin-sensitive PP2A regulatory subunit, alpha 4, to microtubules: implications for the clinical variability of X-linked Opitz GBBB syndrome and other developmental disorders. BMC Cell Biol. 2002; 3:1. https://doi.org/10.1186/1471-2121-3-1 PMID: 11806752; PubMed Central PMCID: PMCPMC64779.

26. Kim J, Kim I, Yang JS, Shin YE, Hwang J, Park S, et al. Rewiring of PDZ domain-ligand interaction network contributed to eukaryotic evolution. PLoS Genet. 2012; 8(2):e1002510. Epub 2012/02/22. https://doi.org/10.1371/journal.pgen.1002510 1002510 PGENETICS-D-11-01934 [pii]. PMID: 22346764.

27. Liu YC, Couzens AL, Deshwar AR, LD BM-C, Zhang X, Puviindran V, et al. The PPFIA1-PP2A protein complex promotes trafficking of Kif7 to the ciliary tip and Hedgehog signaling. Sci Signal. 2014; 7(355): ra117. Epub 2014/12/11. 7/355/ra117 [pii] https://doi.org/10.1126/scisignal.2005608 PMID: 25492966.

28. Spangler SA, Hoogenraad CC. Liprin-alpha proteins: scaffold molecules for synapse maturation. Biochem Soc Trans. 2007; 35(Pt 5):1278–82. Epub 2007/10/25.BST0351278 [pii] https://doi.org/10.1042/BST0351278 PMID: 17956329.

29. Rual JF, Venkatesan K, Hao T, Hirozane-Kishikawa T, Dricot A, Li N, et al. Towards a proteome-scale map of the human protein-protein interaction network. Nature. 2005; 437(7062):1173–8. Epub 2005/09/29. nature04209 [pii] https://doi.org/10.1038/nature04209 PMID: 16189514.

30. Higa S, Tokoro T, Inoue E, Kitajima I, Ohtsuka T. The active zone protein CAST directly associates with Ligand-of-Numb protein X. Biochem Biophys Res Commun. 2007; 354(3):686–92. https://doi.org/10.1016/j.bbrc.2007.01.036 PMID: 17257582.

31. Wang Y, Liu X, Biederer T, Sudhof TC. A family of RIM-binding proteins regulated by alternative splicing: Implications for the genesis of synaptic active zones. Proc Natl Acad Sci U S A. 2002; 99 (22):14464–9. https://doi.org/10.1073/pnas.182532999 PMID: 12391317; PubMed Central PMCID: PMCPMC137906.

32. Dho SE, French MB, Woods SA, McGlade CJ. Characterization of four mammalian numb protein isoforms. Identification of cytoplasmic and membrane-associated variants of the phosphotyrosine binding domain. J Biol Chem. 1999; 274(46):33097–104. Epub 1999/11/07. PMID: 10551880.

33. Endoh-Yamagami S, Evangelista M, Wilson D, Wen X, Theunissen JW, Phamluong K, et al. The mammalian Cos2 homolog Kif7 plays an essential role in modulating Hh signal transduction during development. Curr Biol. 2009; 19(15):1320–6. Epub 2009/07/14. S0960-9822(09)01323-2 [pii] https://doi.org/10.1016/j.cub.2009.06.046 PMID: 19592253.

34. Suzuki M, Hara Y, Takagi C, Yamamoto TS, Ueno N. MID1 and MID2 are required for Xenopus neural tube closure through the regulation of microtubule organization. Development. 137(14):2329–39. Epub 2010/06/11. dev.048769 [pii] https://doi.org/10.1242/dev.048769 PMID: 20534674.

35. Guerrier S, Coutinho-Budd J, Sassa T, Gresset A, Jordan NV, Chen K, et al. The F-BAR domain of srGAP2 induces membrane protrusions required for neuronal migration and morphogenesis. Cell. 2009; 138(5):990–1004. Epub 2009/09/10. S0092-8674(09)00794-6 [pii] https://doi.org/10.1016/j.cell.2009.06.047 PMID: 19737524.

Supplemental Table 1. Proteomic analysis of GST-LNX1-PDZ2 interacting proteins purified from brain lysates Previously known interactions are underlined, as are carboxyl-terminal cysteines. An asterisk indicates proteins identified as interacting with both LNX1 and LNX2 PDZ2 domains.

Gene Symbol	Mascot Score	Name	Carboxyl terminus
*Erc1**	7959	Erc1 ELKS/Rab6-interacting/CAST family member 1	DQDEEEGIWA
Ppfia3	4094	Ppfia3 Liprin-alpha-3	DGVSVRTYSC
*Erc2**	2235	Erc2 ELKS/Rab6-interacting/CAST family member 2	DQDDEEGIWA
*Lrrc16a**	2180	Lrrc16a Leucine-rich repeat-containing protein 16A	EEAEKEFIFV
*Fchsd2**	2109	Fchsd2 FCH and double SH3 domains protein 2	KMEDVEITLV
Ppfia4	1549	Ppfia4 liprin-alpha-4	EPSTVRTYSC
*Fermt2**	1467	Fermt2 Fermitin family homolog 2	MFYKLTSGWV
Ppfia2	1441	Ppfia2 Liprin-alpha-2	DNSTVRTYSC
Ppfia1	1358	Ppfia1 Liprin-alpha-1	DSATVRTYSC
Ppp2r5d	968	Ppp2r5d Protein phosphatase 2A B56 delta subunit	TGSRNGREGK
Prkcc	843	Prkcc Protein kinase C gamma type	PTSPVPVPVM
*Akap11**	792	Akap11 A-kinase anchor protein 11	ANRLQTSMLV
Ndrg3	749	N-myc downstream regulated gene NDRG3	DRHQTMEVSC
Ppp2r5c	724	Ppp2r5c Isoform 2 of Serine/threonine-protein phosphatase 2A 56 kDa regulatory subunit gamma isoform	ASELLSQDGR
*Pafah1b1**	710	Pafah1b1 Isoform 1 of Platelet-activating factor acetylhydrolase IB subunit alpha	DQTVKVWECR
*Ndel1**	668	Ndel1 Isoform 1 of Nuclear distribution protein nudE-like 1	SAPGMLPLSV
*Sphkap**	656	Sphkap A-kinase anchor protein SPHKAP	EQKERTPSLF
*Prkar1a**	592	Prkar1a cAMP-dependent protein kinase type I-alpha regulatory subunit	QYNSFVSLSV
Slc1a3	570	Slc1a3 Excitatory amino acid transporter 1	KPVADSETKM
Klhl11	567	Klhl11 Isoform 1 of Kelch-like protein 11	RRVPSSQIEC
*Ppp3ca**	559	Ppp3ca Isoform 1 of Serine/threonine-protein phosphatase 2B catalytic subunit alpha isoform	SNGSNSSNIQ
*Prkar1b**	518	Prkar1b cAMP-dependent protein kinase type I-beta regulatory subunit	RYNSFISLTV
Camk2d	449	Camk2d Isoform 1 of Calcium/calmodulin-dependent protein kinase type II subunit delta	SGGTSLWQNI
Ndrg2	422	Ndrg2 Isoform 1 of Protein NDRG2	PPGHTMEVSC
Trim9	418	Trim9 Isoform 2 of E3 ubiquitin-protein ligase TRIM9	AVKSPQAPAP
Cyfip1	384	Cyfip1 Isoform 1 of Cytoplasmic FMR1-interacting protein 1	PPIHQSLASS
*Ywhag**	382	Ywhag 14-3-3 protein gamma	QDDDGGEGNN
*Kazn**	320	Isoform 1 of Kazrin	GYGSLEVTNV
Atp2b3	305	Atp2b3 plasma membrane calcium ATPase 3	AGNPGGESIP
*Iqsec1**	301	Iqsec1 IQ motif and SEC7 domain-containing protein 1 isoform b	QPPQPPVLCS
Wasf1	282	Wasf1 Wiskott-Aldrich syndrome protein family member 1	SEFDEVDWLE
Dgcr8	272	Dgcr8 Microprocessor complex subunit DGCR8	GGEPLCTVDV
Hspa1b	270	Hspa1b Heat shock 70 kDa protein 1B	GSGPTIEEVD
Clec16a	267	Clec16a Isoform 5 of Protein CLEC16A	NPEPAEPTEH
Unc-13	265	- Unc-13 homolog B	SESRSTEEGS
Srgap1	254	Srgap1 SLIT-ROBO Rho GTPase-activating protein 1	QGPTDKSCTM
Hnrnph1	239	Hnrnph1 Heterogeneous nuclear ribonucleoprotein H	NSSDFQSNIA
Ctnnd2	238	Ctnnd2 Isoform 1 of Catenin delta-2	HYPASPDSWV

Supplemental Table 1 continued.

Gene Symbol	Mascot Score	Name	Carboxyl terminus
Mios	236	Mios WD repeat-containing protein mio	NLVPAETVQP
Tufm	230	Tufm Isoform 1 of Elongation factor Tu, mitochondrial	TEEDKNIKWS
Phldb1	219	Phldb1 Uncharacterized protein	GAEGYTQFMN
*Ywhaz**	214	Ywhaz 14-3-3 protein zeta/delta	EAEAGEGGEN
Snap47	200	Snap47 Isoform 1 of Synaptosomal-associated protein 47	KQNRRMRKLM
Hspa4l	194	Hspa4l Isoform 1 of Heat shock 70 kDa protein 4L	DKKLPEMDID
Ywhab	185	Ywhab Isoform Long of 14-3-3 protein beta/alpha	DEGDAGEGEN
Krt15	183	Krt15 keratin, type I cytoskeletal 15	KVVSSRKREI
Cct2	180	Cct2 T-complex protein 1 subunit beta	IKRVPDHHPC
Srcin1	170	Srcin1 Uncharacterized protein	FGARNSSISF
*Ywhaq**	166	Ywhaq;LOC100503129 Isoform 1 of 14-3-3 protein theta	ECDAAEGAEN
Krt13	162	Krt13 Isoform 1 of Keratin, type I cytoskeletal 13	NSGRPDFRKY
Tecpr1	158	Tecpr1 Isoform 1 of Tectonin beta-propeller repeat-containing protein 1	EARGPGPVCC
Hspa4	150	Hspa4 Heat shock 70 kDa protein 4	HTDSGEMEVD
*Pfkl**	145	Pfkl 6-phosphofructokinase, liver type	TRRTLSIDKF
Hepacam	143	Hepacam Hepatocyte cell adhesion molecule	DESGQVEISA
Camsap1	141	Camsap1 Isoform 1 of Calmodulin-regulated spectrin-associated protein 1	TVPKKTQTRK
Vwa5a	140	Vwa5a von Willebrand factor A domain-containing protein 5A	LSVNPAVFGV
Add1	139	Add1 Isoform 1 of Alpha-adducin	LKKSKKKSDS
Ppfibp1	136	Ppfibp1 Isoform 3 of Liprin-beta-1	ASITDEDSNV
AW555464	128	AW555464 Isoform 1 of Protein KIAA0284	FLPDAERFLI
Wars	127	Wars Isoform 1 of Tryptophanyl-tRNA synthetase, cytoplasmic	FHFQCFCFDT
Ap1b1	123	Ap1b1 AP-1 complex subunit beta-1	YQAYETILKN
Ndrg1	119	Ndrg1 Protein NDRG1	AGPKSMEVSC
Dtna	118	Dtna Isoform 1 of Dystrobrevin alpha	DEAYQVSLQG
*Ldb1**	116	Ldb1 Isoform 1 of LIM domain-binding protein 1	SENPTSQASQ
Gstm7	116	Gstm7 Glutathione S-transferase Mu 7	FTKMATWGSN
*Ctnna2**	115	Ctnna2 Isoform 1 of Catenin alpha-2	LSEFKAMDSF
Tbce	113	Tbce Tubulin-specific chaperone E	ENGDCLLVRW
Atp4a	113	Atp4a Uncharacterized protein	GSWWDQDFYY
Atp12a	112	Atp12a Potassium-transporting ATPase alpha chain 2	GSWWDKNMYY
Cdk14	108	Cdk14 Isoform 1 of Cyclin-dependent kinase 14	YGKSLSNSKH
Entpd2	104	Entpd2 Isoform Long of Ectonucleoside triphosphate diphosphohydrolase 2	VRSAKSPGAL
Bcr	104	Bcr Breakpoint cluster region protein	RQSILFSTEV
Cttnbp2	103	Cttnbp2 Cttnbp2 protein	KHEQVEKPNK
Nptn	103	Nptn Isoform 2 of Neuroplastin	DKNLRQRNTN
*Slc6a1**	101	Slc6a1 Sodium- and chloride-dependent GABA transporter 1	GSSASKEAYI
*Rpn1**	100	Rpn1 Dolichyl-diphosphooligosaccharide--protein glycosyltransferase subunit 1	TKIDHILDAL
Atl1	99	Atl1 Atlastin-1	MQTCKVLPLE
*Ctnnb1**	96	Ctnnb1 Catenin beta-1	NQLAWFDTDL

Supplemental Table 2. Proteomic analysis of GST-LNX2-PDZ2 interacting proteins purified from brain lysates Previously known interactions are underlined, as are carboxyl-terminal cysteines. An asterisk indicates proteins identified as interacting with both LNX1 and LNX2 PDZ2 domains.

Gene Symbol	Mascot Score	Name	Carboxyl terminus
*Erc1**	3181	Erc1 ELKS/Rab6-interacting/CAST family member 1	DQDEEEGIWA
*Sphkap**	2692	Sphkap A-kinase anchor protein SPHKAP	EQKERTPSLF
*Lrrc16a**	2270	Lrrc16a Isoform 1 of Leucine-rich repeat-containing protein 16A	EEAEKEFIFV
*Fchsd2**	1938	Fchsd2 Isoform 2 of FCH and double SH3 domains protein 2	KMEDVEITLV
Srgap2	1935	Srgap2 SLIT-ROBO Rho GTPase-activating protein 2	PQATDKSCTV
*Akap11**	1576	Akap11 A-kinase anchor protein 11	ANRLQTSMLV
*Fermt2**	1287	Fermt2 Fermitin family homolog 2	MFYKLTSGWV
*Erc2**	1139	Erc2 ELKS/Rab6-interacting/CAST family member 2	DQDDEEGIWA
Atp2a2	1125	Atp2a2 Isoform SERCA2B of Sarcoplasmic/endoplasmic reticulum calcium ATPase 2	DTNFSDMFWS
Rrbp1	1059	Rrbp1 ribosome-binding protein 1 isoform a	GSSSKEGTSV
*Kazn**	560	Isoform 1 of Kazrin	GYGSLEVTNV
Eml3	549	Eml3 Echinoderm microtubule-associated protein-like 3	SLSPASSLDV
*Prkar1b**	507	Prkar1b cAMP-dependent protein kinase type I-beta regulatory subunit	RYNSFISLTV
*Prkar1a**	504	Prkar1a cAMP-dependent protein kinase type I-alpha regulatory subunit	QYNSFVSLSV
Ktn1	500	Ktn1 Uncharacterized protein	EVNQQLTKET
Kcnj10	327	Kcnj10 ATP-sensitive inward rectifier potassium channel 10	SALSVRISNV
Slc4a4	322	Slc4a4 Isoform 1 of Electrogenic sodium bicarbonate cotransporter 1	STFLERHTSC
Ckap4	292	Ckap4 Cytoskeleton-associated protein 4	LKVEKIHEKI
*Ndel1**	287	Ndel1 Isoform 1 of Nuclear distribution protein nudE-like 1	SAPGMLPLSV
Gria2	278	Gria2 Isoform 1 of Glutamate receptor 2	NVYGIESVKI
*Ctnnd2**	272	Ctnnd2 Isoform 1 of Catenin delta-2	HYPASPDSWV
Kif5a	236	Kif5a Kinesin heavy chain isoform 5A	FPLHQETAAS
Exoc4	230	Exoc4 Exocyst complex component 4	ATKDKKITTV
*Rpn1**	224	Rpn1 Dolichyl-diphosphooligosaccharide-protein glycosyltransferase subunit 1	TKIDHILDAL
Agap2	215	Agap2 Isoform 1 of Arf-GAP with GTPase, ANK repeat and PH domain-containing protein 2	GRVDTTIALV
*Ywhag**	207	Ywhag 14-3-3 protein gamma	QDDDGGEGNN
Mtmr1	204	Mtmr1 Myotubularin-related protein 1	HSATPVHTSV
C2cd2l	197	C2cd2l C2 domain-containing protein 2-like	KANGNPSPQL
Ddost	185	Ddost Dolichyl-diphosphooligosaccharide--protein glycosyltransferase 48 kDa subunit	LHMKEKEKSD
Amigo1	176	Amigo1 Isoform 1 of Amphoterin-induced protein 1	SVFSDTPIVV
Exoc2	176	Exoc2 Exocyst complex component 2	QAASPAVMKT
C230096C10Rik	175	C230096C10Rik Isoform 1 of Uncharacterized protein KIAA0090	QVKLLNRAWR
Rpn2	172	Rpn2 Dolichyl-diphosphooligosaccharide-protein glycosyltransferase subunit 2	AQHAVKRTAH
Sbf2	153	Sbf2 SET-binding factor 2	DRIQSCLSDA
*Slc6a1**	153	Slc6a1 Sodium- and chloride-dependent GABA transporter 1	GSSASKEAYI

Supplemental Table 2 continued.

Gene Symbol	Mascot Score	Name	Carboxyl terminus
Nrxn1	150	Nrxn1 Uncharacterized protein	KKNKDKEYYV
*Ppp3ca**	149	Ppp3ca Isoform 1 of Serine/threonine-protein phosphatase 2B catalytic subunit alpha isoform	SNGSNSSNIQ
Nomo1	144	Nomo1 Nodal modulator 1	QTKKQKTRRT
Cds2	144	Cds2 Phosphatidate cytidylyltransferase 2	GILTSALEDE
Srr	138	Srr Isoform 1 of Serine racemase	RPAPYQTVSV
Exoc1	136	Exoc1 Uncharacterized protein	DYCSSIAQSH
Slc25a12	131	Slc25a12 Calcium-binding mitochondrial carrier protein Aralar1	AQPKAAAAAQ
*Ywhaz**	129	Ywhaz 14-3-3 protein zeta/delta	EAEAGEGGEN
Canx	129	Canx Calnexin	SPRNRKPRRE
*Ywhaq**	129	Ywhaq;LOC100503129 Isoform 1 of 14-3-3 protein theta	ECDAAEGAEN
*Iqsec1**	125	Iqsec1 IQ motif and SEC7 domain-containing protein 1 isoform b	QPPQPPVLCS
*Ldb1**	124	Ldb1 Isoform 1 of LIM domain-binding protein 1	SENPTSQASQ
Ppp2r1b	123	Ppp2r1b serine/threonine-protein phosphatase 2A 65 kDa regulatory subunit A beta isoform isoform a	AQEAISVLAA
Stt3a	120	Stt3a Putative uncharacterized protein	DLDNRGLSRT
Ilvbl	117	Ilvbl Isoform 1 of Acetolactate synthase-like protein	TDFRDGSISV
*Pfkl**	113	Pfkl 6-phosphofructokinase, liver type	TRRTLSIDKF
Myl1	113	Myl1 Isoform MLC1 of Myosin light chain 1/3, skeletal muscle isoform	EAFVKHIMSV
Snd1	110	Snd1 Staphylococcal nuclease domain-containing protein 1	DDADEFGYSR
*Pafah1b1**	109	Pafah1b1 Isoform 1 of Platelet-activating factor acetylhydrolase IB subunit alpha	DQTVKVWECR
Prkacb	107	Prkacb Isoform 1 of cAMP-dependent protein kinase catalytic subunit beta	EKCGKEFCEF
Ssbp3	107	Ssbp3 Isoform 1 of Single-stranded DNA-binding protein 3	NYSPSMTMSV
Lamc1	103	Lamc1 Uncharacterized protein	CFNTPSIEKP
*Ctnnb1**	102	Ctnnb1 Catenin beta-1	NQLAWFDTDL
Atp1b2	101	Atp1b2 Sodium/potassium-transporting ATPase subunit beta-2	VAFKLRINKT
Clptm1	100	Clptm1 Cleft lip and palate transmembrane protein 1 homolog	PKPAEDKKKD